Physical Aspects of Local Solid Tumor Growth

Von der Fakultät für Physik und Geowissenschaften

der Universität Leipzig

genehmigte

DISSERTATION

zur Erlangung des akademischen Grades

Doktor der Naturwissenschaften

doctor rerum naturalium

Dr. rer. nat.,

vorgelegt von M.Sc. Hans Kubitschke,
geboren am 25.10.1987 in Leipzig.

Erster Gutachter: Prof. Josef A. Käs
Zweiter Gutachter: Prof. Paul Janmey

Tag der Verleihung: 23.03.2020

Bibliografische Beschreibung

Kubitschke, Hans

Physical Aspects of Local Solid Tumor Growth

Universität Leipzig, Fakultät für Physik und Geowissenschaften
162 Seiten, 276 Literaturzitate, 12 Abbildungen

Zusammenfassung:

Krebszellen haben gemeinsame Eigenschaften, wie unbegrenztes Wachstumspotential und die Vermeidung von Apoptose. Krebs kann als systemische Erkrankung angesehen werden und es reicht daher nicht aus, molekulare Details von Krebs zu verstehen, sondern auch emergente physikalische Eigenschaften von Krebs auf mehreren Größenskalen von Genen über Zellen bis hin zu Geweben.

Diese Arbeit konzentriert sich auf physikalische Eigenschaften die an der Krebsprogression, der Migration von Krebszellen und dem Krebswachstum beteiligt sind. Die Migration von Krebszellen führt zur Fähigkeit zur Metastasierung, der häufigsten Ursache für krebsbedingten Tod. Der Schlüssel zu diesem Prozess ist die Verformbarkeit von Krebszellen beim Durchqueren der dichten Mikroumgebung aus extrazellulärer Matrix und anderen Zellen. Der genaue Beitrag des Aktin- und Mikrotubuli-Netzwerks zur zellulären elastischen Verformung und Entspannung ist wichtig und wurde untersucht. Ein wichtiges Ergebnis ist, dass bei kleinen Verformungen (<5%) die Aktin-Filamente die viskoelastische Zellverformung unter mechanischer Belastung dominieren und Mikrotubuli die Zellrelaxation bestimmen, während bei größeren Verformungen (>5%) Aktin-Filamente und Mikrotubuli gleichermaßen zur Zellverformung und -relaxation beitragen. So sind die Mikrotubuli für die Migration in Mikroumgebungen von größerer Bedeutung, als es die aktuelle Literatur vermuten lässt.

Ein initial gebildeter bösartiger Tumor tritt typischerweise in eine Wachstumsphase ein, in der das umgebende Gewebe verdrängt und eingedrungen wird. Für ein optimales klinisches Behandlungsergebnis sollte der Primärtumor so gut wie möglich entfernt werden, was die genaue Erkennung der Tumorfront und die Identifizierung der Gewebe mit dem Risiko einer Krebsinfiltration beinhaltet. In dieser Arbeit werden natürliche Hindernisse und Grenzen für das Krebswachstum, wie z.B. Fasziengewebsgrenzen oder Gewebekompartimentgrenzen, basierend auf klinischen Daten von Gebärmutterhalskrebs analysiert, die aus der pathologischen Untersuchung von chirurgisch resezierten Tumoren von 518 Patienten gewonnen wurden. Die Wachstumsgrenzen wurden als embryonale Gewebeentwicklungsgrenzen identifiziert und betonen, dass Krebs Entwicklungsmerkmale aufweist, die häufig in der Embryogenese vorkommen. Das gefundene Tumorwachstumsmuster und die -form widersprechen dem das das vorherrschende Dogma der isotropen Tumorwachstum, welches der chirurgischen Tumorresektion und Strahlentherapie zugrunde liegt. Die Tumorform-Distribution weist starke Abweichungen von sphärischer Symmetrie auf, was darauf hindeutet, dass Tumore durch entwicklungsbiologische Kompartimente und deren Kompartimentsgrenzen begrenzt und geformt werden. Computersimulationen liefern auch den Nachweis, dass die klinisch gefundene Tumorinfiltrationswahrscheinlichkeit von Geweben nicht auf der metrischen Entfernung des gefährdeten Gewebes zum Gewebe der Tumorherkunft basiert, sondern auf der ontogenetischen Verwandtschaft der Gewebe.

Bibliographic description

Kubitschke, Hans

Physical Aspects of Local Solid Tumor Growth

Universität Leipzig, Fakultät für Physik und Geowissenschaften
162 Pages, 276 References, 12 Figures

Summary:

Cancer cells share common properties, such as unlimited replicative potential and evasion of apoptosis, coined the "Hallmarks of Cancer". Cancer can be considered a systemic disease and it is therefore not sufficient to understand molecular details of cancer, but also emergent physical properties of cancer on multiple scales from genes over cells to tissues.

This thesis focuses on physical characteristics and physics involved in cancer progression, cancer cell migration, and cancer growth. Migration of cancer cells results in the ability of metastasis, the most common cause of cancer-related death. Key for this process is the deformability of cancer cells when squeezing through dense microenvironment of extra-cellular matrix and other cells. The precise contribution of the actin and microtubule network towards both cellular elastic deformation and relaxation is important and is evaluated. A major finding is that on small deformations (<5%), actin filaments dominate cell's viscoelastic response under stress application and microtubules determine the cell relaxation under stress release, whereas for larger strains (>5%) actin filaments and microtubules equally contribute to cell deformation and relaxation. Thus, the microtubules are of greater importance for the migration in microenvironments than current literature suggests.

An initially formed malignant tumor typically enters a growth phase where surrounding tissue is displaced and invaded. For best clinical treatment outcomes, the primary tumor should be removed as best as possible which includes the precise detection of the tumor front and identification of the tissues at risk of cancer infiltration. In this thesis, natural obstacles and boundaries for cancer growth, such as fascial tissue boundaries or tissue compartment boundaries, are analyzed based on clinical data of cervical cancers obtained from pathological examination of surgical resected tumors of 518 patients. the growth boundaries were identified as embryonic tissue developmental boundaries emphasizing that cancer exhibit developmental features commonly found in embryogenesis. The found tumor growth pattern and shape contradicts the isotropic tumor growth which is the prevailing dogma guiding tumor resection and radiotherapy. The tumor shape distribution display strong deviations from spherical symmetry advocating that tumors are confined and shaped by developmental compartments and their compartment boundaries. Computer simulations also provide evidence that the clinical found tumor infiltration probability of tissues is not based on metric distance of the tissue at risk to the tissue of tumor origin, but on the ontogenetic relatedness of the tissues.

Table of Content

List of Figures

1 Introduction

Despite the vast accumulated knowledge about cancers by now, cancer paradoxically developed towards an omnipresent disease with improved overall public health and – as a consequence of the former – increased overall life expectancy, especially since the second industrialization. This development led to signing of the *National Cancer Act* back in 1971 by United States president Richard Nixon with the intended goal of finding a cure for cancer. Nonetheless, cancer remains a major cause of death even nearly half a century after the declaration of the "War on Cancer" [1–3] only second to cardiovascular disease [4], illustrated in *Figure 1.1* and *Figure 1.2*.

Why is this "War on Cancer" a paramount battleground with rather limited progress compared to (former) major diseases like tuberculosis, influenza, chronic obstructive pulmonary disease, lower respiratory infections, or diarrheal diseases? The "flaw" of numerous other diseases is that they often can be treated or prevented with vaccines or other proven standardized treatment or prevention options, whereas cancer has not achieved such standardized treatment. The cardinal reason is that most other major diseases are caused by bacteria and not by the organism's own cells.

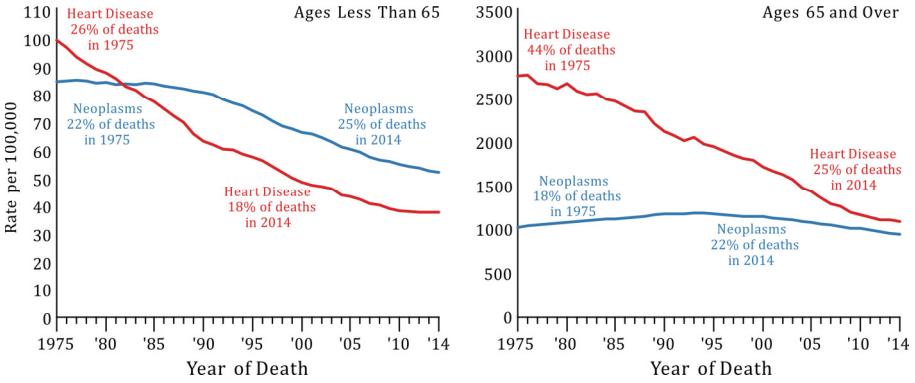

Figure 1.1: Development of death rates of heart diseases and cancers after the signing of the *National Cancer Act*. While the death rates for cancer significantly decreased for age less than 65, the death rates are still high for age 65 and over signifying that cancer is an age-related disease such as heart diseases. In contrast, death rates for heart diseases declined in the same time frame. Illustration adapted from NHI SEER, SEER Cancer Statistics Review [5].

Cancer is a collective disease family where the disease progression and development usually show similar patterns, but the microscopic cause and origin may vary strongly. Astonishingly, the *National Cancer Institute* is already distinguishing over 200 different types of cancer [6], yet virtually all cancers share properties of lost growth regulations, strategies to evade apoptosis, among others factors coined the "hallmarks of cancer" [7–9]. This illustrates, that cancer develops into a systemic disease with molecular origin but macroscopic developmental steps. The crucial step in cancer progression is the metastasizing stage which causes approx. 66.7% and higher of all cancer related deaths [10]. The ability of cancer cell to migrate across tissue boundaries and survive in different microenvironments is therefore the most intriguing transition to study in cancer progression. Thus, it is imperative to fully grasp the concepts of cancer cell migration from a physical point of view. As a consequence, the tissue level presumably is an appropriate level of observation for cancer progression [11]. It is therefore not sufficient to study molecular details of cancer alone, but cancer progression has to be understood on multiple scales, from genes over cells to tissues.

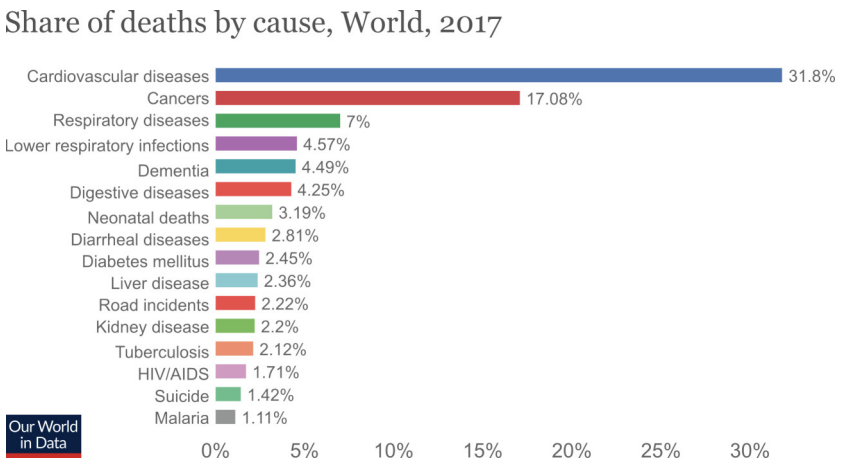

Figure 1.2: Shared death rates by cause worldwide in 2017. Data refers to the specific cause of death, which is distinguished from risk factors for death, such as air pollution, diet and other lifestyle factors. This is shown by cause of death as the percentage of total deaths. Illustration adapted from IHME, Global Burden of Disease [4].

For instance, more recent studies revealed over 70 former unknown genetic variations, single nucleotide polymorphisms (SNPs), associated to common cancers of breast, prostate and ovaries [12–15] thereby doubling the known common risk variants linked to cancer. However, these genetic studies reveal no clear cause-and-effect. Comparing current treatment options to the accumulated knowledge of cancer, a discrepancy is revealed that the quality of treatment options lacks behind the knowledge about cancer.

Surgery, radiotherapy and general chemotherapy are the prevalent treatment strategies in broad clinical practice. Another promising strategy of immunotherapy has received a throwback after researchers have discovered why some cancers do not respond to certain types of immunotherapy, coined “checkpoint inhibitors” (CPI), and up to 85 percent of patients with certain cancers treated with checkpoint inhibitors do not properly benefit [16] and most patients treated with CPI eventually develop progressive disease [17]. Nonetheless, immunotherapy is still a promising treatment option. From a historical perspective, the three major treatment strategies are can be considered as classical strategies: modern cancer surgery, i.e. Halsted’s *Radical Cancer Surgery* in *Figure 1.3*, dates back to the end of the 19th century, radiotherapy emerged at the verge to the 20th century, first chemotherapy was approved in the 1940’s. They stood the test of time

and were refined and optimized, however, novel insights in cancer are often difficult to translate to the classic treatment strategies and – unfortunately – the classical approaches have not fundamentally evolved beyond optimization and healthy tissue sparing practice since then. As a result, the patient morbidity was decreased and the survival rate increased, however, apparent limitations of treatability and survival rate of advanced cancers are still present [18].

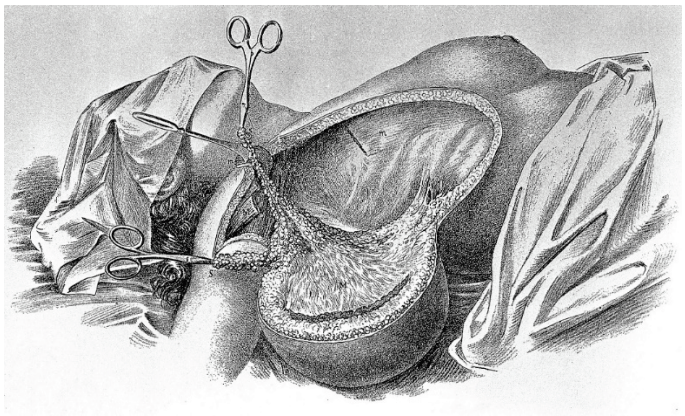

Figure 1.3: Illustration of Radical Mastectomy Technique from William Halsted prior to final amputation of the breast. Adopted from [19].

Crucial for cancer therapy of the 21st century are novel, promising approaches which may also translatable to the standard approaches of surgery, radiotherapy and chemotherapy. In the long run, approaches such as immunotherapy will likely be of great importance and practicability, however, they are not adequately realizable in the short run as broad clinical practice. Furthermore, considering how much money was already provided in investigating the prevalent understanding of cancer, it begs the questions: Are the current tenets of cancer in need of readjustments and what alternative theories of cancer may be beneficial to be investigated?

Arguably, the narrow genomic view on cancer is not sufficient. Treatment relevant descriptions, such as staging and grading, may include molecular details, nonetheless, they are predominantly of physical characteristics, such as tumor size and shape, breached boundaries and invaded tissues, and lymph node infiltration and metastases formation.

The focus should fall on the limiting factors of cancer progression since genome damage is inevitable and it is thus impossible to keep track

of all damaged sites rendering molecular approaches inefficient in most current clinical scenarios. However, these limiting factors are – in essence – of physical nature. In amendment, physical characteristics are associated to certain length scales, which is also reflected in cancer progression, i.e. loss of growth control enables local tumor growth and invasion in other tissues by displacement on length scales of single cells, tens of micrometers, whereas the gain of migratory modes and motility of cancerous cells enables them to surpass several cell lengths in distance and ultimately to form metastases.

This thesis focuses on physical characteristics and physics involved in cancer progression, migration, and growth. Motility and migration of cancerous cells is a tightrope act of (traction) force generation and cell deformability as they squeeze through a tight meshwork of surrounding cells and ECM [20,21]. In order to perform this task most efficiently, cancerous cells need to be deformable, but also be capable in sufficient directed force generation, both processes which require considered restructuring of the cytoskeleton outlined in Kubitschke et al. 2018 [22]. I will describe which components of the cytoskeleton contribute to cellular elastic deformation and relaxation for different strain regimes and show that a single-focused view on actin cytoskeleton is insufficient for migration in microenvironments but the microtubule network is also important, especially in regimes of larger deformations, which is part of Kubitschke et al. 2017 [23].

Lastly, when a sufficient number of cancer cells conglomerate in one cluster and form an initial solid tumor, they slowly alter their microenvironment. Most commonly, the extra-cellular matrix stiffens which in turn is in itself a tumor promoter resulting in further tumor progression [20,21,24–26]. In the accompanying tumor growth phase, the surrounding healthy tissue is slowly displaced, invaded or recruited by the tumor. Nonetheless, there are further boundaries for the solid tumor and cancer cells to overcome. Most prominent are fascial tissue boundaries such as basement membrane or tissue compartment boundaries, both comprised of densely packed and aligned extracellular macrofilaments. Presented in Kubitschke et al. 2019 [27], with vast clinical data of cervical cancers obtained from pathological examination of surgical resected tumors of 518 patients, I have analyze such tumor growth boundaries and obstacles and show that clinically found growth of solid tumors contradicts the assumption of isotropic random tumor

growth which is the prevailing dogma guiding tumor resection and radiotherapy.

Peculiarly, the identified growth boundaries are, in fact, embryonic tissue development boundaries underlining that cancer cells exhibit embryonic developmental features, which is too often ignored in cancer development. In case of the uterine cervix, the herein analyzed data displays a predictable tumor infiltration pattern of reversed embryogenetic tissues development. Thus, knowing the embryological origin of any tissue in which cancer arises, one can derive a relative likelihood of different adjacent tissues to be infiltrated by tumor cells, depending on their ontogenetic proximity to the tissue of cancer origin, deduce an ontogenetic tumor stage, and tailor surgical resection and/or radiation exactly to the tissue at risk.

Clearly, patients will benefit if surgeons and radiotherapists caring for them have a high-resolution roadmap at hand which can help them navigate through the tissues surrounding the tumor. While the prevailing *wide excision method* plainly adds an "safety margin" of presumably healthy tissue excised around the tumor with the goal of surgically removing or radiating all tumor cells which might have preceded the solid tumor front, an ontogenetic resection and radiation approach defines all already invaded embryogenetic-derived tissues and tissue compartments as to be resected and/or radiated, but spares all further tissues regardless of the proximity to the solid tumor. The thereby well-defined and reproducible approach can often spare certain functional tissues, such as nerves for bladder or rectum functionality, and therefore reducing the patient's morbidity after treatment. Furthermore, by surgically removing or radiating all tumor infested tissue compartments, all initially suitable microenvironments for tumor cell proliferation are treated, thus any occult tumor cell will not find a proper habitable microenvironment and presumably not proliferate any further. In the time of individualized precision medicine, a "safety margin" strategy based on a concept which defines tissue at risk using metrical distances is no longer acceptable. It is time to scrutinize data of tumor infiltration patterns in additional cancers, relate these patterns to ontogenetic anatomy and to develop novel resection and radiation strategies.

2 Background

2.1 Cellular Structure and Biomechanical Properties

From a biophysical point of view, the cytoskeleton and the cell membrane are of primary interest for almost all mechanical properties of cells. Among many functional roles in the cell, the cytoskeleton is the backbone for the mechanical stability of a cell and majorly contributes to the cell's viscoelastic properties. The cytoskeleton is connected to the cell membrane which is the barrier and gatekeeper of the internal and external environment of the cell. The cell membrane serves as intermediary for enacting cell-cell and cell-ECM connections and therefore cellular adhesion and cell signaling.

In cancers, the paramount concern for treatment outcome is the ability of the primary solid tumor to form metastases. The connected biophysical ingredients to accomplish this are manifold, however, the ability of cancer cells to migrate through densely packed microenvironments of extracellular matrix (ECM) and other cells are of utmost importance. Key is the deformability of cancer cells and the ability to squeeze through narrow openings of ECM and surrounding cells. With such a toolkit cancer cells can leave the primary tumor, intravasate into the blood vessels, extravasate at a new location and ultimately form a far metastasis. While tissue invasion and formation of

metastasizes is a multi-step process involving multitude of changes in order for cancerous cells to acquire the ability to metastasize [7,8,28], the cytoskeleton can be pinpointed as the main contributor. In order to metastasize, cancerous cells need to be deformable, but also be capable in sufficient directed force generation, both processes which require considered restructuring of the cytoskeleton. It is thus important to understand the contributions of individual constituents of the cytoskeleton and its role in cellular deformability and force generation.

The central observations of my publication Kubitschke et al. 2017 [23] as part of this thesis are that the actin and microtubule network are differentially responsible for the cell's deformability and strain relaxation for different strain regimes of low and large strains. Thus, in the following subsections I will provide the background knowledge needed for the composition and the fundamental rheological properties and characterization of the cytoskeleton.

2.1.1 Cellular Cytoskeleton

The cytoskeleton, the main contributor of the cell's mechanics, is an actively regulated biopolymer network. It is composed of biofilaments which constantly self-assemble and disassemble, entangle and crosslink themselves. The cytoskeleton is therefore an exceptionally dynamic scaffold under continuous internal rearrangement, nonetheless, provides a cell's mechanical integrity and enables whole-cell locomotion and suits as internal cargo transport system [22,29]. The biofilaments assemble from monomers or dimers (few nanometers in size) to compose filaments up to few tens of micrometer. In eukaryotic cells are three major filaments present, actin filaments, intermediate filaments and microtubules, all with different physical, molecular and functional differences. Their distinct molecular structure of the monomers and dimers results in different assembly and disassembly motifs. Therefore, they contribute towards the mechanical integrity of the cytoskeleton on different length and time scales and enabling cytoskeletal adaptation on external stimuli.

The three major filament classes, actin, microtubules and intermediate filaments, are also distinguishable from their physical

characteristics by their bending stiffness (or flexural rigidity). In polymer physics, the bending stiffness is commonly described by a characteristic length scale on which the polymer's direction of the ends (tangent vector) loses its correlation by bending due to thermal fluctuations. This length scale is coined persistence length. As illustration, the tangent vectors of the ends of uncooked spaghetti point in the same direction, hence the contour length of spaghetti would be much shorter than its persistence length. Uncooked spaghettis would therefore be considered "stiff polymer". Whereas cooked spaghettis lose their correlation of the tangent vectors at their ends and would be considered flexible. The classification of stiff, flexible and semiflexible based on persistence to contour length ratio is seen in these three major filament classes of the cytoskeleton: The intermediate filaments are considered flexible, $p > l_P$, with a persistence length of approx. 1 µm [30]. The actin filaments are semiflexible as their persistence length is in the same range than the contour length with $l_P \approx 17$ µm [31,32] and their length ranging between few micrometers and 100µm. The contour length of microtubules ranges from approx. 2 to 500 µm and their persistence length display an increase with contour length from approx. 100 to 5'000 µm [33], therefore, microtubules are considered as stiff polymers, $p \ll l_P$. All further, detailed characterization and background of biopolymers is given in chapter 5.2 of Kubitschke et al. 2018 [22].

2.1.2 Viscoelastic Material Properties of Cells

While cells and tissues are living entities and are active in their response to environmental changes, such as acting forces and deformations, they can under certain conditions be considered as quasi-passive materials. The time scale is often the crucial condition since cellular adaptations are not infinitely fast. Hence, all measurements and experiments which probe cell mechanics on shorter scales than cellular "reaction time" can be considered as quasi-passive material probing. Cells and tissues react to external mechanical cues partly as viscous fluids and partly as elastic solids. Their response is characterized as viscoelastic.

The viscoelastic properties are essential in cancer cell migration. Without the proper structural backbone, cancer cells are not able to generate sufficient traction forces for migration nor to squeeze through surrounding cells and gaps in the extra-cellular matrix. The exact contribution and best-suited mechanical properties are under ongoing debate [34–37]. One argument is that cancer cells should be stiff enough to push against its surrounding enabling a solid tumor to grow in the first place, other arguments point in the direction that softness helps with migration. Furthermore, others have pointed out that the best physical characteristics of solid tumors likely lies in broad distribution of cellular material properties of individual cancer cells [38]. In such a case, the more rigid cells give rise to a sturdy mechanical backbone for the solid tumor [39–42] while the softer cells harbor the potential of migration and metastasizing later during cancer progression.

The information given in this section is a brief introduction of viscoelastic material properties and their definitions, the foundation of the theoretical background for my publication Kubitschke et al. 2018 [22].

Generally, the bulk material properties of cells and tissues is of interest. For that, one can consider a unit cuboid of biological material and applying forces or deformations to its surface. An applied uniaxial force F onto two counter-facing unit surfaces A will induce a stress (force per unit area). The mechanical stress is thus defined as

$$\sigma = \frac{F}{A} .$$

Consequential, the mechanical strain γ is then the relative deformation along the axis of force application, given by

$$\gamma = \frac{\Delta x}{x}$$

with the absolute deformation Δx and the thickness of the cuboid x along the axis of force application. An elongation along one axis usually also induces a compression or retraction of the bulk material along the transverse axes y and z of force application. This property is captured in the Poisson ratio:

$$\mu = -\frac{\Delta y / y}{\Delta x / x} = -\frac{\gamma_{\perp}}{\gamma_{\parallel}} .$$

For instance, elastic rubber is to large extend incompressible (its density is conserved), the volume of the initial and deformed cuboid will be identical, whereas concrete and glasses are compressible and can vary their density to some extent. For isotropic materials, the Poisson ratio is generally between 0 and 0.5 (no lateral contraction upon pulling and incompressible). Biological material and hydrated cytoskeleton are nearly incompressible with a Poisson ratio of approx. $0.45 - 0.5$ [43,44].This simplest case of elastic behavior is known as Hooke's law, the strain γ is linear proportional to the applied stress σ with a proportionality constant describing the material property, the elastic or Young's modulus E, of the spring: $\sigma = E\gamma$. In analog, applying a strain and measuring the stress provides the tensile compliance D of the material $\gamma = D\sigma$ with the relation $E \coloneqq 1/D$.

Biological materials show elastic behavior on short time scales of seconds and less, however, biological material can also display permanent deformations when stresses are applied for a prolonged time. The continuous deformation under constant applied stress is captured as the viscosity of a material. The introduced energy while deforming is then internally dissipated due friction and the material will not relax back to its initial shape. The viscous flow, i.e. strain rate $\dot{\gamma}$, is linear proportional to the applied stress σ with a proportionality constant η, the Newtonian viscosity: $\sigma = \eta\dot{\gamma}$.

As introduced, biological matter like tissues, cells and the cytoskeleton show elastic and viscous material responses, and are from there called viscoelastic materials. Viscoelastic responses are more complex since they can depend on the direction of stress application (compression, tension or shear) and the time scale of applied stresses or strains. It follows, that for biological matter the stress response depends on the strain γ and on the strain rate $\dot{\gamma}$ of the material in a non-trivial relation like for perfect elastic solids or Newtonian fluids.

As an approximation to this complex behavior, constitutive models and equations are used, typically involving a combination of elastic springs and viscous dashpots in parallel and series configuration in order to mimic the response of the viscoelastic material. While constitutive equations based on arrays of springs and dashpots are purely top-down approaches without taking molecular details into consideration, they are still useful to describe viscoelastic materials to a certain extent. In addition, there are also bottom-up models like the worm-like or glassy

worm-like chain were developed to elucidate the molecular origins of material properties of biopolymers [45,46]. A more thoroughly background on rheological properties of cells is provided in chapter 5.3 of Kubitschke et al. 2018 [22] and chapter 2.3 and 2.4 [47].

2.2 Optical Stretcher

The mechanical strain response of cells to external force stimuli can be classified in general as viscoelastic and as active or passive depending on time scale. Cellular mechanics are of importance in various cell functions, such as cell migration, adhesion and (force) polarization. Many different tools are used to characterize the rheological properties of cell, i.e. a summary is given in Kubitschke et al. 2018 [22], and provided insights into the role of cell and nuclear mechanics is key attributes in various diseases, such as inflammation, cardiovascular diseases and predominantly cancers [48–51]. Peculiarly, the provided values of rheological parameters in literature, such as elastic modulus and viscosity of cells, vary by two to three orders of magnitude for the same cell type with various measurement devices [34]. The major factor for these broad variations is vast differences in general cell culture conditions. While some parameters can easily be controlled, such as temperature, passage number, pH value, cell medium composition, other factors, such as substrate-cell interactions and cell-cell interactions, are not in direct control. Cells are mechanosensitive and adapt their cytoskeletal composition and mechanical properties to their microenvironment. This leaves a large source of mechanical cell properties uncontrolled and therefore unspecified.

In order to circumvent the influence of the microenvironment onto cells, a well-controlled, isotropic and/or homogeneous microenvironment should ideally be provided. Suspending cells in culture medium for biomechanical measurements is thus a viable strategy because its highly reproducible and interactions of cells with

their environment are reduced to a minimum. Therefore, the "ground state" of the mechanical properties of cells without microenvironmental alterations can be measured. Furthermore, biological cells show a broad distribution of mechanical parameter values [22,23,34,38] and thus a technique with high throughput is also favorable in order to achieve proper statistics.

Two devices capable of contact-free biomechanical measurements and sufficiently high throughput are the optical stretcher [52] and the real-time deformability cytometry [53,54] where cells are stored in suspension and subsequently are stretched via laser light or hydrodynamic forces, respectively. The lab of Prof. Käs is providing a state-of-the-art optical stretcher, thus, the mechanical response of different biofilaments of the cytoskeleton can be efficiently probed with high statistical resolution.

The properties and characteristics of the cytoskeleton provide insights for cellular functions such as cell motility and ability to migrate, which is the key ingredient in cancer cell metastasis. When cells migrate through their environment, the cytoskeleton is under considerable mechanical stress and strain and various cytoskeletal components provide different functions. In this thesis, I used the optical stretcher to differentially dissect the individual mechanical contribution of the actin and microtubule network towards cell mechanics and concluded that both cytoskeletal networks are differentially responsible for the cell's deformability and strain relaxation for small and large strain regimes[23]. In the forthcoming section I will introduce the functional principle of the optical stretcher which provides is the foundation for Kubitschke et al. 2017 [23] as part of this thesis.

The earliest detection of optical scattering and gradient forces on micron sized particles dates back nearly half a century ago in 1970 by Athur Ashkin [55] who developed subsequently the first optical trap, the optical tweezer, in 1986 [56], for whom he got awarded the Nobel prize in physics in 2018.

The optical stretcher invented by Jochen Guck and Josef Käs [48,52,57] is a divergent dual-beam optical trap with two coaxial, anti-parallel aligned laser fibers. Like for optical tweezers, its working principle is based on momentum transfer at the interface of dielectric objects, usually biological cells, for applying forces. In short, the

momentum transfer is created due to the change of the refractive index at the interface and the change in momentum of the photons. As the total momentum of the system is conserved, a counteracting momentum at the surface is induced. In contrast to the optical tweezer, where dielectrics are only trapped by the optical gradient forces, the optical stretcher is also capable to deform dielectrics via the strong photon momentum transfer.

The optical stretcher setup comprises a microfluidic flow chamber with quadratic profile perpendicular to the laser axis for delivery of suspended cells to be stretched. The setup was used on an inverted phase-contrast microscope and the cells during stretch were captured by a CMOS camera at 30 frames per second. The set-up and cell reservoir are cooled to 18 °C during the whole measurement. The stretching process is controlled by a custom-made LabVIEW program and the image series of the cells were evaluated by a custom-made edge detection algorithm in MATLAB. The detailed components of the automated microfluidic stretcher are given in the methods section of [58] and additional upgrades/changes are described in my publication Kubitschke et al. 2017 [23].

The applied stretching force is linear proportional to the laser power and was chosen to be a step-stress profile. Therefore, the setup is designed such that the creep compliance of biological cells is measured. In detail, the cells were initially trapped with 100 mW for one second, stretched for 2 seconds at 750 or 1200 mW, corresponding to stress regime of several Pascals, and trapped at 100 mW for cell relaxation. The whole cell acquisition, trapping and stretching is fully automated allowing to measure up to 300 cells per hour. Typical deformation-response curves to applied step stresses are provided in *Figure 5.4* of Kubitschke et al. 2018 [22] and *Figure 1a* and *1d* of Kubitschke et al. 2017 [23].

While the precise force calculations of cells within the dual-beam trap was done with generalized Lorenz-Mie theory of scattering [59–62], a simplified geometrical ray optics approach for force calculation [52,57] is often sufficient assuming that the cells are much larger than the incident wavelength [62]. The ray optics calculation of [52,57] is best suited to illustrate the working principle of the optical stretcher and will be sketched in the following section.

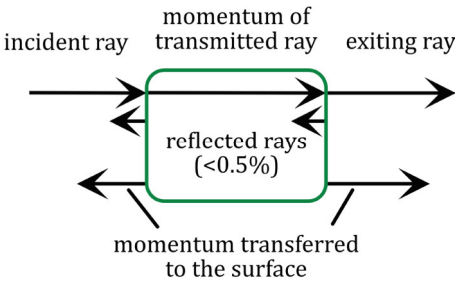

Figure 2.1: Schematic photon momentum transfer on an interface of an idealized cell. Cells have slightly higher refractive index than the surrounding medium (typically cell culture medium with refractive index of water). Illustration adopted from [52]. Copyright © 2001 Elsevier, license number 4700731196957.

In a one-dimensional case along the laser axes, the dielectric can be considered as two plane surfaces, i.e. a square, see illustration *Figure 2.1*. An incident ray of light is carrying the energy of a photon. The momentum of the photon is given via Einstein's energy-momentum relation of the Four-momentum:

$$E = cp = \frac{c_0}{n} p \,,$$

with the energy of a photon E, the momentum of the photon p, the speed of light in the medium c, the speed of light in vacuum c_0 and the refractive index of the medium n. The total momentum is conserved, therefore, when a photon traverses an interface of different refractive indices the momentum of the photon increases and induces a counter-acting momentum transfer onto the interface. A surpassing laser beam through a cell induces consequentially a force on the front and an antiparallel force on the back side of a biological cell, thus, the cell is getting stretched.

2.3 Cell Motility

Despite that organisms are to a large extend structurally stable and the largest fraction of cells are set in their particular place and do not migrate and perambulate through the organism, cell motility plays a crucial role in various processes, predominantly during embryogenesis,

wound healing and immune response. All processes of cell motility are highly regulated and controlled in organisms. There are, however, also instances where the ability to crawl through tissues are misused, particular in diseases such as cancer invasion and metastasis. In order to migrate through dense extra-cellular matrix crowded with obstacles, cells must continuously generate forces and consume energy to push themselves forward. Microscopic objects like cells live in a regime of low Reynolds number and thus cannot rely on their inertia to propagate [63,64]. Cell migration of healthy cells is often directed by environmental factors such as chemical gradients (chemo- and haptotaxic) which are sensed via specialized transmembrane receptors [65] and mechanical stimuli (mechano- and durotaxis) which is probed by cellular protrusions and protrusive forces [66].

In contrast, the ability of cancer cells to migrate and to form colonies far from the primary solid tumor – the ability to metastasize – is in essence a severe diagnosis in clinical practice as this is often fatal for a patient [10]. The ingredients for metastasizing are (I) the general capability of cancer cell to migrate, i.e. leaving the primary tumor and subsequentially crawling through healthy tissue, and (II) the ability to overcome boundaries and hinderances of migration, i.e. basal membranes, endothelium and inter-tissue fascial boundaries. In this subsection, I will elucidate different forms of migration which are observed in mammalian cells in various circumstances to fulfil certain specialized tasks which are often adopted and misused in cancer cell migration and ultimately metastasis formation.

The herein reviewed modes of cell migration are mainly textbook-like knowledge summarized in review articles by Condeelis [67,68], Wirtz [51,69], and Friedl et al. [70–72] if not stated otherwise. The role of migratory barriers, such as inter-tissue fascial structures, will be elaborated in subsequent subchapters.

Only a fraction of cell types is naturally able to migrate in given circumstances, such as embryonic cells in embryogenesis, epithelial cells in wound healing or immune cells for preying on pathogenic bacteria. These cells have different possible ways of locomotion with varying efficacy depending on the microenvironment. In many cases, eukaryotic cells use amoeboid motion, which is a crawling-like type of movement accomplished by protrusion of cytoplasm of the cell and is accompanied

by a dynamically changing cell morphology [73]. Amoeboid motion is a combination of crawling motion, characterized by expansion of the actin network at the cell front, and blebbing motion, where active network contractions causing formation of pressure-driven blebs [74]. An overview of various modes of migration is concluded in *Figure 2.2*.

The best studied type of motion is the crawling motion on flat substrates such as Petri dishes. The driving part is the actin network which undergoes directed growth by enhancing polymerization at the leading edge of the cell and thereby inducing polymerization forces inducing a flat protrusion at the leading edge coined lamellipodia. The lamellipodia is attached to the substrate via focal adhesions which provides sufficient traction for the cell. With help of the actin cytoskeleton, the back side of the cell contracts, pushing the cell slightly forward, and disengages adhesion sites. The surplus of filamentous actin on the back side is then depolymerized. This cyclic process is characterized by a myosin-driven treadmilling of actin, coined retrograde flow, where filamentous actin is transported from the leading edge to the back side of the cell and globular actin is transported to the leading edge. [75–78]

In blebbing motion, on the other hand, the force generation for locomotion is generated in a different way. The initial step is the creation of a bleb, which is a bulging of the cell membrane caused by detachment from the basal actin cortex [79–81]. The intracellular pressure driven by actin-myosin contraction and cortical tension afterwards expands the bleb by an inflow of cytosol [79,80]. As last step of this cycling process, actin polymerizes in the bleb, attaches to the cell membrane and reforms the actin-cortex. As there are no directed actin treadmilling required compared to crawling motion the blebbing motion is most suitable in structured 3D environments with obstacles enabling the cell to migrate reasonable fast through 3D matrices, such as the ECM, and micron sized pores [70,79,82,83].

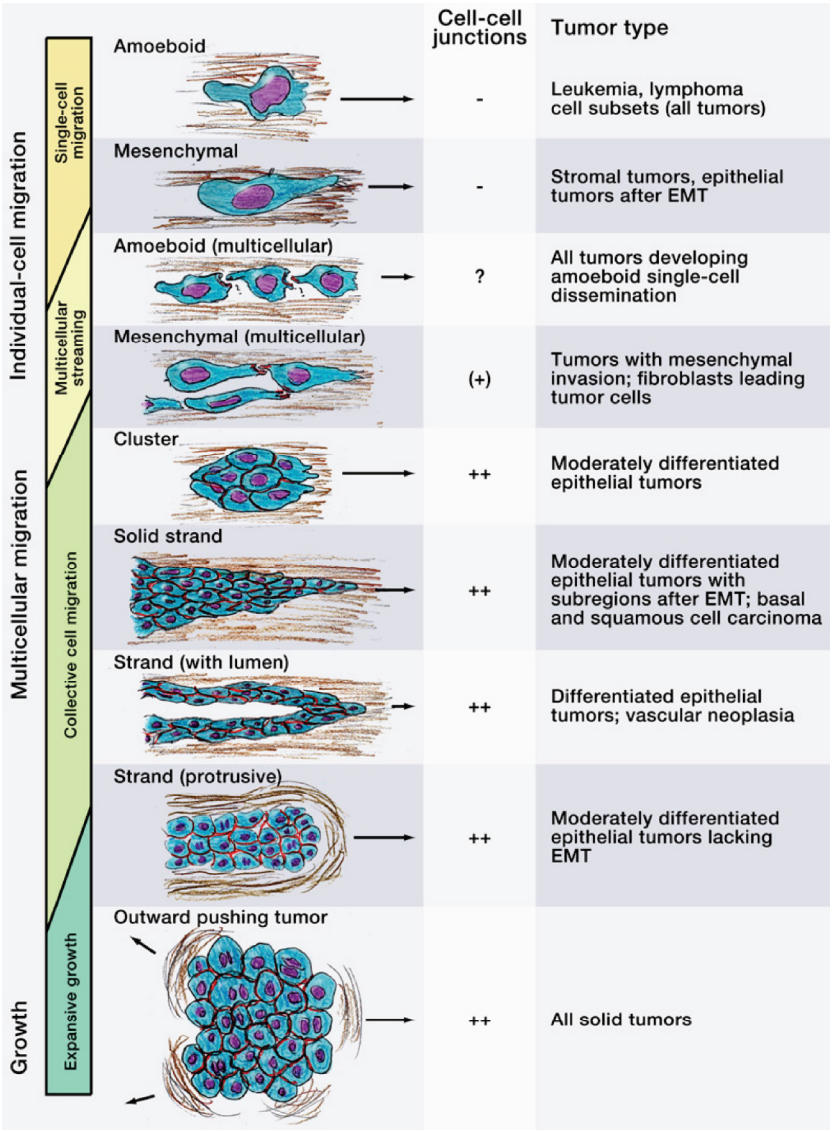

Figure 2.2: Modes of migration during cancer invasion ranked by quantity of involved cells in migration. Adopted from [72]. Copyright © 2011 Elsevier Inc. under license number 4691380641040.

In fact, blebbing motion is superior since it enables “squeezing” through smallest gaps in cell-filled ECMs often without the need to degrade the surrounding ECM [70,84]. The drawback is, however, that it demands a higher cellular deformability and restructuring and a subsequent restoration of the cytoskeleton. Moreover, the cell’s nucleus as the largest and most crucial organelle, requires temporal adaptation during squeezing through pores of smaller than the nucleus size [83,85,86].

A special type of amoeboid motion is the coined mesenchymal motion. The classification of mesenchymal motion by Friedl et al. 2011 [72] refers to large extend to the definition of the crawling motion in three dimensions. However, the mesenchymal cells form strong adhesive contacts with the microenvironment by focal attachments and migrate in a rather fibroblast-like fashion [87], whereas classical crawling motion only utilize weak adhesive and poorly localized contacts to the substrate.

The similarity of the former introduced modes of migration is also highlighted in the ability of cells to switch to different modes of migration. Especially cancer cells are recognized to efficiently shift between these migration modes, which is a crucial ability in order to form metastases [29,51,71,87]

Besides the introduced modes of migration for individual cells, an agglomeration of cells can interactively migrate as collective, cohesive multicellular unit [72,87]. Often, the previous properties of individual migration are partly conserved and the additional interaction and interconnectivity is achieved by promoting cell-cell junctions. Introducing multicellularity enables novel modes of migration for the cell agglomeration, such as formation of multicellular tubes and strands, or rather irregularly shaped clusters [72]. When cell-cell contacts of the cell cluster are not tight and individual cells may transiently form and resolve cell-cell contacts, the loosely connected cluster of cells can perform a mode of migration in between individual and collectively motion, commonly denoted as multicellular streaming [88,89], which is hypothesized as a major migration mode in tumor cells to surpass the endothelium and to intravasate [90–92].

The acto-myosin cytoskeleton is the cardinal component to enable cell motility as it is the main force carrier and transducer in locomotion. However, when moving through dense, cell-filled ECM the deformability and shape recovery are also of utmost importance. The priority of the acto-myosin complex is also often highlighted in this case in common literature and marginalizing the microtubule network and intermediate filaments. Although, not only the active processes, but also active and passive rheological properties of the cytoskeletal components are relevant. For instance, intermediate filaments are remarkable extensible without breaking enabling them to mechanical stabilize cells by strain-hardening and enabling mechanotransduction [30,93–99], and

microtubules are able to regulate the dynamics of actin and cell migration [100–104] and provide the rigid backbone to oppose contractile forces allowing cells to extend and retract their leading edge [105,106]. As part of this thesis, I will elucidate and deepen the understanding of the specific contributions of actin filaments and microtubules towards the mechanical stability in cells for small and large deformations and strain relaxation [23], which is the foundation for cell migration.

2.4 Concepts of Embryogenesis and Cancer Progression

The genesis of a large-scale mammalian organism from a single fertilized cell is a remarkably intricate process. Even more remarkable, it is also an incredible organized and accurate procedure. The precise spacial and temporal arrangement, rearrangement and differentiation of tissues is the indispensable process of ontogenesis, especially in embryogenesis. Without any doubt, molecular and genetic processes like signaling and genetic pathway regulations are of importance, however, physical principles also play a crucial role. For instance, differential adhesion strength of different cell types supporting demixing and segregation of differentiated cell types, thus enables the formation of specific tissue types and tissue compartments [107,108].

Cancer Progression, on the other hand, can be seen as a de-differentiation of cells thereby slowly losing functional specialization of the originating cell type and acquiring former silenced cell functions and processes [109–111]. The most prominent reacquired function of any cancer is the ability of limitless, uncontrolled cell proliferation. In any multicellular organism, and especially in highly functionalized such as mammals, cell proliferation is tightly controlled and predominantly found during embryogenesis and wound healing and is only occasionally re-activated in adult animals. The re-acquiring of certain embryogenic cell functions is a key characteristic in cancer progression [7,8,112,113].

Beyond cell proliferation are other dualities of embryogenesis and cancer progression which will be elucidated in the following subchapters. Therein, I will focus on tissue compartment formation and cell type segregation, which will form natural growth and migration boundaries for cells and therefore also for cancer cells to a certain extent. Identification of growth boundaries for cancers may provide great treatment possibilities for surgical resection of primary tumors and their associated invaded tissue compartments, decreasing recurrence rates and therefore increasing patient survival rate and decreasing surgery-related morbidity.

2.4.1 Cell Differentiation and Morphogenesis

The origin and development of shapes animals and animal body parts provides a vast variation in forms and patterning. While certain patterns like striped or speckled fur are directly visible and their function are often directly recognized, i.e. camouflage or herd recognition, most pattern formations are happening unseen during animal development in order to form specialized tissues, body parts and organs. In fact, stable pattern formation, symmetry breaking and polarization is an essential attribute from the very beginning of embryogenesis throughout maturation of all known metazoans [114–116]. These developmental process for the generation of form and shape, and therefore tissue organization is summarized as morphogenesis. Alongside cell differentiation and regulation of timing, patterning and morphogenesis build up the four key intertwined classes of crucial developmental processes.

D'Arcy Wentworth Thompson with his book *On Growth and Form* published in 1917 [117] can be regarded as the pioneer of mathematical-quantitative analysis of the morphogenesis of animal organisms and as one of the first biomathematicians. He showed that many body forms can be explained as changes in the shape of a coordinate network, which is laid over the organism, and that often quite simple growth allometries are effective in explaining the transition from one form to another. Today, these can be interpreted as the expression of developmental

genes of different expression strengths along a gradient of a molecular trigger molecules, commonly coined morphogens.

The terminology of *morphogens* was introduced more than three decades later by Alan Turing in his pioneering work *The Chemical Basis of Morphogenesis* in 1952 [118] where a chemical mechanism based on reaction-diffusion equations of proposed morphogens is described which gives rise for biological pattern formation out of a homogeneous, uniform state. In fact, Turing already proposed that mechanical motions and forces, and spatial-temporal chemical reactions should be tightly intertwined in pattern formation. Due to the mathematical complexity of mechanical and chemical coupling, he limited his proposed theory to chemical reactions and diffusion[118]. Since then (non-linear) reaction–diffusion theory of morphogenesis, has served as a fundamental model in theoretical biology, especially embryogenesis [119], decades before the formation of so-called Turing-patterns were experimentally rigorously demonstrated [120].

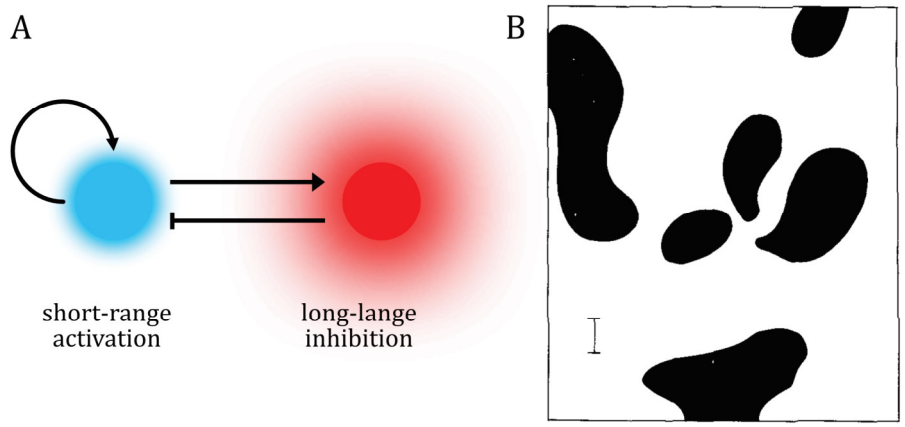

Figure 2.3: Alan Turing's chemical interaction scheme of Morphogenesis. Figure (A) displays the first proposed regulatory interaction network of two diffusing morphogens (activator in blue, inhibitor in red) by Alan Turing. The activating morphogen (blue) auto-catalytically promotes locally the production and increase of both morphogens. The inhibitory morphogen (red) inhibits the former morphogen and has a high diffusibility, thus the inhibitory morphogen has a long-ranged inhibitory effect. Figure (B) illustrates the original published "dappled" pattern of the presented interaction network in two dimensions from *The Chemical Basis of Morphogenesis* [118]. Copyright © 1990 Springer Nature, license number 4698240535575.

The general form of Turing's initial proposed system of two interacting morphogens (or chemicals in general) is given by two differential equations:

$$\frac{\partial c_1}{\partial t} = D_1 \nabla^2 c_1 + \gamma R_1(c_1, c_2)\,,$$
$$\frac{\partial c_2}{\partial t} = D_2 \nabla^2 c_2 + \gamma R_2(c_1, c_2)\,,$$

with the two chemicals denoted as i (usually one activator and one inhibitor), chemical concentrations c_i with diffusion constants D_i and the chemical interaction terms R_i and the strength of the interaction γ. The central feature of this set of reaction-diffusion system is, that with rather simple reaction terms the two chemicals can transform an initial unpatterned, time-dependent system into a spatial patterned, quasi time-independent system. The peculiar concept of Turing instability is to consider a spatially homogeneous, linearly stable system, which is unstable in the inhomogeneous case, if diffusion is described by suitably chosen diffusion coefficients, which is coined *diffusion-driven instability*. This concept was novel, since diffusion is generally regarded as a stabilizing factor in the field of partial differential equations.

As illustrated in *Figure 2.3*, Turing's first proposed reaction-diffusion system of morphogens is based on the inhibitor which diffuses faster than the activator. At the beginning, locations with high activator concentration, often coincide with higher inhibitor concentrations. However, this does not lead to the disappearance of the activator substance, as the inhibitor quickly evaporates due to the rapid diffusion.

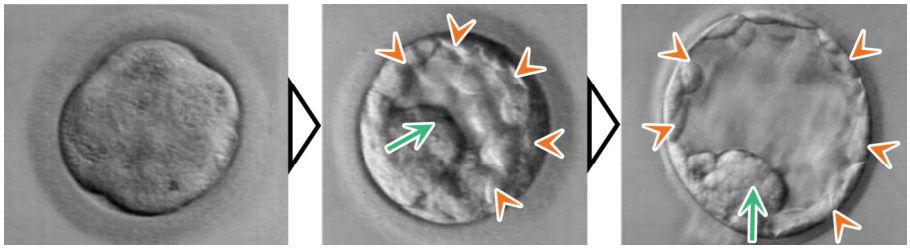

Figure 2.4: Human development *in vitro* is depicted from a compacted morula (left) to the early blastocyst (middle) to the hatched blastocyst (right) with trophoblast (orange arrowheads) and inner cell mass (green arrow). Adopted from *Larsen's Human Embryology*, Copyright © 2016 Springer Nature [121].

Turing's proposed regulatory mechanism in *The Chemical Basis of Morphogenesis* found wide-spread applications in theoretical biology and is not limited to fur patterning. Furthermore, regulatory interaction networks like given in *Figure 2.3* are now basic concepts of protein, gene and pathway interactions. In embryogenesis, cell differentiation and tissue formation are driven by interacting morphogens, such as

transcription factors *Bicoid* and *Hunchback*, or growth factors like *Wingless*, *Hedgehog* and *TGF-β*. In fact, for many morphogenetic steps in the early embryo the interacting morphogens are identified. For instance, cells of the morula differentiate into cells which will later form the *inner cell mass* (ICM) or the *trophectoderm* (TE) of the primordial embryo, depicted in *Figure 2.4*. This cell differentiation is founded on auto-catalytic and inhibitory interactions of *Oct4* and *Cdx2* such that *Oct4* is expressed in the ICM and *Cdx2* is expressed in the TE, as illustrated in *Figure 2.5*.

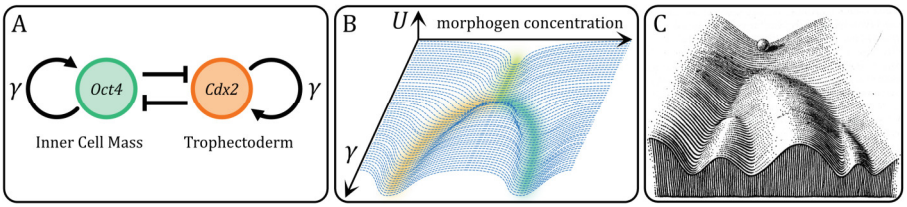

Figure 2.5: Working Principles of regulatory networks. (A) The bi-stable regulatory network deciding cell fate of the morula's cells towards ICM (Oct4, green) or Trophectoderm (Cdx2, orange) when the self-amplification parameter γ is increased. (B) Quasi-energy landscape of the bi-stable switch. For low self-amplification γ of the morphogens (yellow branch), both morphogens are coexpressed. When γ reaches a critical value, the former stable branch bifurcates into a state with high *Oct4* and low *Cdx2* expression (green branch) and high *Cdx2* and low *Oct4* expression (orange branch). (C) Waddington's classical mechanical interpretation on cell fate determination. The landscape is shaped by interacting genes. A cell (represented as a pebble) perambulates along the bifurcating valleys and reaching one of the final valleys. Waddington's epigenetic landscape in (C) is adopted from [122].

One advantage of the regulatory network formalism is that they can be constructed independent from the exact knowledge of the underlying, quantitative partial differential equation, but possible discrete, stable states can still be determined even for larger networks. From that formalism quasi-energy landscapes can be derived for simple networks [123,124], such as for the bi-stable switch of *Oct4* and *Cdx2* shown in *Figure 2.5 A* and *B*. Historically, the classical interpretation of cell fate determination as a rolling pebble in a bifurcation landscape, *Figure 2.5C*, was already proposed a few years after Turing's seminal paper on morphogenesis by Conrad Hal Waddington in his work on *The Strategy of the Genes* in 1957 [122]. However, for non-equilibrium, non-gradient systems such as large genetic networks, it is not directly possible to obtain a strict potential function without ad hoc amendments and assumptions [125]. Details about the representation as quasi-energy

landscapes were worked on in the following decades after the two seminal works of Turing and Waddington. Further discussion of epigenetic landscapes is included in chapter *Link between Cancer Progression and Embryogenesis*.

After the discovery of intracellular constituents such as cytoskeletal filaments and motor proteins, and active transport, it became apparent that the link between mechanical and chemical cues of morphogenesis is crucial in pattern formation on tissue level and development [126]. Active transport of morphogens and mechanical forces when connected to chemical interactions can provide patterning length scale more intricated than simple diffusion processes [119,126,127]. Ultimately, developing embryos do not only undergo cell differentiation steps based on morphogens and gradients but also cell type segregation and mechanical alterations such as tissue folding events inducing topological changes of the organism and subsequent formation of compartments, which is content of the subsequent chapter.

2.4.2 Compartmentalization and Segregation

The segregation of cell types and formation of tissues, known as compartmentalization, is a pivotal step in the development of the internal and external morphology of an organism and is accomplished in parallel to cell differentiation from the beginning of embryogenesis [128] Cells differentiation is usually initialized by morphogenetic signaling molecules, named morphogens, forming a morphogenetic gradient and cells adopting their phenotype according to the sensed morphogen concentration by activating or deactivating certain selector genes [129–131]. Often, morphogens cause a cascade of cellular reactions and adaptions in form of epigenetic regulations, such as cell polarity, cell-cell adhesion, cell-ECM adhesion, ECM degradation and cytoskeletal rearrangements. Furthermore, complex morphogenesis may be understood as an emergent property of local cell interactions guided by cell-cell interaction and cooperation, chemical and bioelectrical signals, and physical cues such as pressure and tension [113].

These morphogens can be understood as epigenetic regulators which can trigger fundamental processes like the epithelial-

mesenchymal transition (EMT), where previous polarized, immotibe epithelial cells acquire migratory and invasive properties that enables these cells to extend filopodia, migrate through ECM and pass other cells, and thus becoming mesenchymal cells [51,132–134]. This transition from an immobile to mobile phenotype and its inverse process – mesenchymal-epithelial transition (MET) – are vital during embryogenesis and wound healing, where cells have to coordinately re-localize, and is also a re-acquired function of cancer cells in order to form initial solid tumors, invade other tissues and ultimately metastasize to distant sides [135–137].

When an initial tissue is composed of cells with different phenotype, these different cells often spontaneously de-mix and segregate. It was shown in numerous publications that different cells of all early steps of embryogenesis de-mixing based on physical principles of differences in the cell-cell adhesiveness [107,108,138,139], following the exact same principle of de-mixing of an oil-water mixture where the segregation of oil and water is a consequence of differences in the attractive forces and energy minimization of the liquid-liquid interface. As result, cells with same phenotype have the affinity to colocalize resulting in a complete segregation of the different phenotypes based on physics-driven principles.

The formation of two localized tissues of different cell types gives rise to initial meta-compartments, or morphogenetic fields, where cells are still able to transgress from one meta-compartment to another but changing thereby their phenotypic fate. The formed meta-compartments are afterwards solidified by short-ranged signaling induced border cells [140], which in turn coordinate the growth and fate of the tissue via long-range signaling [131,141]. After this initial morphogenetic imprinting, the cells express compartment-specific selector genes thereby regulating the fate of the compartments [128,142,143] and the compartments will not directly interact and influence anymore [129,144]. The compartments are now rendered predominantly self-sufficient with well-defined lineage boundaries and can be treated as developmental sub-systems [131,145] which often sub-divide in further sub-compartments during development leading to a whole morphogenetic differentiation tree, also called ontogenetic tree, of differentiating cells and compartments [142]. This type of modularization and standardization is reflected in the responsible genes for

compartmentalization. The so-called homeobox genes are the gene family responsible for gene expression regulation and control of processes of morphogenesis and cell differentiation, particular the *Hox* genes for orchestrating compartmentalization [112,128,146]. The *Hox* genes also display an astonishing functional and phylogenetically conservation across Metazoans in compartment development [147], for instance, replacing a certain *Hox* gene of *drosophila* by its analog *Hox* gene of chicken results in to a certain extent functioning flies [148] despite that their most recent common ancestor lived over half a billion years ago [149].

After embryogenesis, initial differentiation steps of compartment and organ formation are concluded and the organism enters fetogenesis where the further development of the organs and differentiation of tissues takes place. It should be noted that the definition of organs and compartments differs substantially. As illustrated in the previous section, compartments are developmental sub-units derived from their primordial tissue or lineage caused be morphogenetic differentiation. Organs, however, are classified as functional (sub)-units of an organism since they fulfil a limited and specialized task. While the ultimate fate of differentiating cells during compartmentalization are the formation of highly specified tissues with well-defined functional roles, it does not conclude that the final structure will be a certain single organ. In essence, there is an assured correlation between ontogenetic compartments and organs, however, both classifications can be distinguished and can display considerable differences. In particular, many organs, such as the bladder, are structurally supported by fatty connective tissue, which itself can be considered an endocrine organ [150]. However, these two functional distinct structures, or organs, arose from the same primordial compartment (bladder compartment). In general, tissues can be tracked back to their embryological defined primordial compartments of origin [151], which for instance has been done in meticulous detail for the female urogenital ducts for cervix [144,152–158] and vulva [158–162].

One peculiar aspect important for my work in Kubitschke et al. 2019 [27] – and possibly for future works – is the tissue composition of the compartments around the uterine cervix. All compartments arose from the primordial mesoderm during embryogenesis and the major compartments have multiple types, mainly fibrous connective tissue and muscular tissue, see *Figure 1* (anatomical maps of the female pelvis) of

Kubitschke et al. 2019 [27]. Functionally speaking, the fibrous connective tissue of all compartments of this region are of same nature, fulfil the same function and are not properly distinguishable in their physical properties. Engulfed in these connective tissues are the corresponding organs or functional units, e.g. cervix, bladder muscle, rectum muscle and ureter, which have different physical properties compared to fibrous connective tissues. These two points of view, the physical and the ontogenetic view, have different and partially opposing implications for tumor growth and infiltration. The detailed implications are outlined in chapter *Initial Steps in Tumor Formation and Progression* and *Link between Cancer Progression and Embryogenesis*.

2.4.3 Physical Characteristics of Hallmarks of Cancer

The vast complexity of cancer is displayed by its origin of often seemingly random genetic and epigenetic alterations and hence the characterization of over 200 different forms of cancer with varying genetic profiling and therapeutic strategies [163]. Consequently, cancer is considered a collection of diseases with common schemes of the ability of cancer cells to invade adjacent tissues and often forming metastases in far regions of the organism [38].

However, most forms of cancer progress and ultimately be fatal in the same way, which is in contrast to the broad range of genotype variations found in cancers. Cancer is in general considered a systemic disease [164–168]. These apparent similarities give rise for coarse-grained view on cancer based on emergent properties than the molecular view based on genetic defects and alterations. On one hand, the biological details can be generalized leading to the *Hallmarks of Cancer*, common schemes in cancer development found in virtually all cancers. On the other hand, the common schemes are results from underlying functional principles and many of them have a physical interpretation. While certain cancers can be pinpointed to certain genetic defects and can be treated accordingly, the vast majority cannot be efficiently treated on the genetic level. Thus, especially the physical point of view is treatment relevant in the general case and many treatment options are of this origin. For instance, most chemotherapies are based on disrupting cell

division processes. As cancer cells are dividing much more rapidly than healthy tissue cells, cancer cells are therefore indirectly more affected by chemotherapeutics. In addition, most cancer related deaths are caused by metastases and the best treatment option against the formation of metastases is physically removing the primary tumor and preventing cancer cells to migrate and cross tissue barriers in the body. While therapeutic agents are acting on the molecular level, the desired effect is of purely physical nature. Therefore, the characterization of cancers based on physical and genetic properties is valid.

Cancers are categorized by their tissue where they originate from, for instance, the most common type of cancers, carcinomas, arise from epithelial cells. Precancerous stages of tumors do not spread into surrounding tissues and are considered to be benign tumors. In essence, cancers can arise from every tissue, however, the incidence rate is strongly dependent on age and other risk factors, such as tobacco (lung cancer) and extended UV light exposure (skin cancer) [169].

The common theme in cancers are genetic mutations and alterations and is thus in the focus of large parts of the scientific community. The DNA of an average mammalian cell gets damaged in various ways, for example by the action of reactive oxygen species or ionic radiation with the resulting damage ranging from single nucleotide mutations to whole DNA double-strand breaks, with a total of over 100,000 damages per day [170]. As countermeasure to the permanent degradation of the cell's most vital functional unit, many cellular safety features are at work to prevent and/or repair damages whenever possible [refs]. The DNA repair mechanisms are unfortunately inherently limited, and all cells and organisms, given enough time, will suffer from the burden of damaged DNA. Fortunately, most genetic mutations have a negative impact on the survivability of the affected cells, thus critical mutations are often accompanied by a timely death of the cell. However, some mutations can persist and proliferate and eventually can lead to cancer. The mutation rate for cancer is strongly dependent on the genomic region [171] and is increasing under further genetic instability [8,172,173]. On the epigenetic level, the mutagenic rates are estimated to be an order of magnitude higher than the genetic layer [174] and is considered to be a major driver for cancer development [123,175,176].

Consecutively, a database project to detect and catalogize common genetic mutations in cancers using whole genome sequencing [163] was

initiated by the National Cancer Institute and the National Institute of Health in 2005, known as *The Cancer Genome Atlas* (TCGA). It is undisputed that the genetic layer of cancer is crucial, for it is the origin of cancer, however, the outcome of cancer diagnosis, treatment and prevention of the TCGA project was, at best, conservative measured by the investments taken [177]. The main reasons are, first, once cancer progression is initiated be genetic defects, cancer evolves towards a systemic disease and progresses even without further major genetic alterations, for instance, subtle epigenetic changes, microenvironment interactions, inflammation and changes of the gene regulatory network [158,164–168,175,176,178–182]. Secondly, even within a single tumor there is intratumor phenotypic and genotypic heterogeneity [183–186] and it is reasonable that cancer cells of one tumor display also physical heterogeneity, and thus functional heterogeneity, such as physical properties [38,42,48,187].

The bottom line of this initial project is that the diversity of genes involved in cancer progression is so cardinal that drug targeting single genes is effectively futile in predominant number of cases [188] and voices emerged to discard the paradigm of cancer genetics and move towards cancer as an epigenetic tissue-level disease [189]. Consequential, with ongoing development of genome sequencing techniques, especially next generation single cell RNA sequencing, the epigenetic layer of tissues and cancer steadily unveils. For instance, the Genotype-Tissue Expression project (GTEx) established a data base of genetic variation and gene expression in multiple human tissues from over 50 different sites of the body, e.g. brain, skin, colon, breast, to unravel the epigenetic differences in tissues and to elucidate the genetic basis of common disease [190].

In an attempt to unify the structure and process of cancer development from a biological point of view, Hanahan and Weinberg have mapped out and proposed six fundamental and four subsequent “Hallmarks of Cancer” [7,8]:

- Self-sufficiency in growth signals,
- Insensitivity to anti-growth signals,
- Evading apoptosis,
- limitless replicative potential,
- Sustained angiogenesis,

- Tissue invasion and metastasis,
- Deregulated metabolism,
- Evading the immune system,
- Genome instability,
- Inflammation.

These hallmarks are of more descriptive nature and while they stem from a biologist's point of view, they should universal translate to other scientific domains, like physical and mathematic sciences. As example, if a cell becomes independent of external growth signals, then modelling cell growth becomes independent from modelling promoter and inhibitor distribution, see chapter *Cancer Growth Modelling*. Thus, *self-sufficiency in growth signals* and *insensitivity to anti-growth signals* can be straight-forwardly interpreted as a de-coupling of a set of previously coupled partial differential equations (cPDEs), e.g.

$$\frac{\partial n_c}{\partial t} = D_c \nabla^2 n_c + R_c(n_c, n_n)$$
$$\frac{\partial n_n}{\partial t} = D_n \nabla^2 n_n + R_n(n_n, n_c) \,,$$

were n_i are two cell population densities of a given tissue– presumably pre-cancerous indicated with c and normal cells with n – with corresponding diffusive motility constant D_i and coupling term R_i describing the growth rates of both cell populations and interaction. Healthy cells in tissue are subject to contact inhibition preventing uncontrollable cell growth which can be captured in the interaction term, i.e. for high cell density the growth term approaches zero. Loss of described interaction, thus being *self-sufficient in growth signals* and *insensitive to anti-growth signals*, is then equivalent to the coupling term R_c losing its dependency on n_n. Therefore, cancerous cell growth and promoter and inhibitor distribution rendering tumor progression less reliant to external factors, as seen in interaction terms in above PDEs, as they are. In fact, all hallmarks can be precise translated to a biophysical description [21,51,179] and generally categorized as elements of tumor growth, neoplasm transformation or transformation of cancer cell towards aggressive and metastatic sub types [21].

While the descriptive character of the Hallmarks of Cancer is regarded as valid, the detailed biological foundation is challenged as original data and the rationale of the underlying somatic mutation theory

is not consistent [158,189]. For instance, the first five hallmarks also hold true for benign tumors and solely the ability to invade and metastasize is reserved for malignant cells [191]. More elaborate, cell proliferation can be argued to be the "default state" in the light of evolutionary theory and is a necessity in embryogenesis and a requirement for life and adult cells entering quiescence is an artificial/cooperative state of rest. From the same perspective, cell motility can also be considered as a default state, again, a necessity in embryogenesis and a requirement for life. To no surprise, cancer has been hypothesized by others as a state of primitive metazoan life of loosely interacting colonies of poorly differentiated cells [192,193]. Therefore, cancer is not *per se* gaining certain new traits and functions but is re-acquiring already available.

Nonetheless, cancer research's primarily focus lies on molecular and genetic ground unison with the Hallmarks of Cancer as the biological basis of the disease [189,194]. Furthermore, the central dogma of cancer being a Neo-Darwinian genetic process still stands despite that there is extended experimental and clinical data inconsistent with such theory, e.g. somatic mutations specifically associated for metastatic process still cannot be provided today [195,196], despite that this is a crucial hallmark which separates benign and malignant tumors. From a biophysical point of view, malignant progression and metastasis formation undoubtfully requires various biomechanical changes of at least a certain fraction of cells of the tumor and its microenvironment. For tumors to grow in a densely packed environment, the cancer cells have to be able to withstand and proliferate under higher homeostatic pressure than the surrounding normal cells [39–41]. Metastasis formation can only occur when cancer cells harbor the ability to migrate and overcome obstacles such as interfacial tissue boundaries. Thus, changes in the mechanical properties (cancer) cells, changes in restructuring and stiffening of the physical microenvironment are essential for cancer progression [21,38,179,197–199].

The clinical relevance of these hallmarks lies within the staging systematics of cancers. Many forms of cancers have meticulous staging parameters dependent on tumor size, shape, graininess of tumor boundary and infiltrated tissues and lymphatic system, For instance for cervical cancers, the staging of the *Fédération Internationale de Gynécologie et d'Obstétrique* (FIGO) discriminates five stages ascending in severity from carcinoma *in situ*, confined to the organ of origin,

invasion of surrounding organs or tissue, spread to distant nodes, to tissue within the pelvis and distant metastases. However, despite the metastasizing stage of cancer, the distinct hallmarks are not directly transferred to cancer stages, but the physical characteristics of mainly tumor growth, neoplasm formation and transformation of tumor cells. While the hallmarks are generalizing principles, they are not sufficiently adaptable to treatment-related clinical practice, but the purely physical interpretations are. Furthermore, the hallmarks do not provide a concrete treatment strategy except that the metastatic stage is of least treatment success, whereas tumor growth characteristics does, such as provided in Kubitschke et al. 2019 [27].

2.4.4 Initial Steps in Tumor Formation and Progression

Tumor growth, progression and evolution is a systemic disease with malignant transformations on different time and length scales. On the smallest length scale, the microscopic sub-cellular domain, cancer development is rooted to alterations in gene expression, exchange and conversion of nutrients, receptor (in-)activity and regulation of cellular functions, such as cell division, migration and cell-cell signaling. The initiation of carcinogenesis and the appearance of first pre-malignant cells is accompanied with genetic defects and alterations.

Nonetheless, genetic defects and alterations leading to limitless replicative potential, insensitivity to growth inhibitory signals from its environment and self-sufficiency in growth signals are the initial and crucial steps for (pre)cancerous cells to emerge [191]. These genetic defects of the microscopical layer lead to abnormal and excessive cell growth forming a carcinoma *in situ* in case of cancers of epithelial origin. This neoplasia is usually characterized by a comparable slow, tissue displacing growth dynamics which is well differentiated and separated from the surrounding normal tissue. Already in this stage the microscopic, genetic details are coarse-grained to certain cellular and tissue functions describing carcinogenesis and tumor progression, such as the Hallmarks of Cancer [7,8]. A neoplasia which is confined to the epithelial layer is considered benign since the crucial malignant property of tissue invasion and metastasis is not acquired.

The transition from a benign tumor towards a malignant tumor involves further cellular and tissue level changes. For the initial formation of most primary malignant tumor from epithelial origin, precancerous cells (former differentiated epithelial cells) of the benign tumor have to transgress the basal membrane of the epithelium and embed into the underlying tissue. In most cases, some precancerous cells separate from the benign tumor by undergoing a transition from a non-motile to a motile phenotype and steadily losing cell-cell connections, such as adherens junctions and desmosomes, and thereby losing the organized dense cell-layer structure and apical-basal polarity. The cells down-regulate their cell-cell contact, prominently E-cadherins [51], and ultimately separate by changing to a motile mesenchymal phenotype enabling them to penetrate the basal membrane and intrude the underlying tissue. This process is commonly denoted as epithelial-mesenchymal transition (EMT) [51,132–134,200–202] and is a crucial process in embryogenesis for the formation and transformation of embryogenic tissues and wound healing. In fact, EMT and its reverse transition, mesenchymal-epithelial transition (MET), are non-linear multidimensional process regulating and being regulated by cell motility, cell polarity, cell-cell adhesion and interaction with the microenvironment [202], which gives rise to intermediate and hybrid states of epithelial and mesenchymal phenotype [203–208]. These processes are accompanied with drastic changes of biomechanical properties. The concept of EMT and MET as binary processes and states is therefore challenged [202]. The second path for benign tumor cells to break through the basal membrane is not by individualizing and adopting a mesenchymal phenotype, but by mode of collective motion [72].

Malignant transformed tumors, however, are not necessarily bound to single modes of migration, and therefore tissue invasion, but can re-activate and misuse all of the aforementioned modes of migration leading to an elevated adaptability of cancer cells to their microenvironment and invasiveness. Nonetheless, the common adopted mode of migration to transgress the basal membrane is via (collective) epithelial-mesenchymal transition. Peculiarly, other tissue interfaces, such as interfaces of tissues of different embryogenic origin, are structurally very similar to the basal membrane and are built up by collagen fiber networks [209], but are often not consecutively

transgressed in many cases of cervical cancers despite that the tumor cells initially have the migratory ability, as shown in Kubitschke et al. 2019 [27]. Therefore, it can be hypothesized that switching of migration modes, such as EMT and MET, are not utmost important considerations when facing tumor growth on locoregional scale. However, other migratory boundaries, such as ontogenetic linage boundaries of different compartments, are crucial parameters for identification of tumor growth inhibitory factors.

Once the underlying tissue got invaded by malignant cells, these cells may re-differentiate back to epithelial phenotype and a primary malignant tumor emerges [200]. With the appearance of the first neoplasia the physical characteristics of cancer and physical properties on tissue level are emerging, thus they are emergent properties which cannot directly be derived from the genetic defects alone, but integration of complex cell-cell interactions. The most prominent emergent properties are found in the properties of the tumor microenvironment with its restructured and stiffened extra-cellular matrix, chronic inflammation and cell recruitment [21,179,210–213]. Hereby, interactions between tumor cells and other cell types, e.g. endothelium, lymphocytes, adipocytes and macrophages, are in focus.

From a clinical perspective, in this stage of primary tumor formation and growth lies the greatest opportunity in increasing the treatment outcome for patients. The malignant transformed cells have reached a critical size to influence its surrounding tissue, alter the microenvironment and cause inflammation and therefore can cause symptoms and health issues in patients. Furthermore, the solid tumor often reached a size detectable by examination, palpation or medical imaging. In its non-metastatic stage, the survival rates after treatment are exceptional for many forms of cancer compared to metastatic stage which corresponds on average 66,7% of cancer related deaths and can be as high as 90% [10]. To no surprise, characterization of tumor progression in this stage is predominantly based on treatment options and outcome, thus size or direct extent of the primary tumor, degree of spread to regional lymph nodes, and presence of distant metastasis are key characteristics of the TNM Classification of Malignant Tumors. The characterization of tumor progression is not directly connected to certain genetic defects and alterations but described as function and ability of tumors and cancer cells to transgress and to migrate through

boundaries and other tissues. Thus, the crucial steps in tumor progression have a predominantly physical characteristic.

2.4.5 Link between Cancer Progression and Embryogenesis

Concepts of cancer initiation and progression have mostly been based on Darwinian assumptions [185,214–217]. In this context, cells are regarded as competitors for vital resources, e.g. oxygen and nutrients. High cell division rates in tumors are thought to generate large numbers of random mutations leading to a multitude of phenotypically diverse sub-clones. Thus, malignant progression is fueled by natural microenvironmental selection of the fittest tumor clone. This concept is coined as the *clonal evolution model*. It is assumed that mutagenic processes are generally non-purposeful and non-directional. Recurring phenotypic traits which are shared by many cancers are thought to represent the impact of selective forces [216]. The ability of cancer cells to develop resistance to chemotherapeutic drugs can also be explained by the acting selective pressure and the broad heterogeneity of cancer cells. However, the clonal evolutionary model only provides an explanation for the historic steps and is limited to the past but is not capable of providing any outlook into the future of cancer progression. Peculiarly, while the microscopic machinery of cancer progression is argued to be quasi-random mutations, the observable macroscopic cancer progression usually follows the same principles and actions summarized in the hallmarks of cancer.

Nonetheless, it is important to note that most phenotypic characteristics which are reminiscent of cancer cells and which are conveniently summarized as hallmarks of cancer [7,8] are shared by cells during embryonic development and can be brought about without a single mutation by epigenetically switching of the gene regulatory network [175,182], for instance, a simple overexpression of the unmutated *ras* gene can already lead to reactivation of mesenchymal-like features and thus leading to metastatic malignant phenotype [218]. In fact, it has been recognized for a long time that cancer cells exhibit embryonic features [219,220] and many known embryonic pathways, such *Notch*, *Hedgehog*, *Wnt*, *Hippo*, *TGF-β* and *FGF*s, are (re-)activated in

cancer and harbor therapeutic potential [221–223]. While somatic mutations certainly play an important role in the initiation phase of cancer development [195,224], malignant progression might rely less on mutations but depend more on the coordinated activation of transcriptional programs [175,182].

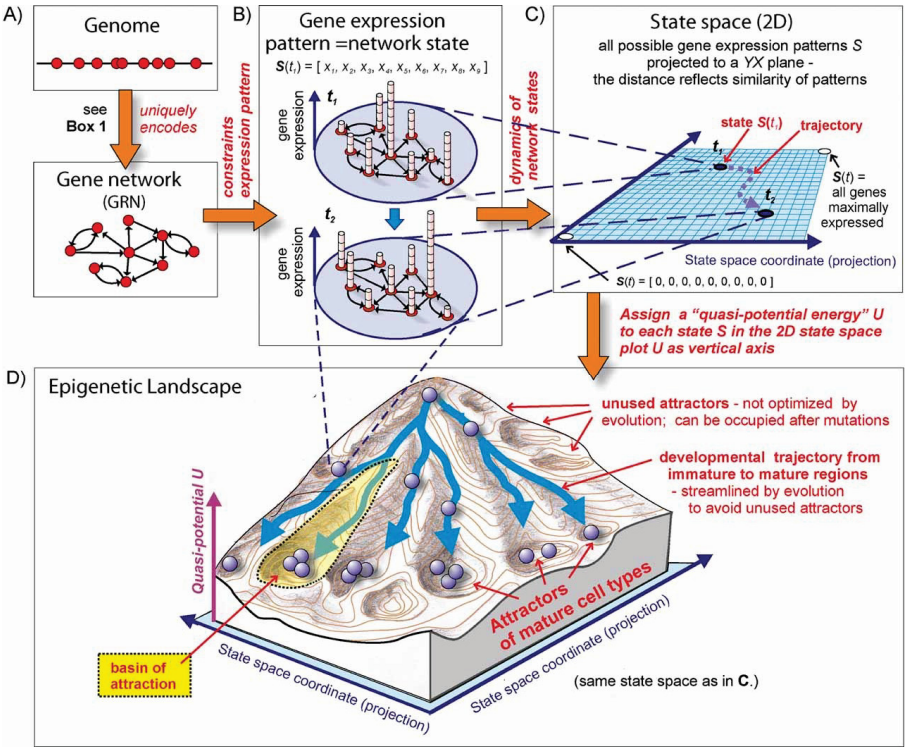

Figure 2.6: Hierarchical Emergence of the epigenetic landscape from the gene network. (A) The linear genomic sequence encodes the specific molecular interactions between gene loci. The gene loci give rise to the gene regulatory network and its fixed network architecture. (B) A fixed genetic network architecture has various possible gene expression pattern including metastable and transitional states. (C) The network states of n genes can be mapped to a n-dimensional state space and the trajectory from one expression state to another can be mapped by a trajectory. (D) Different expression states S_i may have different probabilities. A quasi-potential can be mapped as $U \sim P(S_i)$. Most likely expression states can be interpreted as attractor states. Waddington's epigenetic landscape can be represented in such a fashion. Graphic adopted from Huang 2012 [123]. Copyright © 2011 John Wiley and Sons, license number 4691380149182.

Genes can regulate the expression of other genes via intricated molecular interactions which are transcribed in the genome. This gives rise to the gene regulatory network (GNR) of interacting genes and enables the cell to have various stable expression pattern, thus

phenotypes, without the need for changes in the genome. Changes in the constraints of the network, e.g. activation of certain pathway, can induce a cascade of changing expression pattern, which is outlined in *Figure 2.6*.

The recurrent phenotypic similarity between cancer cells and embryonic (stem) cells can be explained well by the orchestrated expression of the same array of genes in normal and cancer stem cells [225]. Reproducibility in such highly complex cellular differentiation processes implies the existence of underlying transcriptional programs which sequentially activate and silence specific genes. These programs are executed by gene regulatory networks (GRNs), which are defined as units of interacting transcriptional elements which exhibit a specific regulatory relationship and therefore cause a predictable pattern of gene expression with a defined structural and functional output [226]. GRN's enable cells to concertedly change protein expression patterns in response to environmental changes and have a tendency to stabilize themselves [227]. Stable gene regulatory states can thus be considered attractors in a high-dimensional spaces of the cell's genetic expression profiles [176,228]. As a physical interpretation illustrated in *Figure 2.6*, the state space of the gene regulatory network displays as an n-dimensional landscape for the corresponding n regulated genes. Valleys of this quasi-landscape are then attractor states, meaning that these represent stable gene expression profiles. Switching from one expression state to another, is accompanied by a transition from one stable gene regulatory state to another, often initiated by key regulators. Cell differentiation is then described by an initial cell population with a meta-stable, transitional expression profile ("basin of attraction" in the GRN quasi-landscape) which becomes instable due to key regulators and the cells switch to a new (meta-)stable expression state of the bifurcating GRN. Thus, the GRN with its bifurcations determines the cell fate. The inverse process of cell fate determination in the GRN gives rise to cell dedifferentiation, which is a key component of cancer progression. For this process, mutated cells may have altered network dynamics which allows for reoccupation of previous, undifferentiated expression states or occupying new expression states outside of the developmental trajectory from immature to mature cells.

For instance, often pairs of antagonizing transcription factors – the simplest two-dimensional GRN – determine the cell fate choice and timing during embryogenesis, such as *Oct4* and *Cdx2* for the

differentiation of the Oocyte to an inner cell mass (*Oct4* up and *Cdx2* down regulated) and Trophoectoderm (*Cdx2* up, *Oct4* down) [229–232]. In fact, bifurcations as a principle of development were already introduced about 60 years ago by Waddington in his epigenetic landscape proposition [122] based on the pioneering work by Turing [118]. This theoretic work was confirmed experimentally many decades later [127] and bifurcational tissue differentiation has remained an essential paradigm in our understanding of cell fate decision and development [124].

In effect, GRNs are at the center of a holistic concept integrating all epigenetic and genetic aspects of cell fate decision [123]. Genomic alterations and instability that can be caused by a variety of environmental factors such as irradiation, chronic inflammation and viral infections might lead to the re-activation of previously silenced developmental GRN's [123,175,182]. The gene regulatory network provides a framework for structured tumor progression without the need that random mutations are the driver of cancer progression as there are more possibilities to de- or reactive (epi)genetic programs without direct somatic mutations targeting key transcription factors, as the clonal evolution model would suggest.

To a certain extent, this leads to a predictable evolution which is reflected by the acquisition of all hallmarks of cancer on a cellular level. Furthermore, others have shown that stiffening of the extracellular matrix (which again can be caused by a variety of environmental factors) can induce a cancerous phenotype in epithelial cells without the necessity of new mutations [24–26,233].

As there are striking similarities between cancer development and embryonal developmental plans, the question rises if and how strongly intertwined are carcinogenesis and embryogenesis? For one, the Hallmarks of Cancer reflect cellular function crucial in embryogenesis, second, during embryogenesis cell differentiate and specialize during maturing whereas cancer cells slowly lose their differentiated and specialized phenotype during cancer progression. During embryogenesis, different tissues arose in a stepwise bifurcational process of differentiation, these initial precursor tissues formed stable tissue compartments and are segregated via dense collagen fascia as compartment boundaries in matured organisms [209]. Cancer progression, on the other hand, is accompanied by steadily acquiring

more traits and characteristics of embryonic developmental origin due to a loss of differentiation and gained adaptivity. Peculiar, the transformation of metastatic tumor cells into healthy and differentiated mature tissues was also shown to be possible via transplanting the malignant tumor cells into transplanted into various embryo models [113,178,234,235]. This line of thought resulted in a hypothesis of *Inverse Morphogenesis* coined by Prof. Höckel of the University Clinic Leipzig [158]. The theory proposes that carcinogenesis has self-organizing similarities like morphogenesis presumably based on attractor-driven progression due to changes in the gene regulatory networks. From the view point of the pioneering works on reversion of malignant tumor cells and phenotype into healthy mature tissues based on tumor cell interaction in embryonic tissues [113,178,234,235], the connection is strikingly profound when considering cancer as a systemic disease emerging on tissue level [11].

From a perspective of Waddington's epigenetic landscape [122–124], the fate of a cell is determined on the path the precursor cell takes in the gene regulatory network through a sequence of stable states, perambulating through the bifurcating valleys of the epigenetic landscape. Thus, every bifurcation in the GRN can give rise to further cell differentiations. As the embryogenic tissue evolves via differentiation – one primordial cell type bifurcates into two different cell types – with subsequent segregation towards more mature tissues. Thereby, cellular features and functions of embryogenic origin are slowly silenced, such as cell proliferation and cell migration, as they are not necessary or harmful for the originated mature tissue. Carcinogenesis can thus be considered to be the *inverse* process of morphogenesis, thus *inverse morphogenesis*, where embryonic functions are re-activated with cell proliferation and migration being the key features [219,220]. On a grand scheme, this theory provides additional *ad-hoc* predictions for carcinogenesis and tumor progression. As cells differentiate and segregate during ontogenesis, cancer cells of a certain compartment of origin should regain a more de-differentiated state and the capability to life and thrive in other ontogenetic distant tissue compartments. For the very first steps in carcinogenesis, this is a necessity to form an initial tumor: malignant transformed epithelial cells acquire the trait to break through the basal membrane and invading the underlying tissue, a different sub-compartment [142]. Furthermore, the compartment, where the tumor

first formed, originated from another differentiated, primordial embryogenic tissue. Thus, *inverse morphogenesis* would predict, that the next tissues at risk of tumor invasion will be all further tissues which arose from the primordial embryogenic tissue. In addition, cancer progression relies less on genetic mutations since minuscule changes in the GRN can amplify to large effect in the expression pattern and thus influence the cancer phenotype.

To a certain extend it is shown that the correlation of carcinogenesis and ontogenesis has treatment-related implications and can used as a guideline for surgical approaches to remove primary tumors for various tumor entities, i.e. cervix [156,157,161,236,237], vulva [159,160], rectum [238], pancreas[239], and mid-facial skin cancers [240], wherein the local tumor spread can be described well with embryological structures such as compartments and fusion planes. In short, tumors often do not transgress embryogenic compartment boundaries of ontogenetic distant tissues but are more likely of passing compartment boundaries of ontogenetic close tissues. With further tumor progression the tumor acquires the ability to overcome the compartment boundaries of ontogenetic distant tissues. This raises the question if the association between cancer progression and embryogenic development is a general concept and can the ontogenetic relatedness of tissues be used to predict which local tissues are at risk of cancer infiltration.

As part of this thesis, I tested the hypothesis of *Inverse Morphogenesis* for the case of cervical cancers based on vast clinical data of tumor infiltration from a physical point of view: A purely physical microenvironmental description of tumor growth and invasion agnostic of any embryogenetic influence will predict different invasion likelihoods of various tissues and different tumor shape than an ontogenetic-derived tumor growth description. I included analysis of the clinical data of tumor shape and size as well tumor growth modelling to outline that a purely physical microenvironmental model of cancer progression, as suggested by the Darwinian-based somatic mutation theory of cancer, is not sufficient to describe tumor progression properly.

2.5 Cancer Growth Modelling

As introduced in the previous chapter *Initial Steps in Tumor Formation and Progression*, when a cancer commences into the metastases-forming state, the chances of curing the disease rapidly decreases. Thus, it is imperative to detect the tumor as early and detailed as possible, and remove the primary tumor accordingly before metastatic colonies emerge. The primary tumor growth phase is consequently the most crucial phase for predicting treatment outcome.

While various effects of carcinogenesis are acting on different length and time scales, without doubt they are not disconnected and the scales are strongly intertwined. However, some phenomena of one length scale are emergent effects of actions of the underlying smaller scale. Modelling tumor growth is therefore a non-trivial task since bridging the scale difference is cumbersome and often involves *ad-hoc* assumptions. Thus, many tumor growth modelling approaches elucidate only one scale and are thus inherently limited. This crucial aspect also highlights that, depending which approach is used, the type of modelling is critical for which tumor properties can be analyzed. On the other hand, tumor progression is also a process on multiple scales with cellular factors, e.g. gene expression and mutation, cell adaptation and mechanics, and epigenetic and phenotypic changes, and microenvironmental factors, e.g. ECM density and fiber alignment, chemo- and haptotaxic. In order to grasp tumor growth and the multiscale nature of cancer, modeling approaches of different length and time scales are interwoven giving rise to hybrid models which combine discrete and continuous processes, such as cell division and nutrient transport, respectively.

Modelling of the inflational growth phase has many interesting aspects as it is a multiscale problem predominantly located on the

mesoscopic and macroscopic scale and therefore may include coarse-grained aspects of the microscopic scale and also may include a descriptive outlook how the macroscopic scale might emerge from the mesoscopic layer. Some of the coarse-grained aspects are the introduction of implicit mutations altering certain cellular parameter, such as resistance to drugs, growth rate and metabolic rates, hiding the genetic details on molecular level. After all, tumor growth dynamics occur on the phenotypic level of cells despite that mutations happen on the molecular genetic level, thus, tumor growth dynamics is largely an microenvironmental-driven process.

For the meso- and macrocosmos, deterministic reaction-diffusion equations have been used to model time- and space-dependent growth and spread of tumors [241–243]. The general assumptions for such an approach are a coarse-grained description of chemical interactions in form of partial differential equations (PDEs) and general assumptions of conservation laws and continuum equations. Thus, the most fundamental conservation equation for cell proliferation and migration holds:

$$\frac{\partial n}{\partial t} = -\nabla \cdot \vec{j} + g(n, \dots) ,$$

where $n = n(\vec{x}, t)$ is the density of cells at position $\vec{x}$ and time t, $\vec{j}$ is the flux of cells across a surface, and $g(n, \dots)$ is the net proliferation rate. The growth rate depends on the cell density n among various other parameter, such as promoter and inhibitor concentrations c_i (e.g. *EGF*, *TGF*, …). The flux of cells in tissues is then the migration of cells through the surrounding microenvironment, which is comprised of random undirected motility and directed, gradient following haptotactic/durotactic motility [244–247]:

$$-\nabla \cdot \vec{j} = -\nabla \cdot (D \nabla n) - \nabla \cdot (a_1 n \nabla \mathrm{c}_1 + a_2 n \nabla c_2 + \cdots)$$

where D is the diffusion coefficient of random cell motility, and c_i is the concentration of attractant or repellant of type i with cell affinity a_i. The concentrations of various attractants and repellants may also follow reaction-diffusion equations. Such continuum equations are successfully used in modelling various biological phenomena with cancer growth and progression one of the most prominent examples [248–253].

With the given set of coupled reaction-diffusion equations describing cell growth, cell mobility, cell attractant and repellant, cell proliferation promoter and inhibitor, tumor growth can be modeled to a

large extent. There is, however, a drawback of often hitherto unknown parameters of the models and limited computational power. In order to tackle these issues, models can often only focus on certain aspects of tumor growth and progression. Moreover, to keep the computational cost, the system of coupled differential equations is often simplified by (often) reasonable assumptions such as symmetry arguments, rescaling of parameters, and linearization of equations.

Tumor growth modelling is, however, still limited in tumor size in terms that the predictive power diminishes rapidly. Whereas for modelling smaller tumors aspects of evolutionary fitness and microenvironmental interaction can be studied, modelled and compared with experimental data, modelling larger tumors are afflicted by lack of clinical and experimental data, thus parametrizing and/or validating large scale models is cumbersome and ultimately directly testable hypotheses are lacking. Unfortunately, the largest modelling scale of local and regional tumor sizes is the scale with greatest clinical implications. Any validated prediction of such a large-scale model will have an impact on treatment options such as surgery and radiotherapy. On this scale, the cellular details of individual cancer cell are of lesser importance and coarse-grained properties like size, shape and infiltrated structures are measure of the associated tumor stage, e.g. FIGO staging for cervical cancers discriminates between tumors confined to the organ of origin, invasion of surrounding organs or tissue and spread to distant sides.

The aim of large scale modelling presented in Kubitschke et al. 2019 [27] is to identify growth limitations of primary solid tumors within the human body based on clinical data of cervical cancers obtained from pathological examination of surgical resected tumors of 518 patients and simulations. Therefore, the microscopic layer is represented in a coarse-grained manner and the later cancer progression events of the macroscopic layer, such as metastases formation, have to be omitted in order to keep the model computational cost feasible and enabling to support all parameters of the model with quantitative clinical data, such as net growth rate of tumors. In contrast to various other approaches, where often spherical symmetry of tumor growth is an assumption, I focus on the analysis of anisotropic tumor growth. Thus, spherical symmetry is explicitly allowed, and partially enforced, for local tumor growth. The hypothesis of *Inverse Morphogenesis* is tested whether it

predicts tumor growth, invasion and shape better than the prevailing tumor growth assumption of random isotropic growth and its associated wide excision method for surgical resection. In Kubitschke et al. 2019 [27] the tumor infiltration pattern and order in surrounding ontogenetic compartments are analyzed which is used to evaluate the feasibility and advantages of novel surgical methods based on embryogenic compartment theory.

3 Results and Discussion

3.1 First Publication

The content of this chapter has been published in the manuscript "Physical Properties of Single Cells and Collective Behavior"

DOI: 10.1007/978-3-319-65924-4

Physical Properties of Single Cells and Collective Behavior

5

Hans Kubitschke, Erik W. Morawetz, Josef A. Käs, and Jörg Schnauß

Abstract

Cells display a high degree of functional organization, largely attributed to the intracellular biopolymer scaffold known as the cytoskeleton. This inherently complex structure drives the system out of equilibrium by constantly consuming energy to conserve or reorganize its structure. Thus, the active, structurally organized cytoskeleton is the key player for the emergent mechanical properties of cells, which further determine properties of cell clusters and even multicellular organisms. In this spirit, this chapter introduces the physical principles on the different levels of biological complexity ranging from single biopolymers to tissues. The emergent mechanical properties and their respective effects on each level will be highlighted with a strong emphasis on their intertwined nature.

5.1 Introduction

The tremendous complexity of biological matter emerges from the interplay between intertwined levels or scales, with each level contributing a rich repertoire of physical principles. To uncover these principles and their interplay has proven to be a nontrivial task since processes, which we consider the fundamentals of life, exist far from thermodynamic equilibrium. Thus, traditional, purely reductionist approaches are unsuitable to fully elucidate and describe biological soft matter [1–3].

H. Kubitschke • E.W. Morawetz • J.A. Käs
Peter Debye Institute for Soft Matter Physics, Universität Leipzig, Leipzig, Germany
e-mail: hans.kubitschke@uni-leipzig.de

J. Schnauß (✉)
Peter Debye Institute for Soft Matter Physics, Universität Leipzig, Leipzig, Germany

Fraunhofer Institute for Cell Therapy and Immunology, Leipzig, Germany
e-mail: joerg.schnauss@uni-leipzig.de

I. Sack, T. Schaeffter (eds.), *Quantification of Biophysical Parameters in Medical Imaging*, https://doi.org/10.1007/978-3-319-65924-4_5

Generally, complex systems are difficult to capture by intuitive understanding, which rather impedes an abstraction of the system in form of a model. When dealing with living matter, we can refer to different levels of complexity, which can be assigned to physical scales [4]. In this framework, a higher level contains the lower level, and complexity necessarily increases, which can even lead to entirely new properties [1]. If principles of the macrostate are absent in the underlying microstate, they are considered emergent (e.g., a single fish cannot exhibit swarm behavior). The term emergence describes the process leading to novel emergent properties, with the prefixes "micro" and "macro" not referring to definite length scales but to different levels of biological complexity [4]. For biological matter, a possible hierarchy might be described as

protein → filament → network → cell → tissue.

Using this hierarchy as a point of departure, we can aim at describing a given system only on the basis of the next underlying level of complexity, an approach termed hierarchical reductionism or coarse-graining [5, 6]. A biological tissue, for example, can be described as an accumulation of cells and extracellular matrix without considering subcellular structures. Further, cell mechanics can be described in terms of principles of networks of filaments. In this process, the problem is reduced, losing the detail of lower levels, similar to the use of computers, where not every single transistor has to be considered to operate the machine.

This chapter describes the physical principles emerging at the different levels of complexity and how they can be scaled up. In this context, it is important to clearly distinguish the concepts of self-organization (processes driven by energy dissipation) and self-assembly (processes driven by minimization of free energy, i.e., no energy is dissipated) [7–10]. With these terms at hand, we begin by introducing the lowest level of complexity, i.e., monomers and filaments, and proceed to the higher levels, successively describing the physical principles of cells, cell clusters, and tissues.

5.2 The Cytoskeleton

The cytoskeleton is a scaffold lending cells mechanical integrity and stability. It consists of three main constituents: actin, intermediate filaments (IFs), and microtubules (MTs). These components form fibers in the micrometer range by polymerizing their monomers into specific arrangements, resulting in a different intrinsic filament stiffness for each class [11] (Fig. 5.1). The stiffness is commonly characterized via the so-called persistence length (l_p) [12, 13]. This material-specific parameter is a measure of the fluctuation correlation along the filament backbone, quantifying over which distance an oscillation at a specific point (S_0) at the backbone becomes uncorrelated to the movement of another point (S_2) at the filament (Fig. 5.1). The persistence length can be directly observed, for instance, by analyzing the average transverse fluctuations of filaments observed over time or by

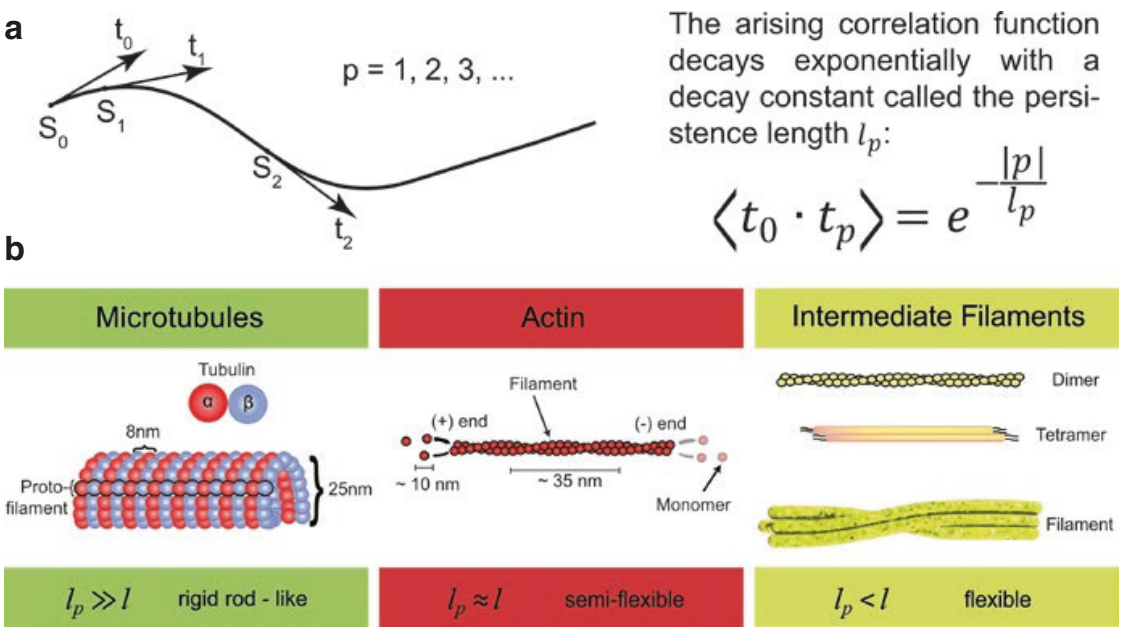

Fig. 5.1 (**a**) Points (S) along the contour of a semiflexible polymer have different tangent vectors (t). If points are close to each other (S_0 and S_1), their tangent vectors are correlated and roughly point in the same direction. When points are further apart (S_0 and S_2), their tangent vectors are uncorrelated and point in different directions. (**b**) illustrates the stiffness regimes of the three major cytoskeletal components—microtubules (MTs), actin, and intermediate filaments (IFs). Different mechanical properties are a direct result of the differing filament architectures. l denotes the length of the filament and l_p the persistence length [7]

evaluating their tangent–cosine correlation function [14]. Based on these methods, actin filaments have an l_p of ~10 μm [15, 16], while MTs have a much longer l_p in the range of millimeters [17]. Note that l_p of natural biopolymers cannot be freely tuned and new model systems have to be used to derive the respective scaling laws [13, 18–20]. Since l_p is derived via thermal fluctuations (imagine a fluctuating cooked spaghetti), it is a temperature-dependent parameter and cannot be considered a material-defining constant. However, by multiplying thermal energy, k_BT, with the temperature, T, and the Boltzmann constant, k_B, a new temperature-independent parameter called bending stiffness, $\kappa = k_BTl_p$, can be derived.

Besides their mechanical properties, which have a static function and serve as the cellular skeleton, the cytoskeletal filaments are also very dynamic structures, enabling rapid adaptive organization of the entire cytoskeleton to fulfill functions such as cell migration or division. Fascinatingly, the cell can use the same components for these somehow contradictory tasks, which is only possible because of permanent energy dissipation, permitting rapid transition between different states. Furthermore, although the cytoskeletal building blocks are preserved in almost every eukaryotic cell, induced morphologies vary substantially among different cell types. Even within a single cell, the cytoskeleton spatially organizes into various different structures responsible for differing sets of functions—a strategy known as multifunctionality.

The different filament architectures not only result in a wide range of different bending rigidities but also determine their role in dynamic processes. MTs, for instance, are very rigid and thus typically appear as individual fibers, extending

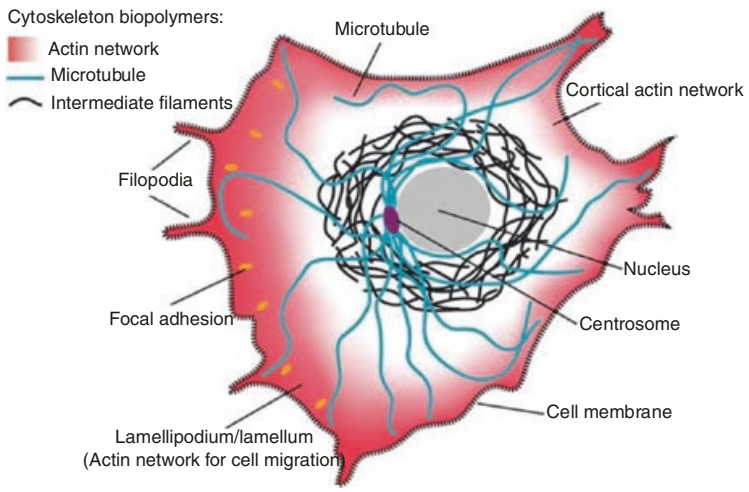

Fig. 5.2 Schematic drawing of a crawling cell on a 2D substrate showing the most prominent locations for the three types of cytoskeleton biopolymers. MTs are typically nucleated at the centrosome and span the largest portion of the cell. IFs are most commonly found around the cell nucleus, whereas actin filaments form dense networks close to the cell membrane. Particularly, dense and dynamic actin networks are found at the leading edge of migrating cells (forming lamellipodia and filopodia) [7]

from the cell interior to the membrane (Fig. 5.2). Due to their outreach and rather straight structures, they are especially well suited for intracellular transport and for providing directed forces during mitosis and for organelle positioning [7]. Actin filaments, on the other hand, are semiflexible polymers and are typically arranged into networks and bundles driving processes such as cell migration. Actin filaments polymerize near the membrane (leading to high local concentrations as illustrated in Fig. 5.2) and effectively push the boundary of the cell forward. In this dynamic process, actin monomers depolymerize at the filament ends pointing toward the cell center. These monomers subsequently travel to the front to reenter the polymerization cycle, a process called treadmilling [7, 21]. Due to their highly dynamic nature, actin filaments can trigger rapid cellular changes. Additional components such as cross-linking proteins or active myosin motors substantially enrich both their mechanical and dynamic phase spaces. It should be noted here that biological force generation is commonly attributed to the activity of molecular motors [11]. However, recent studies have demonstrated that actin as well as MT-based force generation can be driven solely by entropic arguments without requiring any energy dissipation [22–28].

In general, actin turnover and interactions with molecular motors are persistent processes in biological matter, resulting in substantial energy consumption. In eukaryotic cells, for instance, actin turnover alone can reach up to ~50% of the total energy consumption [29, 30], which in turn indicates that minimizing energy consumption has not been the most dominant evolutionary factor. Apart from molecular motors, all other actin accessory proteins influence the filament or network properties without consuming energy in a form of ATP or GTP. Accordingly, regulatory functions can be roughly classified as modifications of either polymerization dynamics, cross-linking, or filament nucleation [7, 21].

IFs are much less studied than the other two main components of the cytoskeleton. Additionally, IFs describe not only one specific polymer but a rather heterogeneous class of biopolymers, which form extended networks and thus substantially contribute to cell mechanics [31, 32]. Different types of IFs performing specific cellular tasks have been identified [33]. However, a general feature of all these cytoskeletal biopolymers is that they undergo growth and shrinkage by addition or subtraction of monomers. Therefore, their length is adjustable in a dynamic fashion and highly depends on stochastic fluctuations [32, 34, 35]. Further, their dynamic organization is largely determined by a complex interplay with a multitude of molecular accessory proteins, which nucleate, sever, cross-link, weaken, strengthen, or transport individual filaments [11]. The dynamic, self-organizing cytoskeleton is powered by energy-dissipating ATP or GTP consumption, mainly fueling two key processes: hydrolysis-powered depolymerization/polymerization of filaments and molecular motor-driven filament/motor transport [7]. Unlike IFs, MTs and actin are polar structures due to their asymmetrical polymerization and depolymerization dynamics (treadmilling) caused by their differing critical concentrations at the two ends. These two different critical concentrations are a direct result of ATP or GTP consumption, thus reflecting the intrinsic non-equilibrium process, which exerts substantial pushing forces [36]. The arising polarity is crucial for molecular motors to be able to move in a specific direction, enabling controlled cargo transport as well as directed pulling forces [37].

5.3 Rheology

Rheology is the study of deformation responses of materials to applied forces. The deformation response to constantly acting forces depends on whether the material is categorized as a solid or a fluidlike material. In solid materials, the magnitude of the deformation, typically elongation, scales with the applied force, e.g., an elastic spring under tension. Solid responses may also include plastic deformations such as overstretching a spring beyond its elastic limit, which permanently deforms it. The so-called viscous deformation response of a fluidlike material describes how the deformation *rate* scales with the applied force, e.g., ketchup flowing out of a bottle or squeezing glue out of a tube.

For biological samples—in this chapter single cells and soft tissues—viscoelastic responses to small forces have two distinct time scales: on short time scales, from split seconds to minutes, tissue deformation is proportional to applied forces and will recover to return to its initial form after stress release. This is easily confirmed by pressing against muscular or fatty tissue, where responses are nearly elastic. On long time scales (days to months), tissues tend to behave like highly viscous fluids, enabling body modification such as stretching lips by inserting lip discs, as, for example, practiced by the tribes of Mursi and Surma residing in Ethiopia [38] and the south American peoples of the Kayapo and Botocudo [39], or earspools ("flesh tunnel") in western subcultures and various African and American tribes [38, 40]. Materials which are governed by both

elastic and viscous behaviors, such as most biological tissues, are considered viscoelastic materials. Examples of deformation responses are presented in Fig. 2.5 of Chap. 2.

Besides these passive responses, cells and tissues can actively react to environmental cues. Well-known active force generators are myosin motors, which exert pulling forces on actin filaments. This interaction is crucial on the cellular level for processes such as single-cell motility as well as on the tissue level, e.g., for muscle contraction. Many active processes are complexly intertwined with cellular pathways or immune responses and can highly influence the material properties of cells and tissues.

While the qualitative description of biological materials is straightforward, quantitative descriptions involve a profound theoretical background and mathematical models. The main goal of quantitative description is to gather material parameters from biological tissues. Since material parameters should describe intrinsic properties, they should be—in the best possible case—independent of features of the experimental setup such as applied forces, size of the tissue, or type of experiment conducted. This chapter will outline the *theoretical minimum* needed to adequately describe single cells and biological tissues later on and will introduce the concepts and terminology needed to understand the following chapters. Special cases such as nonlinearity and temperature dependencies are deliberately neglected here and are partially discussed later.

5.3.1 Step Experiment

As a starting point, consider a cuboid of tissue. The deformation response will depend on the strength of the force and how it is applied, i.e., on which side and in which direction. Vice versa, if a given deformation is forced upon the material, an internal force will arise accordingly. For the sake of simplicity—mathematical and explanatory—we restrict the possible types of force and deformation application to the types illustrated in Fig. 5.3: a longitudinal sudden force experiment and a transverse shear experiment.

In the stretching experiment, the force is applied equally on two counter-facing sides (red-dashed lines), resulting in an applied stress σ (force per area). The material will expand by Δx in the stretching direction and retract by $-\Delta y$ perpendicular to it. The resulting elongation is measured as strain, i.e., relative extension $\gamma = \Delta x/x$ (a tensor notation of linear strain is given in Eq. (2.6) of Chap. 2). Contraction occurs due to internal forces of the material, usually since many materials, such as water, are nearly incompressible. The relation between axial strain and transverse strain is captured in the Poisson ratio ν given by

$$\nu = -\frac{\Delta y / y}{\Delta x / x} = \frac{1}{2}\left(1 - \frac{\Delta V}{V}\frac{x}{\Delta x}\right), \tag{5.1}$$

with volume V of the cuboid and all further parameters as sketched in Fig. 5.3a. The Poisson ratio is a dimensionless unit and typically ranges from 0 to 0.5. A value

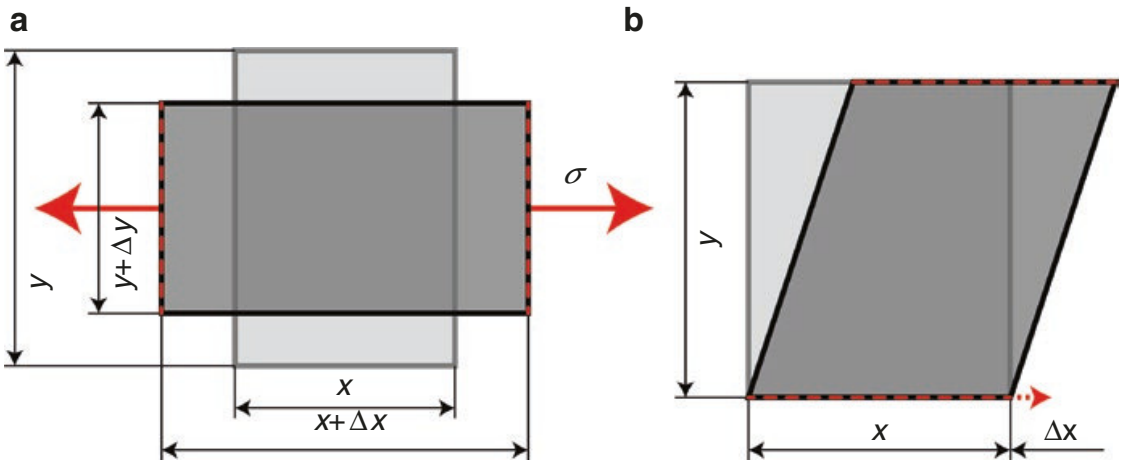

Fig. 5.3 The two archetypes of deformation response experiments in rheology. (**a**) shows the stretching mode, where two counter-facing sides are pulled apart perpendicular to the surface. The material elongates in the direction of the applied force and contracts perpendicular to it. (**b**) shows the shear mode. A strain is applied on the upper side, and the strain response is measured on the lower side

close to 0 means nearly no lateral contraction upon pulling, while a value close to 0.5 means that the material is nearly incompressible. The Poisson ratio for biological microtissue samples was found to be on the order of $\nu = 0.45$ [41]. Lower values can be found in multiphasic tissues, in which a fluid phase is allowed to freely move (see Chaps. 3 and 4).

For simplicity, only constant step stresses, as illustrated in Fig. 2.5 of Chap. 2, are considered in the following. When applying such a constant stress profile, σ_0, starting at $t = 0$, strain γ can be expressed as

$$\gamma(t) = D(t)\sigma_0 \quad \text{or} \quad D(t) = \frac{\gamma(t)}{\sigma_0}, \tag{5.2}$$

where t denotes time and $D(t)$ denotes *tensile creep compliance*. This parameter is usually unique to the type of material measured. For a perfect elastic, springlike material, tensile creep compliance reduces to a constant, $D(t) = 1/E$, where Young's modulus E describes the stiffness of a solid material under forces very similar to the spring constant of an elastic spring. The higher it is, the stiffer the material. Muscle tissue, for example, has an average Young's modulus of 2.12 ± 0.91 kPa [42], while cancellous/trabecular bone has 14.8 ± 1.4 GPa [43, 44]. An overview of elastic properties of tissues has been presented in a review by Akhtar et al. [45].

For a perfect viscous, fluidlike material, the tensile creep compliance will follow $D(t) = t/\eta$, where η is the viscosity of the fluid. The higher the viscosity of a material, the slower the flow speed for given forces will be. Honey, for instance, has a viscosity between 2.54 and 23.4 Pa · s (at 25°C, depending on moisture and sugar composition) [46], while blood has 4 mPa · s [47].

For viscoelastic materials, the detailed time-dependent response will be more complicated. Examples for illustration are presented in Fig. 2.5 and Fig. 5.4.

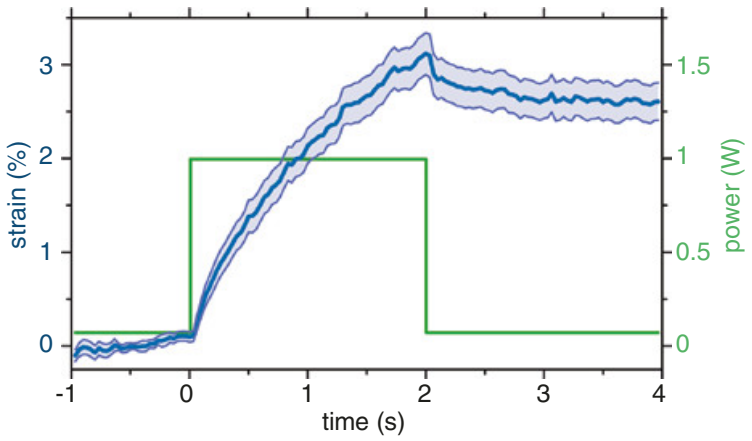

Fig. 5.4 Graph of the strain response of cells (blue, including confidence interval) under a step stress in an optical stretcher. The applied stress is proportional to the laser power (green). After 2 s, the stress is released and the cell relaxes again. A detailed description of the optical stretcher can be found in the next chapter

If a step strain γ_0 is applied, instead of a step stress, the corresponding stress response $\sigma(t)$ will be given by

$$\sigma(t) = E(t)\gamma_0 \quad \text{or} \quad E(t) = \frac{\sigma(t)}{\gamma_0}, \tag{5.3}$$

with the *elastic modulus* $E(t)$, also known as time-dependent Young's modulus, which is in principle the inverted tensile creep compliance. The two material parameters—tensile creep compliance and elastic modulus—are not independent. In fact, one can translate tensile creep compliance to elastic modulus and vice versa. The conversion can be done using Laplace transform $\mathcal{L}$:

$$\mathcal{L}\left[E(t)\right]\mathcal{L}\left[D(t)\right] = \frac{1}{s^2}, \tag{5.4}$$

with the complex frequency parameter $s = \sigma + i\omega$. Because the interpretation of elastic modulus $E(t)$ is more straightforward—the higher the modulus, the stiffer the material—it is more commonly used in the scientific community than creep compliance.

5.3.2 Oscillatory Experiment

The second measurement archetype is the shear experiment (Fig. 5.3b), in which a cuboid of material is fixed between two plates. On one plate, a shear stress is applied, and, in the opposite plate, the strain response is measured. Vice versa, applying a strain and measuring a stress response would give the same qualitative result. Commonly, forced strain γ_{in} is a sinusoidal alternation at frequency ω with a chosen maximum strain amplitude γ_0:

$$\gamma_{in}(t) = \gamma_0 \cos(\omega t). \tag{5.5}$$

The response to stress on the second plate will depend on the material, either elastic, viscous, or viscoelastic. In Fig. 5.5 the three types of responses are illustrated for applying a shear strain and measuring the stress response and vice versa.

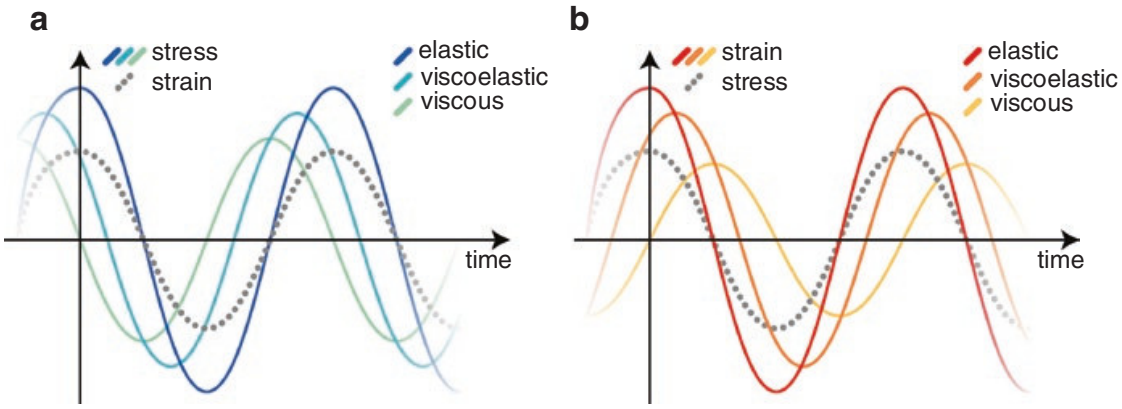

Fig. 5.5 Sketches of the shear–strain relation in the shear experiment. In (**a**), a shear strain is applied (gray), and the stress response is measured, while in (**b**) a shear stress is applied, and strain is measured. An elastic response (blue and red, respectively) is in phase, while a viscous response is phase shifted by 90° (positive direction in (**a**), negative direction in (**b**)). The phase shift will be between 0° and 90° for a viscoelastic response

In either case, the response is also sinusoidal but phase shifted, if the material is not purely elastic. Since cases (a) and (b) in Fig. 5.5 give principally the same results, but with inverted cause and effect, we henceforth focus on case (a), applying strain and measuring stress, as this is the more common experimental method.

As the viscoelastic stress response will be sinusoidal with an added phase shift—the strain lags behind the stress—it is possible to use some basic trigonometric identities for dealing with sines and cosines in an elegant way. Nonetheless, the solution for viscoelastic materials can already be explained qualitatively since the response of elastic and viscous materials is already known.

For elastic materials, the resulting stress, σ_{ela} , is proportional to the applied strain, γ_{in}, giving

$$\sigma_{\mathrm{ela}}(t) = \sigma_{0,\mathrm{ela}} \cos(\omega t), \tag{5.6}$$

since γ_{in} is also a cosine function. In contrast, for a viscous material, the strain *rate* is proportional to stress, meaning that stress will be highest when strain changes the fastest and stress will be zero when strain is constant. Therefore, the viscous stress response will be out of phase by 90°:

$$\sigma_{\mathrm{vis}}(t) = -\sigma_{0,\mathrm{vis}} \sin(\omega t). \tag{5.7}$$

Intuitively, the stress response of a viscoelastic material can be found as the sum of the elastic and the viscous response:

$$\sigma_{\mathrm{VE}}(t) = \sigma_{0,\mathrm{ela}} \cos(\omega t) - \sigma_{0,\mathrm{vis}} \sin(\omega t). \tag{5.8}$$

Analogous to the tensile creep compliance presented in the previous chapter, we can define the *complex shear modulus* given by

$$G^*(\omega,t) = \frac{\sigma_{\mathrm{VE}}(\omega,t)}{\gamma_0} = G'(\omega)\cos(\omega t) - G''(\omega)\sin(\omega t), \tag{5.9}$$

with storage modulus G' and loss modulus G''.

A viscoelastic material can therefore be characterized by the ratio of the viscous and the elastic stress response amplitude for a given frequency [13]. The higher the viscous amplitude relative to the elastic amplitude, the more viscous than elastic a material is at that given frequency. The elastic and viscous response can be different for varying shear frequencies (see Fig. 5.6. The ratio of both amplitudes also defines phase shift angle δ, like in Fig. 5.5, given by the following equation (see Eq. (2.44) in Chap. 2):

$$\tan\delta(\omega) = \frac{\sigma_{0,\mathrm{vis}}}{\sigma_{0,\mathrm{ela}}} = \frac{G''(\omega)}{G'(\omega)}. \tag{5.10}$$

For the quantitative part, the basic trigonometric identities mentioned above are needed. As the elastic and viscous amplitudes cannot be measured independently in shear experiments, we have to convert G^* from a sum of a sine and a cosine to a single cosine (or sine) including phase shift. After conversion, we obtain

$$G^*(\omega,t) = \left|\boldsymbol{G}^*(\omega)\right| \cos(\omega t + \delta), \tag{5.11}$$

where $|\boldsymbol{G}^*(\omega)|$ denotes the measured absolute amplitude given by

$$\left|\boldsymbol{G}^*(\omega)\right| = \sqrt{G'(\omega)^2 + G''(\omega)^2}. \tag{5.12}$$

The storage and loss modulus can be recovered via $G'(\omega) = |\boldsymbol{G}^*|\cos\delta$ and $G''(\omega) = |\boldsymbol{G}^*|\sin\delta$.

This representation of complex shear modulus G^* is most suited for experimental data since it includes absolute amplitude $|\boldsymbol{G}^*(\omega)|$ and phase shift δ, both of which are quantities that are easily measurable in any oscillatory shear experiment for any frequency. Complex shear modulus $G^*(\omega)$ is the favored material parameter in the scientific community since it has a more convenient interpretation, basically the

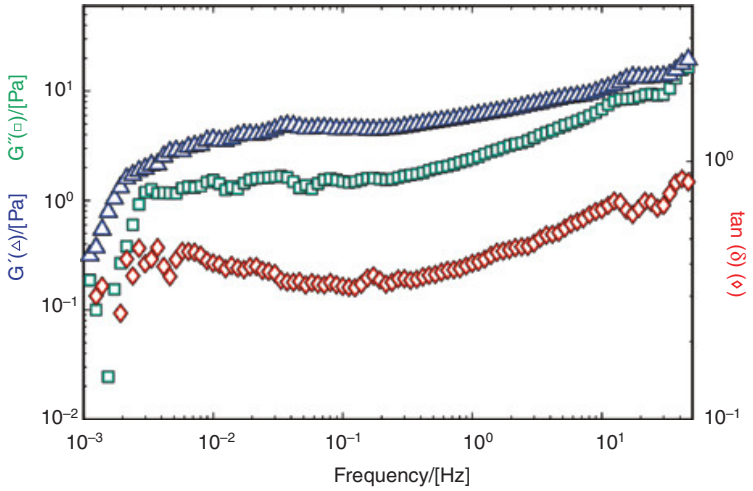

Fig. 5.6 Graph of the elastic and viscous shear modulus (extracted from the complex shear modulus) and phase angle of an actin polymer network measured with a rotation shear rheometer. For low frequencies (10^{-2} Hz and lower), actin is easier to deform on long time scales of 100 s, which cause a significantly lower storage (blue) and modulus (green). Deformability, both elastic and viscous, increases with frequency. As the phase angle increases with frequency, actin becomes more and more viscous in its response

same as elastic modulus E. Also, rotation shear rheometers are predominantly used for oscillatory shear experiments, which can directly measure the storage and loss modulus for a broad frequency range. If instead a shear stress is applied and a strain response is measured (Fig. 5.5a), the calculations above can be done analogously and will result in the complex inverse of $G^*(\omega)$, i.e., complex compliance $J^*(\omega) = 1/G^*(\omega)$. A typical complex shear modulus graph is depicted in Fig. 5.6, showing the frequency-dependent response of an actin network under strain load.

In addition, the previously introduced elastic modulus $E(t)$ and tensile creep compliance $D(t)$ can also be converted to complex shear modulus $G^*(\omega)$. Details of the conversion will be omitted since it involves advanced calculus and will not give more insight into the material properties of biological tissues.

5.3.3 Modeling Viscoelasticity

Modeling the complex time dependence of tensile creep compliance or the elastic modulus of viscoelastic materials is often done via constitutive equations and/or models. In a simplified, coarse-grained vision, cells can be considered as polymer scaffolds (cytoskeleton) filled with a viscous fluid (cytosol) and functional entities (organelles, which are obstacles in the polymer meshwork), or, put simply, the cytoplasm responds like a *water-filled sponge* [48]. The cytoskeleton is the main contributor to elastic behavior, while the flow and friction of the cytosol and organelles contribute to the viscous response. The combination of both results in an overall viscoelastic response.

An ideal spring with its elastic response, simulating the cytoskeleton, and an ideal dashpot, simulating the viscosity of the cytosol, can be interconnected to set up toy models simulating viscoelastic responses. We will give here only a short and shallow overview on how viscoelastic properties can arise from the combination of perfectly elastic and viscous subunits. When combining a spring and a dashpot in parallel in the so-called Kelvin–Voigt model, the applied stress is distributed between the spring and the dashpot as captured in the following simple equation:

$$\sigma_{\text{total}} = \sigma_{\text{spring}} + \sigma_{\text{dashpot}}. \tag{5.13}$$

In addition, the strain of the spring and dashpot will be the same as the total strain:

$$\gamma_{\text{total}} = \gamma_{\text{spring}} = \gamma_{\text{dashpot}}. \tag{5.14}$$

With this set of equations, the time-dependent strain response $\gamma(t)$ of the Kelvin–Voigt model (and analogously for the Maxwell model) for *any* given time-dependent stress $\sigma(t)$ can be calculated. With the recipe given above, more complex models, possibly featuring more material details for different time scales, can be set up using more than one spring and dashpot. Introduction of another dashpot in series, for instance, accounts for permanent plastic deformation. Furthermore, these models can be applied to any type of experiment—shear and pulling/pushing mode, stress or strain application, and oscillatory and stepping mode—rendering them universally applicable. These models are therefore widely used in the scientific community as a first top–down approach.

Another modeling approach originates from polymer physics allowing to derive many scaling laws from basic principles [12]. Scaling laws are powerful, predictive tools and are generally found in biological systems [49–51]. For instance, the basal metabolic rate P of mammals is approximately proportional to their mass M to the power of three fourths ($P \propto M^{3/4}$). For single cells and tissues, scaling laws can be found for the strain response under stress load ($\gamma \propto \sigma_0 \cdot t^{\alpha}$) [52–54]. For a scaling exponent α between 0 and 1, a viscoelastic response can be modeled, including the limit cases of $\alpha = 0$ and $\alpha = 1$, corresponding to a purely elastic and purely viscous response, respectively. Indeed, scaling behaviors of material parameters, such as G^* and E, can be found in various biological systems [55]. They can be also derived from more fundamental principles of polymer interactions [12] and hold even for advanced theories, i.e., the glassy wormlike chain [56, 57] including nonlinearities like strain hardening and softening [58]. More modeling approaches for cells and tissues can be found in [59, 60].

However, many approaches assume a passive material, which might not be the case for biological matter on time scales of minutes or longer [60]. Introducing active responses, and therefore active force generation, in models is a challenging task since many active processes cannot be described with ease in a coarse-grained manner. Modeling force generation of myosin motors, however, has made significant advances, and appropriate models have been introduced [61–65].

Besides active responses, when probing the mechanical properties of biological matter, the effect of temperature should not be neglected. The temperature should always be in a physiological range since many processes in organisms are highly temperature dependent, e.g., polymerization and depolymerization rates of actin and microtubules [66, 67] as well as motor activity of myosin, dynein, and kinesin [68]. Temperature also affects passive material properties as many materials become less viscous at higher temperatures. Honey, for instance, is much more viscous at lower temperatures [46]. In detail, the viscosity of honey follows an Arrhenius law [69]:

$$\eta(T) = \eta(T_{\text{ref}})\, e^{-\left(\frac{E_A}{k_B T}\right)}, \tag{5.15}$$

where $\eta(T_{\text{ref}})$ is the viscosity of the material at a given reference temperature, k_B the Boltzmann constant, and E_A the activation energy of a transition of states, usually energy barriers of chemical reactions or binding energies. This effect, commonly known as time–temperature superposition, can be observed for single cells [70]. However, many cells do not show this clear relation, and the temperature dependency of their responses is more complex [71].

5.4 Mechanics on the Cellular Level

Modeling is often limited by strong interactions across multiple levels of complexity. Already on a cellular level, the many cell organelles and functional groups make it difficult to grasp the cell "as a whole" in terms of a coarse-grained system. As the internal structures of cells are already highly anisotropically distributed, it might

appear counterintuitive to describe the behavior of a whole cell as a coarse-grained system. It turns out, however, that many of the introduced concepts are no oversimplifications *per se* and that biological systems can often be described in such a simplified manner. As long as cells (and/or tissues) are not actively reacting to applied forces and deformations, cell mechanics can be understood as an emergent consequence of the cytoskeletal network level. To push this conceptual approach even further, key aspects of cell migration [72] or cell shape [73] can be described without considering details of the filamentous or the molecular level by solely using very fundamental hydrodynamics-based descriptions [74].

Biological cells can be structurally regarded as polymer-filled entities enclosed by a nearly impenetrable membrane. Due to the considerable backbone stiffness of actin filaments and microtubules, mechanical integrity is already given for relatively large mesh sizes and low-volume fraction. An analogy for this concept is a tent, which mechanically stabilizes a certain volume with enough space for passive and active molecular transport. As described in the cytoskeleton chapter, the three main components, actin, microtubules, and intermediate filaments, can form emergent structures such as networks and bundles [7, 75]. Although cells come in a broad phenotypic diversity, including keratinocytes, fibroblasts, and neurons, the cytoskeletal composition does not necessarily need a thorough overhaul. Usually, slight compositional variation or introduction of active processes, i.e., molecular motors, is often sufficient to generate this rich pool of structural appearances. Additionally, many other cellular components contribute to the mechanical behavior.

The main actors in this scenario are the nucleus, the cytoskeleton, and the cell membrane. While these structures are functionally and mechanically intertwined, effects can be specifically attributed to certain subcellular structures. Whole-cell deformations like squeezing or stretching of the cell body are mostly affected by the cytoskeleton as it is the most extensive structure in the cell. Small deformations in the linear regime (up to 5% [58]) are dominated by actin and intermediate filaments [76]. For larger deformations between 5 and 25% strains, nonlinear effects of the actin cytoskeleton can result in nonlinear responses, e.g., strain stiffening [77–79] and—paradoxically—also strain softening [80, 81] (the paradox is resolved in [58]). Even larger elongations are intercepted by microtubules and ultimately limited by the integrity of the membrane. Lamellipodia and other protrusions also rely on the stabilization by cytoskeletal filaments. Nuclear mechanics come into play when cells are moving in narrow spaces or are heavily compressed [82, 83]. Passing of narrow channels is dependent on the viscous response of the nucleus to such confinement [83–85], and the nuclear lamina will actively respond to environmental stiffness [86, 87]. The mechanical response of cells is also influenced by their membrane, and diseases such as cancer can often cause membrane alterations [88, 89]. Small indentations (tenth of cell diameter) and pulling forces (sub-nano-Newton) are a matter of membrane bending rigidity, while global (and quasi-global) indentations are influenced by effective membrane tension [89, 90]. Furthermore, membrane rigidity influences the extent of mechanosensing signaling pathways. This also holds for self-induced invaginations and blebbing, i.e., exo- and endocytosis, receptor binding, and treadmilling. When discussing processes beyond these

circumstances and on the scale of a whole cell, the entanglement of these differently behaving structures has to be taken into account. Still, the cytoskeleton can be considered the most influential part of the cell regarding mechanical behavior.

The strong influence of the cytoskeleton on the overall mechanical properties is striking when looking at the elastic modulus E of most cells. It ranges from unexpected low values [52] of some hundred Pa in glial or neuronal cells [91] to tens of kPa in human thrombocytes [92], illustrating the high variability and adaptivity of cells compared to classical and synthetic materials. As parts of the cytoskeleton are in constant treadmilling, appearance and mechanical structure are not persistent and allow the cell to adapt to its environment, rendering the cytoskeleton self-regulatory.

From the broad range of elastic moduli of different cell types and completely different functions, it is apparent that cell mechanics is a vital component of cellular functioning [93–97] including mitosis, where the cytoskeleton undergoes a significant overhaul enabling controlled cell division [98].

5.4.1 Probing Techniques

Cell rheology probes the response of cells to applied disturbances. As already explained in detail in the rheology chapter, responses and disturbances are usually forces and deformation or vice versa. Since material parameters like the complex shear modulus are in principle independent of the probing technique, a variety of techniques have been established based on different physical concepts to generate stresses or strains. Table 5.1 summarizes the most common probing techniques for single cells. Another reason for this variety is that every technique has its own working range of stresses and strains and temporal resolution and probes a cell either locally or globally. Nonetheless, due to the high structural heterogeneity of single cells including local mechanical alterations, it has turned out that directly comparable, consistent results are difficult to obtain. One eminent question is *what* exactly is probed since the main components of the cytoskeleton already differ in their mechanical properties. Also, adherent cells, which form prominent stress fibers on substrates [99], differ in their responses from suspended cells, in which actin conglomerates to a shell-like cortex below the membrane [100, 101]. It remains an open question whether (and how) results obtained for adhered and suspended cells compare.

The comparably simple and inexpensive micropipettes were one of the first tools for characterizing cell mechanics via micropipette aspiration [117], albeit it is limited by inherently lower throughput due to long preparation and measurement times. In the earliest application of this method, blood cells with different diameters were used and analyzed with regard to their response to higher or lower suction pressure (=stress). In general, any suspended cell can be probed including isolated cells from tissues [103]. If a very small pipette diameter is chosen, the local mechanical properties can be probed, whereas larger pipettes can be used to suck in cells for global probing on time scales from seconds to hours [102], and deformations far from the linear regime can be obtained.

Table 5.1 Cell mechanics probing techniques

Technique	Range of application
Micropipette aspiration 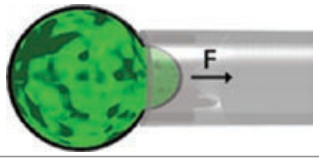	Local or global probing of strain and stress depending on diameter Time range 1–1000 s [102, 103]
AFM/SFM indentation 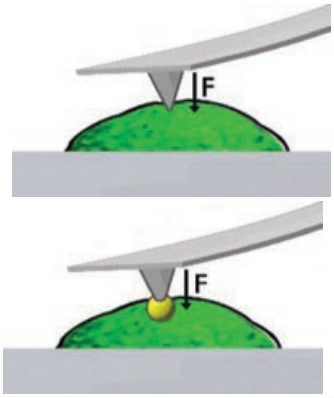	Low and high strains possible Local or averaged probing Frequency range 1–300 Hz Force range pN–nN [93, 104, 105]
Active and passive optical trap rheology 	Probing of overall force and fraction of force transmitted to the environment Local or global probing of stresses (Pa) Force range pN–nN [106]
Passive bead rheology 	Passive method Local properties of viscosity via diffusion Energies of order k_BT [107–109]
Magnetic bead rheology 	Local probing of elastic response Frequency range 0.01–1000 Hz Torques up to 130 Pa, linear [54, 110]
Optical stretcher 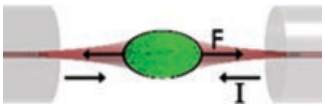	Local or global probing of stresses (Pa) Forces 0.1 nN Small strains of 1−10% [97, 101, 111–113]
Real-time deformation cytometer (RT-DC) 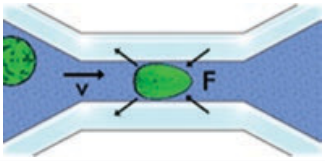	Global probing of deformation under high pressures Stresses up to 500 Pa [114–116]
Micro-constriction array 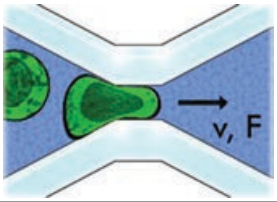	Global probing of deformation of cells Cell nuclei deformation probing Stresses up to 400 Pa [83]

Another well-established method to determine mechanical properties of cells, which can be also extended to small tissue samples, is atomic (scanning) force microscope (AFM). Depending on the geometry of the cantilever, cells can be probed very locally by using a pointy tip [93], broadly locally by using a beaded tip [91, 104, 118], or globally by using a flat tip [119]. In terms of stress and strain application, the AFM is versatile, allowing indention times from milliseconds to minutes, only limited by drifting of experimental stages (which can be stabilized with slight sophistication [120]). The force application ranges from pN to nN, including forces beyond the linear limit [121, 122]. Furthermore, using an oscillating cantilever to induce oscillatory stresses allows complex shear modulus measurements [41, 105]. One drawback of the AFM is the comparably low throughput due to possible long preparation times of the experiments, and since adherent cells are very flat, substrate stiffness and roughness affect the results and have to be considered [104]. Stretching of cells can also be done by letting the cell adhere to the cantilever first and subsequently pulling it away [123].

To circumvent the bottleneck of low throughput, further techniques make use of parallel preparation of cells by incorporating tracing beads and using passive Brownian motion (passive microrheology) or probing beads and actively displacing them (active microrheology) [124, 125]. The established method of analysis is based on cross-correlation of the motion of different beads and correction for local heterogeneities [109, 126]. Since artificial beads may be invasive, naturally present "tracers" such as storage granules, mitochondria, and other submicron particles were used with success [108, 127].

With the small size of the beads relative to cell size, both active and passive microrheologies are best suited to probe local rather than global mechanical properties. As microrheology is a contact method, it is highly dependent on the type and strength of linkage between the beads and the surrounding cellular structures [124, 128] and, due to the heterogeneity of cells, a controlled binding affinity is yet to be achieved [124].

The most common active microrheological method is magnetic twisting cytometry, which involves manipulation (usually twisting) of magnetic beads with an external magnetic field [54, 110, 129]. Since oscillating magnetic fields can be easily generated, many cells can be probed in parallel at once across a range of over four decades of frequencies. Limiting factors degrading measurement accuracy, however, include the exact determination of the bead's magnetic moment along with bead-to-bead variation and the applied external magnetic field.

All probing techniques discussed so far are contact based and are therefore prone to be invasive and might measure cell mechanics in an altered state. Furthermore, for all techniques, cells have to be at least weakly adherent, introducing additional problems due to substrate influences even for techniques based on optically trapped probing beads [106]. These limitations and difficulties can be overcome by using optical manipulation and microfluidic techniques to measure single suspended cells.

For optical manipulation, the optical stretcher has been established. This technique is based on the momentum transfer of photons on interfaces with changing refractive indices. Two antiparallel laser fibers with divergent beam profiles can

generate an optical pressure force [130] enabling optical trapping at lower laser powers and deformation of cells at higher powers [101]. The optical stretcher can apply step stresses over a time-range from 0.1 s to tens of seconds, enabling creep compliance measurements [111, 112]. Applied stresses are in the Pa range, corresponding to sub-nano-Newton forces, which depend on fiber-to-fiber distance and cell size. Cell mechanics can be probed locally for large cells and small fiber distances or globally for small cells and increased fiber distances. Since cells can be optically trapped for a prolonged period of time, active responses of single cells can be observed, for instance, active contractions of cells under force load [131]. Oscillatory stress application is also possible, however, with the restriction that only positive stresses (stretching of cells) and no negative stresses (squeezing of cells) can be applied [132, 133]. Therefore, the stress pattern will include an offset stress: $\sigma(t) = \sigma_0 + \sigma_0 \sin(\omega t)$. Embedded in a microfluidic setup, the optical stretcher allows serial measurements of up to 300 cells per hour and subsequent sorting, which can be challenged by the global heterogeneity of cell stiffness [97, 101].

Related techniques are able to deform cells in a similar contact-free manner but are based on hydrodynamic instead of optical forces [116]. Here, cells are pushed through capillaries in a continuous flow. Sudden changes in capillary geometry alter the flow profile locally. Shear flow velocities are applied that are sufficient to generate force differences large enough to deform whole-cell bodies. With these techniques, immense throughputs can be achieved [114–116]. However, the very limited observation time for one cell (millisecond range) impedes long-term deformation measurement, reducing measurable cell mechanics to the relative deformation of the cells after entering the measurement channel, i.e., the (time-independent) elastic modulus E.

Further details and comparisons of the different commonly applied probing techniques can be found in [52, 55, 60, 121, 134, 135].

5.4.2 Comparability and Interpretation

The broad range of experimental techniques and their intrinsic advantages and disadvantages make it challenging to compare results obtained with different techniques, especially quantitative results. Responses of suspended and adherent cells (as well as resting and migrating) will inherently differ from each other due to their altered geometries. Furthermore, probing a cell locally might not yield the same results as probing it globally. Even focusing on a single technique, defining the mechanical properties of a certain cell type is already nontrivial as cell-type stiffness follows a broad, non-Gaussian distribution (which can be tackled by averaging over many cells in large cell monolayer shear measurements [136]).

Despite the given quantitative challenges, the broad range of experimental techniques has yielded a comprehensive qualitative picture of cell mechanics covering various orders of stress and strain regimes [52, 124]. For instance, measurements with different techniques show a common power-law behavior of the complex shear modulus with only a slightly varying power-law exponent [107, 124, 134, 137, 138].

Nonetheless, in order to compare experimental techniques, one has to overcome some drawbacks of these techniques, which often involve poor statistics and the lack of standardized measurement protocols. For some of the methods presented here, it is difficult to obtain enough data during the short time in which the mechanical properties are altered actively in response to environmental changes. On the other hand, the diversity of probing techniques is also an advantage. As different cell types occur in different environments, cell mechanics differ to suit their environment, e.g., red blood cells are more elastic since they have to squeeze through capillaries [11]. Thus, the most suitable technique for a given cell type can be chosen. Suspended cells like RBCs, for instance, can be measured more easily and rapidly in an optical stretcher or real-time deformation cytometer [83, 112, 115, 139].

5.5 Tissues

The mechanics of systems consisting of multiple cells are changed drastically by two elements that are not present at the single-cell level: adhesive contacts between cells and between cells and the extracellular matrix (ECM), enabling active responses of cells to their neighbors. Cell–cell communication via very basic interactions, such as chemical feedback loops, can already lead to collective behavior of cells, e.g., swarm-like collective migration of keratinocytes [140] and collective cell migration during invasion and metastatic spread of malignant tumors [141]. Furthermore, strength and type of adhesive contacts direct force transmission and modulate cell migration and motility. As a consequence, cells can show collective structural behavior on different length scales ranging from organization of smaller subdomains in tissues with individual properties up to global quasi-frozen, glass-like states with no (relative) cell migration as in epithelial layers [142], which commonly occurs as soon as increased adhesion force and cell density are introduced. Since active processes of tissues are emergent phenomena, they can strongly influence mechanical responses. Adhesive cell–cell contacts and ECM can highly contribute to the stiffness and fluidity of tissues and span a phase space ranging from quasi-solid responses, e.g., epithelial tissue, to quasi-fluid materials such as migratory cells in mesenchymal tissues.

5.5.1 Cell–Cell and Cell–Matrix Adhesion

Most types of cell adhesion are mediated by proteins of the family of cell adhesion molecules (CAMs). CAMs are typically transmembrane proteins with binding sites for the cytoskeleton as well as sites for *trans*- and *cis*-interactions with other CAMs or the ECM in the extracellular domain. In addition to adhesion, they function as cytoskeletal anchors and play significant roles in mechanosignaling [11], which elegantly illustrates the intertwined nature of the different levels of complexity.

CAMs are often calcium dependent, and one of the most prominent CAM families is cadherins (a portmanteau word combining *ca*lcium and *adherin*g). Cadherins come in three flavors and are usually associated with certain tissues (but are not restricted to these): E-cad, epithelial cells; N-cad, neuronal cells, and P-cad, pancreatic cells. They can appear as single free molecules but are usually ordered as nanoclusters linked to actin or as more complex desmosomes linked to the keratin cytoskeleton [143]. Differences in the function of these proteins are still under investigation, but changes in their expression rate can be correlated to changes of phenotype and behavior. In epithelial-to-mesenchymal transition (EMT), for example, cells lose their well-structured belt-like distribution of E-cadherins in favor of P- and N-cadherins [144]. At the same time, cells will regain their ability to move through tissue, a hallmark step in tumorigenesis and metastasis [145, 146]. In malignant tumors, this switch can promote directed invasion into the surrounding tissue of small cell clusters, often regulated by messenger RNA (mRNA). For instance, upregulation of miR-9, a short, noncoding RNA gene involved in gene regulation, leads to increased cell motility and invasiveness [147]. The increased expression of P-cad triggers polarization and directed movement [148]. This results in cells moving in single file (Indian filing) out of the tumor, with a tumor cell or fibroblast as the leading cell [149]. The polarization of the fibroblast that moves away from the cancer cells is mediated by N-cad adhesive sites [150].

Contact to the ECM is mainly established by integrins, which consist of two subunits, the α- and β-units, and can bind collagen, glycoproteins of the ECM (e.g., fibronectin), or both. There are several types of α- and β-units and consequentially a broad range of different integrins. Like cadherins, they cluster into functional domains by focal adhesions. Binding of integrins to extracellular structures induces signaling cascades that intervene with basic cellular functions such as cell growth and apoptosis. Depending on the range of expression of different integrins, and subsequently the composition of focal adhesions, signaling pathways can be promoted or suppressed. Integrins such as $\alpha_v\beta_3$ or $\alpha_5\beta_1$, for instance, are often found in cancer cells and seem play a role in cancer development. They influence the mechanical behavior [151], invasiveness in ECM-rich surroundings [152], and cellular survival [153]. In addition, some integrins are known to form complexes with growth factors that induce EMT [154] and increase proliferation [155].

The mechanical feedback of cell–cell and cell–ECM interactions is a fundamental parameter for cellular regulation and shows its drastic influence in diseases such as cancer [156]. Cells can modify their morphology and mechanical properties in response to a changing microenvironment [99]. Especially since cells can and do modulate their ECM and CAMs, they can be a strong promoter of metastasis formation [157]. This active reaction of cells to their microenvironment becomes stronger with increasing malignancy, e.g., metastatic cells can mimic mechanical properties of neuronal cells [158] by reactivating (epigenetically) silenced genes [159–161].

5.5.2 Tissue Dynamics and Collective Cell Behavior

It is a great challenge to define simple mechanical parameters for tissues. At small time scales and low strains, tissues show frequency-dependent complex shear moduli [162]. At larger time scales, tissues can lose their viscoelastic behavior and show fluidlike mechanics—usually coupled to movement of single cells in the tissue and in a regime far from equilibrium dynamics. The two established main models describe tissues as glass-like, amorphous materials or as yield stress fluids. With both models, the active contribution of cells in the system is of interest. Softness of the cell body, adhesion strength to neighboring cells, and matrix as well as active forces determine whether a cell is able to migrate or not [163].

Analogies to glassy materials can be found in liquid- to solid-like glass transition. When the temperature of a glassy material drops below the glass transition point, molecules are strongly confined in their motion and fixed in a chaotic lattice. A cell system that reaches a certain density due to proliferation will exhibit similar behavior. Additionally, density-independent transitions can be observed when adhesion and stiffness of cells are modulated [164]. Inhibited migration and proliferation mark the point at which the system goes into a static (glassy) state [165, 166], a concept which can be transferred to tissues under high stresses. Epithelial layers, for example, have been shown to exert constant pulling forces that can influence their behavior [167].

Yield stress fluids show viscoelastic behavior to the point where a certain energy barrier has been overcome, when the material will start to flow. In this model, single-cell mechanics and stresses acting on the tissue are the main contributors [168]. Stress on the tissue, intrinsic or extrinsic, interacts with local adhesive mechanics, giving rise to either fluidlike or solid-like behavior. Especially homeostatic stresses determine the flow of the tissue, and a tissue with higher homeostatic stress will invade surrounding tissues either as small, separate islands or as a front [169] (Fig. 5.7A1, A2).

In both cases, transitions can occur for the whole tissue at once, cell clusters in confinement, or for single cells within a tissue. Even when a tissue is above the transition point and remains static, some cells might be in a different state and still able to pass through it (Fig. 5.7).

A rheological approach to access the different states of tissues is measuring phase angle δ. Although this approach does not account for active cell migration, it allows estimating the fluidity of the tissue. δ near 0° (purely elastic) indicates a jammed state, while viscous, flowing tissue approaches 90°. To probe local properties of tissues, scanning force microscopy can be employed to create a map of viscoelasticity of a tissue slice that can be attributed to processes in the sample [170]. With standard bulk shear rheometers, global measurements can be performed to determine the overall viscoelastic properties [171]. Methods such as magnetic resonance elastography enable direct measurement of complex shear moduli of a whole tissue or with spatial resolution [162, 172].

When parameters of single cells, such as adhesive and viscoelastic properties, are known, these can be used to draw conclusions regarding tissue dynamics. The differential adhesion hypothesis (DAH) states that a mixture of cells

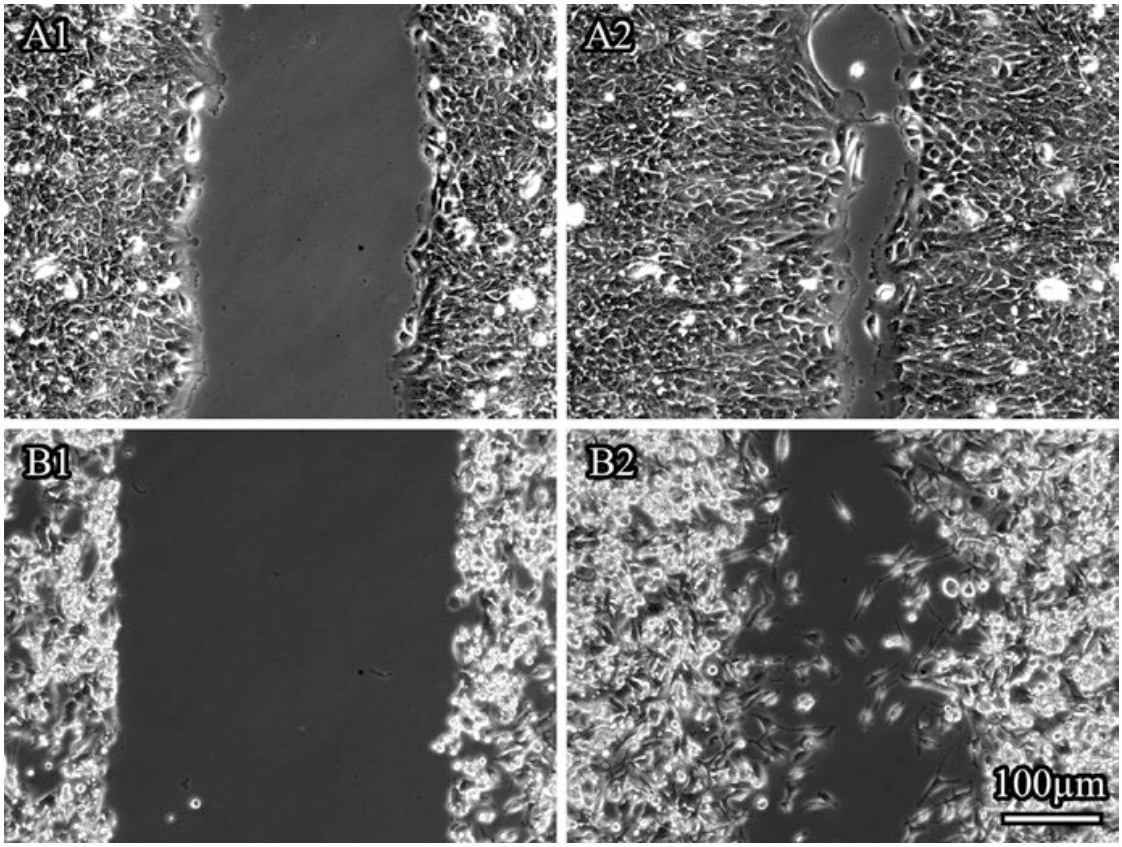

Fig. 5.7 Wound-healing assay of two different cell types. In the upper panel, A1 and A2, an epithelial cell layer starts at a certain time (A1) and closes the wound after 30 h (A2). The epithelial cell layer maintains its cell front and shows a coordinated, collective motion. A mesenchymal cell layer, B1 and B2, loses its front (B1) in this process and shows randomly walking single cells and no coordinated, collective motion after 30 h (B2)

with different adhesiveness develops into an ordered state, separating subpopulations accordingly [173]. The DAH holds true in morphogenesis, where cells demix like fluids with different surface tensions [174], but fails for cancer development. When cells undergo EMT, demixing can be observed, which seems to follow a more complex behavior [175]. Local jamming, unjamming, and tumor cell invasion are strongly related to these observations. When a malignant neoplasm forms, it constitutes a clearly separated bulk of tissue within the healthy stroma. Cells in the tumor exhibit altered mechanical behavior and heavily remodel the ECM, but there is no obvious reason why a distinct boundary exists. As soon as the cells lose their epithelial phenotype, they show increased invasion [176]. Still, the primary tumor grows to a certain size before cells escape, which might have its origins in cellular jamming. Fibrosis, for instance, leads to a very stiff ECM [177], and the growth of the tumor creates pressure on the surrounding tissue and the tumor itself [178]. In other words, the tumor embeds itself in a strong matrix. This goes hand in hand with a tumor being a rigid mass, although single malignant cells tend to be softer when becoming more invasive [179]. While the self-driven confinement creates a jammed state within the tumor [180], the mechanical feedback leads to further

transitioning toward more malignant phenotypes [181]. Over time, the distribution of cellular softness becomes broader [97], and expression of CAMs is altered [144] up to the point where some cells undergo an unjamming transition and start to move out of the tumor [182]. It has to be noted that this cellular escape does not occur in a random pattern. Similar to embryogenesis, where cells follow the DAH, self-organization within the tissue is the first step. Collective migration in 2D assays can be observed, when the confluency of the layer confines cells, before the layer becomes jammed [183] (Fig. 5.7 A2). In 3D, this cellular streaming has also been observed: small conglomerates of cells in an unjammed state form and migrate collectively, often following a leader cell [184]. This marks the start of metastatic spread, and the moment at which invasion begins heavily depends on the individual neoplasm. Some tumors will grow to immense sizes over months or even years before cells pass the boundaries, while others metastasize within weeks of the original tumor formation.

Conclusion

The eukaryotic cell is well studied with decades of research dedicated to various branches and aspects ranging from classification of whole-cell types down to molecular details of protein folding processes [11, 185]. With the advancement of techniques and detailed insights into biological matter, the cause and effect of many diseases could be attributed to certain functional or structural units and levels of complexity within the cell; for instance, sickle cell disease is often caused by only a single-nucleotide polymorphism (SNP) of the beta-globin gene, which results in strand-like clustering of defective hemoglobin and consequently stiffening of red blood cells [186, 187]. Especially cancer—as one of the most prominent maladies—is well studied on many levels of complexity [188], and crucial developmental steps and many biological changes in tumorigenesis were found and described [145, 146]. The development of cancer is accompanied by major changes of the cytoskeleton, which are necessary for cancer cells to migrate and invade other tissues [97, 189]. The cytoskeleton usually gets softer with increased malignancy, as shown with different cellular probing techniques [115, 116, 179, 188–194]. These important insights render rheological material characterization of a viable tumor marker. At the tissue level, however, tumors are found to be stiffer than healthy surrounding tissue due to a stiffer stroma and elevated cytoskeletal tension [177] although they are constituted of softer cells. While many emergent phenomena on the microtissue level will influence mechanical properties, many of them are physically characterized and quantified. While the biophysics of tumorigenesis and tissue mechanics is qualitatively well studied. Still, the quantitative description of demixing, jamming, and surface tension is under current investigation and remains promising with ongoing research on this frontier of science [163, 164, 183, 195–201].

Acknowledgments We thank Till Möhn, Jürgen Lippoldt, Martin Glaser and Benjamin Wolf for their very helpful comments, discussions, advices for illustrations, and language editing.

Glossary

*Self-organization***:** Self-organization is an active, non-equilibrium process of an open system where energy is constantly dissipated and needs to be resupplied, for instance, to generate forces (such as the actin–myosin power stroke) or to organize dynamic structures (such as the lamellipodium for cell migration) far from the thermodynamic equilibrium [10].

Self-assembly: Self-assembly processes are solely based on equilibrium dynamics and are independent of energy dissipation. They occur spontaneously and tend to minimize the free energy of the system driving it toward its thermodynamic equilibrium without an additional energy source such as ATP or GTP. Self-assembly can occur in closed systems [10].

Persistence Length: Mechanical property quantifying the stiffness of a polymer relative to its length. The length scale on which the direction vectors of both ends of a filament lose their correlation.

Bending Stiffness: The resistance of a beam with unit diameter and length while undergoing bending. The higher the bending stiffness, the harder to flex the unit beam.

Molecular Motors: Molecular machines which consume energy (e.g., ATP, GTP) and convert it into motion or mechanical work.

Treadmilling: Steady-state phenomenon of cytoskeletal filaments, mostly actin, where one filament end depolymerizes and the other end polymerizes, leading to shrinkage and growth at the ends with no net length change of the filament.

Tensile Creep Compliance: The magnitude of the creep response of a unit bulk material for a given unit force load. The higher the tensile creep compliance, the easier it deforms under force load.

Elastic Modulus (Young's Modulus) or Shear Modulus: The resistance of a unit bulk material under axial load or under shearing load, respectively. The higher the elastic modulus or shear modulus, the harder to deform the material. In incompressible materials, the elastic modulus is three times the shear modulus.

Exocytosis: Active transport of molecules out of the cell via a secretory vesicle as transport carrier.

Endocytosis: Active transport of molecules into the cell via encapsulation of the molecules with the cell membrane and formation of a vesicle as transport carrier.

Receptor Binding: Binding of signaling molecules to transmembrane proteins used for cellular and tissue response.

Mechanosignaling: Sensing and signaling of cells induce a response to mechanical, environmental cues.

Glass-like Material: Solid-phase state of a material, where the strong, non-crystalline entanglement of the molecules, usually polymer chains, prevents an unhindered liquid-like flow and movement of the molecules for low thermal energy. Above the glass transition temperature, the material can flow again.

Amorphous Material: Noncrystalline solid with no long-range order, usually consisting of many clustered domains with different (crystalline) orientations and substructures.

Yield Stress Fluid: A fluid which only starts to flow above a critical stress, the yield stress. For stresses below the yield stress, it behaves like a solid.

Homeostatic Stress: Internal stress of a tissue generated by adhesion forces, which is actively regulated to remain close to constant.

Differential Adhesion Hypothesis: Hypothesis for cellular movement in tissues of different cell types based on thermodynamic principles. Cells with different adhesion forces will minimize their free energy by moving to other cells with similar adhesion forces in order to maximize bonding strength.

Jamming: A quasi-phase transition of a material, where rigidity suddenly increases and fluidity suddenly decreases when the density of cells (or molecules) increases above a critical level.

References

1. Anderson PW. More is different. Science. 1972;177(4047):393–6. https://doi.org/10.1126/science.177.4047.393.
2. Laughlin RB, Pines D. The theory of everything. Proc Natl Acad Sci U S A. 2000;97(1):28–31. https://doi.org/10.1073/pnas.97.1.28.
3. Schrödinger E. What is life?: the physical aspect of the living cell, Canto. Cambridge: Cambridge University Press; 2010.
4. Ryan AJ. Emergence is coupled to scope, not level. Complexity. 2007;13(2):67–77. https://doi.org/10.1002/cplx.20203.
5. Dawkins R The blind watchmaker: why the evidence of evolution reveals a universe without design. New edition [reissue] ed. New York: W. W. Norton; 1996.
6. Schuster P. A beginning of the end of the holism versus reductionism debate?: molecular biology goes cellular and organismic. Complexity. 2007;13(1):10–3. https://doi.org/10.1002/cplx.20193.
7. Huber F, Schnauss J, Ronicke S, et al. Emergent complexity of the cytoskeleton: from single filaments to tissue. Adv Phys. 2013;62(1):1–112. https://doi.org/10.1080/00018732.2013.771509.
8. Huber F, Kas J. Self-regulative organization of the cytoskeleton. Cytoskeleton. 2011;68(5):259–65. https://doi.org/10.1002/cm.20509.
9. Halley JD, Winkler DA. Classification of emergence and its relation to self-organization. Complexity. 2008;13(5):10–5. https://doi.org/10.1002/cplx.20216.
10. Halley JD, Winkler DA. Consistent concepts of self-organization and self-assembly. Complexity. 2008;14(2):10–7. https://doi.org/10.1002/cplx.20235.
11. Alberts B. Molecular biology of the cell: [MBOC]. 6th ed. New York: GS Garland Science; 2015.
12. Doi M, Edwards SF. The theory of polymer dynamics, The international series of monographs on physics, vol. 73. Oxford: Clarendon Press; 2003.
13. Schuldt C, Schnauß J, Händler T, et al. Tuning synthetic semiflexible networks by bending stiffness. Phys Rev Lett. 2016;117(19):197801. https://doi.org/10.1103/PhysRevLett.117.197801.
14. Isambert H, Venier P, Maggs A, et al. Flexibility of actin filaments derived from thermal fluctuations. Effect of bound nucleotide, phalloidin, and muscle regulatory proteins. J Biol Chem. 1995;270(19):11437–44. https://doi.org/10.1074/jbc.270.19.11437.

15. Isambert H, Maggs AC. Dynamics and rheology of actin solutions. Macromolecules. 1996;29(3):1036–40. https://doi.org/10.1021/ma946418x.
16. Greenberg MJ, Wang C-LA, Lehman W, et al. Modulation of actin mechanics by caldesmon and tropomyosin. Cell Motil Cytoskeleton. 2008;65(2):156–64. https://doi.org/10.1002/cm.20251.
17. Janson ME, Dogterom M. A bending mode analysis for growing microtubules: evidence for a velocity-dependent rigidity. Biophys J. 2004;87(4):2723–36. https://doi.org/10.1529/biophysj.103.038877.
18. Yin P, Hariadi RF, Sahu S, et al. Programming DNA tube circumferences. Science. 2008;321(5890):824–6. https://doi.org/10.1126/science.1157312.
19. Schiffels D, Liedl T, Fygenson DK. Nanoscale structure and microscale stiffness of DNA nanotubes. ACS Nano. 2013;7(8):6700–10. https://doi.org/10.1021/nn401362p.
20. Glaser M, Schnauß J, Tschirner T, et al. Self-assembly of hierarchically ordered structures in DNA nanotube systems. New J Phys. 2016;18(5):55001. https://doi.org/10.1088/1367-2630/18/5/055001.
21. Pollard TD, Blanchoin L, Mullins RD. Molecular mechanisms controlling actin filament dynamics in nonmuscle cells. Annu Rev Biophys Biomol Struct. 2000;29:545–76. https://doi.org/10.1146/annurev.biophys.29.1.545.
22. Schnauß J, Händler T, Käs J. Semiflexible biopolymers in bundled arrangements. Polymers. 2016;8(8):274. https://doi.org/10.3390/polym8080274.
23. Schnauss J, Golde T, Schuldt C, et al. Transition from a linear to a harmonic potential in collective dynamics of a multifilament actin bundle. Phys Rev Lett. 2016;116(10):108102. https://doi.org/10.1103/PhysRevLett.116.108102.
24. Lansky Z, Braun M, Ludecke A, et al. Diffusible crosslinkers generate directed forces in microtubule networks. Cell. 2015;160(6):1159–68. https://doi.org/10.1016/j.cell.2015.01.051.
25. Braun M, Lansky Z, Hilitski F, et al. Entropic forces drive contraction of cytoskeletal networks. BioEssays. 2016;38(5):474–81. https://doi.org/10.1002/bies.201500183.
26. Ward A, Hilitski F, Schwenger W, et al. Solid friction between soft filaments. Nat Mater. 2015;14(6):583–8. https://doi.org/10.1038/nmat4222.
27. Hilitski F, Ward AR, Cajamarca L, et al. Measuring cohesion between macromolecular filaments one pair at a time: depletion-induced microtubule bundling. Phys Rev Lett. 2015;114(13):138102. https://doi.org/10.1103/PhysRevLett.114.138102.
28. Huber F, Strehle D, Schnauß J, et al. Formation of regularly spaced networks as a general feature of actin bundle condensation by entropic forces. New J Phys. 2015;17(4):43029. https://doi.org/10.1088/1367-2630/17/4/043029.
29. Daniel JL, Molish IR, Robkin L, et al. Nucleotide exchange between cytosolic ATP and F-actin-bound ADP may be a major energy-utilizing process in unstimulated platelets. Eur J Biochem. 1986;156(3):677–83. https://doi.org/10.1111/j.1432-1033.1986.tb09631.x.
30. Bernstein BW, Bamburg JR. Actin-ATP hydrolysis is a major energy drain for neurons. J Neurosci. 2003;23(1):1–6.
31. Block J, Schroeder V, Pawelzyk P, et al. Physical properties of cytoplasmic intermediate filaments. Biochim Biophys Acta. 2015;1853(11 Pt B):3053–64. https://doi.org/10.1016/j.bbamcr.2015.05.009.
32. Herrmann H, Bar H, Kreplak L, et al. Intermediate filaments: from cell architecture to nanomechanics. Nat Rev Mol Cell Biol. 2007;8(7):562–73. https://doi.org/10.1038/nrm2197.
33. Herrmann H, Aebi U. Intermediate filaments: molecular structure, assembly mechanism, and integration into functionally distinct intracellular scaffolds. Annu Rev Biochem. 2004;73:749–89. https://doi.org/10.1146/annurev.biochem.73.011303.073823.
34. Howard J, Hyman AA. Dynamics and mechanics of the microtubule plus end. Nature. 2003;422(6933):753–8. https://doi.org/10.1038/nature01600.
35. Vavylonis D, Yang Q, O'Shaughnessy B. Actin polymerization kinetics, cap structure, and fluctuations. Proc Natl Acad Sci U S A. 2005;102(24):8543–8. https://doi.org/10.1073/pnas.0501435102.

36. Footer MJ, Kerssemakers JWJ, Theriot JA, et al. Direct measurement of force generation by actin filament polymerization using an optical trap. Proc Natl Acad Sci U S A. 2007;104(7):2181–6. https://doi.org/10.1073/pnas.0607052104.
37. Howard J. Mechanics of motor proteins and the cytoskeleton. Sunderland: Sinauer Associates; 2006.
38. Lockot HW, Uhlig S. Bibliographia aethiopica, Aethiopistische forschungen, vol. 41. Wiesbaden: Steiner; 1998.
39. Bell A, Macfarquhar C. Encyclopaedia britannica: or, a dictionary of arts and sciences, three volumes. Scotland: Edinburgh; 1771.
40. Borel F, Taylor JB, Paris IM. The splendor of ethnic jewelry: from the Colette and Jean-Pierre Ghysels collection, Pbk. ed. New York: H. N. Abrams; 2001
41. Mahaffy RE, Shih CK, MacKintosh FC, et al. Scanning probe-based frequency-dependent microrheology of polymer gels and biological cells. Phys Rev Lett. 2000;85(4):880–3. https://doi.org/10.1103/PhysRevLett.85.880.
42. Chen EJ, Novakofski J, Jenkins WK, et al. Young's modulus measurements of soft tissues with application to elasticity imaging. IEEE Trans Ultrason Ferroelect Freq Contr. 1996;43(1):191–4. https://doi.org/10.1109/58.484478.
43. Rho J-Y, Kuhn-Spearing L, Zioupos P. Mechanical properties and the hierarchical structure of bone. Med Eng Phys. 1998;20(2):92–102. https://doi.org/10.1016/S1350-4533(98)00007-1.
44. Rho JY, Ashman RB, Turner CH. Young's modulus of trabecular and cortical bone material: ultrasonic and microtensile measurements. J Biomech. 1993;26(2):111–9. https://doi.org/10.1016/0021-9290(93)90042-D.
45. Akhtar R, Sherratt MJ, Cruickshank JK, et al. Characterizing the elastic properties of tissues. Mater Today. 2011;14(3):96–105. https://doi.org/10.1016/S1369-7021(11)70059-1.
46. Yanniotis S, Skaltsi S, Karaburnioti S. Effect of moisture content on the viscosity of honey at different temperatures. J Food Eng. 2006;72(4):372–7. https://doi.org/10.1016/j.jfoodeng.2004.12.017.
47. Kesmarky G, Kenyeres P, Rabai M, et al. Plasma viscosity: a forgotten variable. Clin Hemorheol Microcirc. 2008;39(1-4):243–6.
48. Zhou EH, Martinez FD, Fredberg JJ. Cell rheology: mush rather than machine. Nat Mater. 2013;12(3):184. https://doi.org/10.1038/nmat3574.
49. Spence AJ. Scaling in biology. Curr Biol. 2009;19(2):R57–61. https://doi.org/10.1016/j.cub.2008.10.042.
50. Brown JH, West GB, editors. Scaling in biology. Santa Fe Institute studies in the sciences of complexity. Oxford: Oxford University Press; 2000.
51. West GB. A general model for the origin of allometric scaling laws in biology. Science. 1997;276(5309):122–6. https://doi.org/10.1126/science.276.5309.122.
52. Kollmannsberger P, Fabry B. Linear and nonlinear rheology of living cells. Annu Rev Mater Res. 2011;41(1):75–97. https://doi.org/10.1146/annurev-matsci-062910-100351.
53. Sandersius SA, Newman TJ. Modeling cell rheology with the subcellular element model. Phys Biol. 2008;5(1):15002. https://doi.org/10.1088/1478-3975/5/1/015002.
54. Fabry B, Maksym GN, Butler JP, et al. Scaling the microrheology of living cells. Phys Rev Lett. 2001;87(14):148102. https://doi.org/10.1103/PhysRevLett.87.148102.
55. Chen DT, Wen Q, Janmey PA, et al. Rheology of Soft materials. Annu Rev Condens Matter Phys. 2010;1(1):301–22. https://doi.org/10.1146/annurev-conmatphys-070909-104120.
56. Kroy K. Dynamics of wormlike and glassy wormlike chains. Soft Matter. 2008;4(12):2323. https://doi.org/10.1039/B807018K.
57. Kroy K, Glaser J. The glassy wormlike chain. New J Phys. 2007;9(11):416. https://doi.org/10.1088/1367-2630/9/11/416.
58. Wolff L, Fernandez P, Kroy K. Resolving the stiffening-softening paradox in cell mechanics. PLoS One. 2012;7(7):e40063. https://doi.org/10.1371/journal.pone.0040063.
59. Rodriguez ML, McGarry PJ, Sniadecki NJ. Review on cell mechanics: experimental and modeling approaches. Appl Mech Rev. 2013;65(6):60801. https://doi.org/10.1115/1.4025355.

60. Lim CT, Zhou EH, Quek ST. Mechanical models for living cells—a review. J Biomech. 2006;39(2):195–216. https://doi.org/10.1016/j.jbiomech.2004.12.008.
61. Herant M, Marganski WA, Dembo M. The mechanics of neutrophils: synthetic modeling of three experiments. Biophys J. 2003;84(5):3389–413. https://doi.org/10.1016/S0006-3495(03)70062-9.
62. Dai J, Ting-Beall HP, Hochmuth RM, et al. Myosin I contributes to the generation of resting cortical tension. Biophys J. 1999;77(2):1168–76.
63. Peskin CS, Odell GM, Oster GF. Cellular motions and thermal fluctuations: the Brownian ratchet. Biophys J. 1993;65(1):316–24. https://doi.org/10.1016/S0006-3495(93)81035-X.
64. Mogilner A, Oster G. Cell motility driven by actin polymerization. Biophys J. 1996;71(6):3030–45. https://doi.org/10.1016/S0006-3495(96)79496-1.
65. Kuusela E, Alt W. Continuum model of cell adhesion and migration. J Math Biol. 2009;58(1-2):135–61. https://doi.org/10.1007/s00285-008-0179-x.
66. Zimmerle CT, Frieden C. Effect of temperature on the mechanism of actin polymerization. Biochemistry. 1986;25(21):6432–8.
67. Kis A, Kasas S, Kulik AJ, et al. Temperature-dependent elasticity of microtubules. Langmuir. 2008;24(12):6176–81. https://doi.org/10.1021/la800438q.
68. Yengo CM, Takagi Y, Sellers JR. Temperature dependent measurements reveal similarities between muscle and non-muscle myosin motility. J Muscle Res Cell Motil. 2012;33(6):385–94. https://doi.org/10.1007/s10974-012-9316-7.
69. Oroian M, Amariei S, Escriche I, et al. A viscoelastic model for honeys using the time–temperature superposition principle (TTSP). Food Bioprocess Technol. 2013;6(9):2251–60. https://doi.org/10.1007/s11947-012-0893-7.
70. Kießling TR, Stange R, Käs JA, et al. Thermorheology of living cells—impact of temperature variations on cell mechanics. New J Phys. 2013;15(4):45026. https://doi.org/10.1088/1367-2630/15/4/045026.
71. Schmidt BUS, Kießling TR, Warmt E, et al. Complex thermorheology of living cells. New J Phys. 2015;17(7):73010. https://doi.org/10.1088/1367-2630/17/7/073010.
72. Joanny J, Prost J. Active gels as a description of the actin-myosin cytoskeleton. HFSP J. 2009;3(2):94–104. https://doi.org/10.2976/1.3054712.
73. Joanny J-F, Ramaswamy S. A drop of active matter. J Fluid Mech. 2012;705:46–57. https://doi.org/10.1017/jfm.2012.131.
74. Pearson JE. Complex patterns in a simple system. Science. 1993;261(5118):189–92. https://doi.org/10.1126/science.261.5118.189.
75. Strehle D, Schnauss J, Heussinger C, et al. Transiently crosslinked F-actin bundles. Eur Biophys J. 2011;40(1):93–101. https://doi.org/10.1007/s00249-010-0621-z.
76. Goldman RD, Khuon S, Chou YH, et al. The function of intermediate filaments in cell shape and cytoskeletal integrity. J Cell Biol. 1996;134(4):971–83.
77. Pourati J, Maniotis A, Spiegel D, et al. Is cytoskeletal tension a major determinant of cell deformability in adherent endothelial cells? Am J Physiol. 1998;274(5 Pt 1):C1283–9.
78. Wang N, Im T-N, Chen J, et al. Cell prestress. I. Stiffness and prestress are closely associated in adherent contractile cells. Am J Physiol Cell Physiol. 2002;282(3):C606–16. https://doi.org/10.1152/ajpcell.00269.2001.
79. Fernandez P, Pullarkat PA, Ott A. A master relation defines the nonlinear viscoelasticity of single fibroblasts. Biophys J. 2006;90(10):3796–805. https://doi.org/10.1529/biophysj.105.072215.
80. Trepat X, Deng L, An SS, et al. Universal physical responses to stretch in the living cell. Nature. 2007;447(7144):592–5. https://doi.org/10.1038/nature05824.
81. Krishnan R, Park CY, Lin YC, et al. Reinforcement versus fluidization in cytoskeletal mechanoresponsiveness. PLoS One. 2009;4(5):e5486. https://doi.org/10.1371/journal.pone.0005486.
82. Wolf K, Te Lindert M, Krause M, et al. Physical limits of cell migration: control by ECM space and nuclear deformation and tuning by proteolysis and traction force. J Cell Biol. 2013;201(7):1069–84. https://doi.org/10.1083/jcb.201210152.

83. Lange JR, Steinwachs J, Kolb T, et al. Microconstriction arrays for high-throughput quantitative measurements of cell mechanical properties. Biophys J. 2015;109(1):26–34. https://doi.org/10.1016/j.bpj.2015.05.029.
84. Friedl P, Wolf K, Lammerding J. Nuclear mechanics during cell migration. Curr Opin Cell Biol. 2011;23(1):55–64. https://doi.org/10.1016/j.ceb.2010.10.015.
85. Dahl KN, Ribeiro AJ, Lammerding J. Nuclear shape, mechanics, and mechanotransduction. Circ Res. 2008;102(11):1307–18. https://doi.org/10.1161/CIRCRESAHA.108.173989.
86. Swift J, Discher DE. The nuclear lamina is mechano-responsive to ECM elasticity in mature tissue. J Cell Sci. 2014;127(Pt 14):3005–15. https://doi.org/10.1242/jcs.149203.
87. Harada T, Swift J, Irianto J, et al. Nuclear lamin stiffness is a barrier to 3D migration, but softness can limit survival. J Cell Biol. 2014;204(5):669–82. https://doi.org/10.1083/jcb.201308029.
88. Händel C, Schmidt BUS, Schiller J, et al. Cell membrane softening in human breast and cervical cancer cells. New J Phys. 2015;17(8):83008. https://doi.org/10.1088/1367-2630/17/8/083008.
89. Braig S, Schmidt BUS, Stoiber K, et al. Pharmacological targeting of membrane rigidity: implications on cancer cell migration and invasion. New J Phys. 2015;17(8):83007. https://doi.org/10.1088/1367-2630/17/8/083007.
90. Gracià RS, Bezlyepkina N, Knorr RL, et al. Effect of cholesterol on the rigidity of saturated and unsaturated membranes: fluctuation and electrodeformation analysis of giant vesicles. Soft Matter. 2010;6(7):1472. https://doi.org/10.1039/b920629a.
91. Lu Y-B, Franze K, Seifert G, et al. Viscoelastic properties of individual glial cells and neurons in the CNS. Proc Natl Acad Sci U S A. 2006;103(47):17759–64. https://doi.org/10.1073/pnas.0606150103.
92. Radmacher M, Fritz M, Kacher CM, et al. Measuring the viscoelastic properties of human platelets with the atomic force microscope. Biophys J. 1996;70(1):556–67. https://doi.org/10.1016/S0006-3495(96)79602-9.
93. Radmacher M. Studying the mechanics of cellular processes by atomic force microscopy. In: Cell mechanics, vol. 83. London: Elsevier; 2007. p. 347–72.
94. Janmey PA, Winer JP, Murray ME, et al. The hard life of soft cells. Cell Motil Cytoskeleton. 2009;66(8):597–605. https://doi.org/10.1002/cm.20382.
95. Mierke CT, Rosel D, Fabry B, et al. Contractile forces in tumor cell migration. Eur J Cell Biol. 2008;87(8-9):669–76. https://doi.org/10.1016/j.ejcb.2008.01.002.
96. Engler AJ, Sen S, Sweeney HL, et al. Matrix elasticity directs stem cell lineage specification. Cell. 2006;126(4):677–89. https://doi.org/10.1016/j.cell.2006.06.044.
97. Fritsch A, Höckel M, Kiessling T, et al. Are biomechanical changes necessary for tumour progression? Nat Phys. 2010;6(10):730–2. https://doi.org/10.1038/nphys1800.
98. Thery M, Bornens M. Cell shape and cell division. Curr Opin Cell Biol. 2006;18(6):648–57. https://doi.org/10.1016/j.ceb.2006.10.001.
99. Yeung T, Georges PC, Flanagan LA, et al. Effects of substrate stiffness on cell morphology, cytoskeletal structure, and adhesion. Cell Motil Cytoskeleton. 2005;60(1):24–34. https://doi.org/10.1002/cm.20041.
100. Thoumine O, Cardoso O, Meister J-J. Changes in the mechanical properties of fibroblasts during spreading: a micromanipulation study. Eur Biophys J. 1999;28(3):222–34. https://doi.org/10.1007/s002490050203.
101. Wottawah F, Schinkinger S, Lincoln B, et al. Optical rheology of biological cells. Phys Rev Lett. 2005;94(9):98103. https://doi.org/10.1103/PhysRevLett.94.098103.
102. Schmid-Schönbein GW, Sung KL, Tözeren H, et al. Passive mechanical properties of human leukocytes. Biophys J. 1981;36(1):243–56. https://doi.org/10.1016/S0006-3495(81)84726-1.
103. Thoumine O, Ott A. Comparison of the mechanical properties of normal and transformed fibroblasts. Biorheology. 1997;34(4-5):309–26. https://doi.org/10.1016/S0006-355X(98)00007-9.
104. Mahaffy RE, Park S, Gerde E, et al. Quantitative analysis of the viscoelastic properties of thin regions of fibroblasts using atomic force microscopy. Biophys J. 2004;86(3):1777–93. https://doi.org/10.1016/S0006-3495(04)74245-9.

105. Alcaraz J, Buscemi L, Grabulosa M, et al. Microrheology of human lung epithelial cells measured by atomic force microscopy. Biophys J. 2003;84(3):2071–9. https://doi.org/10.1016/S0006-3495(03)75014-0.
106. Mizuno D, Bacabac R, Tardin C, et al. High-resolution probing of cellular force transmission. Phys Rev Lett. 2009;102(16):168102. https://doi.org/10.1103/PhysRevLett.102.168102.
107. Hoffman BD, Massiera G, van Citters KM, et al. The consensus mechanics of cultured mammalian cells. Proc Natl Acad Sci U S A. 2006;103(27):10259–64. https://doi.org/10.1073/pnas.0510348103.
108. Yamada S, Wirtz D, Kuo SC. Mechanics of living cells measured by laser tracking microrheology. Biophys J. 2000;78(4):1736–47. https://doi.org/10.1016/S0006-3495(00)76725-7.
109. Crocker JC, Valentine MT, Weeks ER, et al. Two-point microrheology of inhomogeneous soft materials. Phys Rev Lett. 2000;85(4):888–91. https://doi.org/10.1103/PhysRevLett.85.888.
110. Fabry B, Maksym GN, Butler JP, et al. Time scale and other invariants of integrative mechanical behavior in living cells. Phys Rev E Stat Nonlin Soft Matter Phys. 2003;68(4 Pt 1):41914. https://doi.org/10.1103/PhysRevE.68.041914.
111. Guck J, Ananthakrishnan R, Moon TJ, et al. Optical deformability of soft biological dielectrics. Phys Rev Lett. 2000;84(23):5451–4. https://doi.org/10.1103/PhysRevLett.84.5451.
112. Guck J, Ananthakrishnan R, Mahmood H, et al. The optical stretcher: a novel laser tool to micromanipulate cells. Biophys J. 2001;81(2):767–84. https://doi.org/10.1016/S0006-3495(01)75740-2.
113. Brunner C, Niendorf A, Käs JA. Passive and active single-cell biomechanics: a new perspective in cancer diagnosis. Soft Matter. 2009;5(11):2171. https://doi.org/10.1039/b807545j.
114. Mietke A, Otto O, Girardo S, et al. Extracting cell stiffness from real-time deformability cytometry: theory and experiment. Biophys J. 2015;109(10):2023–36. https://doi.org/10.1016/j.bpj.2015.09.006.
115. Otto O, Rosendahl P, Mietke A, et al. Real-time deformability cytometry: on-the-fly cell mechanical phenotyping. Nat Methods. 2015;12(3):199–202. https://doi.org/10.1038/nmeth.3281.
116. Gossett DR, Tse HTK, Lee SA, et al. Hydrodynamic stretching of single cells for large population mechanical phenotyping. Proc Natl Acad Sci U S A. 2012;109(20):7630–5. https://doi.org/10.1073/pnas.1200107109.
117. Evans EA. Bending elastic modulus of red blood cell membrane derived from buckling instability in micropipet aspiration tests. Biophys J. 1983;43(1):27–30. https://doi.org/10.1016/S0006-3495(83)84319-7.
118. Schulze C, Muller K, Kas JA, et al. Compaction of cell shape occurs before decrease of elasticity in CHO-K1 cells treated with actin cytoskeleton disrupting drug cytochalasin D. Cell Motil Cytoskeleton. 2009;66(4):193–201. https://doi.org/10.1002/cm.20341.
119. Jonas O, Duschl C. Force propagation and force generation in cells. Cytoskeleton. 2010;67(9):555–63. https://doi.org/10.1002/cm.20466.
120. Fuhs T, Reuter L, Vonderhaid I, et al. Inherently slow and weak forward forces of neuronal growth cones measured by a drift-stabilized atomic force microscope. Cytoskeleton. 2013;70(1):44–53. https://doi.org/10.1002/cm.21080.
121. Thoumine O, Ott A, Cardoso O, et al. Microplates: a new tool for manipulation and mechanical perturbation of individual cells. J Biochem Biophys Methods. 1999;39(1-2):47–62. https://doi.org/10.1016/S0165-022X(98)00052-9.
122. Fernandez P, Ott A. Single cell mechanics: stress stiffening and kinematic hardening. Phys Rev Lett. 2008;100(23):238102. https://doi.org/10.1103/PhysRevLett.100.238102.
123. Benoit M, Gabriel D, Gerisch G, et al. Discrete interactions in cell adhesion measured by single-molecule force spectroscopy. Nat Cell Biol. 2000;2(6):313–7. https://doi.org/10.1038/35014000.
124. Hoffman BD, Crocker JC. Cell mechanics: dissecting the physical responses of cells to force. Annu Rev Biomed Eng. 2009;11:259–88. https://doi.org/10.1146/annurev.bioeng.10.061807.160511.

125. Golde T, Schuldt C, Schnauss J, et al. Fluorescent beads disintegrate actin networks. Phys Rev E Stat Nonlinear Soft Matter Phys. 2013;88(4):44601. https://doi.org/10.1103/PhysRevE.88.044601.
126. Levine L. One- and two-particle microrheology. Phys Rev Lett. 2000;85(8):1774–7. https://doi.org/10.1103/PhysRevLett.85.1774.
127. Lau AWC, Hoffman BD, Davies A, et al. Microrheology, stress fluctuations, and active behavior of living cells. Phys Rev Lett. 2003;91(19):198101. https://doi.org/10.1103/PhysRevLett.91.198101.
128. Mijailovich SM, Kojic M, Zivkovic M, et al. A finite element model of cell deformation during magnetic bead twisting. J Appl Physiol. 2002;93(4):1429–36. https://doi.org/10.1152/japplphysiol.00255.2002.
129. Massiera G, van Citters KM, Biancaniello PL, et al. Mechanics of single cells: rheology, time dependence, and fluctuations. Biophys J. 2007;93(10):3703–13. https://doi.org/10.1529/biophysj.107.111641.
130. Kreysing MK, Kießling T, Fritsch A, et al. The optical cell rotator. Opt Express. 2008;16(21):16984. https://doi.org/10.1364/OE.16.016984.
131. Gyger M, Stange R, Kiessling TR, et al. Active contractions in single suspended epithelial cells. Eur Biophys J. 2014;43(1):11–23. https://doi.org/10.1007/s00249-013-0935-8.
132. Maloney JM, Lehnhardt E, Long AF, et al. Mechanical fluidity of fully suspended biological cells. Biophys J. 2013;105(8):1767–77. https://doi.org/10.1016/j.bpj.2013.08.040.
133. Maloney JM, van Vliet KJ. Chemoenvironmental modulators of fluidity in the suspended biological cell. Soft Matter. 2014;10(40):8031–42. https://doi.org/10.1039/C4SM00743C.
134. van Vliet K, Bao G, Suresh S. The biomechanics toolbox: Experimental approaches for living cells and biomolecules. Acta Mater. 2003;51(19):5881–905. https://doi.org/10.1016/j.actamat.2003.09.001.
135. Pullarkat P, Fernandez P, Ott A. Rheological properties of the eukaryotic cell cytoskeleton. Phys Rep. 2007;449(1-3):29–53. https://doi.org/10.1016/j.physrep.2007.03.002.
136. Fernández P, Heymann L, Ott A, et al. Shear rheology of a cell monolayer. New J Phys. 2007;9(11):419. https://doi.org/10.1088/1367-2630/9/11/419.
137. Deng L, Trepat X, Butler JP, et al. Fast and slow dynamics of the cytoskeleton. Nat Mater. 2006;5(8):636–40. https://doi.org/10.1038/nmat1685.
138. Weihs D, Mason TG, Teitell MA. Bio-microrheology: a frontier in microrheology. Biophys J. 2006;91(11):4296–305. https://doi.org/10.1529/biophysj.106.081109.
139. Roth KB, Neeves KB, Squier J, et al. High-throughput linear optical stretcher for mechanical characterization of blood cells. Cytometry A. 2016;89(4):391–7. https://doi.org/10.1002/cyto.a.22794.
140. Szabó B, Szöllösi GJ, Gönci B, et al. Phase transition in the collective migration of tissue cells: experiment and model. Phys Rev E. 2006;74(6):61908. https://doi.org/10.1103/PhysRevE.74.061908.
141. Deisboeck TS, Couzin ID. Collective behavior in cancer cell populations. BioEssays. 2009;31(2):190–7. https://doi.org/10.1002/bies.200800084.
142. Sander EE, van Delft S, ten KJP, et al. Matrix-dependent Tiam1/Rac signaling in epithelial cells promotes either cell-cell adhesion or cell migration and is regulated by phosphatidylinositol 3-kinase. J Cell Biol. 1998;143(5):1385–98.
143. Wu Y, Kanchanawong P, Zaidel-Bar R. Actin-delimited adhesion-independent clustering of E-cadherin forms the nanoscale building blocks of adherens junctions. Dev Cell. 2015;32(2):139–54. https://doi.org/10.1016/j.devcel.2014.12.003.
144. Kalluri R, Weinberg RA. The basics of epithelial-mesenchymal transition. J Clin Invest. 2009;119(6):1420–8. https://doi.org/10.1172/JCI39104.
145. Hanahan D, Weinberg RA. The hallmarks of cancer. Cell. 2000;100(1):57–70. https://doi.org/10.1016/S0092-8674(00)81683-9.
146. Hanahan D, Weinberg RA. Hallmarks of cancer: the next generation. Cell. 2011;144(5):646–74. https://doi.org/10.1016/j.cell.2011.02.013.

147. Ma L, Young J, Prabhala H, et al. miR-9, a MYC/MYCN-activated microRNA, regulates E-cadherin and cancer metastasis. Nat Cell Biol. 2010;12(3):247–56. https://doi.org/10.1038/ncb2024.
148. Plutoni C, Bazellieres E, Le Borgne-Rochet M, et al. P-cadherin promotes collective cell migration via a Cdc42-mediated increase in mechanical forces. J Cell Biol. 2016;212(2):199–217. https://doi.org/10.1083/jcb.201505105.
149. Gaggioli C, Hooper S, Hidalgo-Carcedo C, et al. Fibroblast-led collective invasion of carcinoma cells with differing roles for RhoGTPases in leading and following cells. Nat Cell Biol. 2007;9(12):1392–400. https://doi.org/10.1038/ncb1658.
150. Ladoux B, Mege R-M, Trepat X. Front-rear polarization by mechanical cues: from single cells to tissues. Trends Cell Biol. 2016;26(6):420–33. https://doi.org/10.1016/j.tcb.2016.02.002.
151. Mierke CT. The integrin alphav beta3 increases cellular stiffness and cytoskeletal remodeling dynamics to facilitate cancer cell invasion. New J Phys. 2013;15(1):15003. https://doi.org/10.1088/1367-2630/15/1/015003.
152. Seftor RE, Seftor EA, Gehlsen KR, et al. Role of the alpha v beta 3 integrin in human melanoma cell invasion. Proc Natl Acad Sci U S A. 1992;89(5):1557–61. https://doi.org/10.1073/pnas.89.5.1557.
153. Aoudjit F, Vuori K. Integrin signaling inhibits paclitaxel-induced apoptosis in breast cancer cells. Oncogene. 2001;20(36):4995–5004. https://doi.org/10.1038/sj.onc.1204554.
154. Munger JS, Huang X, Kawakatsu H, et al. A mechanism for regulating pulmonary inflammation and fibrosis: the integrin αvβ6 binds and activates latent TGF β1. Cell. 1999;96(3):319–28. https://doi.org/10.1016/S0092-8674(00)80545-0.
155. Soldi R, Mitola S, Strasly M, et al. Role of alphavbeta3 integrin in the activation of vascular endothelial growth factor receptor-2. EMBO J. 1999;18(4):882–92. https://doi.org/10.1093/emboj/18.4.882.
156. Bissell MJ, Radisky DC, Rizki A, et al. The organizing principle: microenvironmental influences in the normal and malignant breast. Differentiation. 2002;70(9-10):537–46. https://doi.org/10.1046/j.1432-0436.2002.700907.x.
157. Dvorak HF, Weaver VM, Tlsty TD, et al. Tumor microenvironment and progression. J Surg Oncol. 2011;103(6):468–74. https://doi.org/10.1002/jso.21709.
158. Heine P, Ehrlicher A, Käs J. Neuronal and metastatic cancer cells: unlike brothers. Biochim Biophys Acta Mol Cell Res. 2015;1853(11):3126–31. https://doi.org/10.1016/j.bbamcr.2015.06.011.
159. Ibragimova I, de Cáceres II, Hoffman AM, et al. Global Reactivation of Epigenetically Silenced Genes in Prostate Cancer. Cancer Prev Res (Phila). 2010;3(9):1084–92. https://doi.org/10.1158/1940-6207.CAPR-10-0039.
160. Karpf AR, Jones DA. Reactivating the expression of methylation silenced genes in human cancer. Oncogene. 2002;21(35):5496–503. https://doi.org/10.1038/sj.onc.1205602.
161. Cameron EE, Bachman KE, Myohanen S, et al. Synergy of demethylation and histone deacetylase inhibition in the re-expression of genes silenced in cancer. Nat Genet. 1999;21(1):103–7. https://doi.org/10.1038/5047.
162. Riek K, Klatt D, Nuzha H, et al. Wide-range dynamic magnetic resonance elastography. J Biomech. 2011;44(7):1380–6. https://doi.org/10.1016/j.jbiomech.2010.12.031.
163. Bi D, Yang X, Marchetti MC, et al. Motility-driven glass and jamming transitions in biological tissues. Phys Rev X. 2016;6(2):021011. https://doi.org/10.1103/PhysRevX.6.021011.
164. Bi D, Lopez JH, Schwarz JM, et al. A density-independent rigidity transition in biological tissues. Nat Phys. 2015;11(12):1074–9. https://doi.org/10.1038/NPHYS3471.
165. Angelini TE, Hannezo E, Trepat X, et al. Glass-like dynamics of collective cell migration. Proc Natl Acad Sci U S A. 2011;108(12):4714–9. https://doi.org/10.1073/pnas.1010059108.
166. Bi D, Lopez JH, Schwarz JM, et al. Energy barriers and cell migration in densely packed tissues. Soft Matter. 2014;10(12):1885–90. https://doi.org/10.1039/c3sm52893f.

167. Farhadifar R, Roper J-C, Aigouy B, et al. The influence of cell mechanics, cell-cell interactions, and proliferation on epithelial packing. Curr Biol. 2007;17(24):2095–104. https://doi.org/10.1016/j.cub.2007.11.049.
168. Basan M, Prost J, Joanny J-F, et al. Dissipative particle dynamics simulations for biological tissues: rheology and competition. Phys Biol. 2011;8(2):26014. https://doi.org/10.1088/1478-3975/8/2/026014.
169. Podewitz N, Jülicher F, Gompper G, et al. Interface dynamics of competing tissues. New J Phys. 2016;18(8):83020. https://doi.org/10.1088/1367-2630/18/8/083020.
170. Zhu Y, Dong Z, Wejinya UC, et al. Determination of mechanical properties of soft tissue scaffolds by atomic force microscopy nanoindentation. J Biomech. 2011;44(13):2356–61. https://doi.org/10.1016/j.jbiomech.2011.07.010.
171. Schuldt C, Karl A, Korber N, et al. Dose-dependent collagen cross-linking of rabbit scleral tissue by blue light and riboflavin treatment probed by dynamic shear rheology. Acta Ophthalmol. 2015;93(5):e328–36. https://doi.org/10.1111/aos.12621.
172. Reiss-Zimmermann M, Streitberger K-J, Sack I, et al. High resolution imaging of viscoelastic properties of intracranial tumours by multi-frequency magnetic resonance elastography. Clin Neuroradiol. 2015;25(4):371–8. https://doi.org/10.1007/s00062-014-0311-9.
173. Steinberg MS. On the mechanism of tissue reconstruction by dissociated cells. I. Population kinetics, differential adhesiveness. and the absence of directed migration. Proc Natl Acad Sci. 1962;48(9):1577–82. https://doi.org/10.1073/pnas.48.9.1577.
174. Foty RA, Steinberg MS. The differential adhesion hypothesis: a direct evaluation. Dev Biol. 2005;278(1):255–63. https://doi.org/10.1016/j.ydbio.2004.11.012.
175. Pawlizak S, Fritsch AW, Grosser S, et al. Testing the differential adhesion hypothesis across the epithelial–mesenchymal transition. New J Phys. 2015;17(8):83049. https://doi.org/10.1088/1367-2630/17/8/083049.
176. Albini A, Iwamoto Y, Kleinman HK, et al. A rapid in vitro assay for quantitating the invasive potential of tumor cells. Cancer Res. 1987;47(12):3239–45.
177. Paszek MJ, Zahir N, Johnson KR, et al. Tensional homeostasis and the malignant phenotype. Cancer Cell. 2005;8(3):241–54. https://doi.org/10.1016/j.ccr.2005.08.010.
178. Young JS, Llumsden CE, Stalker AL. The significance of the "tissue pressure" of normal testicular and of neoplastic (Brown-Pearce carcinoma) tissue in the rabbit. J Pathol. 1950;62(3):313–33. https://doi.org/10.1002/path.1700620303.
179. Plodinec M, Loparic M, Monnier CA, et al. The nanomechanical signature of breast cancer. Nat Nanotechnol. 2012;7(11):757–65. https://doi.org/10.1038/nnano.2012.167.
180. Nnetu KD, Knorr M, Käs J, et al. The impact of jamming on boundaries of collectively moving weak-interacting cells. New J Phys. 2012;14(11):115012. https://doi.org/10.1088/1367-2630/14/11/115012.
181. Mouw JK, Yui Y, Damiano L, et al. Tissue mechanics modulate microRNA-dependent PTEN expression to regulate malignant progression. Nat Med. 2014;20(4):360–7. https://doi.org/10.1038/nm.3497.
182. Haeger A, Krause M, Wolf K, et al. Cell jamming: collective invasion of mesenchymal tumor cells imposed by tissue confinement. Biochim Biophys Acta. 2014;1840(8):2386–95. https://doi.org/10.1016/j.bbagen.2014.03.020.
183. Park J-A, Kim JH, Bi D, et al. Unjamming and cell shape in the asthmatic airway epithelium. Nat Mater. 2015;14(10):1040–8. https://doi.org/10.1038/nmat4357.
184. Farina KL, Wyckoff JB, Rivera J, et al. Cell motility of tumor cells visualized in living intact primary tumors using green fluorescent protein. Cancer Res. 1998;58(12):2528–32.
185. Wang Y-L, Discher DE, editors. Cell mechanics, Methods in cell biology. London: Elsevier; 2007.
186. Diggs LW. Pathology of sickle cell disease. JAMA. 1971;218(4):600. https://doi.org/10.1001/jama.1971.03190170078040.
187. Platt OS. Sickle cell anemia as an inflammatory disease. J Clin Invest. 2000;106(3):337–8. https://doi.org/10.1172/JCI10726.
188. Weinberg RA. The biology of cancer. 2nd ed. New York: Garland Science; 2014.

189. Seltmann K, Fritsch AW, Käs JA, et al. Keratins significantly contribute to cell stiffness and impact invasive behavior. Proc Natl Acad Sci U S A. 2013;110(46):18507–12. https://doi.org/10.1073/pnas.1310493110.
190. Cross SE, Jin Y-S, Tondre J, et al. AFM-based analysis of human metastatic cancer cells. Nanotechnology. 2008;19(38):384003. https://doi.org/10.1088/0957-4484/19/38/384003.
191. Lichtman MA. Rheology of leukocytes, leukocyte suspensions, and blood in leukemia possible relationship to clinical manifestations. J Clin Invest. 1973;52(2):350–8.
192. Baker EL, Bonnecaze RT, Zaman MH. Extracellular matrix stiffness and architecture govern intracellular rheology in cancer. Biophys J. 2009;97(4):1013–21. https://doi.org/10.1016/j.bpj.2009.05.054.
193. Mofrad MR. Rheology of the cytoskeleton. Annu Rev Fluid Mech. 2009;41(1):433–53. https://doi.org/10.1146/annurev.fluid.010908.165236.
194. Guck J, Schinkinger S, Lincoln B, et al. Optical deformability as an inherent cell marker for testing malignant transformation and metastatic competence. Biophys J. 2005;88(5):3689–98. https://doi.org/10.1529/biophysj.104.045476.
195. Merkel M, Manning ML. Using cell deformation and motion to predict forces and collective behavior in morphogenesis. Semin Cell Dev Biol. 2016;67:167. https://doi.org/10.1016/j.semcdb.2016.07.029.
196. Manning ML, Collins E-MS. Focus on physical models in biology: multicellularity and active matter. New J Phys. 2015;17(4):40201. https://doi.org/10.1088/1367-2630/17/4/040201.
197. Pegoraro AF, Fredberg JJ, Park J-A. Problems in biology with many scales of length: cell–cell adhesion and cell jamming in collective cellular migration. Exp Cell Res. 2016;343(1):54–9. https://doi.org/10.1016/j.yexcr.2015.10.036.
198. Weigelin B, Friedl P. Cancer cells: stemness shaped by curvature. Nat Mater. 2016;15(8):827–8. https://doi.org/10.1038/nmat4711.
199. Te Boekhorst V, Preziosi L, Friedl P. Plasticity of cell migration in vivo and in silico. Annu Rev Cell Dev Biol. 2016;32:491–526. https://doi.org/10.1146/annurev-cellbio-111315-125201.
200. Collins C, Nelson WJ. Running with neighbors: coordinating cell migration and cell–cell adhesion. Cell Adhes Migr. 2015;36:62–70. https://doi.org/10.1016/j.ceb.2015.07.004.
201. Kashef J, Franz CM. Quantitative methods for analyzing cell–cell adhesion in development. Dev Biol. 2015;401(1):165–74. https://doi.org/10.1016/j.ydbio.2014.11.002.

3.2 Second Publication

The content of this chapter has been published in the manuscript "Actin and microtubule networks contribute differently to cell response for small and large strains"

DOI: 10.1088/1367-2630/aa7658

New Journal of Physics
The open access journal at the forefront of physics

Deutsche Physikalische Gesellschaft DPG
IOP Institute of Physics

Published in partnership with: Deutsche Physikalische Gesellschaft and the Institute of Physics

OPEN ACCESS

RECEIVED
19 January 2017

REVISED
27 April 2017

ACCEPTED FOR PUBLICATION
1 June 2017

PUBLISHED
8 September 2017

PAPER

Actin and microtubule networks contribute differently to cell response for small and large strains

H Kubitschke[1], **J Schnauss**[1,2], **K D Nnetu**[1], **E Warmt**[1], **R Stange**[1] and **J Kaes**[1]

[1] Peter Debye Institute for Soft Matter Physics, University Leipzig, Linnestraße 5, D-04103 Leipzig, Germany
[2] Fraunhofer Institute for Cell Therapy and Immunology, Perlickstraße 1, D-04103 Leipzig, Germany

E-mail: hans.kubitschke@uni-leipzig.de

Keywords: optical stretcher, actin filaments, microtubules, latrunculin A, jasplakinolide, nocodazole, paclitaxel

Supplementary material for this article is available online

Abstract

Cytoskeletal filaments provide cells with mechanical stability and organization. The main key players are actin filaments and microtubules governing a cell's response to mechanical stimuli. We investigated the specific influences of these crucial components by deforming MCF-7 epithelial cells at small ($\leqslant$5% deformation) and large strains (>5% deformation). To understand specific contributions of actin filaments and microtubules, we systematically studied cellular responses after treatment with cytoskeleton influencing drugs. Quantification with the microfluidic optical stretcher allowed capturing the relative deformation and relaxation of cells under different conditions. We separated distinctive deformational and relaxational contributions to cell mechanics for actin and microtubule networks for two orders of magnitude of drug dosages. Disrupting actin filaments via latrunculin A, for instance, revealed a strain-independent softening. Stabilizing these filaments by treatment with jasplakinolide yielded cell softening for small strains but showed no significant change at large strains. In contrast, cells treated with nocodazole to disrupt microtubules displayed a softening at large strains but remained unchanged at small strains. Stabilizing microtubules within the cells via paclitaxel revealed no significant changes for deformations at small strains, but concentration-dependent impact at large strains. This suggests that for suspended cells, the actin cortex is probed at small strains, while at larger strains; the whole cell is probed with a significant contribution from the microtubules.

1. Introduction

The ability of cells to sense and adapt to their environment plays a vital role in many of their biologically relevant functions. In the last decade, connections between the mechanical properties of cells and the initiation as well as progress of pathologies such as cancer [1, 2] have been made. These connections highlight the link between molecular changes within the cytoskeleton to morphological and functional changes of the entire cell. In this way, it has been shown that actin filaments and microtubules play significant roles in dynamic cellular processes such as proliferation [3], migration [4–6], differentiation, [7] and apoptosis [8]. Besides their dynamic functions, they lend cells mechanical stability and govern their responses against external, mechanical stimuli. During cancer metastasis, for instance, cells have to squeeze through the underlying extracellular matrix and vascular walls. Extravasation and intravasation during metastasis could lead to small or large deformation of the cells depending on the pore sizes of their surrounding environment. After extravasation, the single cells are transported in suspension to other parts of the body through the blood and spread through the lymph vessel [9].

The interaction between actin filaments and microtubules as well as their contribution to intracellular force balances have been discussed with respect to the traction forces exerted by cells on deformable substrates [10, 11]. These studies revealed the stress bearing ability of microtubules as well as the contractile forces produced by actin filaments together with myosin motors. It remains to be shown that such a force balance mechanism exists in suspended cells. The resistance of cells against deformations has been investigated via

techniques such as magnetic twisting cytometry (MTC) [12, 13], atomic force microscopy (AFM) [14, 15], laser tracking microrheology [13], hydrodynamic stretching with flow-cytometers [16–20], and optical stretcher (OS) [1, 21–24]. These studies were performed on various cell types [7, 25] and often indicate that actin filaments are a major contributor to the mechanical properties of cells. AFM-based studies further showed that microtubule stabilization or disruption did not affect cell elasticity [14, 25] or is only of minor importance [20]. In contrast, MTC studies revealed that destabilization of microtubules inhibited cell stiffness while stabilizing them led to increased cell stiffening [12]. Some of these studies, however, were performed on adherent cells and the measured mechanical properties depend on the local conditions rather than global characteristics [26]. Given the fact that a cell is spatially heterogeneous, the measured mechanical properties vary [13] and are not representative of the response of a cell as a whole to perturbation. In addition, it was shown that also keratin can play a major role in cell stiffness [27].

In contrast, whole cell deformations have been performed either by stretching cells using microplates [28, 29], or by micropipette aspiration [30]. Moreover, cells have been deformed by compression against a glass slide [31] or by use of optical forces such as the OS [7], including contractile force measurements [32], and optical tweezers [33], including force fluctuation measurements [34]. These studies also found that actin filaments are the major contributor to cell elasticity while microtubules contributed to cell relaxation [7]. At large strains, actin filaments have been shown to rupture in *in vitro* studies while the contribution of intermediate filaments and microtubules to cell elasticity becomes dominant [27, 35]. It has also been hypothesized via finite elements simulations [36] that microtubules contribute more to cell elasticity at large strains. Therefore, the disruption of microtubules at large strains has been shown to reduce the non-linearity in whole cell stiffness [37]. In most studies, cells are probed within a linear regime but the magnitude of the deformation (small or large) and its impact on the response of a cell as a whole has not been characterized. Here, we characterize the response of MCF-7 cells to optically applied forces at large and small strains by the means of the previously established automated microfluidic OS [22, 38, 39]. A low and high strain regime were established by employing step stress profiles generated by low and high laser powers. Additionally, target-specific drugs induced cytoskeletal perturbations and according changes in the relative deformation as well as the stress relaxation response of these cells were evaluated. Actin filaments were influenced by latrunculin A (LatA) and jasplakinolide (Jas). LatA disrupted actin filaments by sequestering actin monomers thus reducing the pool of polymerisable actin. In contrast, Jas was used to increase actin nucleation and polymerization and consequently reduced actin depolymerization [40–42]. To interfere with cytoskeletal microtubules, cells were treated with nocodazole (Noc) to destabilize microtubules, which consequently promotes their depolymerization. To achieve the contrary effect, paclitaxel (Tax) was used to stabilize microtubules [43]. Within this approach, the contributions of actin filaments and microtubules to the overall cell mechanics were evaluated in a decoupled manner for small and large strains. In contrast to previous work, we were able to separate the contributions of deformation and relaxation to the mechanical properties of cells for actin and microtubule networks for two orders of magnitude of drug dose concentrations. Here, we single out distinctive contributions for cell mechanical changes of the cytoskeleton.

2. Materials and methods

2.1. Cell culture and drug treatment

The MCF-7 cell line was bought from ATCC (ATCC, HTB-22) and were cultured with Mimimal Essential Medium Eagles with L-Glutamine and Earles salt (Biochrom, FG 0325). The cell culture medium was supplemented with 100 mg ml^{-1} Sodium Pyruvate (Sigma-Aldrich, P 5280), 10 μg ml^{-1} Bovine Insuline (Sigma-Aldrich, I6634), 5 ml of Non-essential amino acids (Biochrom, K 0293), 50 ml Fetal Bovine serum (Biochrom, S 0615), and 1 unit of Penincillin/Streptomycin (Biochrom, A 2212).

LatA (Sigma-Aldrich, L5163), Noc (Sigma-Aldrich, M1404) and Tax (T7402) were obtained from Sigma. Jas (Calbiochem, 420107) was bought from Calbiochem. All drugs were dissolved in 1 ml of dimethyl sulfoxide and 100 μg of the dissolved drug was further dissolve in 5 ml of culture medium. From this, the necessary volume was added to the cells while adherent to obtain the needed concentrations. Cells were incubated with Tax for 18, 10 h for Noc, and 6 h for Jas. LatA, was added to the cells in suspension 2 min before they were measured, thus the cells were measured in a LatA containing medium.

2.2. Automated microfluidic OS

The setup is as described in [39] with minor changes such as the microfluidic and stretching processes being computer controlled. A prototype version was provided by RS Zelltechnik GmbH. The mechanical properties of cells were determined by introducing the cells into the automated microfluidic OS where they are serially trapped and stretched. The cell radius along the laser axis is determined while the cell is trapped for a second at

100 mW. The cell is then stretched at 750 or 1200 mW. During the stretch, images are taken at 30 frames per second. The cells are allowed to relax for 2 s after stress cessation. The time-dependent, relative deformation is defined as $[r_t/r_1 - 1]$, where r_t is the cell's diameter at time t and r_t is the cell's diameter when the cell was trapped. Furthermore, the relative relaxation was defined as $[r_t - r_3]/[r_1 - r_3]$, where r_3 is the cell diameter at end of stretch, $t = 3$ s, and r_t is the cell diameter at time t while relaxing, $t > 3$ s. About 1000 cells were measured for each measurement. The relative deformation of the cells in the large strain regime is underestimated because at very large cell deformations ($\geqslant$20%) the edge detection algorithm was unable to capture the cells' edges accurately due to changes in the contrast.

2.3. The effect of cell size on cell deformation

The deformation of cells within the automated microfluidic OS depends sensitively on the ratio of the radius of the laser beam at the centre of the trap and the cell radius [23]. Recent works have shown that cell deformation increases with increasing cell radius [44], while others showed that cell deformation decreased with increasing cell radius [45]. This contradiction shows the difficulty in normalizing data from the stretcher analytically. To avoid this problem in this work, cells of the same radii were compared (see figures S2a, S2b and S3a, available online at stacks.iop.org/NJP/19/093003/mmedia). However, a maximum change of about ± 1 μm was observed in the averaged cell radius for a couple of measurements (see figure S3b). Considering the calculations in [44] and [45], an increase in cell radius of about ± 1 μm would lead to a relative increase in strain of about 5% compared to normal sized cells. That is, if a cell deforms by 0.07%, an increase in its size by 1 μm would lead to a deformation of 0.0735%. This cell size effect is within our error estimation and is therefore not the cause of the changes in deformation observed in this work. It is however noteworthy that the deformation of cells in the automated microfluidic OS is not largely determined by cell radius as pointed out in [45] because their simulations assumed a homogenous optical property of the cells. A plot of the cell radius against the relative deformation does not show any particular trend (see figure S4). This suggests that there are other factors such as cellular heterogeneity, nuclei size and the stage of the cells in the cell cycle influencing cellular deformation.

2.4. Confocal laser scanning microscopy

A mixture (500 μl) containing 250 μl of Nanofectin (GE Life Sciences, Q051-005) and 250 μl GFP E-MAP tubulin and Lifeact mcherry DNA was added drop-wise to the culture medium in a flask containing MCF7 cells. The cells were culture for 24 h after which the cells were washed with PBS, trypsinized, centrifuged and resuspended. The drugs were added at the appropriate times during culture. The cells were allowed to start settling for 20 min. The cells were then observed on the confocal laser scanning microscope while still having a spherical geometry.

2.5. Spinning disc confocal microscopy

Cells were cultured in μ-Plate 96-wells (ibidi, 89626). Cells were rinsed twice with PBS and kept for 30 min in staining solution. Staining solution was made of PBS containing 200 nM Tubulin Tracker™ Green (ThermoFisher, T34075) and 1 μM SiR-DNA (Spirochrome, SC007). Images were taken with inverted Axio Observer.Z1/Yokogawa CSU-X1A 5000 (Carl Zeiss Microscopy GmbH, Jena, Germany), 63x/1.30 Immersion PH3 Objective, lateral resolution of 235 nm and axial resolution of 460 nm for wavelengths of 490 nm. For cell detachment, we added 1:1 Trypsin-EDTA (Sigma, 59417C) and PBS resulting in final concentration of 0.025% Trypsin and 0.01% EDTA.

3. Results

The low strain regime was obtained with a stretch laser power of 750 mW (stress approx. 14 Pa) resulting in a maximum relative deformation below 5% at the end of the stretch (figure 1(a)). Within this regime, a physiological temperature is maintained [46, 47]. For 1200 mW (stress approx. 23 Pa) a high strain regime was achieved with maximum relative deformations beyond 5% (figure 1(d)). The applied stress of the stretch laser was calculated based on ray-optics studies of concentrically placed, spherical shells of different refractive indices as a model of cells with a cortical layer. The calculations are described in detail in Ananthakrishnan *et al* [36] with additional corrections described in Grosser *et al* [48].

Small deformations in the linear regime (up to 5% [49]) are dominated by actin and intermediate filaments [27, 50]. For larger deformations between 5% and 25% strain, nonlinear effects of the actin cytoskeleton can result in nonlinear responses, e.g., strain stiffening [11, 51, 52] and strain softening [53, 54]. The strain response for small laser powers shows a more pronounced viscous response, whereas for high laser powers a more viscoelastic response is distinguishable. However, the initial rapid, irregular deformation, between 1 and 1.5 s, is partially a result of the nuclear thermal instability of the MCF-7 cells [55]. Since we further investigate the

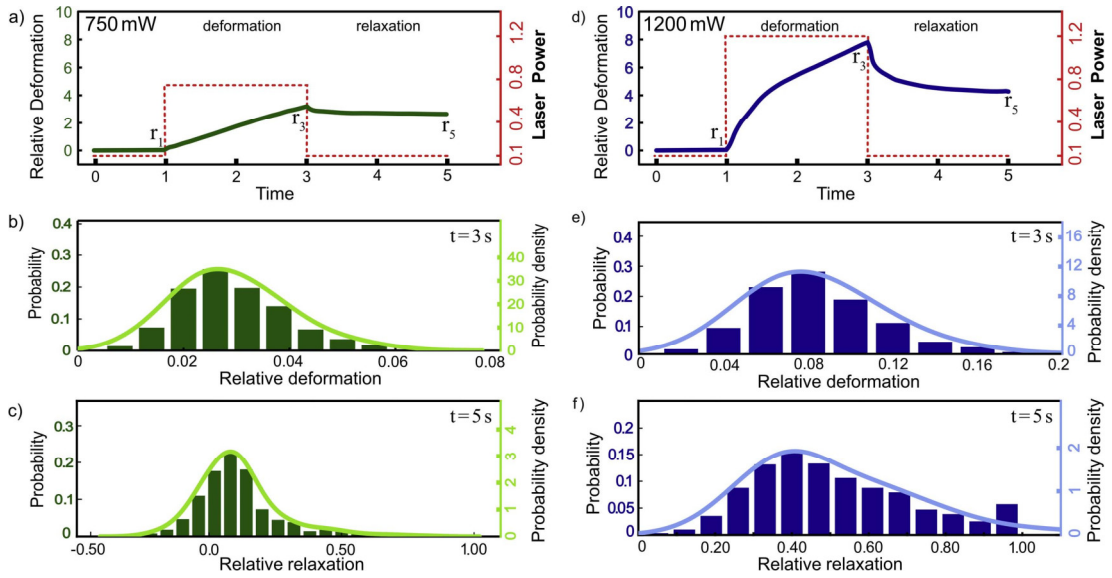

Figure 1. Plots of cells stretched with two different laser powers and the corresponding distributions of the relative deformation and relaxation fitted with the smoothed probability density function. Cells were stretched with a power of 750 mW (a) or 1200 mW (d) for 2 s. The red dashed line indicates the laser power, while the dark green (a) or dark blue (d) is the time-dependent deformation of the cell. (b) Shows the histogram of the relative deformation of cells at small strains and the arising probability density function. The distribution is not completely symmetric, as it would be expected for a normal distribution. (c) The histogram shows the relative relaxation of cells at small strains. The distribution is symmetric as expected for a normal distribution. The minimal optical trapping force (100 mW) of the laser can cause a negative relative relaxation for quasi-viscous mechanical response of cells. Accordingly, for large strains, the histograms of the relative deformation (e) and the relaxation (f) of MCF-7 cells are shown.

cytoskeletal effects of toxins, the induced constant offset in the relative deformation due to nuclear reshaping is not an essential issue in further data analysis.

For small and large strains, we observed asymmetric distributions for the relative deformations at the end of stretch ($t = 3$ s, figures 1(b) and (e)), given as $[r_3/r_1 - 1]$, which broadens for large strains. Furthermore, we define the relative relaxation as a measure of plasticity ($t = 5$ s, figures 1(c) and (f)) as following: $[r_5 - r_3]/[r_1 - r_3]$. The relative relaxation distributions at small strains were symmetric at around $0\% \pm 15\%$ for all measurements (figure 1(c)) but not as broad as the asymmetric relaxation distributions at large strains (figure 1(f)). Since most distributions are asymmetric, the differences in the deformation behaviour of individual cells is not a simple Gaussian function. However, we used a bell curve to calculate the mean and variance of the distributions plotted in the subsequent sections. All comparisons in percentages given in the succeeding sections are done with respect to the relative deformation of untreated cells.

3.1. The impact of actin filaments on cell deformation at small and large strains

At small strains ($\leqslant 5\%$, cells stretched with 750 mW), depolymerization of actin filaments by adding LatA (100 nM) increased the relative deformation of cells up to 75% (figure 2(a)). In contrast to the destabilization, an increased actin nucleation and polymerization due to the addition of Jas resulted in an increase in cell deformation with a maximum increase of about 53% occurring at 200 nM (figure 2(b)).

At large strains ($\geqslant 5\%$, cells stretched with 1.2 W), the disruption of actin filaments led to a maximum increase of 65% in the relative deformation at 1 μM LatA (figure 2(a)), but initiating actin nucleation and polymerization via Jas resulted in no significant change in deformability (figure 2(b)).

3.2. Contribution of actin filaments to cell relaxation

Cell relaxation as considered in this work could also be referred to as the degree of cell plasticity since only a very small percentage of cells relaxed completely in the observation time. Furthermore, at small strains, some cells did not relax while others responded by active elongation. We refer to an active response if the cells expanded after stress release above the maximum deformation during the stretch, i.e. the cells displayed a positive slope in the last second of relaxation resulting in a negative relaxation value. Since these relaxation behaviours cannot be found in an isotropic viscoelastic material, we suspect that this behaviour is caused by active cellular processes such as restructuring of the cytoskeleton [8] and the predominant viscous response in the small strain regime.

The disruption of actin filaments or the enhanced initiation of nucleation and polymerization resulted in the active behaviour of cells at small strains as shown by the negative relaxation values in figures 2(c) and (d). At large strains, this disruption led to a significant decrease in cell relaxation of 32% at 1 μM of LatA (figure 2(c)) implying

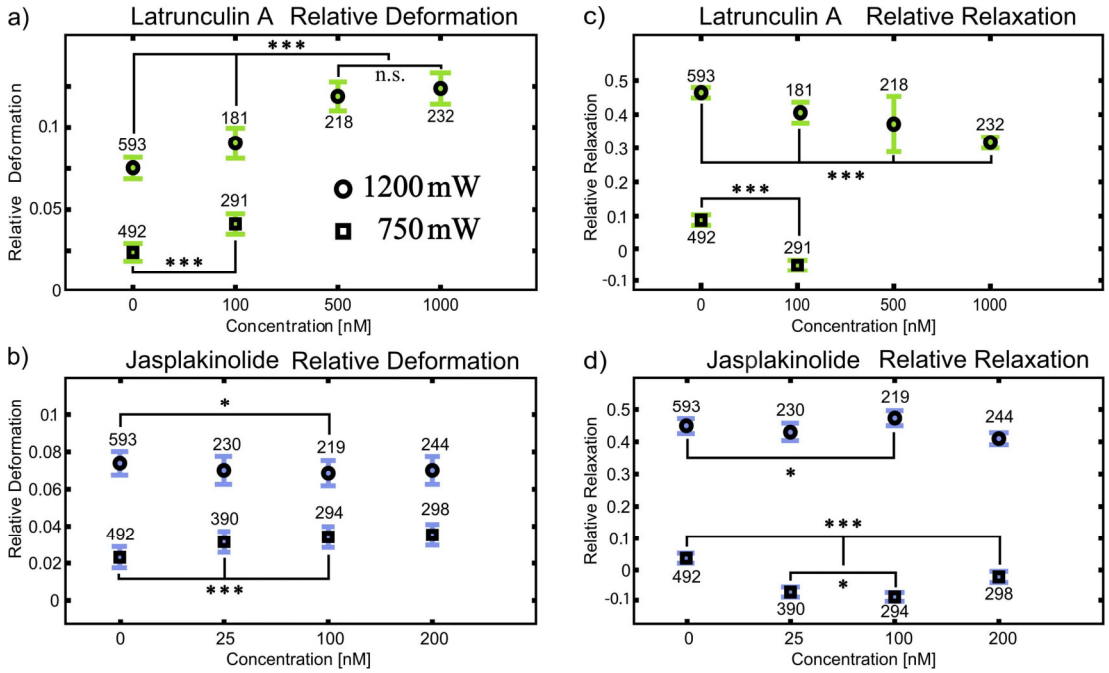

Figure 2. Relative deformation and relaxation of MCF-7 cells treated with latrunculin A and jasplakinolide, respectively. The black circles are the relative deformation at large strains (cells stretched at 1.2 W), while the squares are for the small strains (cells stretched at 750 mW), mean ± (SEM + reproducibility variance). The reproducibility variance was obtained by measuring the cells twice per passage number and for two different passages numbers. The number above each point on the plot is the number of cells from which the mean was obtained. Asterisks indicate the level of significance of the two-sided Kolmogorov–Smirnov test with $p < 0.05$, $p < 0.01$, $p < 0.001$ for one, two and three asterisks, respectively. Branched indicators for significance denote significance between all pairs of included measurements. Sub-branches indicate a lower level of significance between the two samples of the sub-branch. No asterisks denote samples with no significance compared to control measurement. (a) Shown are the relative deformation of LatA treated cells for small (squares) and large (circles) strains. The relative deformation increased significantly with increasing LatA concentration for both small and large strains. An increase from 500 to 1000 nM did not significantly increase the relative deformation. (b) Relative deformations of Jas treated cells for small (squares) and large (circles) strains are displayed. Cell deformation increased substantially with increasing Jas concentration for small strains and concentrations up to 100 nM and showed no significant change at large strains. (c) The relative relaxation, mean ± SEM, of LatA treated cells are illustrated. At small strains (squares), the cells are actively elongating, while at large strains (circles), the cells become significantly more plastic with increasing LatA concentration. (d) The relative relaxation of Jas treated cells revealed that cells actively elongate at small strains (squares) and showed no significant change at large strains (circles).

that the cells became more plastic. In contrast, the enhanced initiation of actin nucleation and polymerization had no significant effect on cell relaxation for all concentrations for measurements at large strains (figure 2(d)).

3.3. The impact of microtubules on cell deformation at small and large strains

As shown in (figure 3(a)) for small strains, disrupting the microtubules by adding Noc (ranging from 1 to 20 μM) had no significant effect on the relative deformation of cells. Stabilizing microtubules using Tax (25 nM to 4 μM) did not affect the relative deformation at small strains either (figure 3(b)).

At large strains, the disruption of microtubules caused by Noc (ranging from 1 to 10 μM) induced no significant change in cell deformation. At 20 μM Noc, however, a significant increase of 20% was observed (figure 3(a)). Stabilization of microtubules via Tax revealed a bipolar effect for measurements at large strains. For low concentrations, cells initially softened, but subsequently the cell populations stiffened for higher Tax concentrations. From 25 to 100 nM, the relative deformation increased by about 32%. The deformation decreased to its original value at 200 nM and remained constant from this concentration to 500 nM. Increasing the concentration from 500 nM to 2 μM Tax resulted in cell stiffening yielding a decrease of about 40% in relative deformation (figure 3(b)).

3.4. Contribution of microtubules to cell relaxation

At small strains, the disruption of microtubules resulted in a significant decrease of 70% in cell relaxation at 20 μM of Noc (figure 3(c)). The stabilization of microtubules in this regime showed no significant effect up to 0.5 μM Tax. However, from 1 μM onwards, cells relaxed actively and expanded after stress release (figure 3(d)). At large strains, microtubule disruption resulted in a decrease in relaxation of about 23% at 20 μM Noc (figure 3(c)) while microtubule stabilization led generally to a decrease in relaxation reaching a maximum of 30% at 50 nM Tax (figure 3(d)).

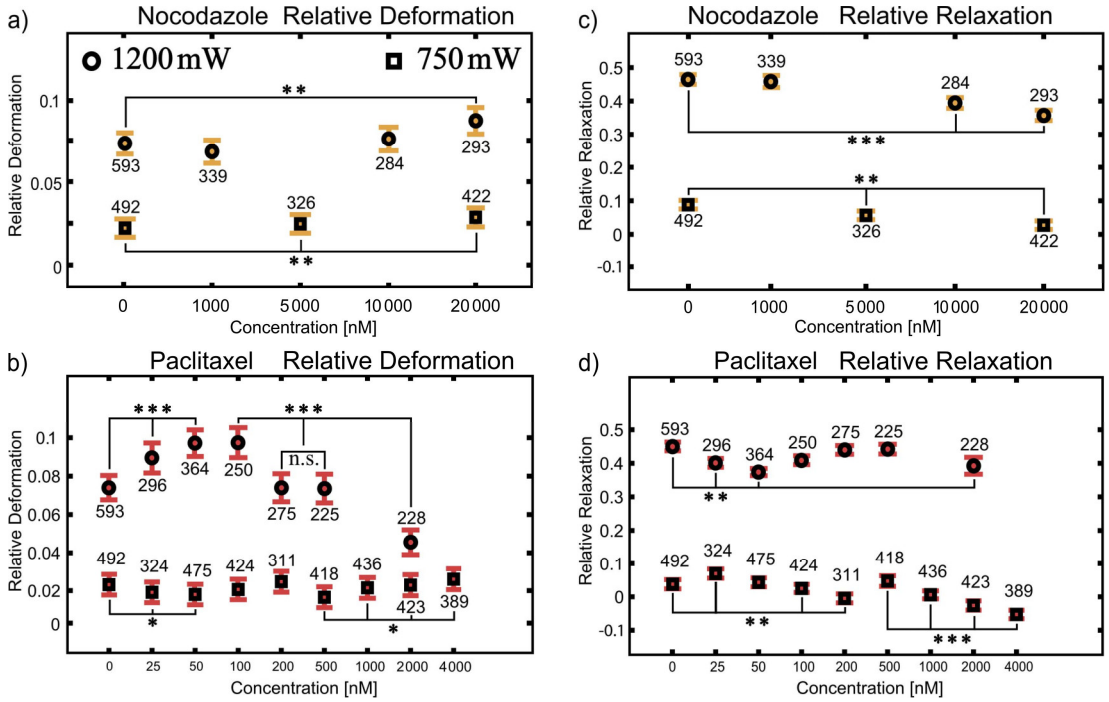

Figure 3. Relative deformation and relaxation of MCF7 cells treated with nocodazole and paclitaxel. The black circles are the relative deformation at large strains (cells stretched at 1.2 W) while the squares are the small strains (cells stretched at 750 mW), mean ± (SEM + reproducibility variance). Asterisks indicate the level of significance of the two-sided Kolmogorov–Smirnov test with $p < 0.05$, $p < 0.01$, $p < 0.001$ for one, two and three asterisks, respectively. Branched indicators for significance denote significance between all pairs of included measurements. Sub-branches indicate a lower level of significance between the two samples of the sub-branch. No asterisks denote measurements with no significance compared to the control measurement. (a) The relative deformation of Noc treated cells is shown. At small strains (squares), Noc was ineffective for all concentrations and displayed only a subtle trend towards higher deformability for increasing concentration. At large strains (circles), a significant increase in cell deformation was only observed at 20 μM Noc. (b) The relative deformation of Tax treated cells revealed no significant overall trend for small strains (squares). For low concentrations, the deformability approaches lower values whereas for higher concentrations, the cells become more deformable again. However, both trends have no considerable impact of cell mechanics. At large strains, the effect of Tax was bipolar and concentration dependent. From 25 to 100 nM Tax, an increase in relative deformation was observed. Above 100 nM, the relative deformation decreased. (c) The relative relaxation of Noc treated MCF7 cells shows that the cells became significantly more plastic at small (squares) and large (circles) strains. (d) The relative relaxation of Tax treated cells is illustrated. At small strains (squares), cellular plasticity increased with increasing concentration and the cells actively elongate from 1 μM Tax and higher concentrations. At large strains (circles), cellular plasticity increased generally but was pronounced at smaller concentration of Tax.

4. Discussion

In suspension, cells develop a well-defined spherical geometry, free of visible stress fibres with the actin cytoskeleton forming an cortex-like structure which spans the entire cell [56]. Moreover, the microtubules network shows a surprising picture by not clearly indicating whether the microtubules emanate from the microtubule-organizing centre (figure 4). The microtubules form a random network at the cells' interior and pronounced bundles at the periphery (figure 4(a)). This aligned peripheral bundling may be due to collective buckling at the cells' boundary. This is in contrast to the radially outward pointing network found in adherent cells. Microtubules have been shown to have a length-dependent persistence length [57] ranging from 5 to 100 μm, which is substantially stiffer than other cytoskeletal filaments. Therefore, the bending of microtubules within cells emphasizes the presence of compressive forces. We would like to note that local bending can be also induced by forces exerted by active molecular motors or passive cross-linking effects [58, 59]. However, these processes cannot sufficiently explain how several microtubules are bent in parallel, which further indicates the presence of compressive forces. Nevertheless, it remains unclear whether the plasma membrane or the actin cortex can generate such counteracting forces, but previous studies suggested the latter case [60, 61].

The used high concentrations of toxins refer to clinical relevant dosages; whereas a saturated cytotoxicity is strongly preferred, see figure 5. Many toxins, e.g. Tax, show less pronounced toxicity for lower concentrations (figure 5 below 25 nM). Nonetheless, this regime is of interest for fundamental research to investigate functional details of cellular or cytoskeletal structures, respectively [62]. Studying the accumulation dynamics of Tax, for instance, can reveal new insights for cancer diagnostics since it has a high binding affinity to microtubules and accumulates differently in different cell types, pronounced in malignant cells [62–65].

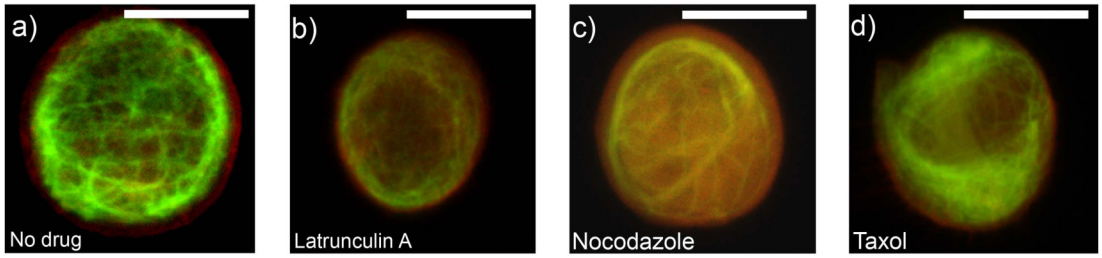

Figure 4. Confocal laser scanning images of MCF-7 cells in suspension showing GFP stained microtubules and RFP stained actin filaments (scale bars 5 μm). The green filaments are the microtubules while the red represents the actin meshwork. (a) In an untreated cell microtubules are highly bend and concentrated at the cell's periphery but form a random network at the cell's interior. Actin is spread throughout the cell. Both microtubules and actin form a cortex at the periphery. (b) A cell was treated with 500 nM LatA to disrupt actin filaments. The microtubule network is maintained as in the non-treated cell with less pronounced actin filaments spread across the entire cell. (c) A cell was treated with 20 μM Noc to disturb microtubules. Actin filaments are spread across the cell and the microtubules network is reduced. Nevertheless, a concentrated region at the cell's periphery is sustained. (d) A cell treated with 2 μM Tax displays a dense network of aligned microtubules along the cell periphery and actin filaments spread throughout the entire cell.

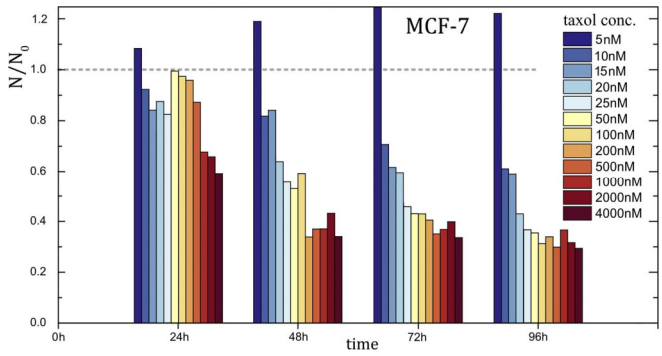

Figure 5. Cytotoxicity Assay for different Tax concentrations for an exposure time of 4 d. Paclitaxel stabilizes microtubules and hinders cell division. For concentrations beyond 25 nM and exposure times of 3 d and more, the toxicity is not majorly increased and nearly independent of the concentration. Below 500 nM, paclitaxel shows a pronounced lag time in its toxicity for the first 24 h. Comparable low concentrations of 5 nM lead to strongly decreased proliferation rates. The doubling time of MCF-7 with no Tax was determined to (38.8 ± 4.2) h. Since the cytotoxicity mainly arises from disrupted cell division and arresting cells in M-phase, only a fraction of cells, which have entered mitosis, are strongly affected by Tax.

In the low concentration regime, a lag time in the cytotoxic effect can be observed. The doubling time, and therefore cell cycle time, is approx. 39 h. Only fractions of cells have entered mitosis and are subject to a major cytotoxic effect of Tax. However, Tax is also toxic in the interphase [66, 67] and solely the mitotic index is not sufficient to explain the efficacy [64]. For concentrations ranging from 80 to 280 nM, Tax is reported to kill tumour cells by inducing multipolar divisions [68] (see supplementary figure S5). Subsequently, the aneuploidy daughter cells will eventually die due to cytokinesis failure and chromosome missegregation [64, 68].

Higher concentrations of Tax (200 nM and above) results in higher fractions of cells forced into mitotic arrest instead of dividing multipolar. In accordance with previous research [63, 64, 66–68], the induced mitotic arrest explains the observed rapidly saturated cytotoxicity for long exposure times. The cytotoxicity is also independent of the concentration if mitotic arrest is induced in cells (200 nM and above, figures 5 and 6).

4.1. Actin filaments dominate cell response at small strains

At small strains, the disruption of actin filaments led to a significant increase in cell deformation (figure 2(a)). Moreover, initiating enhanced actin nucleation and aggregation [69] resulted in an increase in cell deformation (figure 2(b)). This increase in deformation is most likely caused by a reduction of cross-linked actin filaments (figure 4(b)) since he storage modulus strongly dependents on crosslinking density [70, 71]. While actin has a major influence in this deformation regime, destabilization of microtubules had no significant effect on the overall cell deformation (figure 3(a)). At a first glance, these findings do not agree with previous studies reporting that microtubule destabilization initiated acto-myosin contractions in cultured cells [72] while the stabilization of microtubules inhibited acto-myosin contractions [73]. Additionally, acto-myosin contractions have been shown to induce cortical flows that are capable of generating inward forces leading to cytokinesis [74]. A combination of these findings may explain the ineffectiveness of Noc at small strains (figure 3(a)). The reduction

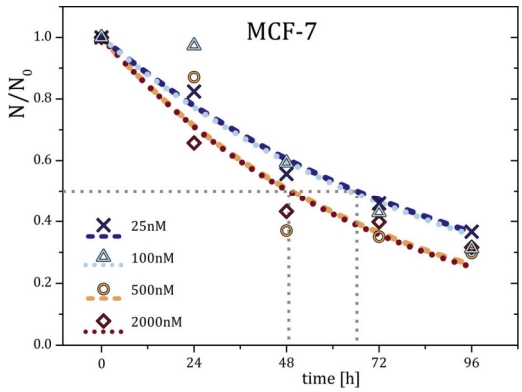

Figure 6. Comparison of time-dependent cytotoxicity of paclitaxel for two orders of magnitude. The dashed and dotted lines are exponential decay fits with toxicological half times (grey dashed lines) in the range of approximately 49–67 h with an SEM of 12 h. For concentrations above 200 nM, the exponential fits show strong deviations for exposure times of 48 h and longer, presumably due to saturation effects and cytotoxic lag times.

in cortical microtubule bundles may be counteracted by strain-hardening effects of the actin filaments caused by increased acto-myosin contractions [75] initiated by microtubule depolymerization. Stabilizing microtubules had no effect on cell deformation at small strains (figure 3(b)) since the imposed stress is not large enough to deform the microtubules within the cytoskeleton. Thus, only the actin cortex is effectively probed. The effect of the stabilized microtubules, however, is indirectly evident as the strengthened microtubules (figure 4(d)) slightly push the actin cortex slightly outwards. The increase in cellular deformation resulting from actin perturbation and the ineffectiveness of microtubule stabilization or disruption suggest that actin filaments alone determine cell mechanics at small strains.

4.2. Microtubules determine cell relaxation at small strains

Cell relaxation at small strains appeared active upon initiating enhanced actin nucleation and surprisingly upon destabilization of actin filaments, which is illustrated by the drop of the relative relaxation below zero for treated cells (figures 2(a) and (b)). In contrast, control cells without drug-induced cytoskeletal perturbations remained inactive displaying a positive value for the relative relaxation (figures 2(a) and (b)). The mechanical properties of actin structures have been shown to dependent on the cross-linker dynamics [70, 76–78], which highlights that stretching cells breaks cross-linkers such as filamin and α-actinin [24]. The weakening of physical inter-filament coupling increases the contribution of viscous deformations and consequently a decrease of elastic contributions since the percolation of the cross-linked network is decreased [70, 79]. Thus, contractile restoring forces are less effectively transmitted through the structure resulting in an increase in cell plasticity. Moreover, microtubules have been shown to buckle upon the active, highly contracting actin cortex during their polymerization [60, 61] (see figure 4). Stress-induced weakening of the actin cytoskeleton by cross-linker breakage suggests that the active behaviour of the entire cell may result from the slow unbuckling of microtubules. In turn, this suggests an entropic origin of the effect, which has been previously reported for both actin and microtubules [58, 78, 80–84]. Destabilizing microtubules resulted in a lack of relaxation, i.e. an increase in plasticity, especially at very high concentrations of Noc. As shown in figure 4(c), Noc treatment resulted in a reduced but aligned network of microtubules within the cells. This emphasizes that the actin cortex does not only cover the restoring force at small strains. The pressure of buckled microtubules also acts as a restoring force to a spherical shape, which is reduced if Noc is added. In contrast, stabilizing microtubules with a concentration of up to 0.5 μM Tax resulted in no significant change in relaxation (figure 3(d)). Beyond 0.5 μM, the cells became more plastic. This increase in plasticity could also result from the unbuckling of microtubules induced by the applied stress in conjunction with microtubule stiffening by Tax treatment. Furthermore, microtubule networks have been shown to release stress over very long times [85], which might explain the general increase in cell plasticity after the stretch.

4.3. Actin filaments and microtubules equally contribute to cell mechanics at large strains

At large strains, disrupting the actin filaments resulted in a significant increase in cell deformation. This increase stems from the loss of mechanical integrity of the actin cytoskeleton and agrees with many reports in literature [7, 24, 25].

The role of the microtubules to cell mechanics has previously often been ignored or underestimated. While the actin cortex is a major contributor to cellular mechanics and stiffness [56], we want to point out that also the microtubule network forms a cortex in suspended state of cells (see figure 7).

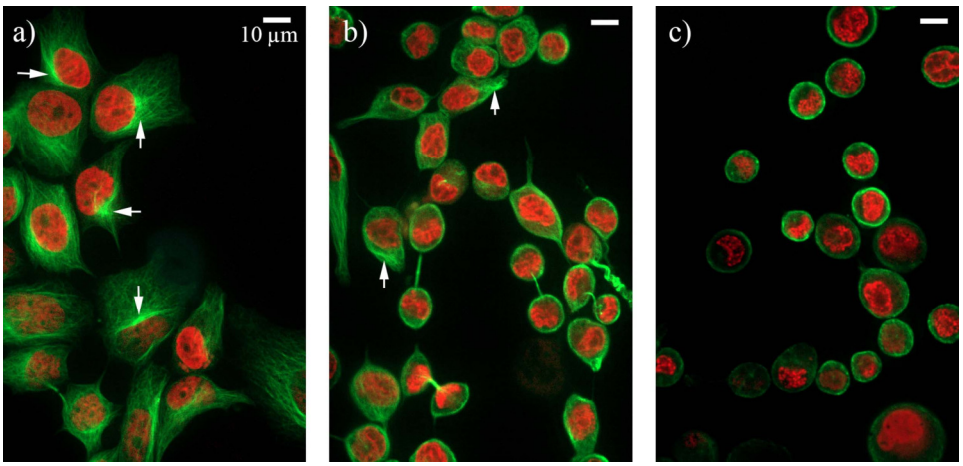

Figure 7. Time series of spinning disc microscope images of cells under influence of low concentration of trypsin-EDTA (0.025%). Microtubules stained in green (Tubulin Tracker Green) and nucleus stained in red (SiR-DNA). (a) Before adding trypsin, cells have well-structured microtubule networks with a microtubule organizing centre (MTOC, white arrows). Microtubule density decreases towards the cell membrane. (b) After 10 min of trypsination, the MTOC is barely recognizable and microtubules start to form a cortex-like structure [56]. (c) After complete detachment from the substrate, the MTOC has dissolved and major parts of the microtubules have formed a microtubule cortex.

Microtubule destabilization increased the overall cell compliance, which is only significant at very high Noc concentrations (figure 3(a)). Noc reduces the microtubule concentration and consequently weakens the observed microtubule network structure (see figure 4(c)) leading to a reduced cell stiffness [85]. These increments in deformation upon destabilizing of both actin filaments and microtubule point towards a cooperative working principle to regulate cellular mechanics at large strains. The initiation of enhanced actin nucleation did not affect the cell deformation. *In vitro* studies showed that actin networks rupture at relatively low strains at constant stress [85]. Therefore, the role of the actin filaments at large strains is negligible while the contributions of other filaments such as the intermediate filaments or microtubules become dominant.

4.4. Stabilizing microtubules has a bipolar effect on cell mechanics at large strains

Stabilizing microtubules by Tax treatment has a concentration-dependent bipolar effect with an increase in deformation at small concentrations of Tax and a decrease at larger concentrations of Tax (figure 3(b)). Microtubule polymerization imposes an outward force on the cell by forming a scaffold, which impedes dynamic instabilities. Thus, their stabilization maintains this imposed force and consequently make cells more compliant. Furthermore, stabilizing microtubules inhibits acto-myosin contractions [73], which oppose cell deformation. From 200 nM onwards, however, cells are stiffened with an effectiveness peaks at 2 µM. This stiffening could be initiated by stabilized microtubules pushing the actin cortex outward to a point where it strain-hardens. Since 200 nM of Tax is approximately the threshold concentration for mitotic arrest, we cannot exclude that cell cycle dependent effects may also play a role. Beyond 2 µM, cells literally explode when higher forces are applied on them (see supplemented video).

4.5. Actin filaments and microtubules both regulate cell relaxation at large strains

Destabilizing actin filaments decreased the cellular relaxation while initiating enhanced actin nucleation had no significant effect (figures 2(c) and (d)). This decline in relaxation originates from a reduction in the elastic strength of the actin cytoskeleton leading to an increased viscous response. Moreover, stabilizing and destabilizing microtubules led to an increased in plasticity (figures 3(c) and (d)). This could result from the disruption of the force balance between the actin cortex and outward pushing buckled microtubule. These large deformations resulting from the high optical forces could also decouple the microtubules from the actin cortex by breaking actin-microtubule crosslinker or actin filaments in general. On the other hand, at large strains, microtubules may no longer be bent and thereby losing their original structural role due to an outstretched configuration, which could lead to an increase in plasticity.

4.6. Different onset of affine and non-affine deformations

To understand the varying effects of the two networks under different strains, we like to emphasize that actin filaments and microtubules are inherently structurally and mechanically different, which is especially reflected in their different persistence lengths [8]. In a more generalized frame, cross-linked networks behave differently than purely entangled networks and cross-linker as well as filament concentrations and length scale distribution

have a rather large impact on the overall network stiffness [71, 86–89]. These concentrations as well as the stiffness of a network's components and their arrangements determine the onset of affine or non-affine deformations, which is consequentially different for actin and microtubule networks. Resulting entropic and enthalpic contributions to mechanical properties can substantially vary for these different networks. It has been stated previously that these differences allow cells to regulate their mechanical responses only by small alterations of cross-linker or filament concentrations to precisely alter the mechanical properties of the cytoskeleton [71]. Gardel *et al* even hypothesized that cell mechanics may vary as a function of external prestress and small variation in force can yield different mechanical responses [71]. Since cellular networks of actin filaments and microtubules substantially vary in all different parameters, their transition from affine to non-affine deformations will be different. While affine deformations of the actin cytoskeleton may govern cell responses in the low strain regime, its dominance is decreased for large strains due to the transition to non-affine deformations resulting in a reduced elastic modulus [90]. Within the range of the used large strains, the microtubule meshwork may still be probed in the affine regime and their mechanical response increases with larger deformations dominating the response of the entire system. Consequently, the ratio of contributions from actin networks and microtubule structures are shifted when probing cells with increasing strains yielding cooperativity effects for the arising mechanical properties.

5. Conclusion

Cells were measured in the suspended state and displayed different morphologies than in the adhered case. Microtubules were shown to form apparent random networks instead of pointing outwards radially from the microtubule organizing centre and actin stress fibres were completely absent. In the suspended state, the microtubule network forms a cortex-like shell in analogy to actin networks of suspended cells. Thus, the mechanical fingerprints of suspended cells have to be clearly distinguished from adhered cells.

By employing cytoskeletal drugs, we have been able to identify the distinct roles of actin filaments and microtubules during deformation of suspended cells. In the case of small strains ($\leqslant 5\%$), the cell deformation is mainly dominated by actin structures and the subsequent relaxation is mainly governed by microtubules due to the initiation of an active cell behaviour. In contrast, at large strains ($>5\%$), we found that actin filaments and microtubules cooperated in maintaining cellular integrity. While the influence of actin filaments appeared minor, microtubules became increasingly dominant upon Tax stabilization. This stabilization yielded concentration dependent, bipolar effects on cell deformation. Here, high Tax concentrations refer to clinical relevant dosage where cytotoxic effects dramatically change a cell's structure and mechanics. A lower dose is especially suitable to study and understand the specific roles of the cytoskeletal components.

In the final case, both actin and microtubules were shown to be responsible for cellular relaxation at large strains. With the implication of microtubules facilitating tumour cell attachment during metastasis by use of microtentacles, the bipolar effect of Tax on cell deformation could help explain the increase in circulating tumour cells in blood when taxane treatment was applied before surgery [91]. To further elucidate the role of these cytoskeletal components, including that of intermediate filaments on cell mechanics, the dynamic change in these filaments during stretching has to be accounted for.

Acknowledgments

We like to thank Tobias R Kießling for fruitful discussions and solving programming problems. We acknowledge funding from the European Commission H2020-PHC-2015-two-stage in the frame of the 'FORCE' project. This work has been supported through the Fraunhofer Attract project 601 683. We acknowledge support from the German Research Foundation (DFG) and University of Leipzig within the program of Open Access Publishing.

Author contributions

DKN, HK, JS, RS, and JAK designed research; DKN, HK and EW performed experiments; DKN, HK and JS analysed data; RS provided analytic tools; DKN, HK, JS and JAK wrote the article.

References

[1] Guck J *et al* 2005 Optical deformability as an inherent cell marker for testing malignant transformation and metastatic competence *Biophys. J.* **88** 3689–98

[2] Suresh S, Spatz J, Mills J P, Micoulet A, Dao M, Lim C T, Beil M and Seufferlein T 2005 Connections between single-cell biomechanics and human disease states: gastrointestinal cancer and malaria *Acta Biomaterialia* **1** 15–30

[3] Ingber D E 1990 Fibronectin controls capillary endothelial cell growth by modulating cell shape *Proc. Natl Acad. Sci. USA* **87** 3579–83
[4] Nnetu K D, Knorr M, Käs J and Zink M 2012 The impact of jamming on boundaries of collectively moving weak-interacting cells *New J. Phys.* **14** 115012
[5] Nnetu K D, Knorr M, Strehle D, Zink M and Käs J A 2012 Directed persistent motion maintains sheet integrity during multi-cellular spreading and migration *Soft Matter* **8** 6913
[6] Nnetu K D, Knorr M, Pawlizak S, Fuhs T and Käs J A 2013 Slow and anomalous dynamics of an MCF-10A epithelial cell monolayer *Soft Matter* **9** 9335
[7] Lautenschläger F, Paschke S, Schinkinger S, Bruel A, Beil M and Guck J 2009 The regulatory role of cell mechanics for migration of differentiating myeloid cells *Proc. Natl Acad. Sci.* **106** 15696–701
[8] Huber F, Schnauss J, Rönicke S, Rauch P, Müller K, Fütterer C and Käs J 2013 Emergent complexity of the cytoskeleton: from single filaments to tissue *Adv. Phys.* **62** 1–112
[9] Gupta G P and Massague J 2006 Cancer metastasis: building a framework *Cell* **127** 679–95
[10] Stamenovic D, Mijailovich S M, Tolic-Norrelykke I M, Chen J and Wang N 2002 Cell prestress: II. Contribution of microtubules *Am. J. Physiol. Cell Physiol.* **282** C617–24
[11] Wang N, Tolic-Norrelykke I M, Chen J, Mijailovich S M, Butler J P, Fredberg J J and Stamenovic D 2002 Cell prestress: I. Stiffness and prestress are closely associated in adherent contractile cells *Am. J. Physiol. Cell Physiol.* **282** C606–16
[12] Wang N 1998 Mechanical interactions among cytoskeletal filaments *Hypertension* **32** 162–5
[13] Hoffman B D, Massiera G, van Citters K M and Crocker J C 2006 The consensus mechanics of cultured mammalian cells *Proc. Natl Acad. Sci. USA* **103** 10259–64
[14] Rotsch C and Radmacher M 2000 Drug-induced changes of cytoskeletal structure and mechanics in fibroblasts: an atomic force microscopy study *Biophys. J.* **78** 520–35
[15] Lam W A, Rosenbluth M J and Fletcher D A 2007 Chemotherapy exposure increases leukemia cell stiffness *Blood* **109** 3505–8
[16] Dudani J S, Gossett D R, Tse H T K and Di Carlo D 2013 Pinched-flow hydrodynamic stretching of single-cells *Lab Chip* **13** 3728–34
[17] Gossett D R, Tse H T, Lee S A, Ying Y, Lindgren A G, Yang O O, Rao J, Clark A T and Di Carlo D 2012 Hydrodynamic stretching of single cells for large population mechanical phenotyping *Proc. Natl Acad. Sci. USA* **109** 7630–5
[18] Mietke A, Otto O, Girardo S, Rosendahl P, Taubenberger A, Golfier S, Ulbricht E, Aland S, Guck J and Fischer-Friedrich E 2015 Extracting cell stiffness from real-time deformability cytometry: theory and experiment *Biophys. J.* **109** 2023–36
[19] Otto O *et al* 2015 Real-time deformability cytometry: on-the-fly cell mechanical phenotyping *Nat. Methods* **12** 199–202
[20] Lange J R, Steinwachs J, Kolb T, Lautscham L A, Harder I, Whyte G and Fabry B 2015 Microconstriction arrays for high-throughput quantitative measurements of cell mechanical properties *Biophys. J.* **109** 26–34
[21] Roth K B, Neeves K B, Squier J and Marr D W M 2016 High-throughput linear optical stretcher for mechanical characterization of blood cells *Cytometry* A **89** 391–7
[22] Guck J, Ananthakrishnan R, Mahmood H, Moon T J, Cunningham C C and Käs J A 2001 The optical stretcher: a novel laser tool to micromanipulate cells *Biophys. J.* **81** 767–84
[23] Guck J, Ananthakrishnan R, Moon T J, Cunningham C C and Käs J A 2000 Optical deformability of soft biological dielectrics *Phys. Rev. Lett.* **84** 5451–4
[24] Wottawah F, Schinkinger S, Lincoln B, Ananthakrishnan R, Romeyke M, Guck J and Käs J A 2005 Optical rheology of biological cells *Phys. Rev. Lett.* **94** 98103
[25] Collinsworth A M, Zhang S, Kraus W E and Truskey G A 2002 Apparent elastic modulus and hysteresis of skeletal muscle cells throughout differentiation *Am. J. Physiol. Cell Physiol.* **283** C1219–27
[26] Heidemann S R and Wirtz D 2004 Towards a regional approach to cell mechanics *Trends Cell Biol.* **14** 160–6
[27] Seltmann K, Fritsch A W, Käs J A and Magin T M 2013 Keratins significantly contribute to cell stiffness and impact invasive behavior *Proc. Natl Acad. Sci. USA* **110** 18507–12
[28] Thoumine O and Ott A 1997 Time scale dependent viscoelastic and contractile regimes in fibroblasts probed by microplate manipulation *J. Cell Sci.* **110** 2109–16
[29] Desprat N, Richert A, Simeon J and Asnacios A 2005 Creep function of a single living cell *Biophys. J.* **88** 2224–33
[30] Trickey W R, Lee G M and Guilak F 2000 Viscoelastic properties of chondrocytes from normal and osteoarthritic human cartilage *J. Orthopaedic Res.* **18** 891–8
[31] Ofek G, Wiltz D C and Athanasiou K A 2009 Contribution of the cytoskeleton to the compressive properties and recovery behavior of single cells *Biophys. J.* **97** 1873–82
[32] Gyger M, Stange R, Kiessling T R, Fritsch A, Kostelnik K B, Beck-Sickinger A G, Zink M and Käs J A 2014 Active contractions in single suspended epithelial cells *Eur. Biophys. J.* **43** 11–23
[33] Nawaz S, Sanchez P, Bodensiek K, Li S, Simons M and Schaap I A T 2012 Cell visco-elasticity measured with AFM and optical trapping at sub-micrometer deformations *PLoS One* **7** e45297
[34] Schlosser F, Rehfeldt F and Schmidt C F 2015 Force fluctuations in three-dimensional suspended fibroblasts *Phil. Trans. R. Soc.* B **370** 20140028
[35] Janmey P A, Euteneuer U, Traub P and Schliwa M 1991 Viscoelastic properties of vimentin compared with other filamentous biopolymer networks *J. Cell Biol.* **113** 155–60
[36] Ananthakrishnan R, Guck J, Wottawah F, Schinkinger S, Lincoln B, Romeyke M, Moon T and Käs J A 2006 Quantifying the contribution of actin networks to the elastic strength of fibroblasts *J. Theor. Biol.* **242** 502–16
[37] Nagayama K and Matsumoto T 2008 Contribution of actin filaments and microtubules to quasi-*in situ* tensile properties and internal force balance of cultured smooth muscle cells on a substrate *Am. J. Physiol. Cell Physiol.* **295** C1569–78
[38] Bow H, Pivkin I, Diez-Silva M, Goldfless S J, Dao M, Niles J C, Suresh S and Han J 2011 A microfabricated deformability-based flow cytometer with application to malaria *Lab Chip* **11** 1065–73
[39] Lincoln B, Wottawah F, Schinkinger S, Ebert S and Guck J 2007 High-throughput rheological measurements with an optical stretcher *Methods Cell Biol.* **83** 397–423
[40] Bubb M R, Spector I, Beyer B B and Fosen K M 2000 Effects of jasplakinolide on the kinetics of actin polymerization. An explanation for certain *in vivo* observations *J. Biol. Chem.* **275** 5163–70
[41] Bubb M R, Senderowicz A M, Sausville E A, Duncan K L and Korn E D 1994 Jasplakinolide, a cytotoxic natural product, induces actin polymerization and competitively inhibits the binding of phalloidin to F-actin *J. Biol. Chem.* **269** 14869–71
[42] Bubb M R 2000 Effects of jasplakinolide on the kinetics of actin polymerization. An explanation for certain *in vivo* observations *J. Biol. Chem.* **275** 5163–70

[43] Rowinsky E K, Cazenave L A and Donehower R C 1990 Taxol: a novel investigational antimicrotubule agent *J. Natl Cancer Inst.* **82** 1247–59
[44] Ekpenyong A E, Posey C L, Chaput J L, Burkart A K, Marquardt M M, Smith T J and Nichols M G 2009 Determination of cell elasticity through hybrid ray optics and continuum mechanics modeling of cell deformation in the optical stretcher *Appl. Opt.* **48** 6344–54
[45] Teo S-K, Goryachev A B, Parker K H and Chiam K-H 2010 Cellular deformation and intracellular stress propagation during optical stretching *Phys. Rev.* E **81** 51924
[46] Kießling T R, Stange R, Käs J A and Fritsch A W 2013 Thermorheology of living cells—impact of temperature variations on cell mechanics *New J. Phys.* **15** 45026
[47] Schmidt B U S, Kießling T R, Warmt E, Fritsch A W, Stange R and Käs J A 2015 Complex thermorheology of living cells *New J. Phys.* **17** 73010
[48] Grosser S, Fritsch A W, Kiessling T R, Stange R and Käs J A 2015 The lensing effect of trapped particles in a dual-beam optical trap *Opt. Express* **23** 5221–35
[49] Wolff L, Fernandez P and Kroy K 2012 Resolving the stiffening-softening paradox in cell mechanics *PLoS One* **7** e40063
[50] Goldman R D, Khuon S, Chou Y H, Opal P and Steinert P M 1996 The function of intermediate filaments in cell shape and cytoskeletal integrity *J. Cell Biol.* **134** 971–83
[51] Pourati J, Maniotis A, Spiegel D, Schaffer J L, Butler J P, Fredberg J J, Ingber D E, Stamenovic D and Wang N 1998 Is cytoskeletal tension a major determinant of cell deformability in adherent endothelial cells? *Am. J. Physiol.* **274** C1283–9
[52] Fernandez P, Pullarkat P A and Ott A 2006 A master relation defines the nonlinear viscoelasticity of single fibroblasts *Biophys. J.* **90** 3796–805
[53] Trepat X, Deng L, An S S, Navajas D, Tschumperlin D J, Gerthoffer W T, Butler J P and Fredberg J J 2007 Universal physical responses to stretch in the living cell *Nature* **447** 592–5
[54] Krishnan R *et al* 2009 Reinforcement versus fluidization in cytoskeletal mechanoresponsiveness *PLoS One* **4** e5486
[55] Warmt E, Kießling T R, Stange R, Fritsch A W, Zink M and Käs J A 2014 Thermal instability of cell nuclei *New J. Phys.* **16** 73009
[56] Salbreux G, Charras G and Paluch E 2012 Actin cortex mechanics and cellular morphogenesis *Trends Cell Biol.* **22** 536–45
[57] Pampaloni F, Lattanzi G, Jonas A, Surrey T, Frey E and Florin E L 2006 Thermal fluctuations of grafted microtubules provide evidence of a length-dependent persistence length *Proc. Natl Acad. Sci. USA* **103** 10248–53
[58] Lansky Z, Braun M, Ludecke A, Schlierf M, ten Wolde P R, Janson M E and Diez S 2015 Diffusible crosslinkers generate directed forces in microtubule networks *Cell* **160** 1159–68
[59] Kent I A, Rane P S, Dickinson R B, Ladd A J C and Lele T P 2016 Transient pinning and pulling: a mechanism for bending microtubules *PLoS One* **11** e0151322
[60] Brangwynne C P, MacKintosh F C, Kumar S, Geisse N A, Talbot J, Mahadevan L, Parker K K, Ingber D E and Weitz D A 2006 Microtubules can bear enhanced compressive loads in living cells because of lateral reinforcement *J. Cell Biol.* **173** 733–41
[61] Brangwynne C P, MacKintosh F C and Weitz D A 2007 Force fluctuations and polymerization dynamics of intracellular microtubules *Proc. Natl Acad. Sci.* **104** 16128–33
[62] Jordan M A, Toso R J, Thrower D and Wilson L 1993 Mechanism of mitotic block and inhibition of cell proliferation by taxol at low concentrations *Proc. Natl Acad. Sci. USA* **90** 9552–6
[63] Jordan M A, Wendell K, Gardiner S, Derry W B, Copp H and Wilson L 1996 Mitotic block induced in HeLa cells by low concentrations of paclitaxel (Taxol) results in abnormal mitotic exit and apoptotic cell death *Cancer Res.* **56** 816–25
[64] Weaver B A 2014 How Taxol/paclitaxel kills cancer cells *Mol. Biol. Cell* **25** 2677–81
[65] Yvon A M, Wadsworth P and Jordan M A 1999 Taxol suppresses dynamics of individual microtubules in living human tumor cells *Mol. Biol. Cell* **10** 947–59
[66] Komlodi-Pasztor E, Sackett D L, Wilkerson J and Fojo T 2011 Mitosis is not a key target of microtubule agents in patient tumors *Nat. Rev. Clin. Oncol.* **8** 244–50
[67] Komlodi-Pasztor E, Sackett D L and Fojo A T 2012 Inhibitors targeting mitosis: tales of how great drugs against a promising target were brought down by a flawed rationale *Clin. Cancer Res.* **18** 51–63
[68] Zasadil L M, Andersen K A, Yeum D, Rocque G B, Wilke L G, Tevaarwerk A J, Raines R T, Burkard M E and Weaver B A 2014 Cytotoxicity of paclitaxel in breast cancer is due to chromosome missegregation on multipolar spindles *Sci. Trans. Med.* **6** 229ra43
[69] Senderowicz A M *et al* 1995 Jasplakinolide's inhibition of the growth of prostate carcinoma cells *in vitro* with disruption of the actin cytoskeleton *J. Natl Cancer Inst.* **87** 46–51
[70] Lieleg O, Claessens M M A E and Bausch A R 2010 Structure and dynamics of cross-linked actin networks *Soft Matter* **6** 218–25
[71] Gardel M L, Shin J H, MacKintosh F C, Mahadevan L, Matsudaira P and Weitz D A 2004 Elastic behavior of cross-linked and bundled actin networks *Science* **304** 1301–5
[72] Kolodney M S and Elson E L 1995 Contraction due to microtubule disruption is associated with increased phosphorylation of myosin regulatory light chain *Proc. Natl Acad. Sci. USA* **92** 10252–6
[73] Danowski B A 1989 Fibroblast contractility and actin organization are stimulated by microtubule inhibitors *J. Cell Sci.* **93** 255–66
[74] Cao L G and Wang Y L 1990 Mechanism of the formation of contractile ring in dividing cultured animal cells: I. Recruitment of preexisting actin filaments into the cleavage furrow *J. Cell Biol.* **110** 1089–95
[75] Alvarado J, Sheinman M, Sharma A, MacKintosh F C and Koenderink G H 2013 Molecular motors robustly drive active gels to a critically connected state *Nat. Phys.* **9** 591–7
[76] Wachsstock D H, Schwarz W H and Pollard T D 1994 Cross-linker dynamics determine the mechanical properties of actin gels *Biophys. J.* **66** 801–9
[77] Strehle D, Schnauss J, Heussinger C, Alvarado J, Bathe M, Käs J A and Gentry B 2011 Transiently crosslinked F-actin bundles *Eur. Biophys. J.* **40** 93–101
[78] Schnauß J, Händler T and Käs J A 2016 Semiflexible biopolymers in bundled arrangements *Polymers* **8** 274
[79] Chelakkot R and Gruhn T 2012 Length dependence of crosslinker induced network formation of rods: a Monte Carlo study *Soft Matter* **8** 11746
[80] Hilitski F, Ward A R, Cajamarca L, Hagan M F, Grason G M and Dogic Z 2015 Measuring cohesion between macromolecular filaments one pair at a time: depletion-induced microtubule bundling *Phys. Rev. Lett.* **114** 138102
[81] Schnauss J, Golde T, Schuldt C, Schmidt B U S, Glaser M, Strehle D, Handler T, Heussinger C and Kas J A 2016 Transition from a linear to a harmonic potential in collective dynamics of a multifilament actin bundle *Phys. Rev. Lett.* **116** 108102
[82] Huber F, Strehle D, Schnauß J and Käs J A 2015 Formation of regularly spaced networks as a general feature of actin bundle condensation by entropic forces *New J. Phys.* **17** 43029
[83] Ellis R 2001 Macromolecular crowding: obvious but underappreciated *Trends Biochem. Sci.* **26** 597–604

[84] Braun M, Lansky Z, Hilitski F, Dogic Z and Diez S 2016 Entropic forces drive contraction of cytoskeletal networks *BioEssays: News Rev. Mol. Cell. Dev. Biol.* **38** 474–81
[85] Lin Y-C, Koenderink G H, MacKintosh F C and Weitz D A 2007 Viscoelastic properties of microtubule networks *Macromolecules* **40** 7714–20
[86] Storm C, Pastore J J, MacKintosh F C, Lubensky T C and Janmey P A 2005 Nonlinear elasticity in biological gels *Nature* **435** 191–4
[87] Broedersz C P and MacKintosh F C 2014 Modeling semiflexible polymer networks *Rev. Mod. Phys.* **86** 995–1036
[88] Schuldt C, Schnauss J, Händler T, Glaser M, Lorenz J, Golde T, Käs J A and Smith D M 2016 Tuning synthetic semiflexible networks by bending stiffness *Phys. Rev. Lett.* **117** 197801
[89] Xu J, Schwarz W H, Käs J A, Stossel T P, Janmey P A and Pollard T D 1998 Mechanical properties of actin filament networks depend on preparation, polymerization conditions, and storage of actin monomers *Biophys. J.* **74** 2731–40
[90] Wen Q, Basu A, Janmey P A and Yodh A G 2012 Non-affine deformations in polymer hydrogels *Soft Matter* **8** 8039–49
[91] Balzer E M, Whipple R A, Cho E H, Matrone M A and Martin S S 2010 Anti-mitotic chemotherapeutics promote adhesive responses in detached and circulating tumor cells *Breast Cancer Res. Treat.* **121** 65–78

Actin and microtubule networks contribute differently to cell response for small and large strains

Supplemental Material

H K, J S, K D, E W, R S and J A K

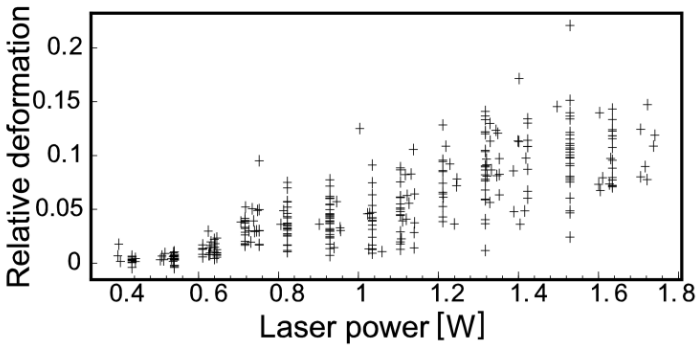

Fig. S1 A plot of the relative deformation of MCF7 cells at various laser powers from 400mW to 1.7W. The cells were stretched with a step stress with the following probing sequence: trapping for 1 second, stretching for 2 seconds, observed relaxation of 2 seconds. The relative deformation of the cells increases linearly with increasing laser power when reaching the threshold of 600mW (n=331).

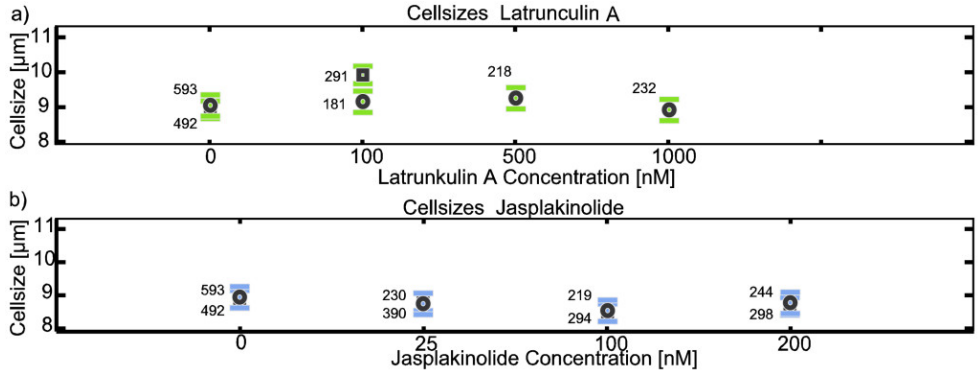

Fig. S2 Averaged cell size of MCF7 cells for various concentrations of Latrunculin A (LatA) and Jasplakinolide (Jas). The digits refer to the number of cells from which the mean was obtained; mean ± SEM. Black circles represent measurements in the large strain regime and the squares in the small strain regime. The averaged cell size remained constant for almost all concentrations of LatA and Jas (only a small deviation of about 1µm at 100nM LatA).

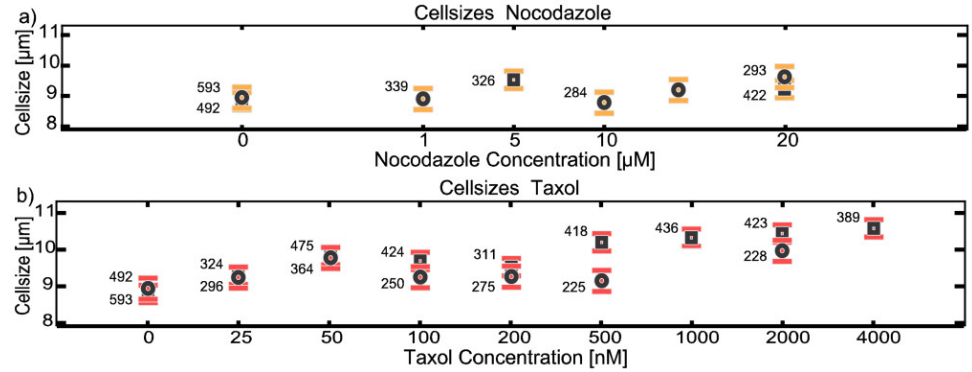

Fig. S3 Averaged cell size of MCF7 cells for various concentrations of Nocodazole (Noc) and Taxol (Tax). Black circles represent measurements in the large strain regime and the squares in the small strain regime. The averaged cell size remained constant for different concentrations of Noc

and deviations were found to be less than 1µm. In case of Tax treated cells, the maximum deviation of 1.5µm has been observed at 4µM Tax. However, this change in cell size does not affect the relative deformation significantly as it is within the error estimation.

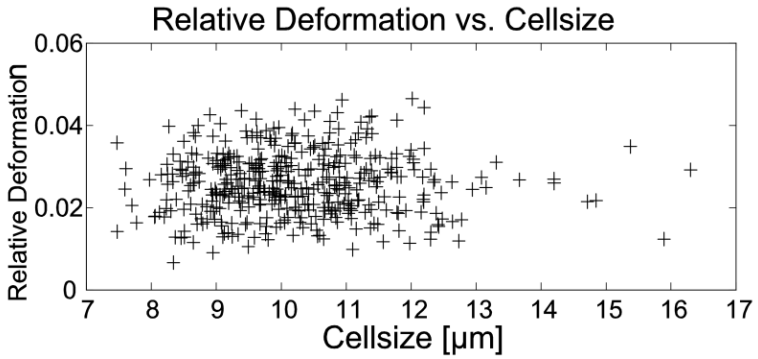

Fig. S4 A plot of the relative deformation of MCF7 cells against the cell size. The relative deformation neither increases nor decreases with increasing cell size. Furthermore, the relative deformation varied significantly for each cell size.

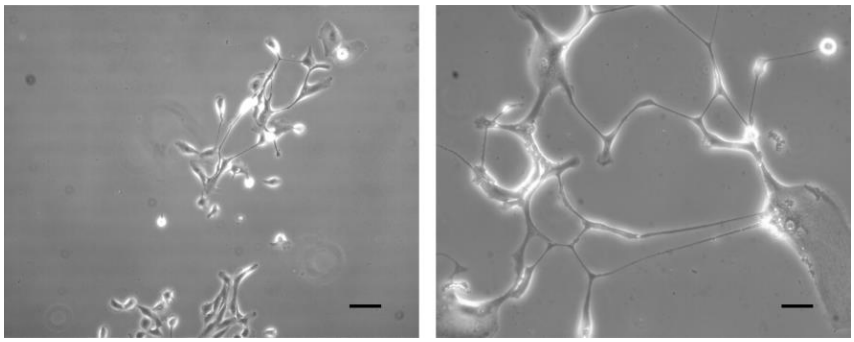

Fig. S5 Images of MCF-10A cells under paclitaxel treatment. Black bar represents 25 µm. MCF-10A have a doubling time of roughly 18 h. Left picture was taken after 24 h and 50 nM paclitaxel. The cell cluster in the upper part shows multipolar divisions. Right picture was taken after 72 h and 200 nM paclitaxel. Multipolar division led to cytokinesis failure and chromosome missegregation. Hardly a cellular structure is visible.

Video S1 The movie shows an MCF7 cell, which was treated with 2µM paclitaxel for 18 hours. During the step stress (cell is trapped at 100mW for a second, stretched at 1.2W for 2 seconds and allowed to relax for 2 seconds) the cell literally exploded. This explosion is a result of very high pressures produced by the stabilized microtubules. The cell's membrane start to burst at the upper right side and the rupture widens along the membrane in analogy to a bursting soap bubble.

3.3 Third Publication

The content of this chapter has been published in the manuscript "Roadmap to Local Tumour Growth: Insights from Cervical Cancer"

DOI: 10.1038/s41598-019-49182-1

SCIENTIFIC REPORTS
nature research

OPEN

Roadmap to Local Tumour Growth: Insights from Cervical Cancer

Hans Kubitschke[1], Benjamin Wolf[2,3], Erik Morawetz[1], Lars-Christian Horn[4], Bahriye Aktas[2,3], Ulrich Behn[5], Michael Höckel[2,3] & Josef Käs[1]

Received: 22 December 2018
Accepted: 21 August 2019
Published online: 04 September 2019

Wide tumour excision is currently the standard approach to surgical treatment of solid cancers including carcinomas of the lower genital tract. This strategy is based on the premise that tumours exhibit isotropic growth potential. We reviewed and analysed local tumour spreading patterns in 518 patients with cancer of the uterine cervix who underwent surgical tumour resection. Based on data obtained from pathological examination of the surgical specimen, we applied computational modelling techniques to simulate local tumour spread in order to identify parameters influencing preferred infiltration patterns and used area-proportional Euler diagrams to detect and confirm ordered patterns of tumour spread. Some anatomical structures, e.g. tissues of the urinary bladder, were significantly more likely to be infiltrated than other structures, e.g. the ureter and the rectum. Computational models assuming isotropic growth could not explain these infiltration patterns. Introducing ontogenetic distance of a tissue relative to the uterine cervix as a parameter led to accurate predictions of the clinically observed infiltration likelihoods. The clinical data indicates that successive infiltration likelihoods of ontogenetically distant tissues are nearly perfect subsets of ontogenetically closer tissues. The prevailing assumption of isotropic tumour extension has significant shortcomings in the case of cervical cancer. Rather, cervical cancer spread seems to follow ontogenetically defined trajectories.

Cancer of the breast, prostate, colorectum, lung, and cervix uteri are among the most commonly diagnosed malignant tumours worldwide[1]. All of these cancers are solid tumours and surgery or (chemo-) radiotherapy are currently the only available options for curative loco-regional treatment[2–5]. Generally, the goal of surgery should be to minimize loco-regional recurrence rates without increasing operative morbidity unnecessarily. To accomplish these objectives, the surgeon is faced with the following central questions: (I) Which tissues are at risk for both visible or occult tumour infiltration and need to be removed? (II) Which tissues can be safely spared, thus minimizing treatment-related morbidity? (III) Which locally advanced tumours can still be submitted to surgical treatment? Conventionally, the answer to these questions has been based on two assumptions: First, that local tumour growth is unpredictable and therefore can occur in any direction, and second, that a microscopically invisible tumour front precedes the identifiable tumour margin. These dogmas of local tumour growth are reflected in the surgical treatment strategy of wide excision. Hereby, a metrically defined circumferential safety margin of healthy tissue is excised around the tumour with the goal of removing all (occult) tumour cells that are thought to permeate this region. Even though a single malignant neoplasm usually does not display isotropic growth, it is thought to have isotropic growth *potential*. As the actual direction of local cancer growth in a given case is assumed to be stochastic, the average growth pattern of multiple tumours is expected to be isotropic. The tissue at risk for infiltration of occult tumour cells is therefore currently defined as an isotropic tissue rim which is removed by wide excision.

However, increasing evidence points to fundamental flaws in the wide excision strategy. Even when adequate wide excision margins are obtained surgically, local relapse rates remain high[6,7]. Furthermore, the width of resection margins would be expected to be one of the most important determinants of local tumour control. However, clinical data does not support this concept as has been demonstrated for several solid tumours, and reports from multiple investigations on resection margins provide conflicting results with some studies indicating that

[1]Peter Debye Institute for Soft Matter Physics, Leipzig University, Leipzig, Germany. [2]Department of Gynecology, Women's and Children's Centre, University Hospital Leipzig, Leipzig, Germany. [3]Leipzig School of Radical Pelvic Surgery, Leipzig University, Leipzig, Germany. [4]Division of Gynecologic, Breast and Perinatal Pathology, University Hospital Leipzig, Leipzig, Germany. [5]Institute of Theoretical Physics, Leipzig University, Leipzig, Germany. Hans Kubitschke and Benjamin Wolf Contributed equally. Correspondence and requests for materials should be addressed to J.K. (email: jkaes@uni-leipzig.de)

the width of resection margins is an important prognostic indicator while others fail to show an effect on local tumour recurrence and survival[8–11]. Imaging modalities are currently not capable of identifying single occult tumour cells that might precede the cancer invasion front. What surgeons need to know, therefore, is which tissues are at risk for *potential* infiltration of occult tumour cells and need to be removed to ensure oncological safety. Likewise, tissues that have a low probability of tumour infiltration should be spared with the goal of decreasing treatment-related morbidity. As a proxy for other solid tumours, we analysed data of cancer of the uterine cervix to demonstrate that local tumour spread is not isotropic but follows predictable growth patterns.

Based on clinical experience during the last two decades[11–14], we hypothesized that these anisotropic growth patterns would fit to an ontogenetic distance map, with tissues exhibiting a lesser ontogenetic distance to the uterine cervix having a higher probability of being infiltrated by the tumour than those of greater ontogenetic distance. The corresponding null-hypothesis would predict that the observed tumour infiltration patterns could be explained by physical distance alone, which is a function of metric distance and physical tissue type (i.e. adipose tissue or muscle). In this investigation, we use data derived from detailed pathology reports of patients who underwent surgical treatment for cervical cancer at our institution. Based on the results from pathological examination of all tissues removed during surgery, we determine in each case which pelvic structures are infiltrated by cancer. We then use area-proportional Euler diagrams and computational tumour growth simulations to determine whether ontogenetic tissue distance (relative to the uterine cervix) is a better parameter for the prediction of cancer infiltration than microenvironmental (physical) distance. The assumption of predictable and ordered rather than stochastic tumour growth patterns could form the basis of a roadmap for local tumour growth which might help surgeons or radiotherapists identify tissues at high risk for tumour infiltration.

Results

Pathological and ontogenetic characterization. To determine the clinical relevance of our findings and to facilitate their clinical application, we characterized our patient sample according to standard criteria; general patient- and tumour characteristics are compiled in Table 1. Our cohort contained a large number of locally advanced cases represented by pathological tumour stages 1b2 and higher in 50.2% of cases. In addition, 33.2% of all patients exhibited regional lymph node metastasis indicating advanced disease. The majority (74.9%) of all cases were squamous cell carcinomas.

Detailed two-dimensional anatomical maps in the sagittal and transversal plane of the pelvis were drawn and tumour infiltration probabilities for different tissues and tissue compartments adjacent to the uterine cervix were mapped to these drawings (Fig. 1A,B) based on pathological-identified infiltrated structures. In addition, different tissue types (e.g. fatty and muscular tissue) were identified and charted in the anatomical maps (Fig. 1C). Furthermore, anatomical tissues were classified and mapped according to their ontogenetic origin (Fig. 1D, described below). Tissues which are ontogenetically close to each other and constitute a functional unit were labelled with similar colours (reddish, greenish, purplish and blueish; Fig. 1D). A detailed description of the ontogenetic anatomy that exhibits some differences to conventional anatomy is available in the methods section.

Tumour size and shape characteristics. We compared the gross tumour diameter with the number of tumour-infiltrated tissue compartments categorised in Fig. 1D. We found a reasonable correlation for small tumours only where three or less tissue compartments were infiltrated (Fig. 2, Spearman's rank order correlation of $\rho = 0.599$). In contrast, we observed only a weak correlation between the two parameters when a higher number, $n \geq 3$, of structures were infiltrated ($\rho = 0.340$). A very similar picture was seen when grouping the tumour data in two sets, one set with tumour diameter $\leq$4 cm in greatest dimension (FIGO staging IB1/IIA1) and one with $>$4 cm (FIGO staging IB2/IIA2). The correlation between infiltrated structures and tumour size for small tumours below 4 cm was again quite reasonable (Spearman's rank order correlation of $\rho = 0.584$), whereas the same correlation was weaker for larger tumours ($\rho = 0.389$).

In Fig. 3 the tumour shape aspect ratio of short to long axis, i.e. the Diameter (Short axis)/Diameter (long axis), is shown which was derived from the metric 3-dimensional measures of the tumours. An aspect ratio of 1 would represent a spherical and 0 a planar (oblate) or needle-shaped (prolate) tumour. We found an average aspect ratio of approx. 0.4.

Descriptive modelling of tumour infiltration. We ran two different *in silico* simulations, each incorporating one of the two models. Results from the tumour growth simulations are shown in Fig. 4. We found that clinical data of tumour infiltration displays a distinct separation of the infiltration probabilities of cervix and bladder associated tissue compartments, and furthermore, of rectum and ureter associated compartments. In the physical microenvironmental model which only considers tissue-type dependent diffusion variation and tumour cell proliferation rates, the invasion probability of spatially close compartments increases with tumour progression almost concurrently. This is displayed by the broad overlapping tumour infiltration probability evolution in Fig. 4A around the inflection points.

In the ontogenetic model (Fig. 4B), tissue compartment boundaries were modelled as additional resistive barriers which limit cancer cell migration. Tissues that are ontogenetically close to the cervix are always invaded before an ontogenetically more distant compartment is infiltrated, e.g. the bladder compartment, the ureter, or the rectum compartment. There is a distinct separation of the infiltration probabilities around the inflection point.

Stepwise tumour infiltration. Tumour infiltration data was gathered from the pathology reports containing the findings of the examination of the surgically resected tissues. Area-proportional Euler diagrams[15–17] of the histopathological data of tumour infiltration were drawn in Fig. 5. The Euler diagram illustrates that up to the ellipse which displays bladder muscle infiltration (yellow), the numbers of patients with tumour infiltration of tissue compartments with successively increasing ontogenetic distance from the uterine cervix are nearly

Parameter	n	%
Total n = 518 Age (median, IQR)	**45 (37–54)**	
Histology		
Squamous cell carcinoma	388	74.9
Adenocarcinoma	103	19.9
Adenosquamous carcinoma	23	4.4
Small cell carcinoma	4	0.8
Type of surgery[a]		
TMMR	437	84.3
EMMR	49	9.5
LEER	32	6.2
Lymphovascular space invasion		
Yes	360	69.5
No	152	29.3
Unknown[b]	6	1.2
Blood vessel invasion		
Yes	66	12.7
No	446	86.1
Unknown[b]	6	1.2
Grading		
G1	75	14.5
G2	253	48.8
G3	185	35.7
Unknown[b]	5	1.0
FIGO Stage		
IA2 – IB1	267	51.5
IB2 – IIB	219	42.3
>IIB	32	6.2
Pathological tumour stage		
1a2 – b1	258	49.8
1b2 – 2b	249	48.1
>2b	11	2.1
Pelvic lymph node metastasis present		
Yes	172	33.2
No	346	66.8
Paraaortic lymph node metastasis present[c]		
Yes	43	8.3
No	475	91.7

Table 1. Patient and tumour data: [a]Total mesometrial resection (TMMR) is a surgical resective procedure by which the adult derivatives of the embryonal Müllerian Anlage (uterus [cervix and corpus], the Fallopian tubes, the proximal vagina, and the vascular and ligamentous mesometrium) are removed. In extended mesometrial resection (EMMR), tissues in addition to those removed by TMMR are resected. Depending on the tumour extension and the surgical situation, this may include the distal ureter and its supporting structure (the mesureter), parts of the urinary bladder wall and its adventitia, the distal vagina, or parts of the peritoneum. In addition to the aforementioned tissues, laterally extended endopelvic resection (LEER) includes removal of pelvic wall structures such as parts of the obturator muscle, the complete bladder with its adventitia and supporting structures, the rectum with its supporting structures, or both. [b]In six cases the entire tumour had been removed by local excision (conisation) for a suspected cervical intraepithelial neoplasia prior to the operation and external pathology reports did not include information on lympho-vascular space invasion. In four of these cases, information on tumour grade was also not available. [c]Periaaortic lymph node status was assessed histopathologically in 100 patients (19.3% of all patients). In the remaining cases paraaortic lymph node status was assumed negative because of histopathologically proven tumour free pelvic nodes and the absence of tumour infiltration of the uterine corpus. In this situation, metastasis in the periaortic region is unlikely.

perfect subsets of the numbers of patients with infiltration of ontogenetically closer compartments. For example, infiltration of the paracervix and the mesometrium was present in 35.7% and 19.4% of cases. The bladder mesentery and the bladder itself were involved by the tumour in 10.4% and 6.2% of cases, the mesureter and ureter in 2.7% and 1.4%, respectively. The rectum, 0.6%, and the mesorectum, 1.4%, showed the lowest likelihood of tumour infiltration. There was only one out of 54 cases of bladder mesentery and bladder muscle infiltration

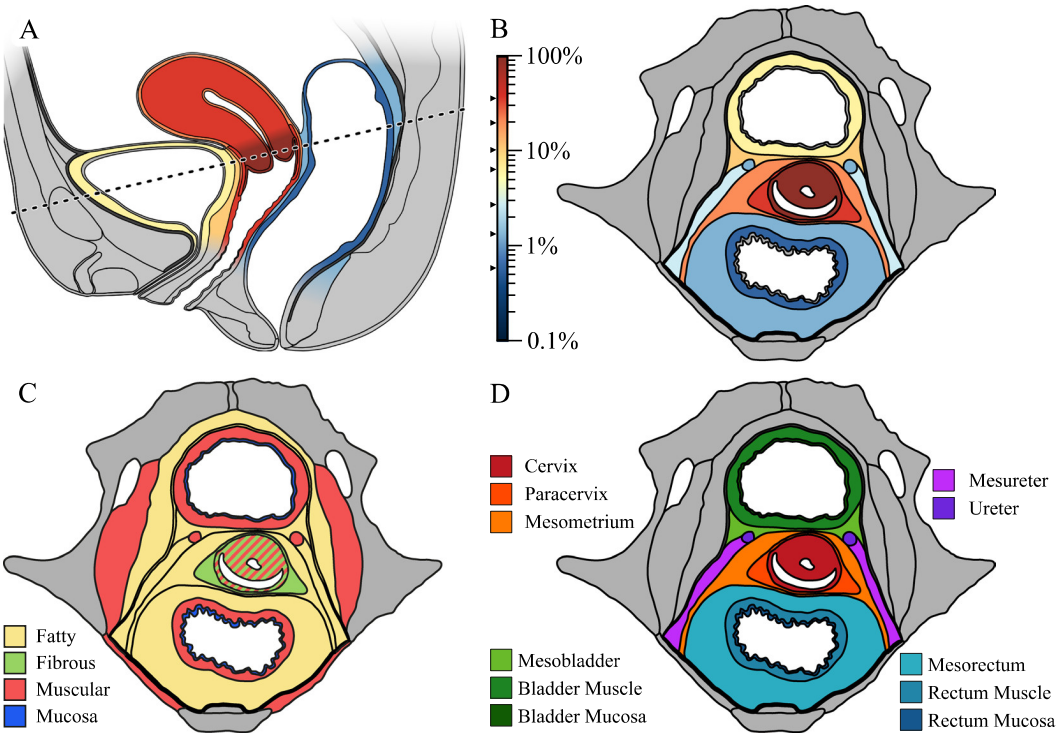

Figure 1. Anatomical maps of the female pelvis at the level of the uterine cervix. Tumour infiltration probability of 518 cervical cancer patients is depicted in the sagittal plane, (**A**) and the transversal plane, (**B**) respectively as heat maps. Despite the circumstance that bladder, rectum, and ureter are in similar metric proximity to the uterine cervix, the infiltration probabilities for each tissue at the time of surgical treatment is different. (**C**) Depicts the color-coded tissue types. Notably, the uterine cervix is surrounded by fibrous-fatty connective tissue in all directions. (**D**) Displays tissue compartments surrounding the uterine cervix classified according to their ontogenetic distance relative to the cervix. These compartments are separated by fine collagen lamellae which can be surgically dissected.

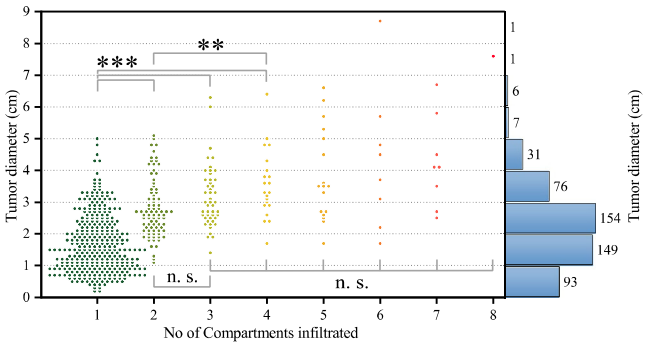

Figure 2. Scatter plot showing the number of infiltrated anatomical compartments with corresponding tumour diameter. An overall tumour diameter histogram is drawn on the right side. While the tumour size correlates with the number of infiltrated compartments for small sizes, especially when three compartments or less are infiltrated (Spearman's rank order correlation of $\rho = 0.599$), the data set of tumour diameters infiltrating more than two structures is only weakly correlated (Spearman's rank order correlation of $\rho = 0.340$). Asterisks indicate the level of significance of the two-sided Kolmogorov–Smirnov test with $p < 0.05$, $p < 0.01$, $p < 0.001$ for one, two and three asterisks, respectively. Branched indicators for significance denote significance between all pairs of included measurements. Importantly, however, there is a wide distribution of tumour sizes for each compartment infiltrated.

without mesometrial involvement (1.9%, green, yellow and blue). Furthermore, we found only one case where the mesorectum was infiltrated without concurrent mesobladder involvement (green and amaranth). Further information about the anatomical structures described here can be found in the methods section and separate diagrams for squamous cell and non-squamous cell carcinomas are included in the Supplement S3.

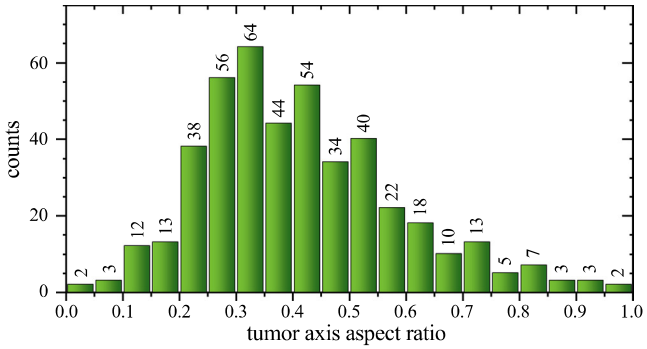

Figure 3. Histogram depicting the distribution of the aspect ratios of our cervical cancer cohort ($n = 518$). A large fraction of tumours has an aspect ratio profoundly deviating from 1 illustrating that the tumours are not of spherical growth.

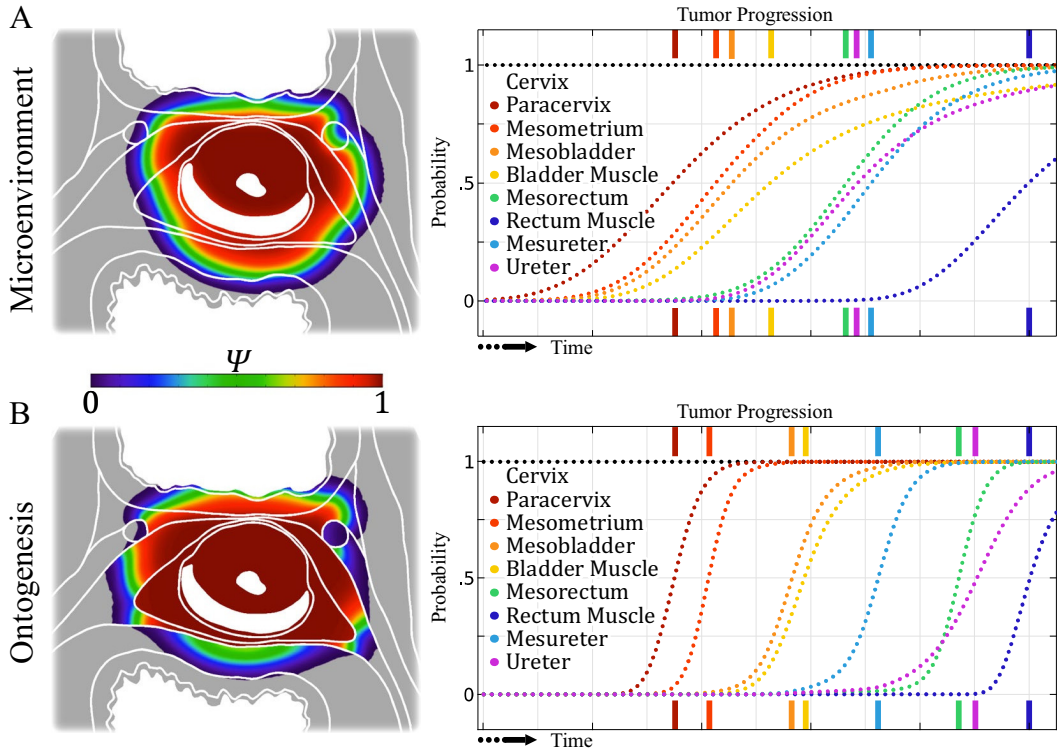

Figure 4. Illustration of the infiltration probability of tissue compartments over time. The model is based on a two-dimensional Fisher-Kolmogorov equation ($n = 1$, $D = 1.7\,m^2/s$, $r_{muscle} = 0.0047 \cdot 1/day$, $r_{fatty} = 0.019 \cdot 1/day$, $r_{fibrous} = 0.014 \cdot 1/day$). The left figures display the color-coded cancer cell probability density Ψ. Histopathological data of tumour infiltration displays distinct separation of infiltration probability of cervix and bladder associated compartments (reddish and yellowish lines) and rectum and ureter associated compartments (greenish and blueish lines). In the microenvironmental model, (**A**) which only considers tissue-type dependent varying diffusion and tumour cell proliferation rates, the invasion probability of spatially close compartments increases with tumour progression almost concurrently. A clear separation of tumour stages is hampered because the invasion probability curves are significantly overlapping. The microenvironmental model does not provide adequate predictions for compartment infiltration. In the ontogenetic model, (**B**) tissue compartment boundaries were modelled as additional resistive passive barriers which limit cancer cell migration, as described in the methods section. Invasion of spatially close compartments happens stepwise, as seen in clinical data. The stepwise order and invasion likelihood of infested compartments can only be correctly represented when considering ontogenetic segregation of tissue compartments.

Discussion

In this work, we demonstrate that local tumour growth potential of cervical cancer is not isotropic and that the infiltration probability differs greatly among different anatomical structures and compartments in close proximity to the uterine cervix.

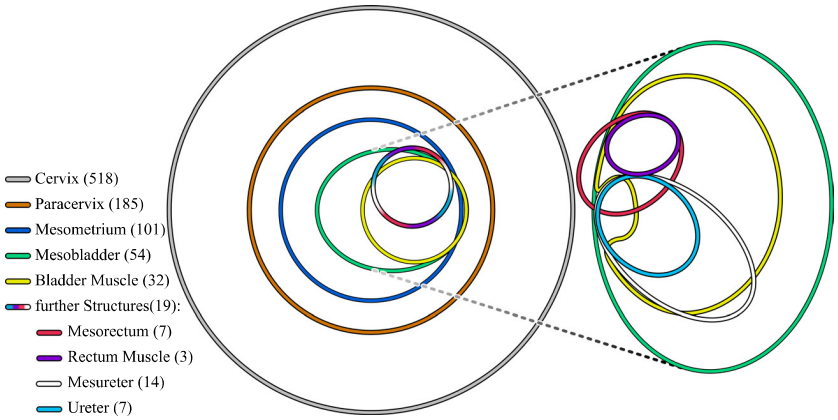

Figure 5. Area-proportional Euler diagram displaying infiltration of endopelvic (sub-) compartments of 518 pooled cervical cancer cases. The patients underwent either Total Mesometrial Resection (TMMR), Extended Mesometrial Resection (EMMR) or Laterally Extended Endopelvic Resection (LEER) as local excisional procedures. The areas of the ellipses are proportional to the total number of reported cases of the corresponding infiltrated compartments and sub-compartments. Overlying areas of two or more ellipses represent cases where several compartments are infiltrated. The intersectional area is also proportional to the number of cases in which multiple compartments are infiltrated. A smaller ellipse that is completely located inside a larger one is therefore a true subset of the larger ellipse. For example, mesometrial infiltration incidents (blue) only occur if the paracervix (orange) has been previously infiltrated. Notably, up to the infiltration of the bladder compartment, the tissue involvement is practically following a stepwise progression which is reflected in ellipses being true subsets of enclosing larger ellipses. Exact definitions of the anatomical structures described here can be found in the methods section.

As a first step to investigate whether tumour growth displays isotropic patterns, we compared the gross tumour diameter with the number of tumour-infiltrated tissue compartments (Fig. 1D). If all surrounding compartments displayed an equal infiltration likelihood, tumour size would be expected to correlate clearly with the number of infiltrated compartments. However, we found a reasonable correlation for small tumours (less or equal to three compartments infiltrated) but only a weak correlation for larger tumours (infiltration of more than three compartments). Notably, while tumours with diameter of 1.5 cm and lower are practically bound to the uterine cervical compartment, larger tumours do not necessarily invade more compartments. Taken together, in contrast to what our null-hypothesis would have predicted, we found that tumours of one size (diameter) can infiltrate a varying number of compartments indicating that local tumour growth does not occur in a purely isotropic manner.

Consequentially, we analysed whether the average tumour shape aspect ratio in our cohort was close to spherical as would have been predicted by our null-hypothesis assuming similar infiltration likelihoods of all surrounding tissues. Contrarily to an idealised, isotropically growing tumour – which is assumed in a wide excision strategy and would have an aspect ratio of very close to 1 – we found that the majority of aspect ratios significantly diverge from 1 with an average aspect ratio of approx. 0.4. While the localisation and shape of the initially formed tumour may influence the shape of the growing tumour, the surgically resected and pathologically analysed tumours presented in Figs 2 and 3 are orders of magnitudes larger in volume. Thus, under the premise of diffusive undirected tumour growth, the shape and aspect ratio of the tumour should exhibit a trend towards a more spherically shaped tumour, which is not observed in the data set. The strong deviation of the found aspect ratio from 1 indicates that cervical cancer tumour growth is not isotropic on average on large scales compared to other tumour entities such as glioblastomas and breast cancers, which grow in a more uniform microenvironment and display a profoundly more spherical aspect ratio close to 0.7[18–20].

To further investigate whether ontogenetic distance is a better parameter than physical (i.e. microenvironmental) distance to predict local tumour growth patterns, we ran *in silico* simulations for a physical microenvironmental and an ontogenetic model. The microenvironmental model is agnostic to ontogenetic compartment boundaries. The infiltration probabilities of different compartments are vastly overlapping, thus the expected number of cases with, for instance, mesorectum infiltration without mesobladder infiltration should be far beyond a singular case as observed in our cohort. Therefore, the microenvironmental model does not adequately reflect tumour infiltration patterns from a probabilistic point of view and physical distance is not a useful parameter in predicting local tumour growth. In the ontogenetic model, however, invasion of spatially close compartments happens stepwise, which is in accordance with the histopathological data. In detail, the tumour infiltration probabilities of tissues with growing ontogenetic distance from the uterine cervix increase suddenly with distinct onsets, in contrast to the overlapping infiltration probabilities of the microenvironmental model. Our tumour growth modelling data shows that introducing ontogenetic distance of tissues relative to the uterine cervix leads to a significant improvement in predicting the clinically observed tumour growth patterns as compared to models assuming isotropic tumour growth in the context of microenvironmental factors alone (microenvironmental or physical distance). However, some points in each model deserve further discussion:

First, one should consider how differences in the tumour microenvironment might lead to preferential infiltration of specific abutting tissues. Fatty, muscular and fibrous connective tissues all constitute different microenvironments in which tumour cells might behave differently. For example, fatty tissue has been shown to promote of tumour growth[21,22] (which would translate into an increased cancer cell proliferation rate r_{ij}). However, tumour cells would be expected to exhibit comparable growth and proliferation behaviour in similar tissue types. The fibro-fatty connective tissues surrounding the uterine cervix ranging to the urinary bladder, the rectum, and the ureter are morphologically very similar and therefore cancer should show similar propensities to extend in either direction rendering tumour growth isotropic on average. Furthermore, the supporting (meso-) structures of bladder, ureter and rectum are all composed of fatty tissue, yet are infiltrated at significantly different rates[13], see Fig. 1C.

Second, during the past decade, there has been an increasing notion that rigidity of the tumour microenvironment plays an important role in directing tumour growth. Extracellular matrix (ECM) stiffness might in fact promote malignant transformation and direct tumour growth along gradients of ECM rigidity, a process termed durotaxis[23,24]. To date, no measurements of stiffness of the tissues surrounding the uterine cervix have been performed; therefore, we could not include tissue stiffness as a parameter in our model. Nonetheless, it seems unlikely that morphologically similar tissues such as the fatty tissue of the bladder mesentery or the rectal mesentery exhibit significantly different degrees of rigidity or rigidity gradients. In fact, morphologically similar cells share important mechanical and regulatory characteristics and respond and adapt to the rigidity of their surroundings in similar ways[23,25–28]. The impact of the microenvironment is also reflected in the active regulation and fine-tuning of the cell's cytoskeleton via crosslinker and filament concentrations[29–35] and therefore the resulting mechanical properties of the cells[36–39]. While it cannot be ruled out that the tissue microenvironment may have an influence of the growth direction and anisotropy, it can be argued that the physical microenvironmental factors cannot be the dominant factor in the process.

Third, it should be assessed whether fascial tissue structures, i.e. dense collagen layers between neighbouring tissues which usually coincide with developmental compartment boundaries, impede tumour growth and thus lead to anisotropic permeation patterns. Recently, using a novel slicing and staining technique, Steinke *et al.* have shown dense, parallel aligned collagen layers between abutting pelvic tissue complexes such as the uterine cervix and the rectum or urinary bladder[40]. These collagen layers may halt locally invading tumour cells. In fact, it has previously been shown that low-to-high concentrated collagen interfaces drastically limit cell migration[25,41–43]. The implementation of collagenous tissue boundaries in our model via uniform, passive resistive boundaries – that is, as a simple mechanical barrier – did not sufficiently lead to the clinically observed growth patterns and shape of cervical cancer. It should be noted, however, that the use of strict inter-compartmental barriers in our model predicts a step-wise tumour progression into neighbouring tissue compartments and thus captures one aspect of the clinically observed tumour permeation pattern. It fails, however, to adequately reflect the anatomical distribution of tumour spread. Nonetheless, dense collagen lamellae remain a crucial physical barrier in (cancer) cell migration. Especially the ontogenetic lineage boundary between the mesometrium and mesorectum, as well as the mesureter, is extraordinary resilient against tumour transmigration, whereas the collagen lamella between the mesometrium and bladder compartment seems to be a minor obstacle; an unexpected observation considering that all collagen lamellae are of comparable thickness and composition and thus should display the same migratory resistance. Given the high spatial density of segregated compartments and therefore proximity of compartment boundaries, the tumour growth is influenced and shaped by these compartment boundaries, described in previous findings[11–14]. However, when interpreting the cancer cell migration resistance across compartment boundaries due to initial ontogenetic tissue incompatibility – that is, cancer can only invade ontogenetically close tissues at first and acquires the trait to invade ontogenetically distant tissue later on – the reason for the migration resilience may become apparent. The bladder compartment is ontogenetically close, whereas the ureter and rectum compartment are ontogenetically far from the uterine cervix compartment. This translates then to a lower hurdle for cervical cancer to acquire the ability to invade the bladder compartment, but a profound step in tumour progression for the rectum and ureter compartment. The patterns of cervical cancer growth that we observed can be mapped to the tissue domains that are identified using the bifurcational developmental paradigm. Crucially, there is a clear correlation between the degree of ontogenetic proximity to the uterine cervix and the likelihood of infiltration by cervical cancer for any pelvic tissue. Indeed, when introducing ontogenetic distance on the tissue tree into our model of local tumour spread, the predicted step-wise tumour infiltration of the various pelvic tissue compartments is nearly identical to the ones observed in clinical practice, as seen in Fig. 4. In contrast, if the isotropic (microenvironmentally influenced) tumour growth model were true, the tumour infiltration probability of different pelvic structures should follow a (quasi-)stochastic process, i.e. the invasion probabilities of two compartments adjacent to the uterine cervix should be independent. Our findings do not support this notion, however. For example, the invasion probabilities of the rectal and ureteral compartments are practically zero if the bladder compartment is not infiltrated, indicating a statistic interaction (e.g. conditional probabilities) between these different infiltration likelihoods.

As a last step, we sought to corroborate our simulation findings concerning the *stepwise* tumour progression which we observed in the ontogenetic tumour progression model. To confirm that ontogenetic tissue compartment infiltration occurs in a predictable and step-wise fashion, tumour infiltration data was gathered by pathological examination of the surgical resected tissues and area-proportional Euler diagrams of the histopathological data of tumour infiltration were drawn (Fig. 5).

Our null-hypothesis of tumour invasion and transmigration based on microenvironmental cues would have predicted that there is a notable probability that the rectum or ureter compartment is infiltrated without infiltration of the bladder compartment. In fact, even by pure chance of probabilistic tumour growth, we would expect to observe a significant number of such tumour situations. Considering its proximity to the uterine cervix, the circumstance that the ureter is spared from tumour infiltration in most of the cases is by itself remarkable. This

is not in support of the notion that microenvironmental factors alone determine tumour growth and invasion. Strikingly, except for one case, the rectum (mesorectum, muscular or mucosal layer) was never infiltrated without simultaneous infiltration of the bladder mesentery which strongly suggests a stepwise tumour progression based on tissue compartments with specifically different risks of tumour infiltration. Interestingly, in the one patient with rectum but without bladder infiltration, the bladder was spared during the initial surgery. After six months, this patient developed a tumour recurrence in the bladder compartment, indicating probable occult involvement of the bladder at the time of the initial operation. The nearly perfect sub-set characteristic of Fig. 5 can only occur if and only if the tumour progression happens in a stepwise fashion as our ontogenetic model would predict. Further information about the anatomical structures described here can be found in the Methods section.

One significant strength of the present work is that it is based on the histopathological data of numerous patients with advanced disease who underwent surgery without any preoperative treatment. Because patients with locally advanced disease are usually submitted to primary chemo-radiotherapy in most institutions, there is generally no comprehensive pathological data available. In a previous series of 88 cases with locally advanced and/or recurrent cervical cancer, the bladder with its support structures showed tumour infiltration in 84%, the rectum in 34% and the ureter in 24% of all cases[14]. In the current analysis examining 518 cases of primary cervical cancer, these patterns were slightly different with the ureter and mesureter exhibiting a greater likelihood of being infiltrated than the rectum and mesorectum. This demonstrates that tumour growth is different in cases of recurrent cancer as previous treatment (e.g. pelvic surgery or irradiation) probably affects ontogenetic compartment boundaries leading to different tumour progression patterns.

There are some weaknesses of our study which should be addressed. First, we used 2-dimensional anatomical maps instead of 3-dimensional anatomic templates. This was due to computational limitations and limited knowledge of the exact 3-dimensional positional information of all pelvic fascia. However, given the fact that the adjacent pelvic planes (sagittal and axial) are nearly identical to the ones we used, 3-dimensional simulation should lead to similar results.

Second, we disregarded other than continuous modes of tumour spread, i.e. lymphatic and haematogenous cancer dissemination. Although these routes of tumour propagation are clinically highly significant and have an important impact on a patient's prognosis, we did not cover them, as our goal was to provide a roadmap for local tumour growth only. Furthermore, constructing precise anatomical templates of the lymphatic and circulatory system as a basis for modelling is currently not feasible. However, considering that lymph nodes receiving drainage from a specific anatomical region display antigens from that region[44], they can be thought of as spatial extensions from that region providing a similarly fertile ground for tumour cell proliferation. We would speculate, that the knowledge about which tissue domain is connected to which lymph nodes could provide the basis for mapping the lymphatic landscape according to the display of antigens characteristic of specified ontogenetic compartments. Consequently, we would expect tumours to proliferate and spread preferentially to lymph nodes displaying antigens of close ontogenetic proximity to the peripheral tissue of tumour origin. Regarding hematogenic cancer spread causing metastasis in distant organs, we would again predict that organs which are ontogenetically closer related to the organ of tumour origin have a higher likelihood of being affected. However, the multitude of organs and anatomic structures sharing equal ontogenetic distance at this late stage of cancer progression makes it difficult to predict patterns of metastasis.

Third, this analysis only includes cervical cancer cases and its applicability to other tumour entities is therefore limited. However, the same principles regarding ontogenetically determined tumour growth seem to apply to vulvar cancer as was demonstrated in a recent clinical trial[45]. Furthermore, the correlation of carcinogenesis and ontogenesis has been shown for various tumor entities, such as rectum[46], pancreas[47], and mid-facial skin cancers[48], wherein the local tumor spread can be well-described with embryological structures such as compartments and fusion planes.

Our findings provide a framework to conceptualize and predict local spread of cervical cancer. As ontogenetic compartment borders can clearly be identified intraoperatively, ontogenetic tissue mapping can probably serve as a roadmap to local cancer growth in other tumour entities. Knowing the embryological origin of any tissue in which cancer arises, one can derive a relative likelihood of different adjacent tissues to be infiltrated by tumour cells, depending on their ontogenetic proximity to the tissue of cancer origin, deduce an ontogenetic tumour stage, and tailor surgical resection exactly to the tissue at risk. In the future, this might help to decrease operative morbidity by sparing low-risk tissue while improving local tumour control by resecting all tissues of potential (occult) tumour infiltration.

What could be the underlying mechanisms on a cellular and molecular level? One explanation might be the existence of transcriptional programs which sequentially activate and silence specific genes. Such programs are executed by gene regulatory networks (GRNs), which are defined as units of interacting transcriptional elements which exhibit specific regulatory relationships and therefore cause a predictable pattern of gene expression with a defined structural and functional output[49]. GRN's enable cells to concertedly change protein expression patterns in response to environmental changes and have a tendency to stabilize themselves including pathological states which might foster tumour progression[50]. This would lead to a predictable evolution which is reflected by the acquisition of all hallmarks of cancer on a cellular level and by specific growth patterns on the tissue level. Interestingly, GRNs seem to play an important role in epithelial-mesenchymal transition (EMT) which is a key mechanism of cell and tissue differentiation, both during ontogenesis and during cancer progression[51–53] including hybrid epithelial/mesenchymal states[54–56]. We hypothesize that the stepwise re-activation of GRNs, which are normally executed during ontogenetic development, leads to the observed growth and infiltration patterns.

In conclusion, we have shown that the potential local tumour growth of cervical cancer is not isotropic. The data representation and our tumour growth simulation indicate that ontogenetic tissue mapping might profoundly help in predicting the probability of tumour invasion into a given tissue by a certain cancer. Future work needs to corroborate these findings, ideally in other cancer entities.

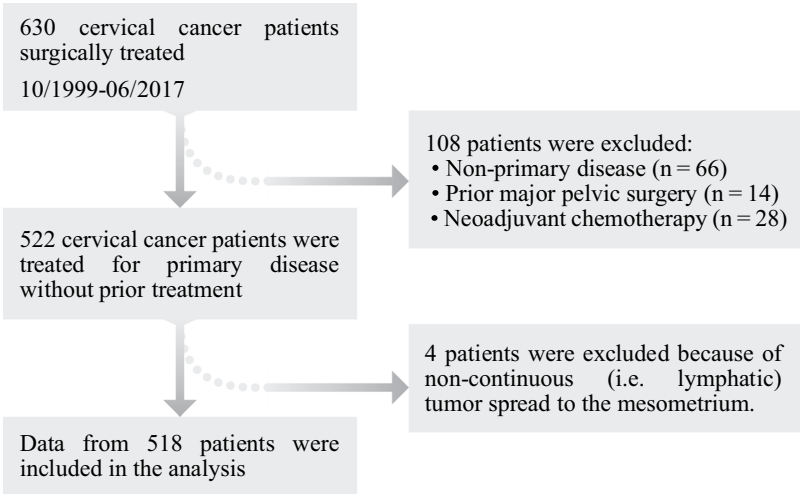

Figure 6. Patient selection process. Initially, 630 patients were enrolled and surgically treated between October 1999 and June 2017 for cervical cancer. Only patients with primary disease and without prior major pelvic surgery were included in the analysis. Four cases were excluded because of locally non-continuous tumour spread. Locally discontinuous tumour spread can occur to the mesometria via lymphatic vessels. Discontinuous local tumour spread to other tissues is anatomically not feasible. Additional information regarding the patient selection process and treatment is available in the Supplement S1.

Methods

Patient selection and data acquisition. In order to obtain histopathological information for further analysis, patient and tumour data was extracted from our institutional study databases. Figure 6 gives an overview over the patient selection process. More information regarding patient selection and treatment can be found in the Supplement S1. The TMMR/EMMR/LEER-Trial (cancer field resection trials) was approved by the ethical committee at the medical faculty of Leipzig University (review board numbers 012 – 13 – 28012013, 192/2001 and 151/366 2000). All aspects of the clinical trial as well as data handling and analysis was carried out in compliance with the relevant guidelines and directives issued by the European Union, the Federal Republic of Germany and the State of Saxony. The patients had given informed consent to participate in this study prior to the operation. This consent included usage of the data for further analysis. As the raw data contains sensitive patient information, it cannot be made accessible to the public. Researchers who meet the criteria to access confidential patient data will be supplied with the requested data on request. Further, non-sensitive data is available in the Supplement S1.

Numerical and qualitative data used for preparation of the Euler diagrams and in-silico models were extracted from the original detailed pathology reports archived in our database. These pathology reports contained all relevant information regarding tumour entity (i.e. squamous or non-squamous histology), tumour size measured directly within the surgical specimen, and extent of infiltration into neighbouring pelvic tissues.

Ontogenetic anatomy. The terms we use to describe pelvic anatomy diverge from the terminology commonly used by gynaecological surgeons. Generally, structures and landmarks in surgical anatomy consist of functional units while "non-functional" connective tissue is frequently not classified any further. In contrast, ontogenetic anatomy provides a means to group all tissues into distinct groups regardless of form and function. Therefore, some of the terms which are less commonly used in conventional surgical anatomy or which have different meanings are described here. Figure 1 gives an anatomic overview.

The Müllerian compartment is the sum of all adult tissues which are derived from the embryonic paramesonephric ducts. Cranio-caudally, this includes the Fallopian tubes, the uterine corpus, the uterine cervix, the proximal two thirds of the vagina and the Müllerian adventitia (see below). Each of these structures constitutes a sub-compartment of the Müllerian compartment.

The para tissues constitute together the Müllerian adventitia. This is a coat of fibrovascular connective tissue enveloping the entire Müllerian compartment. In a cranio-caudal fashion the Müllerian adventitia can be divided into the following segments according to the adjacent organs:

- Fallopian tubes – parasalpinx
- Uterine corpus – paracorpus
- Uterine cervix – paracervix
- Vagina – paracolpos

Each para-tissue constitutes a sub-compartment of the Müllerian compartment.

Note that the term "parametrium" in surgical anatomy conventionally denotes a poorly defined composite structure including more tissues of different ontogenetic origin (paracervix, mesometrium, parts of the

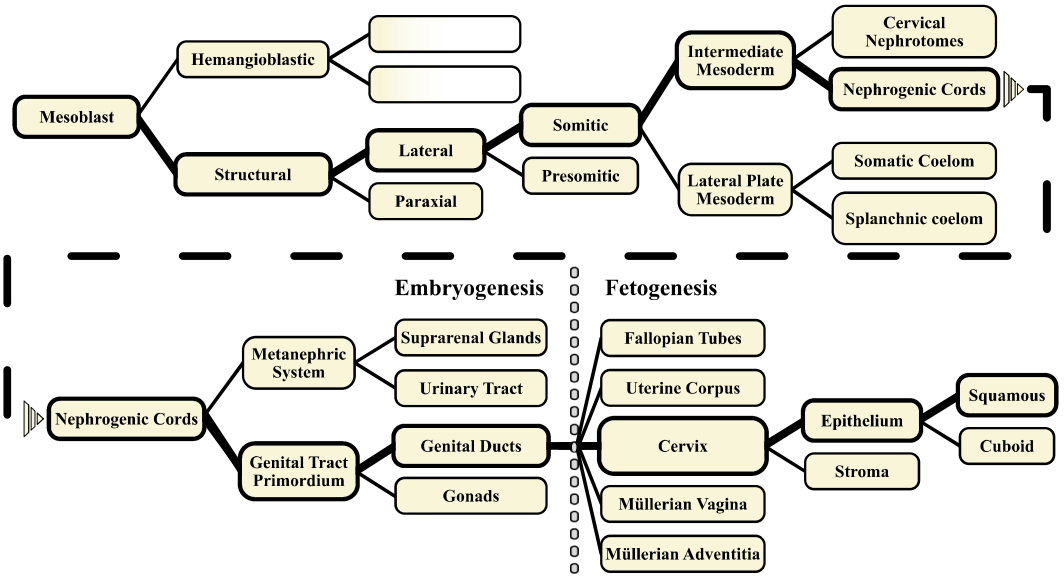

Figure 7. Ontogenetic tissue tree conceptualizing the development of the genital ducts sub-compartments (including the uterine cervix). For example, the nephrogenic cords give rise to the metanephric system and the primordial genital tracts. The primordial genital tracts then bifurcate to produce the gonads and the genital ducts (in the female, these are the Müllerian ducts). The lower Müllerian ducts fuse and develop into the mature reproductive structures including the fallopian tubes, the uterus, the uterine cervix and the proximal (Müllerian) vagina, which all constitute ontogenetic sub-compartments of the adult Müllerian compartment. The diagram depicted can serve as a genealogical tree to trace the ontogenetic development of a given tissue and to deduce the ontogenetic kinship of adjacent tissues. Note that in the post-embryonic (foetal) period indicated by the grey-dashed line, divisions into more than two tissue branches are possible. Contrary to the embryonic period, these developmental steps involve tissue differentiation along defined axes, e.g. craniocaudally without the establishment of new compartments.

mesobladder and the mesureter). The para-tissues contain a tight network of anastomosing arteries and veins as well as lymph vessels and nerves.

The term mesentery is here applied to the connective tissues which connect the pelvic organs to the pelvic and abdominal wall laterally and caudally (and to a lesser extend ventrally in the case of the urinary bladder). The mesenteries are composed primarily of fibrofatty tissue containing lymph- and blood vessels and therefore serve an important nutritional role. In addition, they contain nerves and interspersed condensations of fibrous tissue which serves a suspensory function. Ontogenetically, they are closely related to the organs which they support and are therefore prone for early tumor infiltration. The mesenteries develop and elongate during the embryonic and fetal period as the associated organs move within the abdominal and pelvic cavity as a consequence of differential growth.

Within the pelvis, the urogenital tract is supported by the urogenital mesentery. This mesentery can be subdivided into

- The mesometrium supporting the uterus (corpus and cervix)
- The mesureter supporting the ureter
- The mesobladder supporting the urinary bladder.

In addition, the rectum is supported by the mesorectum.

By conventional nomenclature, only the mesorectum is a proper mesentery (defined as a peritoneal duplication enveloping an intraabdominal organ). From an ontogenetic perspective, the term "mesentery" is broader to include the above-mentioned structures.

Anatomical and ontogenetic mapping. We have previously described embryogenesis in terms of bifurcational tissue differentiation based on morphologic observations in human embryos[12,13]. During the first stage of tissue expansion in a given embryonic domain, cellular proliferation is homogenous and isotropic. At a certain point, presumably when a morphogen gradient is formed, and/or an unstable critical concentration is reached, cellular segregation and the emergence of two new cell populations with new phenotypes can be observed. Figure 7 shows the resulting bifurcational ontogenetic tissue tree in which the ancestry of different tissues can be traced. This tissue tree is the basis for the ontogenetic mapping shown in Fig. 1D.

Modelling. As described in the beginning, singular tumours are usually not of spherical shape and do not necessarily grow isotropically. Nevertheless, permeation of cancer cells into surrounding tissues is assumed isotropic in order to define a safe surgical resection margin, hence they are assumed to have an isotropic growth

potential. Here, we introduce a description of tumour growth dynamics for a *statistically averaged* tumour to show that the clinically assumed isotropic growth is not sufficient for explaining the clinically and pathologically observed tumour growth patterns. The descriptive model is based on the pathological and ontogenetic characterization presented Table 1 and Fig. 7 and is functional for the presented histological cancer types.

The growth dynamics for a statistically averaged tumour were described by the following set of reaction-diffusion equations

$$\partial_t \Psi_{ij,k} = \nabla \cdot \left(D_{ij,k} \nabla \Psi_{ij,k} \right) + R_{ij,k},$$

where $\Psi_{ij,k} = \Psi_{ij,k}(\vec{x}, t)$ denotes the probability density of cancer cells originating from tissue compartment i located in the tissue compartment j at a given time. The index k accounts for the cancer cell's coarse-grained aggressiveness or staging, and $D_{ij,k} = D_{ij,k}(\vec{x}, t)$ denotes the diffusion coefficient of cancerous cells originating from compartment i at the stage k in the compartment j. The local cancer net proliferation rate $R_{ij,k}$ as a bulk may depend, for instance, on the complex cancer cell interactions with its environment. For example, increasing cancer cell density may lead to limited oxygen and nutrient supply per cell and therefore to a reduction in cancer cell division rate, or may lead to tumour hypoxia induced angiogenesis, thus stimulating tumour growth and invasion[57–62]. Some or many of inhibitory factors may lose effect in the progress of tumour progression[63–65], thus altering the cancer proliferation and spreading dynamics. *In vivo*, the local cancer proliferation rate is generally thought to depend on supply of oxygen and nutrients per cancer cell, which is an inverse measure of the local cancer cell density, among potential other physical and chemical microenvironmental factors[42,66–70]. The reaction term can be expanded to include features of nutrient supply, microenvironmental effects or growth factors to create a model closer resembling *in vivo* tumour physiology and allowing for enforced anisotropic tumour growth. Here, the basic tumour growth rate was modelled by a generalized Fisher-Kolmogorov term[71–73] agnostic of microscopic interactions of single cancer cells,

$$R_{ijk} = r_{ijk} \Psi_{ik} (1 - \Psi_{ik}^n),$$

with the individual cancer cell proliferation rate r_{ijk} (as compared to R_{ijk}) and the proliferation inhibition coefficient $(1 - \Psi_{ik}^n)$. The cancer net proliferation rate R_{ijk} initially increases with an increasing number of cancer cells in a given volume and slows down when it approaches the maximum cancer cell density probability $\sum_{ik} \Psi_{ik} = 1$ in that volume. Tissue compartment boundaries were modelled as additional passive resistive barriers which limit cancer cell migration,

$$\hat{\mathrm{n}} \cdot \left(D \nabla \Psi_{ij,k} \right) = \left(\Psi_j - \Psi_i \right) / \rho_{ij,k},$$

with $\hat{\mathrm{n}}$ denoting the normal vector of the interface of neighbouring compartments i and j, and ρ_{ij} the resistance for cancer cell migration across the interface. The resistive barrier simulates an initially low fraction of cancer cells with the acquired capacity of invasion into a neighbouring compartment. The finite-element model was simulated via COMSOL Multiphysics® software[74]. Further detailed descriptions and values of model parameters are given in the Supplement S2.

Data Availability

As the raw patient data of the TMMR/EMMR/LEER-Trial (cancer field resection trials) contains sensitive patient information, it cannot be made accessible to the public. Researchers who meet the criteria to access confidential patient data will be supplied with the requested data on request. Further, all non-sensitive data is available in the methods section and the supplemental information.

References

1. Torre, L. A., Siegel, R. L., Ward, E. M. & Jemal, A. Global Cancer Incidence and Mortality Rates and Trends–An Update. *Cancer epidemiology, biomarkers & prevention: a publication of the American Association for Cancer Research, cosponsored by the American Society of Preventive Oncology* **25**, 16–27, https://doi.org/10.1158/1055-9965.EPI-15-0578 (2016).
2. Cardoso, F. *et al*. Early breast cancer: ESMO Clinical Practice Guidelines for diagnosis, treatment and follow-up. *Annals of oncology: official journal of the European Society for Medical Oncology*, https://doi.org/10.1093/annonc/mdz173 (2019).
3. Parker, C., Gillessen, S., Heidenreich, A. & Horwich, A. Cancer of the prostate: ESMO Clinical Practice Guidelines for diagnosis, treatment and follow-up. *Annals of oncology: official journal of the European Society for Medical Oncology* **26**(Suppl 5), v69–77, https://doi.org/10.1093/annonc/mdv222 (2015).
4. Glynne-Jones, R. *et al*. Rectal cancer: ESMO Clinical Practice Guidelines for diagnosis, treatment and follow-up. *Annals of oncology: official journal of the European Society for Medical Oncology* **28**, iv22–iv40, https://doi.org/10.1093/annonc/mdx224 (2017).
5. Postmus, P. E. *et al*. Early and locally advanced non-small-cell lung cancer (NSCLC): ESMO Clinical Practice Guidelines for diagnosis, treatment and follow-up. *Annals of oncology: official journal of the European Society for Medical Oncology* **28**, iv1–iv21, https://doi.org/10.1093/annonc/mdx222 (2017).
6. Höckel, M. & Dornhöfer, N. The hydra phenomenon of cancer. Why tumors recur locally after microscopically complete resection. *Cancer research* **65**, 2997–3002, https://doi.org/10.1158/0008-5472.CAN-04-3868 (2005).
7. Obrzut, B., Semczuk, A., Naróg, M., Obrzut, M. & Król, P. Prognostic Parameters for Patients with Cervical Cancer FIGO Stages IA2-IIB. A Long-Term Follow-Up. *Oncology* **93**, 106–114, https://doi.org/10.1159/000471766 (2017).
8. Houssami, N. *et al*. Meta-analysis of the impact of surgical margins on local recurrence in women with early-stage invasive breast cancer treated with breast-conserving therapy. *European journal of cancer (Oxford, England: 1990)* **46**, 3219–3232, https://doi.org/10.1016/j.ejca.2010.07.043 (2010).
9. Woelber, L. *et al*. Role of tumour-free margin distance for loco-regional control in vulvar cancer-a subset analysis of the Arbeitsgemeinschaft Gynäkologische Onkologie CaRE-1 multicenter study. *European journal of cancer (Oxford, England: 1990)* **69**, 180–188, https://doi.org/10.1016/j.ejca.2016.09.038 (2016).

10. Landoni, F. *et al*. Class II versus class III radical hysterectomy in stage IB-IIA cervical cancer. A prospective randomized study. *Gynecologic oncology* **80**, 3–12, https://doi.org/10.1006/gyno.2000.6010 (2001).
11. Höckel, M. & Horn, L.-C. The puzzle of close surgical margins is not puzzling. *Gynecologic oncology* **130**, 224–225, https://doi.org/10.1016/j.ygyno.2013.03.017 (2013).
12. Höckel, M. Morphogenetic fields of embryonic development in locoregional cancer spread. *The Lancet Oncology* **16**, e148–e151, https://doi.org/10.1016/S1470-2045(14)71028-9 (2015).
13. Höckel, M., Hentschel, B. & Horn, L.-C. Association between developmental steps in the organogenesis of the uterine cervix and locoregional progression of cervical cancer. A prospective clinicopathological analysis. *The Lancet Oncology* **15**, 445–456, https://doi.org/10.1016/S1470-2045(14)70060-9 (2014).
14. Höckel, M., Wolf, B., Hentschel, B. & Horn, L.-C. Surgical treatment and histopathological assessment of advanced cervicovaginal carcinoma. A prospective study and retrospective analysis. *European journal of cancer (Oxford, England: 1990)* **70**, 99–110, https://doi.org/10.1016/j.ejca.2016.10.016 (2017).
15. Chow, S. & Ruskey, F., Drawing Area-Proportional Venn and Euler Diagrams. In: Liotta G. (eds) *Graph Drawing. GD 2003. Lecture Notes in Computer Science, vol 2912*, edited by G. Liotta, pp. 466–477. Springer, Berlin, Heidelberg, https://doi.org/10.1007/978-3-540-24595-7_44 (2004).
16. Kestler, H. A., Müller, A., Gress, T. M. & Buchholz, M. Generalized Venn diagrams. A new method of visualizing complex genetic set relations. *Bioinformatics (Oxford, England)* **21**, 1592–1595, https://doi.org/10.1093/bioinformatics/bti169 (2005).
17. Kestler, H. A. *et al*. VennMaster. Area-proportional Euler diagrams for functional GO analysis of microarrays. *BMC bioinformatics* **9**, 67, https://doi.org/10.1186/1471-2105-9-67 (2008).
18. Czarnek, N., Clark, K., Peters, K. B. & Mazurowski, M. A. Algorithmic three-dimensional analysis of tumor shape in MRI improves prognosis of survival in glioblastoma: a multi-institutional study. *Journal of neuro-oncology* **132**, 55–62, https://doi.org/10.1007/s11060-016-2359-7 (2017).
19. Mazurowski, M. A. *et al*. Radiogenomics of lower-grade glioma: algorithmically-assessed tumor shape is associated with tumor genomic subtypes and patient outcomes in a multi-institutional study with The Cancer Genome Atlas data. *J Neurooncol* **133**, 27–35, https://doi.org/10.1007/s11060-017-2420-1 (2017).
20. Kasangian, A. A. *et al*. The prognostic role of tumor size in early breast cancer in the era of molecular biology. *PloS one* **12**, e0189127, https://doi.org/10.1371/journal.pone.0189127 (2017).
21. Nieman, K. M., Romero, I. L., van Houten, B. & Lengyel, E. Adipose tissue and adipocytes support tumorigenesis and metastasis. *Biochimica et biophysica acta* **1831**, 1533–1541, https://doi.org/10.1016/j.bbalip.2013.02.010 (2013).
22. Berger, N. A. Obesity and cancer pathogenesis. *Annals of the New York Academy of Sciences* **1311**, 57–76, https://doi.org/10.1111/nyas.12416 (2014).
23. Gilbert, P. M. & Weaver, V. M. Cellular adaptation to biomechanical stress across length scales in tissue homeostasis and disease. *Seminars in cell & developmental biology* **67**, 141–152, https://doi.org/10.1016/j.semcdb.2016.09.004 (2017).
24. Sunyer, R. *et al*. Collective cell durotaxis emerges from long-range intercellular force transmission. *Science* **353**, 1157–1161, https://doi.org/10.1126/science.aaf7119 (2016).
25. Miron-Mendoza, M., Seemann, J. & Grinnell, F. The differential regulation of cell motile activity through matrix stiffness and porosity in three dimensional collagen matrices. *Biomaterials* **31**, 6425–6435, https://doi.org/10.1016/j.biomaterials.2010.04.064 (2010).
26. Discher, D. E., Janmey, P. & Wang, Y.-L. Tissue cells feel and respond to the stiffness of their substrate. *Science (New York, N.Y.)* **310**, 1139–1143, https://doi.org/10.1126/science.1116995 (2005).
27. Yeung, T. *et al*. Effects of substrate stiffness on cell morphology, cytoskeletal structure, and adhesion. *Cell motility and the cytoskeleton* **60**, 24–34, https://doi.org/10.1002/cm.20041 (2005).
28. Chin, L., Xia, Y., Discher, D. E. & Janmey, P. A. Mechanotransduction in cancer. *Current opinion in chemical engineering* **11**, 77–84, https://doi.org/10.1016/j.coche.2016.01.011 (2016).
29. Storm, C., Pastore, J. J., MacKintosh, F. C., Lubensky, T. C. & Janmey, P. A. Nonlinear elasticity in biological gels. *Nature* **435**, 191, https://doi.org/10.1038/nature03521 (2005).
30. Broedersz, C. P. & MacKintosh, F. C. Modeling semiflexible polymer networks. *Rev. Mod. Phys.* **86**, 995, https://doi.org/10.1103/RevModPhys.86.995 (2014).
31. Schuldt, C. *et al*. Tuning Synthetic Semiflexible Networks by Bending Stiffness. *Phys. Rev. Lett.* **117**, 197801, https://doi.org/10.1103/PhysRevLett.117.197801 (2016).
32. Xu, J. *et al*. Mechanical Properties of Actin Filament Networks Depend on Preparation, Polymerization Conditions, and Storage of Actin Monomers. *Biophysical journal* **74**, 2731–2740, https://doi.org/10.1016/S0006-3495(98)77979-2 (1998).
33. Gardel, M. L. *et al*. Elastic behavior of cross-linked and bundled actin networks. *Science (New York, N.Y.)* **304**, 1301–1305, https://doi.org/10.1126/science.1095087 (2004).
34. Kubitschke, H., Morawetz, E. W., Käs, J. A. & Schnauß, J. Physical Properties of Single Cells and Collective Behavior. *Quantification of Biophysical Parameters in Medical Imaging*, edited by I. Sack & T. Schaeffter, pp. 89–121 Springer International Publishing, Cham, https://doi.org/10.1007/978-3-319-65924-4_5 2018.
35. Huber, F. *et al*. Emergent complexity of the cytoskeleton. From single filaments to tissue. *Advances in physics* **62**, 1–112, https://doi.org/10.1080/00018732.2013.771509 (2013).
36. Seltmann, K., Fritsch, A. W., Käs, J. A. & Magin, T. M. Keratins significantly contribute to cell stiffness and impact invasive behavior. *Proceedings of the National Academy of Sciences of the United States of America* **110**, 18507–18512, https://doi.org/10.1073/pnas.1310493110 (2013).
37. Oswald, L., Grosser, S., Smith, D. M. & Käs, J. A. Jamming transitions in cancer. *J. Phys. D: Appl. Phys.* **50**, 483001, https://doi.org/10.1088/1361-6463/aa8e83 (2017).
38. Fritsch, A. *et al*. Are biomechanical changes necessary for tumour progression? *Nature Physics* **6**, 730 EP -, https://doi.org/10.1038/nphys1800 (2010).
39. Kubitschke, H. *et al*. Actin and microtubule networks contribute differently to cell response for small and large strains. *New J. Phys.* **19**, 93003, https://doi.org/10.1088/1367-2630/aa7658 (2017).
40. Steinke, H. *et al*. Periodic acid-Schiff (PAS) reaction and plastination in whole body slices. A novel technique to identify fascial tissue structures. *Annals of anatomy=Anatomischer Anzeiger: official organ of the Anatomische Gesellschaft* **216**, 29–35, https://doi.org/10.1016/j.aanat.2017.10.001 (2017).
41. Carey, S. P., Kraning-Rush, C. M., Williams, R. M. & Reinhart-King, C. A. Biophysical control of invasive tumor cell behavior by extracellular matrix microarchitecture. *Biomaterials* **33**, 4157–4165, https://doi.org/10.1016/j.biomaterials.2012.02.029 (2012).
42. Bordeleau, F., Tang, L. N. & Reinhart-King, C. A. Topographical guidance of 3D tumor cell migration at an interface of collagen densities. *Physical biology* **10**, 65004, https://doi.org/10.1088/1478-3975/10/6/065004 (2013).
43. Mierke, C. T. *et al*. The two faces of enhanced stroma. Stroma acts as a tumor promoter and a steric obstacle. *NMR in biomedicine*. https://doi.org/10.1002/nbm.3831 (2017).
44. Lee, J.-W. *et al*. Peripheral antigen display by lymph node stroma promotes T cell tolerance to intestinal self. *Nature immunology* **8**, 181–190, https://doi.org/10.1038/ni1427 (2007).
45. Höckel, M. *et al*. Vulvar field resection based on ontogenetic cancer field theory for surgical treatment of vulvar carcinoma. A single-centre, single-group, prospective trial. *The Lancet Oncology* **19**, 537–548, https://doi.org/10.1016/S1470-2045(18)30109-8 (2018).

46. MacFarlane, J. K., Ryall, R. D. H. & Heald, R. J. Mesorectal excision for rectal cancer. *The Lancet* **341**(8843), 457–460 (1993).
47. Makino, I. *et al.* Nerve plexus invasion in pancreatic cancer: spread patterns on histopathologic and embryological analyses. *Pancreas* **37**(4), 358–365, https://doi.org/10.1097/MPA.0b013e31818166e6 (2008).
48. Panje, W. R. & Ceilley, R. I. The influence of embryology of the mid-face on the spread of epithelial malignancies. *The Laryngoscope* **89**(12), 1914–1920 https://doi.org/10.1288/00005537-197912000-00003 (1979).
49. Moris, N., Pina, C. & Arias, A. M. Transition states and cell fate decisions in epigenetic landscapes. *Nature reviews. Genetics* **17**, 693–703, https://doi.org/10.1038/nrg.2016.98 (2016).
50. Albergante, L., Blow, J. J. & Newman, T. J. Buffered Qualitative Stability explains the robustness and evolvability of transcriptional networks. *eLife* **3**, e02863, https://doi.org/10.7554/eLife.02863 (2014).
51. Pastushenko, I. *et al.* Identification of the tumour transition states occurring during EMT. *Nature* **556**, 463–468, https://doi.org/10.1038/s41586-018-0040-3 (2018).
52. Saunders, L. R. & McClay, D. R. Sub-circuits of a gene regulatory network control a developmental epithelial-mesenchymal transition. *Development (Cambridge, England)* **141**, 1503–1513, https://doi.org/10.1242/dev.101436 (2014).
53. Denisov, E. V. & Perelmuter, V. M. A fixed partial epithelial-mesenchymal transition (EMT) triggers carcinogenesis, whereas asymmetrical division of hybrid EMT cells drives cancer progression. *Hepatology (Baltimore, Md.)*, https://doi.org/10.1002/hep.29784 (2018).
54. Jolly, M. K. *et al.* Implications of the Hybrid Epithelial/Mesenchymal Phenotype in Metastasis. *Frontiers in oncology* **5**, 155, https://doi.org/10.3389/fonc.2015.00155 (2015).
55. Jordan, N. V., Johnson, G. L. & Abell, A. N. Tracking the intermediate stages of epithelial-mesenchymal transition in epithelial stem cells and cancer. *Cell cycle (Georgetown, Tex.)* **10**, 2865–2873, https://doi.org/10.4161/cc.10.17.17188 (2011).
56. Grosse-Wilde, A. *et al.* Stemness of the hybrid Epithelial/Mesenchymal State in Breast Cancer and Its Association with Poor Survival. *PloS one* **10**, e0126522, https://doi.org/10.1371/journal.pone.0126522 (2015).
57. Krock, B. L., Skuli, N. & Simon, M. C. Hypoxia-induced angiogenesis: good and evil. *Genes & cancer* **2**, 1117–1133, https://doi.org/10.1177/1947601911423654 (2011).
58. Liao, D. & Johnson, R. S. Hypoxia: a key regulator of angiogenesis in cancer. *Cancer metastasis reviews* **26**, 281–290, https://doi.org/10.1007/s10555-007-9066-y (2007).
59. Chouaib, S. *et al.* Hypoxia promotes tumor growth in linking angiogenesis to immune escape. *Frontiers in immunology* **3**, 21, https://doi.org/10.3389/fimmu.2012.00021 (2012).
60. Bergers, G. & Benjamin, L. E. Tumorigenesis and the angiogenic switch. *Nature reviews. Cancer* **3**, 401–410, https://doi.org/10.1038/nrc1093 (2003).
61. Carmeliet, P. & Jain, R. K. Angiogenesis in cancer and other diseases. *Nature* **407**, 249–257, https://doi.org/10.1038/35025220 (2000).
62. Carmeliet, P. & Jain, R. K. Molecular mechanisms and clinical applications of angiogenesis. *Nature* **473**, 298–307, https://doi.org/10.1038/nature10144 (2011).
63. Evan, G. I. & Vousden, K. H. Proliferation, cell cycle and apoptosis in cancer. *Nature* **411**, 342–348, https://doi.org/10.1038/35077213 (2001).
64. McClatchey, A. I. & Yap, A. S. Contact inhibition (of proliferation) redux. *Current opinion in cell biology* **24**, 685–694, https://doi.org/10.1016/j.ceb.2012.06.009 (2012).
65. Elmore, S. Apoptosis: a review of programmed cell death. *Toxicologic pathology* **35**, 495–516, https://doi.org/10.1080/01926230701320337 (2007).
66. Provenzano, P. P. *et al.* Collagen density promotes mammary tumor initiation and progression. *BMC medicine* **6**, 11, https://doi.org/10.1186/1741-7015-6-11 (2008).
67. Weinberg, R. A. The biology of cancer. Chapter 11 - Multi-Step Tumorigenesis, 462 (2014).
68. Oudin, M. J. & Weaver, V. M. Physical and Chemical Gradients in the Tumor Microenvironment Regulate Tumor Cell Invasion, Migration, and Metastasis. *Cold Spring Harbor symposia on quantitative biology* **81**, 189–205, https://doi.org/10.1101/sqb.2016.81.030817 (2016).
69. Weaver, V. M., Fischer, A. H., Peterson, O. W. & Bissell, M. J. The importance of the microenvironment in breast cancer progression: recapitulation of mammary tumorigenesis using a unique human mammary epithelial cell model and a three-dimensional culture assay. *Biochemistry and cell biology=Biochimie et biologie cellulaire* **74**, 833–851 PMCID: PMC2933195 (1996).
70. Hanahan, D. & Weinberg, R. A. Hallmarks of cancer: The next generation. *Cell* **144**, 646–674, https://doi.org/10.1016/j.cell.2011.02.013 (2011).
71. Kametaka, Y. On the nonlinear diffusion equation of Kolmogorov-Petrovskii-Piskunov type. *Osaka Journal of Mathematics* **13**, 11–66 https://doi.org/10.18910/9093 (1976).
72. Menze, B. H. *et al.* A Generative Approach for Image-Based Modeling of Tumor. *Growth. Information processing in medical imaging* **22**, 735–747 https://doi.org/10.1007/978-3-642-22092-0_60 (2011).
73. Clatz, O. *et al.* Realistic Simulation of the 3D Growth of Brain Tumors in MR Images Coupling Diffusion with Biomechanical Deformation. *Ieee Transactions on Medical Imaging* **24**, 1334–1346, https://doi.org/10.1109/TMI.2005.857217 (2005).
74. COMSOL. *Multiphysics® v. 5.3*, www.comsol.com (Stockholm, Sweden).

Acknowledgements

This project has received funding from the European Research Council (ERC-741350/HoldCancerBack). We acknowledge funding from the European Commission H2020-PHC-2015-two-stage as part of the 'FORCE' project (668039/Imaging the Force of Cancer). E.M. was supported by the European Union and the European Social Fond in Saxony (ESF – 100234741). B.W. and M.H. were supported by Stiftung Gynäkologische Onkologie, a non-profit foundation committed to the support of research in gynaecologic oncology.

Author Contributions

All named authors have contributed significantly to this work. H.K. and B.W. have written the original draft of the manuscript. H.K., B.W. and E.M. analysed, curated and synthesized the study data. H.K. and B.W. conducted the research and investigation process and data collection. H.K. prepared the data visualization. H.K., B.W. and U.B. developed the methodology and created the model. L.C.H., B.A., M.H. and J.K. provided study materials (patient and pathological material and clinical data). U.B., M.H. and J.K. administrated and supervised the project and guided the interpretation of the data. All authors provided critical review, commentary, revision and editing for the final version of the manuscript. We acknowledge support from the German Research Foundation (DFG) and University of Leipzig within the program of Open Access Publishing.

Additional Information

Supplementary information accompanies this paper at https://doi.org/10.1038/s41598-019-49182-1.

Competing Interests: The authors declare no competing interests.

Publisher's note: Springer Nature remains neutral with regard to jurisdictional claims in published maps and institutional affiliations.

Supplement
Roadmap to Local Tumour Growth: Insights from Cervical Cancer

Hans Kubitschke[1+], Benjamin Wolf[2,3+], Erik Morawetz[1], Lars-Christian Horn[4], Bahriye Aktas[2], Ulrich Behn[5], Michael Höckel[2,3], Josef Käs[1*]

[1] Peter Debye Institute for Soft Matter Physics, Leipzig University, Germany

[2] Department of Gynecology, Women's and Children's Centre, University Hospital Leipzig, Germany

[3] Leipzig School of Radical Pelvic Surgery, Leipzig University, Germany

[4] Division of Gynecologic, Breast and Perinatal Pathology, University Hospital Leipzig, Germany

[5] Institute of Theoretical Physics, Leipzig University, Germany

S1 Patient selection

Since the beginning of the prospective monocentric studies evaluating the feasibility of total- and extended mesometrial resection (TMMR, EMMR) as well as laterally extended endopelvic resection (LEER) for the treatment of early (TMMR) and locally advanced (TMMR, EMMR and LEER) cancer of the uterine cervix, all clinical, surgical and pathological data was collected prospectively. The surgical procedures in TMMR [1], EMMR [2] and LEER [3] have been described before. As we sought to examine tumour growth unaffected by iatrogenic manipulations, we excluded all non-primary cases (i.e. tumour recurrences or secondary carcinomas). Furthermore, patients who had undergone extensive previous pelvic surgery (e.g. hysterectomy) or had received preoperative chemotherapy were excluded from the analysis as these treatments might affect tumour growth patterns. Because the objective of this study was to investigate continuous tumour spread, we further excluded cases of locally discontinuous (i.e. lymphatic) tumour spread. Locally discontinuous tumour spread can occur, to the mesometria via lymphatic vessels. Discontinuous local tumour spread to other tissues is anatomically not feasible. Pelvic lymph node status was assessed in all patients histopathologically. In 100 patients (19.3%) paraaortic lymph nodes were additionally examined histopathologically because of risk for metastasis to this region. However, we did not further analyse lymph node involvement as the present investigation focuses on local, continuous tumour spread. **Figure 6** of the manuscript gives an overview over the patient selection process. All patients had given written informed consent preoperatively which included permission to use data for further analysis. The TMMR/EMMR and LEER trials have been approved by the local ethics committee.

S2 Modelling

Simulations were carried out with COMSOL Multiphysics 5.3 (www.comsol.com). The set of partial differential equation are

$$\partial_t \Psi_{ij,k} = \nabla \cdot \left(D_{ij,k} \nabla \Psi_{ij,k}\right) + R_{ij,k} \,,$$

$$R_{ij,k} = r_{ij,k} \Psi_{ij,k} \left(1 - \Psi_{ij,k}^{n}\right) ,$$

$$\hat{\mathrm{n}} \cdot (D \nabla \Psi_{ij}) = \left(\Psi_j - \Psi_i\right) / \rho_{ij}$$

as described in the manuscript. The heat transfer module of COMSOL provided the simulation framework. Digitalized transversal planes were acquired from previous publications [4,1,3]. The simulations were done in two dimensions in the transversal plane. A summary of the simulation parameters for the physical-microenvironmental model are given in table 1 and for the ontogenetic model in table 2. For better comprehension, the parameter values here are given in *centimetres* and *days* instead of meters and seconds.

As boundary conditions, the tumour growth starting point is set to the centre of the cervix by imposing the tumour probability density to be $\Psi = 1$ at the external orifice of the cervix. The outer most boundaries of the transversal plane have a zero-probability flux normal to the boundary, meaning that no tumour can leave the body and the whole tumour entity is contained in the simulated transversal plane (the tumour cannot grow outside of the body).

The simulated transversal plane was rasterized into finite, trigonal elements and given differential equations were numerically solved. Initial parameters, e.g. dimensions of the pelvical area and tumour growth rates, were obtained from clinical findings given in the literature [5–10].

Table S1 Parameters for physical microenvironmental model

Parameter		**value**
general		
proliferation inhibition exponent		$n = 1$
diffusion coefficient		$c = 1.467 \cdot 10^{-4}\ \mathrm{cm}^2/\mathrm{d}$
finite element mesh properties		
maximum element size		1.00 cm
minimum element size		0.05 cm
maximum element growth rate		1.3
curvature factor		0.3
simulation time, time step		$0 - 1000$ d , 0.1 d
Tissue characterisation	ontogenetic tissue type	Tumour growth rate
fibrous	cervix paracervix	$r = 1.406 \cdot 10^{-2}\ 1/\mathrm{d}$
fatty	mesometrium mesobladder mesorectum mesureter	$r = 1.875 \cdot 10^{-2}\ 1/\mathrm{d}$
muscular	bladder muscle rectum muscle ureter	$r = 0.469 \cdot 10^{-2}\ 1/\mathrm{d}$

The collagenous and ontogenetic boundaries are simulated as resistive barriers for tumour transgression with resistances given in table 2. The resistivity is perpendicular to the boundary. The ontogenetic compartments are illustrated in **Figure 1D** as grouped colours of same type. The collagenous lamellae are located between neighbouring compartments as described in Steineke et al [11]. The transmigration resistivity between two facing compartments in the ontogenetic model is based on the *distance* in the ontogenetic tree of the invaded compartment and the originating compartment of the tumour cells, given in **Figure 3**. The larger the distance the higher the resistivity. The resistivity is assumed to double for every major bifurcation. The finite-element model was simulatied via COMSOL Multiphysics® software [12]

Table S2 Parameters for onotegenetic model

Parameter		**value**
general		
proliferation inhibition exponent		$n = 1$
diffusion coefficient		$c = 1.467 \cdot 10^{-4}\ \mathrm{cm}^2/\mathrm{d}$
Tissue characterisation	ontogenetic tissue type	Tumour growth rate

fibrous	cervix paracervix	$r = 1.406 \cdot 10^{-2}$ 1/d
fatty	mesometrium mesobladder mesorectum mesureter	$r = 1.875 \cdot 10^{-2}$ 1/d
muscular	bladder muscle rectum muscle ureter	$r = 0.469 \cdot 10^{-2}$ 1/d
Migration from tissue i…	…into tissue j	Transmigration resistivity ρ_{ij}
Paracervix	Mesometrium	$0.217 \cdot 10^3$ d/cm^2
Mesometrium	Mesobladder	$0.434 \cdot 10^3$ d/cm^2
Mesometrium Mesobladder	Mesureter Ureter	$0.868 \cdot 10^3$ d/cm^2
Mesometrium	Mesorectum	$1.736 \cdot 10^3$ d/cm^2

S3 Step-wise Tumour Infiltration

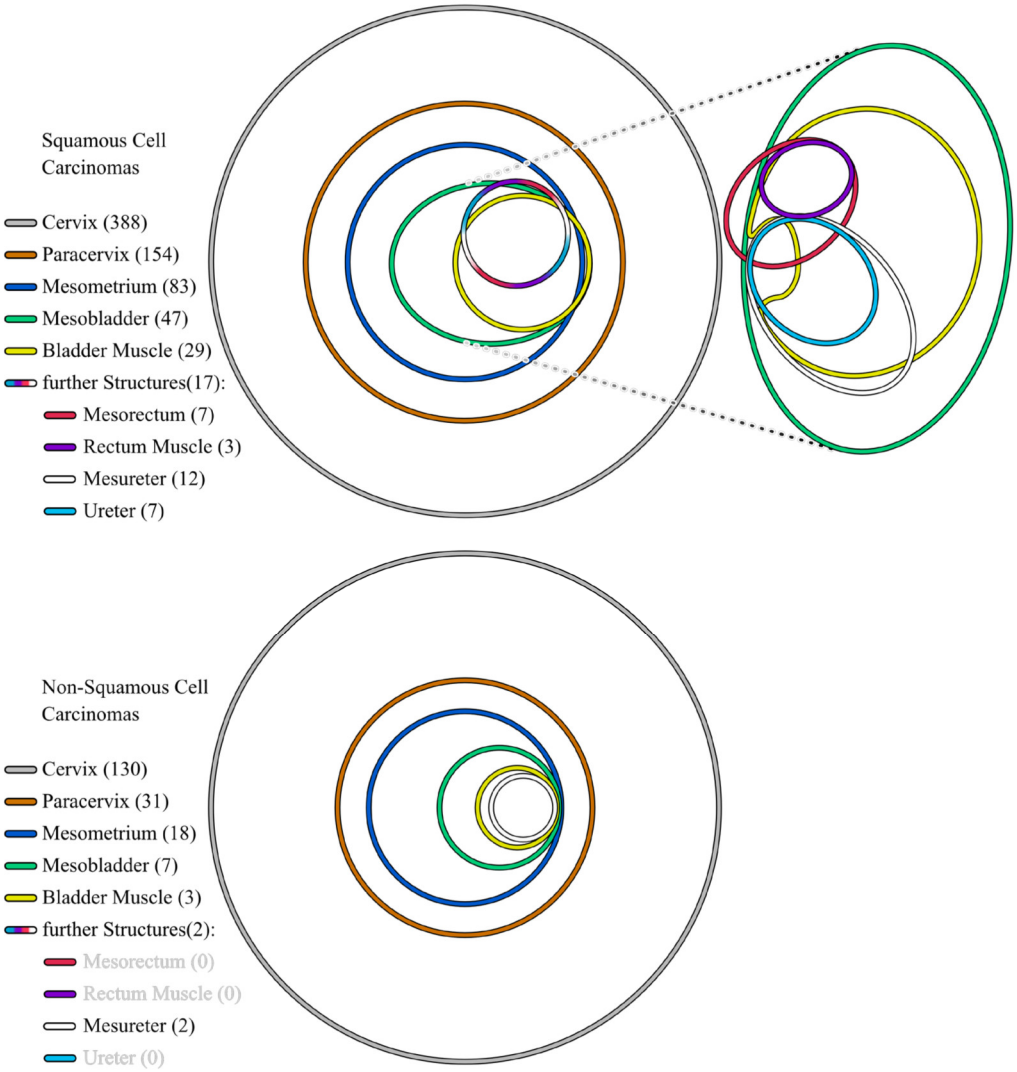

Figure S1: Separated Area-proportional Euler diagram of infiltration of endopelvic (sub-) compartments of 388 cases of squamous cell carcinomas and 130 cases of non-squamous cell carcinomas of the uterine cervix. Both sub-sets of the larger pooled set of 518 cases show a step-wise tumour infiltration with only a few exceptions.

S4 References

1. Höckel M, Hentschel B, Horn L-C (2014) Association between developmental steps in the organogenesis of the uterine cervix and locoregional progression of cervical cancer. A prospective clinicopathological analysis. The Lancet Oncology 15 (4): 445–456.
2. Wolf B, Ganzer R, Stolzenburg J-U, Hentschel B, Horn L-C et al. (2017) Extended mesometrial resection (EMMR): Surgical approach to the treatment of locally advanced cervical cancer based on the theory of ontogenetic cancer fields. Gynecologic oncology 146 (2): 292–298.
3. Höckel M, Wolf B, Hentschel B, Horn L-C (2017) Surgical treatment and histopathological assessment of advanced cervicovaginal carcinoma. A prospective study and retrospective analysis. European journal of cancer (Oxford, England : 1990) 70: 99–110.
4. Höckel M (2015) Morphogenetic fields of embryonic development in locoregional cancer spread. The Lancet Oncology 16 (3): e148-e151.
5. Zharinov GM, Gushchin VA (1989) Skorost' rosta opukholi i kletochnaia poteria pri rake sheĭki matki. Voprosy onkologii 35 (1): 21–25.
6. Combes PF, Douchez J, Carton M, Naja A. (1968) Etude de la croissance des métastases pulmonaires humaines comme argument objectif d'evaluation du pronostic et des effets thérapiques. Journal de Radiologie et d'Electrologie 49: 893–902.
7. Cosper P, Olsen JR, Siegel B, Dehdashti F, Schwarz JK et al. (2015) Cervical Tumor Volume Doubling Time. A Pilot Study. International Journal of Radiation Oncology*Biology*Physics 93 (3): E258-E259.
8. Harper LM, Odibo AO, Stamilio DM, Macones GA (2013) Radiographic measures of the mid pelvis to predict cesarean delivery. American journal of obstetrics and gynecology 208 (6): 460.e1-6.
9. Trott KR, Kummermehr J (1985) What is known about tumour proliferation rates to choose between accelerated fractionation or hyperfractionation? Radiotherapy and oncology : journal of the European Society for Therapeutic Radiology and Oncology 3 (1): 1–9.
10. Bolger BS, Symonds RP, Stanton PD, MacLean AB, Burnett R et al. (1996) Prediction of radiotherapy response of cervical carcinoma through measurement of proliferation rate. British journal of cancer 74 (8): 1223–1226.
11. Steinke H, Wiersbicki D, Speckert M-L, Merkwitz C, Wolfskämpf T et al. (2017) Periodic acid-Schiff (PAS) reaction and plastination in whole body slices. A novel technique to identify fascial tissue structures. Annals of anatomy = Anatomischer Anzeiger : official organ of the Anatomische Gesellschaft 216: 29–35.
12. COMSOL Multiphysics® v. 5.3. www.comsol.com. Stockholm, Sweden.

4 Summary and Conclusion

The organization of cells and tissues is a intricated process of multicellular life. Many processes of cells are simultaneously orchestrated in tissues in a remarkable reliable fashion to support large organisms. Of the many processes, physical aspects of cells and environment are of utmost importance in motility and structural stability. Peculiarly, the physical and non-physical properties of a tissues are usually not simply a consequence of the properties of the constituting cells of the tissue and the extra-cellular matrix, but can show emergent properties [210–213]. Furthermore, the partial separation and distinction of cell properties and tissue properties can be seen in various diseases and predominantly cancers. Strikingly, tumors are usually stiffer than their surrounding tissues caused by a stiffening of the stroma and increased cytoskeletal tension [233] and can in certain instances be detected by palpation [254–256], whereas single tumor cells are usually softer than their healthy counterparts [48,53,187,257–260], in addition, tumor cells exhibit a very broad distribution of cell elasticity [38,187].

Nonetheless, single cell properties are in the focus as they can reflect the coarse-grained, highly functionalized intracell organization and condition. By probing the elastic response of a cell, the condition of the cytoskeleton can be probed. The physical properties of single cells can often determine the emergent properties of cell clusters or tissues, i.e. metastasizing tumors display a broader and generally softer single cell elasticity distribution [38,187] and it is beneficial for metastasizing

cells to be deformable to crawl through dense tissues. This highlights that rheological characterization of cells and tissues are feasible tumor markers.

In my publication Kubitschke et al. 2018 [22], several orders of magnitudes in rheological properties of biological material were bridged and compared, ranging from cytoskeletal, over cellular towards tissue level. Physical principle governing biomaterial properties are introduced and several cell probing techniques with different probing ranges of stresses and strains, and locally or globally were introduced emphasizing whole cell properties. It is important to note that depending on probing technique that elastic and viscous moduli of cells can vary 1,000-fold and 100-fold [34], respectively. Thus, the emergent and intertwined mechanical properties of different system sizes, cellular and tissue level, is highlighted.

Various diseases and predominantly cancers are accompanied by changes of physical properties and cause and effect is connected to certain functional or structural elements of the cells and/or tissues. The most crucial step in cancer progression deciding approx. 66.7% of all cases about life and death is the ability to form metastases [10]. Thus, the crucial physical characteristics in cancer is cell motility, the ability to migrate caused by substantial remodeling of the cytoskeleton [38,187] and the ability to transgress natural boundaries and barriers for cell migration, such as basal membrane and tissue compartment boundaries.

Consequential, the impact of cytoskeletal components for cell's elastic response were analyzed in Kubitschke et al. 2017 [23]. The different cytoskeletal components contribute mechanical integrity and structure. The primary candidate is actin directly followed by the microtubules determining the cellular response the mechanical cues. The detailed contribution of actin and microtubules towards the response of cells under mechanical cues are still under investigation, however, I elucidated the distinct contributions of actin and microtubules for small and large strains by deforming epithelial cells in the optical stretcher. The cell's response due to optical stretching forces were methodically investigated by treating cells with different cytoskeletal drugs and various dosages spanning two orders of magnitudes. The relative deformation and relaxation were then used to dissect the mechanical contributions of the actin network from the microtubule network. In brief, latrunculin A was used to disrupt the actin network and displayed

a softening independent of the strain regime, whereas jasplakinolide as counterpart for stabilizing actin showed a softening for small strains but no significant alteration of the cellular response on larger strains. For the microtubules, nocodazole for disruption was used resulting in a softening at large strain and no change on small strain of the cellular response. The antagonist, paclitaxel, for stabilizing microtubules resulted in no significant alteration of the cellular response for small strains, but a concentration-dependent bipolar effect for larger strains.

The experiments conclude that for smaller strains the actin cytoskeleton is predominantly probed for the deformation under force load and subsequently the microtubules are more responsible for strain relaxation. Whereas on larger strains, the microtubule and actin network are of equal importance for structural integrity under force load for deformation and relaxation. Peculiarly, when stabilizing microtubules with lower dosages of paclitaxel, the deformability increases first and changes to stiffening of the cells for higher concentrations.

Considering migration of cells through densely packed scaffolds, the importance of the microtubule network becomes eminent, as such environments demand for high deformability and strains. Thus, the microtubule network is likely more accountable for migratory processes, and therefore highly relevant in cancer progression, i.e. metastases formation, as the current literature suggests. In case of cancer, microtubules are in the focus as treatment option as they are forming the mitotic spindle during cell division [261,262]. Furthermore, the microtubule network is responsible for the formation of microtentacles [263–265], microtubular-induced protrusions, which are key player for enabling circulation tumor cells to attach to the cellular wall of the blood vessels and exit the blood stream, thus enabling metastasis formation. Therefore, various chemotherapeutic agents are aiming for the disruption of the microtubules

While approx. 66.7% of cancer deaths are attributed to metastasis formation [10], and thus cancer cell motility, most solid tumors do not possess the ability to disseminate volatile cancer cells with metastasizing potential in their earlier stages [134,214,266]. The metastasizing stage frequently occurs when clinical attempts of local tumor control fail or are not undertaken in the first place. From a clinical perspective, the goal is therefore to detect cancer as soon as possible and remove the solid tumor and tissues at risk of cancer invasion as rigorous as possible under

the premise to keep the treatment-related morbidity at a minimum. In this light of pre-metastatic state of cancer cell growth and migration,

It is important to note, that the predominant treatment strategy for most solid tumors are limited surgical or radio-oncological treatment, but are currently the only available options for curative treatment. Targeted medical therapies have by far not kept their promise to cure solid malignant neoplasms. Furthermore, surgeons and radio-oncologists do not "see" cells, pathways and molecules, but only macroscopic structures. No matter how advanced the genotyping of cancers will be, these advancements will not appropriately translate to surgical and radio-oncological methodology in the near future. It is thus important to provide clinical applicable methods for cancer treatment.

The standard surgical approach is the wide excision where the tumor and an added "safety" margin of presumably healthy but possibly invaded tissue is resected. This method is often agnostic of the type of resected tissue and the treatment-relevant morbidity can be a concern when other vital tissues or organs are close-by the solid tumor.

In my third publication Kubitschke et al. 2019 [27], I provide support to the theory of *Inverse Morphogenesis* that cancers are "aware" of compartment boundaries – like healthy tissues – and stepwise lose the ability to recognize and respect other embryogenic derived tissues and their own tissue of origin, eventually resulting in transgressing compartment boundaries. Over 500 tumor spreading patterns of patients with cancer of the uterine cervix who underwent surgical tumor resection were analyzed. In order to provide arguments for *Inverse Morphogenesis*, the predominant theory of erratic isotropic tumor spread was tested for validity for tumor spreading pattern in uterine cervix and compared to a predicted tumor spread based on the ontogenetic approach of *Inverse Morphogenesis*. In essence, simulations of spreading patterns revealed that the isotropic model is inferior to the ontogenetic model in predicting infiltrated compartments in the pelvical region, i.e. cervix, bladder, rectum and ureter compartments. Assuming an isotropic tumor growth agnostic of compartment boundaries, the tumor shape aspect ratio should display a more spherical shape when growing, however, the found aspect ratios strongly deviated from spherical suggesting that cervical cancers are respecting the anisotropic embryogenic compartment boundaries, which in turn shapes the tumor during its growth. With area-proportional Euler diagrams, the over 500

infiltration patterns confirmed a stepwise tumor infiltration process where ontogenetic closer tissues of the uterine cervix, i.e. the bladder compartment, are always infiltrated first and ontogenetic far tissues, i.e. rectum and ureter compartment, are infiltrated afterward the former is infiltrated. In essence, the prevailing theory of isotropic tumor growth and on this based surgical wide excision strategy have considerable clinically relevant shortcomings and tissue cancer invasion likelihood strongly correlates with ontogenetic relatedness and follows an ontogenetically well-defined path.

In conclusion from a genetic point of view, cancer is an intricated and complex disease with given hallmarks as “checkpoints”, however, cancer progression also obeys physical factors. Therefore, cancer progression can also be described from a physical perspective. Physical characteristics of growth and migration of cancer cells are associated characteristic length scales and harbor a limiting factor for the progression of the disease, e.g. cancer cells without enhanced motility and adaptation will not be able to form metastases thus are limited local spread via growth displacement only.

In many of these aspects, the cytoskeleton is a key player since it harbors the very components to provide the balance of traction force and deformability in order to enable migration. This intrinsically convoluted scaffold drives the cell out of equilibrium by constantly consuming energy to preserve or restructure its shape. Therefore, this organized and well-structured scaffold of biopolymers is essential for the emergent mechanical properties of cells. Any alteration, such as caused by diseases like cancer, is reflected in the mechanical properties of cells. Therefore, measuring the rheological properties of cells can provide insights of the state of cells.

Cell deformation and accompanied cytoskeletal stress and strain is also key in cell migration. When cells migrate and squeeze through the tight meshwork of surrounding cells and extra-cellular matrix, cells have to adapt different modes of migration and deform and relax their cytoskeleton accordingly. As provided in Kubitschke et al. 2017 [23], for smaller deformations and relaxations the actin cytoskeleton is the cardinal player for deformation and microtubules for relaxation, whereas for larger deformations and relaxations the actin and microtubule network are cooperatively supporting one another in maintaining cellular integrity.

A further limiting factor prohibiting cancer progression and invasion can be tissue compartment boundaries. Benign tumors, carcinomas *in situ*, are not transgressing the basal membrane of the epithelial layer and are thus confined in their expansion resulting in exceptional treatment outcome [267–269]. While it is mainly attributed to the missing ability to invade other tissues – the metastatic potential as in Hallmarks of Cancer [7,8] – "disobeying" compartment borders can also be interpreted as dedifferentiation in cancer cells followed by loss of recognition of microenvironmental factors provided by the morphogenetic field of the developmental compartment [158]. The proposed theory is that the terminal attractor for ontogenetic cell differentiation in the gene regulatory network becomes unstable and the cancer cells may transition to the penultimate attractor of differentiation. Consequentially, the cancer cells acquire the capability to the potential to invade more compartments with the same primordial morphogenetic origin. As highlighted, the consequences are far-reaching and have clinical implications. First, tumor spread and invasion can significantly alter and shaped by compartment boundaries. Second, knowing the embryological origin of any tissue in which cancer arises and identifying compartment boundaries can provide a roadmap for tissues at risk of cancer infiltration based on the ontogenetic proximity to the tissues. Therefore, this insight can be used to tailor surgical resection to increase positive treatment outcome while keeping treatment-related morbidity low.

5 Outlook

Carcinogenesis is accompanied by physical changes of the cancer cells. The crucial steps which often decide in the patient survival are the ability to grow and invade locally and globally. While whole organism-wide growth and invasion is a virtual insurmountable threat to the life of the patient, locally confined tumor growth bears a significant better survival rate. Identification of processes and physical characteristics enabling cancers to become a global systemic disease are thus of dire need for the war against cancer. From the clinical point of view, the benchmark always will always be the patient survival rate and treatment-relevant morbidity. It should therefore be noted that most molecular approaches of cancer treatment are often out of reach for clinical treatment methods and/or are not general applicable for a broad spectrum of cancers. There are, nonetheless, some types of cancers have a significant higher risk of occurrence when certain, limited number of genetic defects are inherited, e.g. the risk of a woman with a BRCA1 or BRCA2 mutation developing breast cancer in the course of her life is about 50 to 80 percent and are affected on average about 20 years earlier than women without a family hereditary risk [270,271]. The majority of cancers, however, display such broad genotypic heterogeneity, that a generalized treatment founded on intricated molecular details will probably never be achieved.

Thus, the best line of defense for fighting cancer will be the earliest possible detection of cancer in hope to find cancer before it

reached full metastatic potential, and to identify all tissues of risk of cancer cell invasion in order to tailor more precise surgery and/or radiotherapy. The second line will be the suppression of metastasizing (occult) cancer cells which will include targeting cancer cell proliferation and disruption of cancer cell migration which is the common goal in chemotherapy.

Identification of migratory boundaries, such as developmental compartment boundaries, can provide a strong incentive for guiding surgical tumor resection. The supporting arguments are, first, it is clinically shown, that tumors recognize compartment boundaries, and second, that cancer cells transgress boundaries of ontogenetic closer tissue before ontogenetic distant tissues providing a strong predictive value for tumor infiltration [27,144,154,155,157,159]. Both arguments are beneficial for surgical and radiotherapeutic approaches as both supporting arguments precisely define infiltrated tissues and tissues of further cancer infiltration. Vice versa, the predicted ontogenetic stepwise tumor progression also provides tissues of marginal risk of tumor infiltration which can be spared to reduce treatment morbidity.

Cell migration, especially squeezing through a tight meshwork of ECM and cells is a demanding task for the cell and its cytoskeleton. The delicate balance of force generation and deformability demands a sophisticated and elaborated cytoskeletal architecture. Force generation, transmission and relaxation is achieved via actin and the microtubule network. While the actin network with its shorter persistence length and bending stiffness is the key player for smaller deformations, the microtubule network with its immense persistence length and bending stiffness comes into play for higher deformations.

The third major constituent biopolymer of the cytoskeleton, the intermediate filaments, also play a crucial role in this process. They are mainly responsible for providing mechanical integrity under large deformations [272], which is attributed to their large extensibility without breaking, and enabling mechanotransduction [30,93–99]. In order to complete the picture of cancer invasion, various classes of intermediate filaments, such es vimentin and keratin, have to be incorporated in the framework of cell migration in crowded environments. In fact, vimentin and keratins are already an important cancer progression marker [273–275]. Nonetheless, the physical characterization is incomplete and efforts are made to incorporate more

biophysical details. In this light, it is intriguing to anticipate a complete picture of cell motility and migration from a physical perspective incorporating all three major constituents of the cytoskeleton. The clinical implication would be to minimize the thread inherited by metastasizing cancer cells and ultimately increase positive treatment outcome for advanced cancer stages.

Until the death rate of metastasizing tumors can be reduced to a reasonable level, the cardinal treatment option with best patient outcome is to detect the solid tumor before metastasizing stage and resect it with all corresponding tissues at risk of invasion. Development compartment boundaries and the description of tumor progression based on ontogenetic staging provides a novel ground to identify tissues at risk, tailor surgery according to it, and potentially increase survival rate and decreasing treatment-related morbidity [27,144,156,158]. While the hypothesis is thought through and well-articulated from various theoretical point of views [123,144,158,175,176,182] and evidence from physical and clinical side is provided, e.g. for cervix [156,157,161,236,237], vulva [159,160], rectum [238], pancreas [239], and mid-facial skin cancers [240], the molecular biological and genetic side cannot shown yet.

Unfortunately, all current gene databases are not distinguishing tissues based on their embryogenetic origin, but rather on their localization and functional role. Both spacial localization and functional role of tissues only weakly correlate with ontogenetic relatedness of surrounding tissues. Therefore, the direct link of embryogenesis and cancer progression will involve novel gene databases and tissue characterizations. A great opportunity lies in next generation sequencing techniques such as massively paralleled single cell RNA sequencing. If the ontogenetic relatedness of tissues is a candidate for cancer invasion likelihood, then the genetic signature of healthy tissues and cancerous cells will reflect this relationship. In detail, the transcription factors harboring the morphogenetic differentiation events in ontogenesis should be identified in given healthy tissues and then compared to cancerous cells. If a set of transcription factors and their caused expression profile decides a cell's fate to become one cell type or another, then cancer cells ought to have an instable expression of said genes and transcription factors enabling them to adapt to both microenvironments of both compartments.

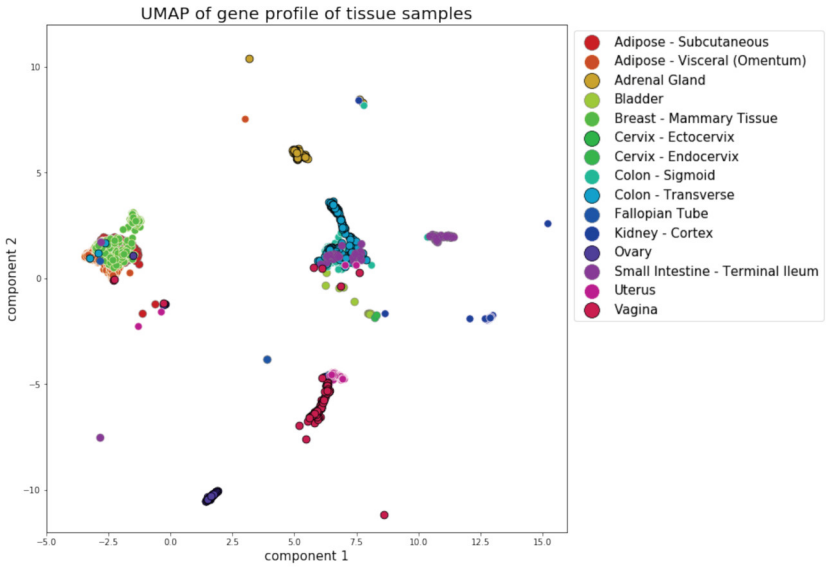

Figure 5.1: 2D mapping with UMAP algorithm of the genetic expression profile of various tissues of the pelvis and other adipose/connective tissues. Tissues of the same kind form clusters which represents a very similar expression profile. Tissues of different origin but functional proximity form a loose cluster with sub-clustering structure, e.g. adipose tissues: subcutaneous, visceral, mammary tissue. Tissues of spacial proximity to not necessarily have a similar expression profile.

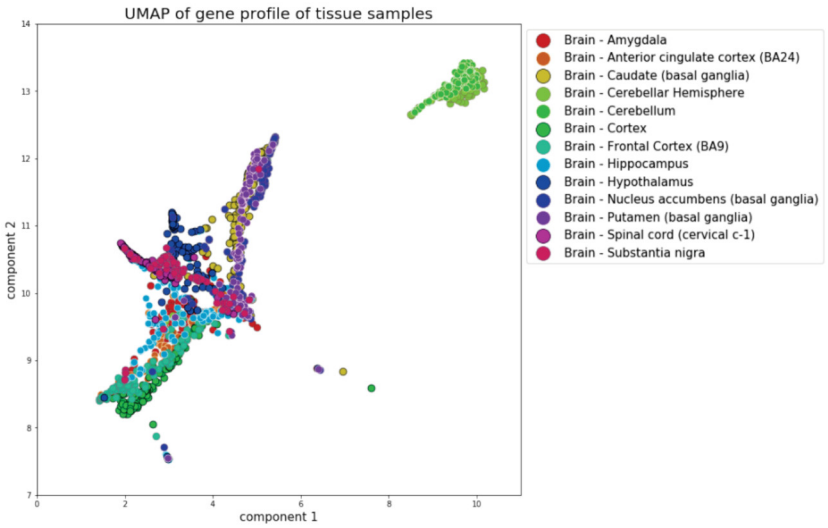

Figure 5.2: 2D mapping with UMAP algorithm of the genetic expression profile of various tissues of the brain. Two main clusters are formed, the cerebellum and cerebrum cluster. Both clusters show detailed sub-clustering of tissues extracted from different regions of the corresponding part of the brain. While the functional properties of the cells of different areas are largely the same, the expression profiles show significant differences revealing an internal organized architecture and thus functionalization.

One such approach for uterine cervix and its related cancer could be to sequence the surrounding fatty connective tissues, e.g. mesometrium, mesobladder, mesorectum and mesureter. These are associated to different developmental compartments, but have the same anatomical function and appear pathological the same. It can be speculated that all genes which show very similar expression patterns can be attributed to "functional genes", that is, they define the function of a fatty connective tissue cell. The remaining, differentially expressed genes are possible candidates of "morphogenetic" genes harboring the genetic code to induce differentiation of cells. *Figure 5.1* illustrates the clustering of gene expression of hundreds of expression profiles of various tissues of origin in vicinity of the uterine cervix. The clustering algorithm is based on Uniform Manifold Approximation and Projection for Dimension Reduction (UMAP) [276]. UMAP is comparable to the more known t-SNE algorithm albeit UMAP outputs are faster to compute, more reproducible and preserve more of the global structure and continuity of a dataset than those from t-SNE.

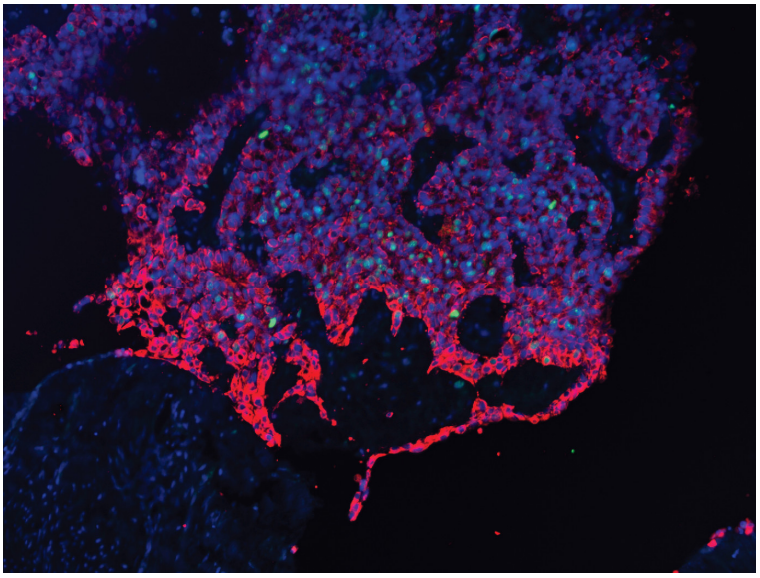

Figure 5.3: Tumor proliferation assay with fluorescent labeling. Cell nuclei are labeled in blue, cytokeratin in red and proliferating cells in green. Cytokeratin is a marker for cancerous cells (reddish area) which includes proliferating cells. Smooth boundaries can be seen in the lower left part of the picture

From the data representation one can extract that functional similar tissue, e.g. subcutaneous and visceral adipose tissue, and connective tissue of the breast, cluster in one region implying that most

genes have similar expression levels. However, it is also visible that these three tissues form distinct sub-clusters within this fatty connective tissue cluster. The sub-clustering of tissues within one major cluster is visible more clearly when analyzing different tissues of the brain from the GTEx database, see *Figure 5.2*. The cerebellum associated samples cluster (greenish colors, upper right corner), all other tissues also cluster and sub-clustering is visible. One can speculate that the expression differences of these tissues include delicate details due to slightly different functional roles within the organism, but also might include genes involved to trace their respective ontogenetic origin.

The functional similarity (if not identity) but ontogenetic disparity of the different fatty connective tissues of the compartments of the uterine cervix can experimentally be investigated, as illustrated in *Figure 5.3*. As example, assuming a low-staged cancer which infiltrated the cervix and the mesometrium. Thus, this cancer is harboring the ability to invade connective tissues if the *Hallmarks of Cancer* are interpreted as purely functional and physical characteristics. One can conduct experiments whether low-staged cancer cells can also invade connective tissues of other ontogenetic origins, e.g. bladder or rectum connective tissue, see *Figure 5.1*. In this experiment, dissected pieces of cancer tissue of patients which underwent cervical cancer removal surgery are placed on top of pieces of ontogenetic different connective tissues of the same patients. The tissue pieces are in direct contact without the physical collagen barrier found between different compartments. If the ontogenetic interpretation of cancer progression is valid, then this cancer will preferentially invade connective tissues of the mesometrium but will spare all other, ontogenetic more distant connective tissues. If only the functional and physical interpretation is important for cancer progression, the type of connective tissue used in the transmigration experiments are of minor importance.

While current tissue-based gene databases may provide some indices for the connection of cancer progression and embryogenesis, in order to fully grasp the duality between cancer and embryogenesis, special refined gene expression profiling of ontogenetic well-defined tissues and compartments have to be done. Fortunately, next generation, single cell sequencing techniques are emerging and will allow for an affordable large-scale sequencing approach. Thus, mapping out

intertwined genetics of cancer progression and embryogenesis is in reach of the scientific progress.

Appendix

Physical Properties of Single Cells and Collective Behavior

By HANS KUBITSCHKE, Erik Winfried Morawetz, Josef Alfons Käs, Jörg Schnauß in *Quantification of Biophysical Parameters in Medical Imaging*, doi.org/10.1007/978-3-319-65924-4

In this publication, I provided optical stretcher and wound healing experiments and Jörg Schnauß provided the rheological measurements. Jörg Schnauß, Erik Morawetz and myself created the graphs, images and illustrations. I provided rheological derivations, deformation and stress evaluation of probing techniques. Major parts of the manuscript were written by myself. Jörg Schnauß provided writing support for the physical description of polymers. Erik Morawetz contributed writing support for description of cell-cell and cell-tissue interaction. Jörg Schnauß and Josef Käs supervised this work by providing suggestions for structuring the manuscript as well as by carefully commenting the manuscript. All authors provided critical review, commentary, revision and editing for the final version of the manuscript.

Actin and microtubule networks contribute differently to cell response for small and large strains

by HANS KUBITSCHKE, Jörg Schnauss, Kenechukwu David Nnetu, Enrico Warmt, Roland Stange and Josef Alfons Käs
in *New Journal of Physics*, Volume 19, 093003, doi.org/10.1088/1367-2630/aa7658

David Nnetu, Jörg Schnauß, Roland Stange, Josef Käs and myself designed the research. I conducted and contributed a significant proportion of the concentration-dependent experiments and experimental data for various cytotoxins. Of the many optical stretcher experiments David Nnetu provided several. The cytotoxicity assays were done by myself. I analyzed and evaluated the optical stretcher data with support from David Nnetu and Jörg Schnauß. I provided the statistical hypothesis testing. David Nnetu and Enrico Warmdt provided fluorescent images and time series of cells undergoing microtubule restructuring. Roland Stange provided support for analytical tools and software for the optical stretcher. I provided all graphs and data visualizations. David Nnetu, Jörg Schnauß and myself have written the manuscript. All authors provided critical review, commentary, revision and editing for the final version of the manuscript.

Roadmap to Local Tumor Growth: Insights from Cervical Cancer

by HANS KUBITSCHKE, Benjamin Wolf, Erik Winfried Morawetz, Lars-Christian Horn, Bahriye Aktas, Ulrich Behn, Michael Höckel, Josef Alfons Käs
in *Scientific Reports*, 9(1), doi.org/10.1038/s41598-019-49182-1

In this publication Benjamin Wolf, Lars-Christian Horn, Bariye Aktas and Michael Höckel provided access to the anonymized, raw clinical patient data including MRI images. Benjamin Wolf and myself developed the patient selection criteria for further analysis. Benjamin Wolf provided access to the patient and tumor characteristics. All further patient data analysis, e.g. tumor size, tumor shape, tissue infiltration pattern, and statistical hypothesis testing, was done by myself including all corresponding graphs and illustrations. Michael Höckel and Josef Käs provided suggestions for the data interpretation. I

created the anatomical tissue maps and illustrations from MRI images as well as the tumor growth simulations and derivations. Ulrich Behn supported the development of the model and its interpretation. Michael Höckel and Benjamin Wolf provided the ontogenetic tissue tree which were illustrated by myself. The manuscript was mainly written by Benjamin Wolf and myself. Benjamin Wolf provided several of the medical descriptions and termini. I provided all physical descriptions and interpretations. All authors provided critical review, commentary, revision and editing for the final version of the manuscript.

Bibliography

1. M. J. Thun, J. O. DeLancey, M. M. Center, A. Jemal, and E. M. Ward, "The global burden of cancer: priorities for prevention," Carcinogenesis **31**(1), 100–110 (2010).
2. A. Jemal, M. M. Center, C. DeSantis, and E. M. Ward, "Global Patterns of Cancer Incidence and Mortality Rates and Trends," Cancer Epidemiol. Prev. Biomark. **19**(8), 1893–1907 (2010).
3. J. Peto, "Cancer epidemiology in the last century and the next decade," Nature **411**(6835), 390 (2001).
4. IHME, "Causes of Death, Global Burden of Disease," https://ourworldindata.org/causes-of-death.
5. "SEER Cancer Statistics Review (CSR) 1975-2014," https://seer.cancer.gov/archive/csr/1975_2014/.
6. NIH, "What Is Cancer?," https://www.cancer.gov/about-cancer/understanding/what-is-cancer.
7. D. Hanahan and R. A. Weinberg, "The Hallmarks of Cancer," Cell **100**(1), 57–70 (2000).
8. D. Hanahan and R. A. Weinberg, "Hallmarks of cancer: the next generation," Cell **144**(5), 646–74 (2011).
9. Y. A. Fouad and C. Aanei, "Revisiting the hallmarks of cancer," Am. J. Cancer Res. **7**(5), 1016–1036 (2017).
10. H. Dillekås, M. S. Rogers, and O. Straume, "Are 90% of deaths from cancer caused by metastases?," Cancer Med. **8**(12), 5574–5576 (2019).
11. S. Dinicola, F. D'Anselmi, A. Pasqualato, S. Proietti, E. Lisi, A. Cucina, and M. Bizzarri, "A Systems Biology Approach to Cancer: Fractals, Attractors, and Nonlinear Dynamics," OMICS J. Integr. Biol. **15**(3), 93–104 (2011).
12. R. A. Eeles, A. A. A. Olama, S. Benlloch, E. J. Saunders, and The PRACTICAL (Prostate Cancer Association Group to Investigate

Cancer-Associated Alterations in the Genome) Consortium, "Identification of 23 new prostate cancer susceptibility loci using the iCOGS custom genotyping array," Nat. Genet. **45**(4), 385–391 (2013).

13. K. Michailidou, P. Hall, A. Gonzalez-Neira, kConFab Investigators, Hereditary Breast and Ovarian Cancer Research Group Netherlands (HEBON), The Breast and Ovarian Cancer Susceptibility Collaboration, and The GENICA (Gene Environment Interaction and Breast Cancer in Germany) Network, "Large-scale genotyping identifies 41 new loci associated with breast cancer risk," Nat. Genet. **45**(4), 353–361 (2013).

14. P. D. P. Pharoah, Y.-Y. Tsai, S. J. Ramus, Australian Cancer Study, and Australian Ovarian Cancer Study Group, "GWAS meta-analysis and replication identifies three new susceptibility loci for ovarian cancer," Nat. Genet. **45**(4), 362–370 (2013).

15. L. C. Sakoda, E. Jorgenson, and J. S. Witte, "Turning of COGS moves forward findings for hormonally mediated cancers," Nat. Genet. **45**, 345–348 (2013).

16. V. Verma, R. K. Shrimali, S. Ahmad, W. Dai, H. Wang, S. Lu, R. Nandre, P. Gaur, J. Lopez, M. Sade-Feldman, K. Yizhak, S. L. Bjorgaard, K. T. Flaherty, J. A. Wargo, G. M. Boland, R. J. Sullivan, G. Getz, S. A. Hammond, M. Tan, J. Qi, P. Wong, T. Merghoub, J. Wolchok, N. Hacohen, J. E. Janik, M. Mkrtichyan, S. Gupta, and S. N. Khleif, "PD-1 blockade in subprimed CD8 cells induces dysfunctional PD-1 + CD38 hi cells and anti-PD-1 resistance," Nat. Immunol. **20**(9), 1231–1243 (2019).

17. N. D. Klemen, M. Wang, P. L. Feingold, K. Cooper, S. N. Pavri, D. Han, F. C. Detterbeck, D. J. Boffa, S. A. Khan, K. Olino, J. Clune, S. Ariyan, R. R. Salem, S. A. Weiss, H. M. Kluger, M. Sznol, and C. Cha, "Patterns of failure after immunotherapy with checkpoint inhibitors predict durable progression-free survival after local therapy for metastatic melanoma," J. Immunother. Cancer **7**(1), 196 (2019).

18. S. A. Narod, J. Iqbal, and A. B. Miller, "Why have breast cancer mortality rates declined?," J. Cancer Policy **5**, 8–17 (2015).

19. A. M. Cotlar, J. J. Dubose, and D. M. Rose, "History of surgery for breast cancer: radical to the sublime," Curr. Surg. **60**(3), 329–337 (2003).

20. C. T. Mierke, F. Sauer, S. Grosser, S. Puder, T. Fischer, and J. A. Käs, "The two faces of enhanced stroma: Stroma acts as a tumor

promoter and a steric obstacle," NMR Biomed. **31**(10), e3831 (2018).

21. C. T. Mierke, "Physical break-down of the classical view on cancer cell invasion and metastasis," Eur. J. Cell Biol. **92**(3), 89–104 (2013).

22. H. Kubitschke, E. W. Morawetz, J. A. Käs, and J. Schnauß, "Physical Properties of Single Cells and Collective Behavior," in *Quantification of Biophysical Parameters in Medical Imaging*, I. Sack and T. Schaeffter, eds. (Springer International Publishing, 2018), pp. 89–121.

23. H. Kubitschke, J. Schnauss, K. D. Nnetu, E. Warmt, R. Stange, and J. Kaes, "Actin and microtubule networks contribute differently to cell response for small and large strains," New J. Phys. **19**(9), 093003 (2017).

24. T. Yeung, P. C. Georges, L. A. Flanagan, B. Marg, M. Ortiz, M. Funaki, N. Zahir, W. Ming, V. Weaver, and P. A. Janmey, "Effects of substrate stiffness on cell morphology, cytoskeletal structure, and adhesion," Cell Motil. Cytoskeleton **60**(1), 24–34 (2005).

25. D. T. Butcher, T. Alliston, and V. M. Weaver, "A tense situation: forcing tumour progression," Nat. Rev. Cancer **9**(2), 108–122 (2009).

26. P. M. Gilbert and V. M. Weaver, "Cellular adaptation to biomechanical stress across length scales in tissue homeostasis and disease," Semin. Cell Dev. Biol. **67**, 141–152 (2017).

27. H. Kubitschke, B. Wolf, E. Morawetz, L.-C. Horn, B. Aktas, U. Behn, M. Höckel, and J. Käs, "Roadmap to Local Tumour Growth: Insights from Cervical Cancer," Sci. Rep. **9**(1), (2019).

28. F. van Zijl, G. Krupitza, and W. Mikulits, "Initial steps of metastasis: Cell invasion and endothelial transmigration," Mutat. Res. Mutat. Res. **728**(1), 23–34 (2011).

29. F. Huber, J. Schnauß, S. Rönicke, P. Rauch, K. Müller, C. Fütterer, and J. Käs, "Emergent complexity of the cytoskeleton: from single filaments to tissue," Adv. Phys. **62**(1), 1–112 (2013).

30. N. Mücke, L. Kreplak, R. Kirmse, T. Wedig, H. Herrmann, U. Aebi, and J. Langowski, "Assessing the flexibility of intermediate filaments by atomic force microscopy," J. Mol. Biol. **335**(5), 1241–1250 (2004).

31. Ott, Magnasco, Simon, and Libchaber, "Measurement of the persistence length of polymerized actin using fluorescence

microscopy," Phys. Rev. E Stat. Phys. Plasmas Fluids Relat. Interdiscip. Top. **48**(3), R1642–R1645 (1993).

32. F. Gittes, B. Mickey, J. Nettleton, and J. Howard, "Flexural rigidity of microtubules and actin filaments measured from thermal fluctuations in shape," J. Cell Biol. **120**(4), 923–934 (1993).

33. F. Pampaloni, G. Lattanzi, A. Jonáš, T. Surrey, E. Frey, and E.-L. Florin, "Thermal fluctuations of grafted microtubules provide evidence of a length-dependent persistence length," Proc. Natl. Acad. Sci. U. S. A. **103**(27), 10248–10253 (2006).

34. P.-H. Wu, D. R.-B. Aroush, A. Asnacios, W.-C. Chen, M. E. Dokukin, B. L. Doss, P. Durand-Smet, A. Ekpenyong, J. Guck, N. V. Guz, P. A. Janmey, J. S. H. Lee, N. M. Moore, A. Ott, Y.-C. Poh, R. Ros, M. Sander, I. Sokolov, J. R. Staunton, N. Wang, G. Whyte, and D. Wirtz, "A comparison of methods to assess cell mechanical properties," Nat. Methods **15**(7), 491–498 (2018).

35. T. Harada, J. Swift, J. Irianto, J.-W. Shin, K. R. Spinler, A. Athirasala, R. Diegmiller, P. C. D. P. Dingal, I. L. Ivanovska, and D. E. Discher, "Nuclear lamin stiffness is a barrier to 3D migration, but softness can limit survival," J. Cell Biol. **204**(5), 669–682 (2014).

36. P. A. Janmey, J. P. Winer, M. E. Murray, and Q. Wen, "The Hard Life of Soft Cells," Cell Motil. Cytoskeleton **66**(8), 597–605 (2009).

37. B. L. Bangasser, G. A. Shamsan, C. E. Chan, K. N. Opoku, E. Tüzel, B. W. Schlichtmann, J. A. Kasim, B. J. Fuller, B. R. McCullough, S. S. Rosenfeld, and D. J. Odde, "Shifting the optimal stiffness for cell migration," Nat. Commun. **8**(1), 1–10 (2017).

38. A. Fritsch, M. Höckel, T. Kiessling, K. D. Nnetu, F. Wetzel, M. Zink, and J. A. Käs, "Are biomechanical changes necessary for tumour progression?," Nat. Phys. **6**, 730–732 (2010).

39. T. Büscher, N. Ganai, G. Gompper, and J. Elgeti, "Tissue evolution: Mechanical interplay of adhesion, pressure, and heterogeneity," ArXiv191003263 Q-Bio (2019).

40. N. Ganai, T. Büscher, G. Gompper, and J. Elgeti, "Mechanics of tissue competition: interfaces stabilize coexistence," New J. Phys. **21**(6), 063017 (2019).

41. N. Podewitz, F. Jülicher, G. Gompper, and J. Elgeti, "Interface dynamics of competing tissues," New J. Phys. **18**(8), 083020 (2016).

42. L. Oswald, S. Grosser, D. M. Smith, and J. A. Käs, "Jamming transitions in cancer," J. Phys. Appl. Phys. **50**(48), 483001 (2017).

43. M. Radmacher, "Studying the mechanics of cellular processes by atomic force microscopy," Methods Cell Biol. **83**, 347–372 (2007).

44. R. E. Mahaffy, C. K. Shih, F. C. MacKintosh, and J. Käs, "Scanning Probe-Based Frequency-Dependent Microrheology of Polymer Gels and Biological Cells," Phys. Rev. Lett. **85**(4), 880–883 (2000).

45. A. R. Bausch and K. Kroy, "A bottom-up approach to cell mechanics," Nat. Phys. **2**(4), 231 (2006).

46. K. Kroy and J. Glaser, "The glassy wormlike chain," New J. Phys. **9**(11), 416–416 (2007).

47. S. Hirsch, T. Schaeffter, and I. Sack, "The Fundamentals of Transport in Living Tissues Quantified by Medical Imaging Technologies," in *Quantification of Biophysical Parameters in Medical Imaging*, I. Sack and T. Schaeffter, eds. (Springer International Publishing, 2018), pp. 9–43.

48. J. Guck, S. Schinkinger, B. Lincoln, F. Wottawah, S. Ebert, M. Romeyke, D. Lenz, H. M. Erickson, R. Ananthakrishnan, D. Mitchell, J. Kas, S. Ulvick, and C. Bilby, "Optical deformability as an inherent cell marker for testing malignant transformation and metastatic competence," Biophys. J. **88**(5), 3689–98 (2005).

49. J. Lammerding, P. C. Schulze, T. Takahashi, S. Kozlov, T. Sullivan, R. D. Kamm, C. L. Stewart, and R. T. Lee, "Lamin A/C deficiency causes defective nuclear mechanics and mechanotransduction," J. Clin. Invest. **113**(3), 370–378 (2004).

50. N. Bufi, M. Saitakis, S. Dogniaux, O. Buschinger, A. Bohineust, A. Richert, M. Maurin, C. Hivroz, and A. Asnacios, "Human Primary Immune Cells Exhibit Distinct Mechanical Properties that Are Modified by Inflammation," Biophys. J. **108**(9), 2181–2190 (2015).

51. D. Wirtz, K. Konstantopoulos, and P. C. Searson, "The physics of cancer: the role of physical interactions and mechanical forces in metastasis," Nat. Rev. Cancer **11**(7), 512–522 (2011).

52. J. Guck, R. Ananthakrishnan, H. Mahmood, T. J. Moon, C. C. Cunningham, and J. Käs, "The optical stretcher: a novel laser tool to micromanipulate cells.," Biophys. J. **81**(2), 767–784 (2001).

53. O. Otto, P. Rosendahl, A. Mietke, S. Golfier, C. Herold, D. Klaue, S. Girardo, S. Pagliara, A. Ekpenyong, A. Jacobi, M. Wobus, N. Töpfner, U. F. Keyser, J. Mansfeld, E. Fischer-Friedrich, and J. Guck, "Real-time deformability cytometry: on-the-fly cell mechanical phenotyping," Nat. Methods **12**(3), 199–202 (2015).

54. M. Herbig, M. Kräter, K. Plak, P. Müller, J. Guck, and O. Otto, "Real-Time Deformability Cytometry: Label-Free Functional Characterization of Cells," Methods Mol. Biol. Clifton NJ **1678**, 347–369 (2018).

55. A. Ashkin, "Acceleration and Trapping of Particles by Radiation Pressure," Phys. Rev. Lett. **24**(4), 156–159 (1970).

56. A. Ashkin and J. M. Dziedzic, "Optical trapping and manipulation of viruses and bacteria," Science **235**(4795), 1517–1520 (1987).

57. J. Guck, R. Ananthakrishnan, T. J. Moon, C. C. Cunningham, and J. Käs, "Optical deformability of soft biological dielectrics," Phys. Rev. Lett. **84**(23), 5451–5454 (2000).

58. B. Lincoln, F. Wottawah, S. Schinkinger, S. Ebert, and J. Guck, "High-Throughput Rheological Measurements with an Optical Stretcher," in *Methods in Cell Biology*, Cell Mechanics (Academic Press, 2007), **83**, pp. 397–423.

59. P. B Bareil, Y. Sheng, and A. Chiou, "Local scattering stress distribution on surface of a spherical cell in optical stretcher," Opt. Express **14**(25), 12503–12509 (2006).

60. J. Guck, R. Ananthakrishnan, C. C. Cunningham, and J. Käs, "Stretching biological cells with light," J. Phys. Condens. Matter **14**(19), 4843–4856 (2002).

61. L. Boyde, K. J. Chalut, and J. Guck, "Interaction of Gaussian beam with near-spherical particle: an analytic-numerical approach for assessing scattering and stresses," JOSA A **26**(8), 1814–1826 (2009).

62. L. Boyde, A. Ekpenyong, G. Whyte, and J. Guck, "Comparison of stresses on homogeneous spheroids in the optical stretcher computed with geometrical optics and generalized Lorenz-Mie theory," Appl. Opt. **51**(33), 7934–7944 (2012).

63. E. M. Purcell, "Life at low Reynolds number," Am. J. Phys. **45**(1), 3–11 (1977).

64. D. B. Dusenbery, *Living at Micro Scale: The Unexpected Physics of Being Small* (Harvard University Press, 2009).

65. P. J. M. V. Haastert and P. N. Devreotes, "Chemotaxis: signalling the way forward," Nat. Rev. Mol. Cell Biol. **5**(8), 626 (2004).

66. P. C. Georges and P. A. Janmey, "Cell type-specific response to growth on soft materials," J. Appl. Physiol. **98**(4), 1547–1553 (2005).

67. J. J. Bravo-Cordero, L. Hodgson, and J. Condeelis, "Directed cell invasion and migration during metastasis," Curr. Opin. Cell Biol. **24**(2), 277–283 (2012).

68. H. Yamaguchi, J. Wyckoff, and J. Condeelis, "Cell migration in tumors," Curr. Opin. Cell Biol. **17**(5), 559–564 (2005).

69. P.-H. Wu, D. M. Gilkes, and D. Wirtz, "The Biophysics of 3D Cell Migration," Annu. Rev. Biophys. **47**(1), 549–567 (2018).

70. P. Friedl and K. Wolf, "Tumour-cell invasion and migration: diversity and escape mechanisms," Nat. Rev. Cancer **3**(5), 362–74 (2003).

71. P. Friedl and K. Wolf, "Tumour-cell invasion and migration: diversity and escape mechanisms," Nat. Rev. Cancer **3**(5), 362–374 (2003).

72. P. Friedl and S. Alexander, "Cancer invasion and the microenvironment: plasticity and reciprocity," Cell **147**(5), 992–1009 (2011).

73. Y. Nishigami, M. Ichikawa, T. Kazama, R. Kobayashi, T. Shimmen, K. Yoshikawa, and S. Sonobe, "Reconstruction of Active Regular Motion in Amoeba Extract: Dynamic Cooperation between Sol and Gel States," PLOS ONE **8**(8), e70317 (2013).

74. T. Lämmermann and M. Sixt, "Mechanical modes of 'amoeboid' cell migration," Curr. Opin. Cell Biol. **21**(5), 636–644 (2009).

75. C. H. Lin, E. M. Espreafico, M. S. Mooseker, and P. Forscher, "Myosin Drives Retrograde F-Actin Flow in Neuronal Growth Cones," Neuron **16**(4), 769–782 (1996).

76. A. Ponti, M. Machacek, S. L. Gupton, C. M. Waterman-Storer, and G. Danuser, "Two Distinct Actin Networks Drive the Protrusion of Migrating Cells," Science **305**(5691), 1782–1786 (2004).

77. C. Jurado, J. R. Haserick, and J. Lee, "Slipping or Gripping? Fluorescent Speckle Microscopy in Fish Keratocytes Reveals Two Different Mechanisms for Generating a Retrograde Flow of Actin," Mol. Biol. Cell **16**(2), 507–518 (2004).

78. N. A. Medeiros, D. T. Burnette, and P. Forscher, "Myosin II functions in actin-bundle turnover in neuronal growth cones," Nat. Cell Biol. **8**(3), 216 (2006).

79. G. T. Charras, "A short history of blebbing," J. Microsc. **231**(3), 466–478 (2008).

80. J.-Y. Tinevez, U. Schulze, G. Salbreux, J. Roensch, J.-F. Joanny, and E. Paluch, "Role of cortical tension in bleb growth," Proc. Natl. Acad. Sci. **106**(44), 18581–18586 (2009).

81. E. Paluch, M. Piel, J. Prost, M. Bornens, and C. Sykes, "Cortical Actomyosin Breakage Triggers Shape Oscillations in Cells and Cell Fragments," Biophys. J. **89**(1), 724–733 (2005).

82. P. Friedl, "Prespecification and plasticity: shifting mechanisms of cell migration," Curr. Opin. Cell Biol. **16**(1), 14–23 (2004).

83. P. Friedl, K. Wolf, and J. Lammerding, "Nuclear mechanics during cell migration," Curr. Opin. Cell Biol. **23**(1), 55–64 (2011).

84. S. Even-Ram and K. M. Yamada, "Cell migration in 3D matrix," Curr. Opin. Cell Biol. **17**(5), 524–532 (2005).

85. C. M. Denais, R. M. Gilbert, P. Isermann, A. L. McGregor, M. Te Lindert, B. Weigelin, P. M. Davidson, P. Friedl, K. Wolf, and J. Lammerding, "Nuclear envelope rupture and repair during cancer cell migration," Science **352**(6283), 353–8 (2016).

86. K. Wolf, M. Te Lindert, M. Krause, S. Alexander, J. Te Riet, A. L. Willis, R. M. Hoffman, C. G. Figdor, S. J. Weiss, and P. Friedl, "Physical limits of cell migration: control by ECM space and nuclear deformation and tuning by proteolysis and traction force," J. Cell Biol. **201**(7), 1069–84 (2013).

87. P. Friedl and K. Wolf, "Plasticity of cell migration: a multiscale tuning model," J. Cell Biol. **188**(1), 11–19 (2010).

88. E. M. Davis and J. P. Trinkaus, "Significance of cell-to cell contacts for the directional movement of neural crest cells within a hydrated collagen lattice," J. Embryol. Exp. Morphol. **63**, 29–51 (1981).

89. J. M. Teddy and P. M. Kulesa, "In vivo evidence for short- and long-range cell communication in cranial neural crest cells," Development **131**(24), 6141–6151 (2004).

90. A. G. Clark and D. M. Vignjevic, "Modes of cancer cell invasion and the role of the microenvironment," Curr. Opin. Cell Biol. **36**, 13–22 (2015).

91. E. T. Roussos, M. Balsamo, S. K. Alford, J. B. Wyckoff, B. Gligorijevic, Y. Wang, M. Pozzuto, R. Stobezki, S. Goswami, J. E. Segall, D. A. Lauffenburger, A. R. Bresnick, F. B. Gertler, and J. S. Condeelis, "Mena invasive (MenaINV) promotes multicellular streaming motility and transendothelial migration in a mouse model of breast cancer," J. Cell Sci. **124**(13), 2120–2131 (2011).

92. A. Patsialou, J. J. Bravo-Cordero, Y. Wang, D. Entenberg, H. Liu, M. Clarke, and J. S. Condeelis, "Intravital multiphoton imaging reveals multicellular streaming as a crucial component of in vivo cell migration in human breast tumors," IntraVital **2**(2), e25294 (2013).

93. O. I. Wagner, S. Rammensee, N. Korde, Q. Wen, J.-F. Leterrier, and P. A. Janmey, "Softness, strength and self-repair in intermediate filament networks," Exp. Cell Res. **313**(10), 2228–2235 (2007).

94. E. E. Charrier and P. A. Janmey, "Mechanical properties of intermediate filament proteins," Methods Enzymol. **568**, 35–57 (2016).

95. J. Block, V. Schroeder, P. Pawelzyk, N. Willenbacher, and S. Köster, "Physical properties of cytoplasmic intermediate filaments," Biochim. Biophys. Acta BBA - Mol. Cell Res. **1853**(11, Part B), 3053–3064 (2015).

96. D. Fudge, D. Russell, D. Beriault, W. Moore, E. B. Lane, and A. W. Vogl, "The Intermediate Filament Network in Cultured Human Keratinocytes Is Remarkably Extensible and Resilient," PLoS ONE **3**(6), (2008).

97. H. Herrmann, H. Bär, L. Kreplak, S. V. Strelkov, and U. Aebi, "Intermediate filaments: from cell architecture to nanomechanics," Nat. Rev. Mol. Cell Biol. **8**(7), 562–573 (2007).

98. Z. Qin, L. Kreplak, and M. J. Buehler, "Hierarchical Structure Controls Nanomechanical Properties of Vimentin Intermediate Filaments," PLoS ONE **4**(10), (2009).

99. J. Block, H. Witt, A. Candelli, E. J. G. Peterman, G. J. L. Wuite, A. Janshoff, and S. Köster, "Nonlinear Loading-Rate-Dependent Force Response of Individual Vimentin Intermediate Filaments to Applied Strain," Phys. Rev. Lett. **118**(4), (2017).

100. B. Zhao, D. P. Meka, R. Scharrenberg, T. König, B. Schwanke, O. Kobler, S. Windhorst, M. R. Kreutz, M. Mikhaylova, and F. Calderon de Anda, "Microtubules Modulate F-actin Dynamics during Neuronal Polarization," Sci. Rep. **7**, (2017).

101. A. Mikhailov and G. G. Gundersen, "Relationship between microtubule dynamics and lamellipodium formation revealed by direct imaging of microtubules in cells treated with nocodazole or taxol," Cell Motil. **41**(4), 325–340 (1998).

102. E. J. Ezratty, M. A. Partridge, and G. G. Gundersen, "Microtubule-induced focal adhesion disassembly is mediated by dynamin and focal adhesion kinase," Nat. Cell Biol. **7**(6), 581 (2005).

103. X.-D. Ren, W. B. Kiosses, and M. A. Schwartz, "Regulation of the small GTP-binding protein Rho by cell adhesion and the cytoskeleton," EMBO J. **18**(3), 578–585 (1999).

104. C. M. Waterman-Storer, R. A. Worthylake, B. P. Liu, K. Burridge, and E. D. Salmon, "Microtubule growth activates Rac1 to promote lamellipodial protrusion in fibroblasts," Nat. Cell Biol. **1**(1), 45 (1999).

105. H. Yang, A. Ganguly, and F. Cabral, "Inhibition of Cell Migration and Cell Division Correlates with Distinct Effects of Microtubule Inhibiting Drugs," J. Biol. Chem. **285**(42), 32242–32250 (2010).

106. A. Ganguly, H. Yang, R. Sharma, K. D. Patel, and F. Cabral, "The Role of Microtubules and Their Dynamics in Cell Migration," J. Biol. Chem. **287**(52), 43359–43369 (2012).

107. R. A. Foty, C. M. Pfleger, G. Forgacs, and M. S. Steinberg, "Surface tensions of embryonic tissues predict their mutual envelopment behavior," Dev. Camb. Engl. **122**(5), 1611–1620 (1996).

108. G. Forgacs, R. A. Foty, Y. Shafrir, and M. S. Steinberg, "Viscoelastic Properties of Living Embryonic Tissues: a Quantitative Study," Biophys. J. **74**(5), 2227–2234 (1998).

109. H. Gabbert, R. Wagner, R. Moll, and C.-D. Gerharz, "Tumor dedifferentiation: An important step in tumor invasion," Clin. Exp. Metastasis **3**(4), 257–279 (1985).

110. D. Friedmann-Morvinski and I. M. Verma, "Dedifferentiation and reprogramming: origins of cancer stem cells," EMBO Rep. **15**(3), 244–253 (2014).

111. Y. Yamada, H. Haga, and Y. Yamada, "Concise Review: Dedifferentiation Meets Cancer Development: Proof of Concept for Epigenetic Cancer," Stem Cells Transl. Med. **3**(10), 1182–1187 (2014).

112. M. Mark, F. M. Rijli, and P. Chambon, "Homeobox Genes in Embryogenesis and Pathogenesis," Pediatr. Res. **42**(4), 421 (1997).

113. M. Levin, "Morphogenetic fields in embryogenesis, regeneration, and cancer: Non-local control of complex patterning," Biosystems **109**(3), 243–261 (2012).

114. D. J. Marston and B. Goldstein, "Symmetry Breaking in C. elegans: Another Gift from the Sperm," Dev. Cell **11**(3), 273–274 (2006).

115. S. Roth and J. A. Lynch, "Symmetry Breaking During Drosophila Oogenesis," Cold Spring Harb. Perspect. Biol. **1**(2), (2009).

116. A. Ajduk and M. Zernicka-Goetz, "Polarity and cell division orientation in the cleavage embryo: from worm to human," Mol. Hum. Reprod. **22**(10), 691–703 (2016).

117. D. W. Thompson, *On Growth and Form* (Dover, 1992).

118. A. Turing, "The chemical basis of morphogenesis," Philos. Trans. R. Soc. Lond. B. Biol. Sci. **237**(641), 37–72 (1952).

119. B. J. Copeland, J. Bowen, M. Sprevak, and R. Wilson, *The Turing Guide*, First edition (Oxford University Press, 2017).

120. T. W. Hiscock and S. G. Megason, "Orientation of Turing-like Patterns by Morphogen Gradients and Tissue Anisotropies," Cell Syst. **1**(6), 408–416 (2015).

121. G. C. Schoenwolf, S. B. Bleyl, P. R. Brauer, and P. H. Francis-West, *Larsen's Human Embryology*, Fifth edition (Churchill Livingstone, 2015).

122. C. H. Waddington, *The Strategy of the Genes* (2014).

123. S. Huang, "The molecular and mathematical basis of Waddington's epigenetic landscape: A framework for post-Darwinian biology?," BioEssays **34**(2), 149–157 (2012).

124. J. E. Ferrell, "Bistability, Bifurcations, and Waddington's Epigenetic Landscape," Curr. Biol. **22**(11), R458–R466 (2012).

125. J. Wang, L. Xu, E. Wang, and S. Huang, "The potential landscape of genetic circuits imposes the arrow of time in stem cell differentiation," Biophys. J. **99**(1), 29–39 (2010).

126. J. Howard, S. W. Grill, and J. S. Bois, "Turing's next steps: the mechanochemical basis of morphogenesis," Nat. Rev. Mol. Cell Biol. **12**(6), 392–398 (2011).

127. N. Tompkins, N. Li, C. Girabawe, M. Heymann, G. B. Ermentrout, I. R. Epstein, and S. Fraden, "Testing Turing's theory of morphogenesis in chemical cells," Proc. Natl. Acad. Sci. **111**(12), 4397–4402 (2014).

128. M. Kirschner and J. Gerhart, *The Plausibility of Life: Resolving Darwin's Dilemma* (Yale University Press, 2005).

129. A. Garcia-Bellido, P. Ripoll, and G. Morata, "Developmental Compartmentalisation of the Wing Disk of Drosophila," Nature. New Biol. **245**(147), 251 (1973).

130. C. Tickle, D. Summerbell, and L. Wolpert, "Positional signalling and specification of digits in chick limb morphogenesis," Nature **254**(5497), 199–202 (1975).

131. P. A. Lawrence and G. Struhl, "Morphogens, compartments, and pattern: lessons from drosophila?," Cell **85**(7), 951–961 (1996).

132. D. H. Kim, T. Xing, Z. Yang, R. Dudek, Q. Lu, and Y.-H. Chen, "Epithelial Mesenchymal Transition in Embryonic Development, Tissue Repair and Cancer: A Comprehensive Overview," J. Clin. Med. **7**(1), (2017).

133. J. P. Thiery and J. P. Sleeman, "Complex networks orchestrate epithelial-mesenchymal transitions," Nat. Rev. Mol. Cell Biol. **7**(2), 131–142 (2006).

134. M. Bacac and I. Stamenkovic, "Metastatic Cancer Cell," Annu. Rev. Pathol. Mech. Dis. **3**(1), 221–247 (2008).

135. V. Mittal, "Epithelial Mesenchymal Transition in Tumor Metastasis," Annu. Rev. Pathol. **13**, 395–412 (2018).

136. I. Pastushenko and C. Blanpain, "EMT Transition States during Tumor Progression and Metastasis," Trends Cell Biol. **29**(3), 212–226 (2019).

137. J. H. Tsai and J. Yang, "Epithelial–mesenchymal plasticity in carcinoma metastasis," Genes Dev. **27**(20), 2192–2206 (2013).

138. R. A. Foty and M. S. Steinberg, "The differential adhesion hypothesis: A direct evaluation," Dev. Biol. **278**(1), 255–63 (2005).

139. R. A. Foty, G. Forgacs, C. M. Pfleger, and M. S. Steinberg, "Liquid properties of embryonic tissues: Measurement of interfacial tensions," Phys. Rev. Lett. **72**(14), 2298–2301 (1994).

140. K. Basler and G. Struhl, "Compartment boundaries and the control of Drosopfiffa limb pattern by hedgehog protein," Nature **368**(6468), 208 (1994).

141. M. Zecca, K. Basler, and G. Struhl, "Sequential organizing activities of engrailed, hedgehog and decapentaplegic in the Drosophila wing," Dev. Camb. Engl. **121**(8), 2265–2278 (1995).

142. K. D. Irvine and C. Rauskolb, "Boundaries in development: formation and function," Annu. Rev. Cell Dev. Biol. **17**, 189–214 (2001).

143. C. Dahmann and K. Basler, "Compartment boundaries: at the edge of development," Trends Genet. TIG **15**(8), 320–326 (1999).

144. M. Höckel, "Morphogenetic fields of embryonic development in locoregional cancer spread," Lancet Oncol. **16**(3), e148-151 (2015).

145. P. Simpson and G. Morata, "Differential mitotic rates and patterns of growth in compartments in the Drosophila wing," Dev. Biol. **85**(2), 299–308 (1981).

146. S. Stein, R. Fritsch, L. Lemaire, and M. Kessel, "Checklist: vertebrate homeobox genes," Mech. Dev. **55**(1), 91–108 (1996).

147. J. C. Glover, "Correlated patterns of neuron differentiation and Hox gene expression in the hindbrain: a comparative analysis.," Brain Res. Bull. **55**(6), 683–693 (2001).

148. B. Lutz, H. C. Lu, G. Eichele, D. Miller, and T. C. Kaufman, "Rescue of Drosophila labial null mutant by the chicken ortholog Hoxb-1 demonstrates that the function of Hox genes is phylogenetically conserved.," Genes Dev. **10**(2), 176–184 (1996).

149. F. J. Ayala, A. Rzhetsky, and F. J. Ayala, "Origin of the metazoan phyla: Molecular clocks confirm paleontological estimates," Proc. Natl. Acad. Sci. **95**(2), 606–611 (1998).

150. E. E. Kershaw and J. S. Flier, "Adipose Tissue as an Endocrine Organ," J. Clin. Endocrinol. Metab. **89**(6), 2548–2556 (2004).

151. M. M. Chan, Z. D. Smith, S. Grosswendt, H. Kretzmer, T. M. Norman, B. Adamson, M. Jost, J. J. Quinn, D. Yang, M. G. Jones, A. Khodaverdian, N. Yosef, A. Meissner, and J. S. Weissman, "Molecular recording of mammalian embryogenesis," Nature **570**(7759), 77 (2019).

152. M. Höckel, L.-C. Horn, B. Hentschel, S. Höckel, and G. Naumann, "Total mesometrial resection: high resolution nerve-sparing radical hysterectomy based on developmentally defined surgical anatomy," Int. J. Gynecol. Cancer Off. J. Int. Gynecol. Cancer Soc. **13**(6), 791–803 (2003).

153. M. Höckel, L.-C. Horn, and H. Fritsch, "Association between the mesenchymal compartment of uterovaginal organogenesis and local tumour spread in stage IB-IIB cervical carcinoma: a prospective study," Lancet Oncol. **6**(10), 751–756 (2005).

154. M. Höckel, L.-C. Horn, N. Manthey, U.-D. Braumann, U. Wolf, G. Teichmann, K. Frauenschläger, N. Dornhöfer, and J. Einenkel, "Resection of the embryologically defined uterovaginal

(Müllerian) compartment and pelvic control in patients with cervical cancer: a prospective analysis," Lancet Oncol. **10**(7), 683–692 (2009).

155. M. Höckel, "Cancer permeates locally within ontogenetic compartments: clinical evidence and implications for cancer surgery," Future Oncol. Lond. Engl. **8**(1), 29–36 (2012).

156. M. Höckel, B. Hentschel, and L.-C. Horn, "Association between developmental steps in the organogenesis of the uterine cervix and locoregional progression of cervical cancer: a prospective clinicopathological analysis," Lancet Oncol. **15**(4), 445–456 (2014).

157. B. Wolf, R. Ganzer, J.-U. Stolzenburg, B. Hentschel, L.-C. Horn, and M. Höckel, "Extended mesometrial resection (EMMR): Surgical approach to the treatment of locally advanced cervical cancer based on the theory of ontogenetic cancer fields," Gynecol. Oncol. **146**(2), 292–298 (2017).

158. M. Höckel and U. Behn, "The Order of Cancer: A Theory of Malignant Progression by Inverse Morphogenesis," Front. Oncol. **9**, 416 (2019).

159. M. Höckel, K. Schmidt, K. Bornmann, L.-C. Horn, and N. Dornhöfer, "Vulvar field resection: novel approach to the surgical treatment of vulvar cancer based on ontogenetic anatomy," Gynecol. Oncol. **119**(1), 106–113 (2010).

160. M. Höckel, S. Trott, N. Dornhöfer, L.-C. Horn, B. Hentschel, and B. Wolf, "Vulvar field resection based on ontogenetic cancer field theory for surgical treatment of vulvar carcinoma: a single-centre, single-group, prospective trial," Lancet Oncol. **19**(4), 537–548 (2018).

161. M. Höckel, L.-C. Horn, R. Illig, N. Dornhöfer, and H. Fritsch, "Ontogenetic anatomy of the distal vagina: relevance for local tumor spread and implications for cancer surgery," Gynecol. Oncol. **122**(2), 313–318 (2011).

162. M. Höckel and N. Dornhöfer, "Vulvovaginal reconstruction for neoplastic disease," Lancet Oncol. **9**(6), 559–568 (2008).

163. K. Tomczak, P. Czerwińska, and M. Wiznerowicz, "The Cancer Genome Atlas (TCGA): an immeasurable source of knowledge," Contemp. Oncol. **19**(1A), A68–A77 (2015).

164. G. Zajicek, "Cancer as a systemic disease," Med. Hypotheses **4**(3), 193–207 (1978).

165. A. J. Redig and S. S. McAllister, "Breast cancer as a systemic disease: a view of metastasis," J. Intern. Med. **274**(2), 113–126 (2013).

166. Y. Hüsemann, J. B. Geigl, F. Schubert, P. Musiani, M. Meyer, E. Burghart, G. Forni, R. Eils, T. Fehm, G. Riethmüller, and C. A. Klein, "Systemic Spread Is an Early Step in Breast Cancer," Cancer Cell **13**(1), 58–68 (2008).

167. G. R. Prout, P. P. Griffin, and W. U. Shipley, "Bladder carcinoma as a systemic disease," Cancer **43**(6), 2532–2539 (1979).

168. D. P. Sohal, R. M. Walsh, R. K. Ramanathan, and A. A. Khorana, "Pancreatic Adenocarcinoma: Treating a Systemic Disease With Systemic Therapy," JNCI J. Natl. Cancer Inst. **106**(3), (2014).

169. M. R. Stratton, "Exploring the genomes of cancer cells: progress and promise," Science **331**(6024), 1553–1558 (2011).

170. L. J. Martin, "DNA Damage and Repair: Relevance to Mechanisms of Neurodegeneration," J. Neuropathol. Exp. Neurol. **67**(5), 377–387 (2008).

171. M. Schwartz, E. Zlotorynski, and B. Kerem, "The molecular basis of common and rare fragile sites," Cancer Lett. **232**(1), 13–26 (2006).

172. D. J. Weisenberger, K. D. Siegmund, M. Campan, J. Young, T. I. Long, M. A. Faasse, G. H. Kang, M. Widschwendter, D. Weener, D. Buchanan, H. Koh, L. Simms, M. Barker, B. Leggett, J. Levine, M. Kim, A. J. French, S. N. Thibodeau, J. Jass, R. Haile, and P. W. Laird, "CpG island methylator phenotype underlies sporadic microsatellite instability and is tightly associated with BRAF mutation in colorectal cancer," Nat. Genet. **38**(7), 787–793 (2006).

173. L. A. Loeb, "Human cancers express mutator phenotypes: origin, consequences and targeting," Nat. Rev. Cancer **11**(6), 450–457 (2011).

174. K. D. Siegmund, P. Marjoram, Y.-J. Woo, S. Tavaré, and D. Shibata, "Inferring clonal expansion and cancer stem cell dynamics from DNA methylation patterns in colorectal cancers," Proc. Natl. Acad. Sci. U. S. A. **106**(12), 4828–4833 (2009).

175. S. Huang, "Tumor progression: Chance and necessity in Darwinian and Lamarckian somatic (mutationless) evolution," Prog. Biophys. Mol. Biol. **110**(1), 69–86 (2012).

176. S. Huang and D. E. Ingber, "A non-genetic basis for cancer progression and metastasis: self-organizing attractors in cell regulatory networks," Breast Dis. **26**, 27–54 (2006).

177. S. C. Li, L. M. L. Tachiki, M. H. Kabeer, B. A. Dethlefs, M. J. Anthony, and W. G. Loudon, "Cancer genomic research at the crossroads: realizing the changing genetic landscape as intratumoral spatial and temporal heterogeneity becomes a confounding factor," Cancer Cell Int. **14**(1), 115 (2014).

178. V. M. Weaver, O. W. Petersen, F. Wang, C. A. Larabell, P. Briand, C. Damsky, and M. J. Bissell, "Reversion of the Malignant Phenotype of Human Breast Cells in Three-Dimensional Culture and In Vivo by Integrin Blocking Antibodies," J. Cell Biol. **137**(1), 231–245 (1997).

179. C. T. Mierke, "The fundamental role of mechanical properties in the progression of cancer disease and inflammation," Rep. Prog. Phys. **77**(7), 076602 (2014).

180. L. M. Coussens and Z. Werb, "Inflammation and cancer," Nature **420**(6917), 860–867 (2002).

181. S. Rakoff-Nahoum, "Why Cancer and Inflammation?," Yale J. Biol. Med. **79**(3–4), 123–130 (2006).

182. S. Huang, "Genetic and non-genetic instability in tumor progression: link between the fitness landscape and the epigenetic landscape of cancer cells," Cancer Metastasis Rev. **32**(3–4), 423–448 (2013).

183. I. Dagogo-Jack and A. T. Shaw, "Tumour heterogeneity and resistance to cancer therapies," Nat. Rev. Clin. Oncol. **15**(2), 81–94 (2018).

184. D. L. Dexter, H. M. Kowalski, B. A. Blazar, Z. Fligiel, R. Vogel, and G. H. Heppner, "Heterogeneity of Tumor Cells from a Single Mouse Mammary Tumor," Cancer Res. **38**(10), 3174–3181 (1978).

185. M. C. Lloyd, J. J. Cunningham, M. M. Bui, R. J. Gillies, J. S. Brown, and R. A. Gatenby, "Darwinian Dynamics of Intratumoral Heterogeneity: Not Solely Random Mutations but Also Variable Environmental Selection Forces," Cancer Res. **76**(11), 3136–3144 (2016).

186. R. Fisher, L. Pusztai, and C. Swanton, "Cancer heterogeneity: implications for targeted therapeutics," Br. J. Cancer **108**(3), 479–485 (2013).

187. K. Seltmann, A. W. Fritsch, J. A. Kas, and T. M. Magin, "Keratins significantly contribute to cell stiffness and impact invasive behavior," Proc. Natl. Acad. Sci. **110**(46), 18507–18512 (2013).

188. E. Check Hayden, "Cancer complexity slows quest for cure," Nature **455**(7210), 148–148 (2008).

189. C. Sonnenschein and A. M. Soto, "The aging of the 2000 and 2011 Hallmarks of Cancer reviews: A critique," J. Biosci. **38**(3), 651–663 (2013).

190. "The Genotype-Tissue Expression (GTEx) project," Nat. Genet. **45**(6), 580–585 (2013).

191. Y. Lazebnik, "What are the hallmarks of cancer?," Nat. Rev. Cancer **10**, 232–233 (2010).

192. P. C. W. Davies and C. H. Lineweaver, "Cancer tumors as Metazoa 1.0: tapping genes of ancient ancestors," Phys. Biol. **8**(1), 015001 (2011).

193. H. Chen, F. Lin, K. Xing, and X. He, "The reverse evolution from multicellularity to unicellularity during carcinogenesis," Nat. Commun. **6**(1), 1–10 (2015).

194. D. Nijhawan, T. I. Zack, Y. Ren, M. R. Strickland, R. Lamothe, S. E. Schumacher, A. Tsherniak, H. C. Besche, J. Rosenbluh, S. Shehata, G. S. Cowley, B. A. Weir, A. L. Goldberg, J. P. Mesirov, D. E. Root, S. N. Bhatia, R. Beroukhim, and W. C. Hahn, "Cancer vulnerabilities unveiled by genomic loss," Cell **150**(4), 842–854 (2012).

195. B. Vogelstein and K. W. Kinzler, "The Path to Cancer — Three Strikes and You're Out," N. Engl. J. Med. **373**(20), 1895–1898 (2015).

196. S. Jones, W. -d. Chen, G. Parmigiani, F. Diehl, N. Beerenwinkel, T. Antal, A. Traulsen, M. A. Nowak, C. Siegel, V. E. Velculescu, K. W. Kinzler, B. Vogelstein, J. Willis, and S. D. Markowitz, "Comparative lesion sequencing provides insights into tumor evolution," Proc. Natl. Acad. Sci. **105**(11), 4283–4288 (2008).

197. C. T. Mierke, "Cancer Cells Regulate Biomechanical Properties of Human Microvascular Endothelial Cells," J. Biol. Chem. **286**(46), 40025–40037 (2011).

198. C. T. Mierke, "Role of the endothelium during tumor cell metastasis: is the endothelium a barrier or a promoter for cell invasion and metastasis?," J. Biophys. Hindawi Publ. Corp. Online **2008**, 183516 (2008).

199. C. T. Mierke, "Endothelial cell's biomechanical properties are regulated by invasive cancer cells," Mol. Biosyst. **8**(6), 1639–49 (2012).

200. R. Kalluri and R. A. Weinberg, "The basics of epithelial-mesenchymal transition," J. Clin. Invest. **119**(6), 1420–1428 (2009).

201. J. Roche, "The Epithelial-to-Mesenchymal Transition in Cancer," Cancers **10**(2), (2018).

202. M. K. Jolly, K. E. Ware, S. Gilja, J. A. Somarelli, and H. Levine, "EMT and MET: necessary or permissive for metastasis?," Mol. Oncol. **11**(7), 755–769 (2017).

203. P. Bronsert, K. Enderle-Ammour, M. Bader, S. Timme, M. Kuehs, A. Csanadi, G. Kayser, I. Kohler, D. Bausch, J. Hoeppner, U. T. Hopt, T. Keck, E. Stickeler, B. Passlick, O. Schilling, C. P. Reiss, Y. Vashist, T. Brabletz, J. Berger, J. Lotz, J. Olesch, M. Werner, and U. F. Wellner, "Cancer cell invasion and EMT marker expression: a three-dimensional study of the human cancer-host interface," J. Pathol. **234**(3), 410–422 (2014).

204. Y. Chao, Q. Wu, M. Acquafondata, R. Dhir, and A. Wells, "Partial mesenchymal to epithelial reverting transition in breast and prostate cancer metastases," Cancer Microenviron. Off. J. Int. Cancer Microenviron. Soc. **5**(1), 19–28 (2012).

205. A. Grosse-Wilde, A. Fouquier d'Hérouël, E. McIntosh, G. Ertaylan, A. Skupin, R. E. Kuestner, A. del Sol, K.-A. Walters, and S. Huang, "Stemness of the hybrid Epithelial/Mesenchymal State in Breast Cancer and Its Association with Poor Survival," PloS One **10**(5), e0126522 (2015).

206. R. Strauss, Z.-Y. Li, Y. Liu, I. Beyer, J. Persson, P. Sova, T. Möller, S. Pesonen, A. Hemminki, P. Hamerlik, C. Drescher, N. Urban, J. Bartek, and A. Lieber, "Analysis of epithelial and mesenchymal markers in ovarian cancer reveals phenotypic heterogeneity and plasticity," PloS One **6**(1), e16186 (2011).

207. C. Li, T. Hong, and Q. Nie, "Quantifying the landscape and kinetic paths for epithelial-mesenchymal transition from a core circuit," Phys. Chem. Chem. Phys. PCCP **18**(27), 17949–17956 (2016).

208. M. Lu, M. K. Jolly, H. Levine, J. N. Onuchic, and E. Ben-Jacob, "MicroRNA-based regulation of epithelial-hybrid-mesenchymal fate determination," Proc. Natl. Acad. Sci. U. S. A. **110**(45), 18144–18149 (2013).

209. H. Steinke, D. Wiersbicki, M.-L. Speckert, C. Merkwitz, T. Wolfskämpf, and B. Wolf, "Periodic acid-Schiff (PAS) reaction and plastination in whole body slices. A novel technique to identify

fascial tissue structures," Ann. Anat. - Anat. Anz. **216**, 29–35 (2018).

210. F. Spill, D. S. Reynolds, R. D. Kamm, and M. H. Zaman, "Impact of the Physical Microenvironment on Tumor Progression and Metastasis," Curr. Opin. Biotechnol. **40**, 41–48 (2016).

211. M. J. Oudin and V. M. Weaver, "Physical and Chemical Gradients in the Tumor Microenvironment Regulate Tumor Cell Invasion, Migration, and Metastasis," Cold Spring Harb. Symp. Quant. Biol. **81**, 189–205 (2016).

212. J. W. Ivey, M. Bonakdar, A. Kanitkar, R. V. Davalos, and S. S. Verbridge, "Improving cancer therapies by targeting the physical and chemical hallmarks of the tumor microenvironment," Cancer Lett. **380**(1), 330–339 (2016).

213. D. Fukumura and R. K. Jain, "Tumor microenvironment abnormalities: Causes, consequences, and strategies to normalize," J. Cell. Biochem. **101**(4), 937–949 (2007).

214. P. Mehlen and A. Puisieux, "Metastasis: a question of life or death," Nat. Rev. Cancer **6**(6), 449–58 (2006).

215. L. M. F. Merlo, J. W. Pepper, B. J. Reid, and C. C. Maley, "Cancer as an evolutionary and ecological process," Nat. Rev. Cancer **6**(12), 924–935 (2006).

216. M. Greaves and C. C. Maley, "Clonal evolution in cancer," Nature **481**(7381), 306–313 (2012).

217. R. A. Weinberg, *The Biology of Cancer*, Second edition, Chapter 11: Multi-Step Tumorigenesis (Garland Science, Taylor & Francis Group, 2014).

218. R. Pozzatti, R. Muschel, J. Williams, R. Padmanabhan, B. Howard, L. Liotta, and G. Khoury, "Primary rat embryo cells transformed by one or two oncogenes show different metastatic potentials," Science **232**(4747), 223–227 (1986).

219. I. Ben-Porath, M. W. Thomson, V. J. Carey, R. Ge, G. W. Bell, A. Regev, and R. A. Weinberg, "An embryonic stem cell–like gene expression signature in poorly differentiated aggressive human tumors," Nat. Genet. **40**(5), 499–507 (2008).

220. J. Cohnheim, *Lectures on General Pathology: A Handbook for Practitioners and Students*, Second Edition (London : New Sydenham Society, 1889).

221. W. C. M. Dempke, K. Fenchel, P. Uciechowski, and T. Chevassut, "Targeting Developmental Pathways: The Achilles Heel of Cancer?," Oncology **93**(4), 213–223 (2017).

222. O. Oren and B. D. Smith, "Eliminating Cancer Stem Cells by Targeting Embryonic Signaling Pathways," Stem Cell Rev. Rep. **13**(1), 17–23 (2017).

223. T. Kiesslich, F. Berr, B. Alinger, R. Kemmerling, M. Pichler, M. Ocker, and D. Neureiter, "Current Status of Therapeutic Targeting of Developmental Signalling Pathways in Oncology," https://www.ingentaconnect.com/content/ben/cpb/2012/00000013/00000011/art00009#.

224. B. Vogelstein, N. Papadopoulos, V. E. Velculescu, S. Zhou, L. A. Diaz, and K. W. Kinzler, "Cancer Genome Landscapes," Science **339**(6127), 1546–1558 (2013).

225. H. Chen and X. He, "The Convergent Cancer Evolution toward a Single Cellular Destination," Mol. Biol. Evol. **33**(1), 4–12 (2016).

226. N. Moris, C. Pina, and A. M. Arias, "Transition states and cell fate decisions in epigenetic landscapes," Nat. Rev. Genet. **17**(11), 693–703 (2016).

227. L. Albergante, J. J. Blow, and T. J. Newman, "Buffered Qualitative Stability explains the robustness and evolvability of transcriptional networks," eLife **3**, 02863 (2014).

228. S. A. Kauffman, *The Origins of Order: Self-Organization and Selection in Evolution* (Oxford University Press, 1993).

229. C.-H. Chen, J. Xu, W.-F. Chang, C.-C. Liu, H.-Y. Su, Y. Eugene Chen, F. Du, and L.-Y. Sung, "Dynamic profiles of Oct-4, Cdx-2 and acetylated H4K5 in in-vivo-derived rabbit embryos," Reprod. Biomed. Online **25**(4), 358–370 (2012).

230. G. Wu and H. R. Schöler, "Role of Oct4 in the early embryo development," Cell Regen. **3**(1), 3:7 (2014).

231. H. Niwa, Y. Toyooka, D. Shimosato, D. Strumpf, K. Takahashi, R. Yagi, and J. Rossant, "Interaction between Oct3/4 and Cdx2 Determines Trophectoderm Differentiation," Cell **123**(5), 917–929 (2005).

232. D. Strumpf, "Cdx2 is required for correct cell fate specification and differentiation of trophectoderm in the mouse blastocyst," Development **132**(9), 2093–2102 (2005).

233. M. J. Paszek, N. Zahir, K. R. Johnson, J. N. Lakins, G. I. Rozenberg, A. Gefen, C. A. Reinhart-King, S. S. Margulies, M. Dembo, D. Boettiger, D. A. Hammer, and V. M. Weaver, "Tensional homeostasis and the malignant phenotype," Cancer Cell **8**(3), 241–254 (2005).

234. B. Mintz and K. Illmensee, "Normal genetically mosaic mice produced from malignant teratocarcinoma cells.," Proc. Natl. Acad. Sci. **72**(9), 3585–3589 (1975).

235. J. C. Kasemeier-Kulesa, J. M. Teddy, L.-M. Postovit, E. A. Seftor, R. E. B. Seftor, M. J. C. Hendrix, and P. M. Kulesa, "Reprogramming multipotent tumor cells with the embryonic neural crest microenvironment," Dev. Dyn. **237**(10), 2657–2666 (2008).

236. M. Höckel, B. Wolf, K. Schmidt, M. Mende, B. Aktas, R. Kimmig, N. Dornhöfer, and L.-C. Horn, "Surgical resection based on ontogenetic cancer field theory for cervical cancer: mature results from a single-centre, prospective, observational, cohort study," Lancet Oncol. (2019).

237. M. Höckel, L.-C. Horn, and J. Einenkel, "(Laterally) Extended Endopelvic Resection: Surgical treatment of locally advanced and recurrent cancer of the uterine cervix and vagina based on ontogenetic anatomy," Gynecol. Oncol. **127**(2), 297–302 (2012).

238. J. K. MacFarlane, R. D. H. Ryall, and R. J. Heald, "Mesorectal excision for rectal cancer," The Lancet **341**(8843), 457–460 (1993).

239. I. Makino, H. Kitagawa, T. Ohta, H. Nakagawara, H. Tajima, I. Ohnishi, H. Takamura, T. Tani, and M. Kayahara, "Nerve plexus invasion in pancreatic cancer: spread patterns on histopathologic and embryological analyses," Pancreas **37**(4), 358–365 (2008).

240. W. R. Panje and R. I. Ceilley, "The influence of embryology of the mid-face on the spread of epithelial malignancies," The Laryngoscope **89**(12), 1914–1920 (1979).

241. R. A. Gatenby and E. T. Gawlinski, "A reaction-diffusion model of cancer invasion," Cancer Res. **56**(24), 5745–5753 (1996).

242. M. E. Orme and M. A. J. Chaplain, "A mathematical model of vascular tumour growth and invasion," Math. Comput. Model. **23**(10), 43–60 (1996).

243. A. J. Perumpanani, J. A. Sherratt, J. Norbury, and H. M. Byrne, "Biological inferences from a mathematical model for malignant invasion," Invasion Metastasis **16**(4–5), 209–221 (1996).

244. S. B. Carter, "Principles of Cell Motility: The Direction of Cell Movement and Cancer Invasion," Nature **208**(5016), 1183 (1965).

245. J. A. Lawrence and P. S. Steeg, "Mechanisms of tumor invasion and metastasis," World J. Urol. **14**(3), 124–130 (1996).

246. J. Lacovara, E. B. Cramer, and J. P. Quigley, "Fibronectin enhancement of directed migration of B16 melanoma cells," Cancer Res. **44**(4), 1657–1663 (1984).

247. J. B. McCarthy and L. T. Furcht, "Laminin and fibronectin promote the haptotactic migration of B16 mouse melanoma cells in vitro," J. Cell Biol. **98**(4), 1474–1480 (1984).

248. L. Edelstein-Keshet, *Mathematical Models in Biology*, 1st ed, The Random House/Birkhäuser Mathematics Series (Random House, 1988).

249. N. F. Britton, "Tumour Modelling," in *Essential Mathematical Biology*, N. F. Britton, ed., Springer Undergraduate Mathematics Series (Springer London, 2003), pp. 235–252.

250. J. D. Murray, *Mathematical Biology: I. An Introduction*, 3rd ed., Interdisciplinary Applied Mathematics, Mathematical Biology (Springer-Verlag, 2002).

251. L. Preziosi, ed., *Cancer Modelling and Simulation*, Chapman & Hall/CRC Mathematical Biology and Medicine Series (Chapman & Hall/CRC, 2003).

252. S. Patmanidis, A. C. Charalampidis, I. Kordonis, G. D. Mitsis, and G. P. Papavassilopoulos, "Tumor growth modeling: Parameter estimation with Maximum Likelihood methods," Comput. Methods Programs Biomed. **160**, 1–10 (2018).

253. C. P. Calderón and T. A. Kwembe, "Modeling tumor growth," Math. Biosci. **103**(1), 97–114 (1991).

254. L. Mahoney and A. Csima, "Efficiency of palpation in clinical detection of breast cancer.," Can. Med. Assoc. J. **127**(8), 729–730 (1982).

255. A. Rimsten, B. Stenkvist, H. Johanson, and A. Lindgren, "The diagnostic accuracy of palpation and fine-needle biopsy and an evaluation of their combined use in the diagnosis of breast lesions: report on a prospective study in 1244 women with symptoms.," Ann. Surg. **182**(1), 1–8 (1975).

256. V. Egorov and A. P. Sarvazyan, "Mechanical Imaging of the Breast," IEEE Trans. Med. Imaging **27**(9), 1275–1287 (2008).

257. D. R. Gossett, H. T. K. Tse, S. A. Lee, Y. Ying, A. G. Lindgren, O. O. Yang, J. Rao, A. T. Clark, and D. Di Carlo, "Hydrodynamic stretching of

single cells for large population mechanical phenotyping," Proc. Natl. Acad. Sci. **109**(20), 7630–7635 (2012).

258. M. Plodinec, M. Loparic, C. A. Monnier, E. C. Obermann, R. Zanetti-Dallenbach, P. Oertle, J. T. Hyotyla, U. Aebi, M. Bentires-Alj, R. Y. H. Lim, and C.-A. Schoenenberger, "The nanomechanical signature of breast cancer," Nat. Nanotechnol. **7**(11), 757–765 (2012).

259. S. E. Cross, Y.-S. Jin, J. Tondre, R. Wong, J. Rao, and J. K. Gimzewski, "AFM-based analysis of human metastatic cancer cells," Nanotechnology **19**(38), 384003 (2008).

260. M. R. K. Mofrad, "Rheology of the Cytoskeleton," Annu. Rev. Fluid Mech. **41**(1), 433–453 (2009).

261. C. E. Walczak and R. Heald, "Chapter Three - Mechanisms of Mitotic Spindle Assembly and Function," in *International Review of Cytology*, K. W. Jeon, ed., A Survey of Cell Biology (Academic Press, 2008), **265**, pp. 111–158.

262. K. J. Helmke, R. Heald, and J. D. Wilbur, "Chapter Three - Interplay Between Spindle Architecture and Function," in *International Review of Cell and Molecular Biology*, K. W. Jeon, ed., International Review of Cell and Molecular Biology (Academic Press, 2013), **306**, pp. 83–125.

263. M. A. Matrone, R. A. Whipple, E. M. Balzer, and S. S. Martin, "Microtentacles Tip the Balance of Cytoskeletal Forces in Circulating Tumor Cells," Cancer Res. **70**(20), 7737–7741 (2010).

264. R. A. Whipple, A. M. Cheung, and S. S. Martin, "Detyrosinated microtubule protrusions in suspended mammary epithelial cells promote reattachment," Exp. Cell Res. **313**(7), 1326–36 (2007).

265. R. A. Whipple, E. M. Balzer, E. H. Cho, M. A. Matrone, J. R. Yoon, and S. S. Martin, "Vimentin filaments support extension of tubulin-based microtentacles in detached breast tumor cells," Cancer Res. **68**(14), 5678–88 (2008).

266. T. N. Seyfried and L. C. Huysentruyt, "On the Origin of Cancer Metastasis," Crit. Rev. Oncog. **18**(1–2), 43 (2013).

267. Y. J. Lim, K. Kim, E. K. Chie, W. Han, D. Y. Noh, and S. W. Ha, "Treatment outcome of ductal carcinoma in situ patients treated with postoperative radiation therapy," Radiat. Oncol. J. **32**(1), 1–6 (2014).

268. B. Cutuli, C. Lemanski, B. De Lafontan, M. P. Chauvet, C. T. De Lara, A. Mege, D. Fric, M. Richard-Molard, C. Mazouni, C. Cuvier, A. Carre,

and Y. Kirova, "Ductal carcinoma in situ (DCIS): a French National Survey. Analysis of 2,125 patients.," Clin. Breast Cancer (2019).

269. K. E. Stuart, N. Houssami, R. Taylor, A. Hayen, and J. Boyages, "Long-term outcomes of ductal carcinoma in situ of the breast: a systematic review, meta-analysis and meta-regression analysis," BMC Cancer **15**(1), 890 (2015).

270. J. M. Hall, M. K. Lee, B. Newman, J. E. Morrow, L. A. Anderson, B. Huey, and M. C. King, "Linkage of early-onset familial breast cancer to chromosome 17q21," Science **250**(4988), 1684–1689 (1990).

271. K. Hemminki, X. Li, and K. Czene, "Familial risk of cancer: data for clinical counseling and cancer genetics," Int. J. Cancer **108**(1), 109–114 (2004).

272. L. Kreplak, H. Bär, J. F. Leterrier, H. Herrmann, and U. Aebi, "Exploring the Mechanical Behavior of Single Intermediate Filaments," J. Mol. Biol. **354**(3), 569–577 (2005).

273. P. A. Thomas, D. A. Kirschmann, J. R. Cerhan, R. Folberg, E. A. Seftor, T. A. Sellers, and M. J. C. Hendrix, "Association between Keratin and Vimentin Expression, Malignant Phenotype, and Survival in Postmenopausal Breast Cancer Patients," Clin. Cancer Res. **5**(10), 2698–2703 (1999).

274. H. Polioudaki, S. Agelaki, R. Chiotaki, E. Politaki, D. Mavroudis, A. Matikas, V. Georgoulias, and P. A. Theodoropoulos, "Variable expression levels of keratin and vimentin reveal differential EMT status of circulating tumor cells and correlation with clinical characteristics and outcome of patients with metastatic breast cancer," BMC Cancer **15**(1), 399 (2015).

275. M. E. Kidd, D. K. Shumaker, and K. M. Ridge, "The Role of Vimentin Intermediate Filaments in the Progression of Lung Cancer," Am. J. Respir. Cell Mol. Biol. **50**(1), 1 (2014).

276. L. McInnes, J. Healy, and J. Melville, "UMAP: Uniform Manifold Approximation and Projection for Dimension Reduction," ArXiv180203426 Cs Stat (2018).

Curriculum Vitae

Name	Hans Kubitschke
Geburtsdatum	25th of October 1987
Geburtsort	Leipzig
Staatsangehörigkeit	deutsch

Ausbildung

07/2006	*Allgemeine Hochschulreife (Abitur),* Johannes-Kepler-Gymnasium Chemnitz
10/2006 — 09/2010	*B. Sc. Physik,* Universität Leipzig
10/2010 — 12/2012	*M.Sc. Physik,* Universität Leipzig
Seit 2013	*Wissenschaftlicher Mitarbeiter,* Universität Leipzig

Weitere Qualifikationen

- Lehrerfahrung zwischen 2011 und 2018 (14 Semester) als Tutor in Seminaren und Übungen im Bereich Experimentalphysik, Biophysik und Physik der weichen Materie
- Begutachtung von (ausländischen) Hochschulabschlüssen in den Naturwissenschaften und deren Qualifizierung für lehramts-äquivalente Leistungen
- Hochschuldidaktikzertifikat des Freistaates Sachsen 2017 (HDZ)
- E-Teaching-Zertifikat der Technischen Universität Dresden 2018
- Erweitertes Hochschuldidaktikzertifikat 2019 (HDZ „Plus“)

Declaration of Independence

Hereby I, Hans Kubitschke, declare that I prepared this PhD Thesis without inadmissible aid and only by the usage of the specified resources. I also declare, that I marked the directly or indirectly adopted ideas from external references.

I insure that I do not get any assistance benefits from other persons in selection and evaluation of the material as well as in the preparation of the manuscript.

Furthermore, I hereby declare and confirm that this PhD dissertation is entirely the result of my own investigations except where otherwise indicated. In particular, I insure that I did not make a claim on the aid of a doctoral consultant. Also, I insure that no one has gained, from me or from other persons on behalf on me, immediately or indirectly pecuniary advantages, which are related to the content of this PhD dissertation.

Hereby I insure that this PhD Thesis was not submitted, neither in Germany nor in other countries, in an identical or similar design to another examination office for the purpose of a graduation or another examination procedure.

Hereby I state that I have not been involved in another PhD procedure.

_____ _____

Leipzig, *23.03.2020* Hans Kubitschke

Zusammenfassung der wissenschaftlichen Ergebnisse der Dissertation

Physical Aspects of Solid Tumor Growth

---

der Fakultät für Physik und Geowissenschaften der Universität Leipzig
eingereicht von
M. Sc. Hans Kubitschke
angefertigt am
Peter-Debye-Institut für Physik der weichen Materie,
November 2019

Despite the vast molecular and genetic knowledge cancer developed towards an omnipresent disease and is one of the leading causes of death in the western world. Cancer cells of most cancers share common properties, such as unlimited replicative potential and evasion of apoptosis, coined the "Hallmarks of Cancer" [1,2]. Cancer can be considered a systemic disease with molecular origin but macroscopic progression steps and it is therefore not sufficient to understand molecular details of cancer, but also emergent properties of cancer on multiple scales from genes over cells to tissues.

The physical properties of this particular disease are of great importance [3,4,5] and most treatment strategies, such as surgery, radiotherapy and chemotherapy, are rooted in physical aspects rather than genetic.

This thesis focuses on physical characteristics and physics involved in cancer progression, cancer cell migration, and cancer growth. Migration of cancer cells is a crucial step in cancer progression as this ability often lead to formation of metastasis [6], the most common cause of cancer-related death [7]. Key is the deformability of cancer cells and squeezing through narrow openings of ECM and surrounding cells. Since migration in dense environment crowded with cells and extra-cellular matrix is a tightrope act of traction force generation and cell deformability, the precise contribution of the actin and microtubule network towards both cellular elastic deformation and relaxation is important and is evaluated in this thesis. A major finding is that the single-focused view on actin cytoskeleton alone is insufficient for migration in microenvironments but the microtubule network is also important, especially in regimes of larger deformations which are the common case in migration through dense environments. On small deformations ($< 5\%$), actin filaments dominate cell's viscoelastic response under stress application and microtubules determine the cell relaxation under stress release, whereas for larger strains ($> 5\%$) Actin filaments

and microtubules equally contribute to cell deformation and relaxation.

After the first cancerous cells break through the basal membrane and form the initial malignant tumor, the tumor typically enters the growth phase where surrounding tissue is steadily displaced and invaded by the tumor. For best treatment outcomes, the primary tumor should be removed as best as possible which includes the precise detection of the tumor front and identification of the tissues at risk of cancer infiltration. In this thesis, natural obstacles and boundaries for cancer growth, such as fascial tissue boundaries or tissue compartment boundaries, are analyzed based on clinical data of cervical cancers obtained from pathological examination of surgical resected tumors of 518 patients. Essential findings include the identification of growth boundaries as embryonic tissue developmental boundaries emphasizing that cancer exhibit developmental features commonly found in embryogenesis. Furthermore, the clinically found tumor growth and shape contradicts the isotropic tumor growth which is the prevailing dogma guiding tumor resection and radiotherapy. The found tumor shape distribution display strong deviations from the expected tumor shape of isotropic growth advocating that tumors are shaped and confined in certain developmental compartments which naturally display characteristic shapes.

As a consequence, knowledge of the embryological origin of cancer infested tissues and the ontogenetic relatedness of surrounding tissues can provide a relative likelihood of cancer cell infiltration in adjacent tissues and thus surgical resection and radiotherapy can be tailored precisely to the tissues at risk.

Bibligraphy of Summary

1. D. Hanahan and R. A. Weinberg, "The Hallmarks of Cancer," Cell **100**(1), 57–70 (2000).

2. D. Hanahan and R. A. Weinberg, "Hallmarks of cancer: the next generation," Cell **144**(5), 646–74 (2011).

3. C. T. Mierke, "Physical break-down of the classical view on cancer cell invasion and metastasis," Eur. J. Cell Biol. **92**(3), 89–104 (2013).

4. D. Wirtz, K. Konstantopoulos, and P. C. Searson, "The physics of cancer: the role of physical interactions and mechanical forces in metastasis," Nat. Rev. Cancer **11**(7), 512–522 (2011).

5. C. T. Mierke, "The fundamental role of mechanical properties in the progression of cancer disease and inflammation," Rep. Prog. Phys. **77**(7), 076602 (2014).

6. F. van Zijl, G. Krupitza, and W. Mikulits, "Initial steps of metastasis: Cell invasion and endothelial transmigration," Mutat. Res. Mutat. Res. **728**(1), 23–34 (2011).

7. H. Dillekås, M. S. Rogers, and O. Straume, "Are 90% of deaths from cancer caused by metastases?," Cancer Med. **8**(12), 5574–5576 (2019).

Publication List

Physical Properties of Single Cells and Collective Behavior

HANS KUBITSCHKE, Erik Winfried Morawetz, Josef Alfons Käs and Jörg Schnauß,
Quantification of Biophysical Parameters in Medical Imaging,
doi.org/10.1007/978-3-319-65924-4

Actin and microtubule networks contribute differently to cell response for small and large strains

HANS KUBITSCHKE, Jörg Schnauss, Kenechukwu David Nnetu, Enrico Warmt, Roland Stange and Josef Alfons Käs,
New Journal of Physics, Volume 19, 093003,
doi.org/10.1088/1367-2630/aa7658

Roadmap to Local Tumour Growth: Insights from Cervical Cancer

HANS KUBITSCHKE, Benjamin Wolf, Erik Winfried Morawetz, Lars-Christian Horn, Bahriye Aktas, *Ulrich Behn*, Michael Höckel and Josef Alfons Käs,
Scientific Reports, 9(1),
doi.org/10.1088/1367-2630/aa7658

Dynamics of pore synthesis and degradation in protocells

HANS KUBITSCHKE and Claus Fütterer,
New Journal of Physics, Volume 14, 103008,
doi.org/10.1088/1367-2630/14/10/103008

Detecting heterogeneity in and between breast cancer cell lines

Yang Shen, Sebastian Schmidt, HANS KUBITSCHKE, Erik Winfried Morawetz; Benjamin Wolf, Josef Alfons Käs, Wolfgang Losert,
Cancer Convergence, 4(1):1,
dx.doi.org/10.1186%2Fs41236-020-0010-1

PhD Commission

PROF. DR. CLAUDIA TANJA MIERKE (Chairwoman)
Peter-Debye Institute for Soft Matter Physics
claudia.mierke@uni-leipzig.de

PROF. DR. JOSEF ALFONS KÄS (Supervisor)
Peter-Debye Institute for Soft Matter Physics
jkaes@uni-leipzig.de

PROF. DR. DR. MICHAEL HÖCKEL
Leipzig School of Radical Pelvic Surgery
michael.hoeckel@medizin.uni-leipzig.de

Further Publications

Dynamics of pore synthesis and degradation in protocells

by HANS KUBITSCHKE and Claus Fütterer
in *New Journal of Physics*, Volume 14, 103008, doi.org/10.1088/1367-2630/14/10/103008

I have written major parts of the publication. Claus Fütterer provided writing support. I created the model and the model analysis. I provided all physical descriptions and interpretations. I provided all graphs and data visualizations. Both authors provided critical review, commentary, revision and editing for the final version of the manuscript.

Detecting heterogeneity in and between breast cancer cell lines

by Yang Shen, B U Sebastian Schmidt, HANS KUBITSCHKE, Erik Winfried Morawetz, Benjamin Wolf, Josef A. Käs and Wolfgang Losert
in *BMC Cancer Convergence*, 4(1):1, dx.doi.org/10.1186%2Fs41236-020-0010-1

In this publication the manuscript was written to large extend by Yang Shen and B U Sebastian Schmidt. I provided most of the optical stretcher measurements and data analysis of the experimental data. Erik W Morawetz provided some of the optical stretcher data. Yang Shen and B U Sebastian Schmidt did all further data analysis, statistics and machine learning algorithms. I provided writing support to the manuscript. All authors provided critical review, commentary, revision and editing for the final version of the manuscript.

Supervision and Institutes and Collaborations

My PhD thesis was in general supervised by Prof. Dr. Josef A. Käs from the Peter-Debye Institute for Soft Matter Physics. Most parts of my PhD projects were done at the Peter-Debye Institute. Ulrich Behn from the Institute of Theoretical Physics supported me in model creation and discussion. I was given access to medical data by Lars-Christian Horn from the Institute of Pathology, Bahriye Aktas, Michael Höckel and Benjamin Wolf from the University Clinic. Benjamin Wolf assisted me in the medical data evaluation.

New Journal of Physics
The open-access journal for physics

Dynamics of pore synthesis and degradation in protocells

H Kubitschke[1] **and C Fütterer**[1,2,3]

[1] Institut für Experimentelle Physik I, Universität Leipzig, Linnéstraße 5, Leipzig, Germany

[2] Translationszentrum für Regenerative Medizin, Philipp-Rosenthal Straße 55, 04103, Leipzig, Germany

E-mail: c.fuetterer@biophysik.net

New Journal of Physics **14** 103008 (10pp)

Online at http://www.njp.org/
doi:10.1088/1367-2630/14/10/103008

Abstract. Liposomes have found countless applications as microreactors or for studying the evolution of protocells. However, to keep reactions ongoing, exchange with the environment is required. Based on experiments with nanopores expressed by an enclosed gene expression system, we developed a model describing the observed growth dynamics quantitatively. The model depends on one parameter only and allowed estimations of hitherto unknown parameters: the diffusion coefficient of amino acids through a single pore and the initial amino acid concentration. The long-term consequences of different degradation mechanisms are also discussed: we found a surprisingly sharp threshold deciding on the question of survival of the protocell.

Contents

[3] Author to whom any correspondence should be addressed.

1. Introduction

A large number of bio-molecules can be catalysed from inorganic components in an aqueous medium (pond or ocean) [1–4]. The simultaneous presence of functional combinations of molecules such as ribozymes [5] or nucleotides together with proteins and enzymes is a prerequisite during the genesis of the cell as their function relies on cooperativity. Consequently, the absence of even one partner would prohibit the function and thus be negative for selection and survival. Hence, we assume that the first protocell emerged as an entire functional unit, which is subsequently selected as a whole.

Once polynucleotides and enzymes are present at sufficient concentration, some of those molecules may accidentally get enclosed in a spontaneously forming liposome defining such functional units [6]. Liposomes have been explored previously as model 'protocells' [6–13]. It is conceivable that a very large number of such protocells were created with various combinations of molecules. If only one of those protocells is 'accidentally' able to self-reproduce, its copies may improve and dominate the medium on a long-term scale. On the other hand, however, a price has to be paid: cell membranes are highly impermeable to most bio-molecules and exchange with the environment is largely blocked. As a consequence, the protocell is condemned to equilibrium death. This paper focuses on one possible way out of this dilemma, although important questions are not addressed: where do the presupposed DNA and the enzymes come from, how does a protocell divide, and how do collective phenomena improve the survival of each protocell?

We set up a small theoretical model to address the general problem of feeding the protocell with nutrients by assuming the presence of a complete gene expression system and DNA or RNA encoding nanopores within the vesicle.

The model (figure 1) was inspired by the experiments of Noireaux, Libchaber, Monnard, Luptak and Deamer [6, 14, 15] and is quantitative, as it fits well the experimental data. It is based on liposomes in crystal phase which were filled with, among others, cell extract, plasmid DNA encoding alpha-haemolysin pores (diameter 1.4 nm, molecular mass cut-off 2–3 kDa and monomer sequence length 294 amino acids) and the fluorescent molecule GFP (on the same plasmid). As the pores and GFP were co-expressed, the fluorescent signal allowed measurement of the pore quantity; the system produced pores until the nutrients were depleted. The synthesized α-haemolysin monomers get inserted into the membrane and are self-assembled spontaneously to form pores, creating selective permeability across the membrane. The liposome is then 'fed' with new nutrients and the protein synthesis reaction increases again, which is described later.

Changes in the volume of the liposome (diameter approximately 10 μm) are not considered in [14] and in the presented model. Furthermore, due to the size of the liposome and the high diffusion speed of amino acids, fluctuations are also neglected in our basic model. Extension of the proposed model to accommodate this aspect would be straightforward, however. Fluctuations and noise dominate cellular dynamics at the molecular level. Furthermore, the cell extract used in [14] accounts for a large number of molecules and enzymes. Hence, the noise due to gene expression and translation, diffusion, as well as pore assembly and disassembly is averaged as the time scale of the described dynamics is much larger.

The model is quantitative, robust and therefore an appropriate base for further quantitative extensions towards an artificial cell: it would allow studying the influence of controlled cell membrane permeability on the regulatory feedback loops yielding oscillatory behaviour as

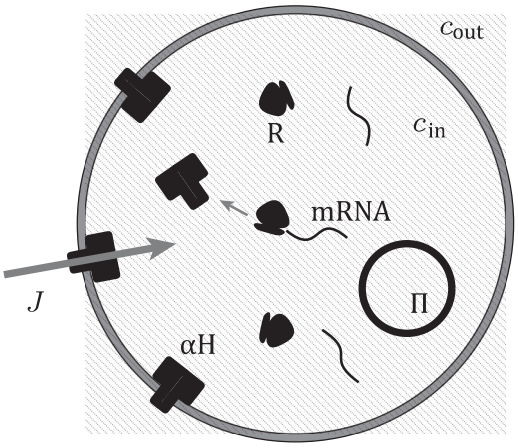

Figure 1. Sketch of a protocell model containing an α-haemolysin pore coding plasmid Π, mRNAs, ribosomes (R), α-haemolysin pores (αH) and cell extract.

described, e.g., by the 'repressilator' model [16]. New unexpected features emerge from multi-cellular systems as synchronization of cellular oscillations [17].

Numerous new features can be obtained by including a pore insertion probability smaller than one. In this case, the probability becomes susceptible to the electrostatic potential differences across the membrane [18]. Degradation and insertion delay can lead to oscillatory behaviour. By integrating calcium-sensitive actin cortex, the membrane tension and consequently mechano-sensitive pores may get modulated as well. Modulated calcium and nutrient concentrations lead to modulation of gene expression [19]. Transporters of amino acids can actively move amino acids in a specific direction across the membrane, using the cross-membrane ion gradient, e.g. sodium [20], as the energy source. Together with passive ion channels, the protocell becomes a highly controllable microreactor for molecular essays down to the single molecule level. Further possibilities consist in the expression of glycine-controlled chloride channels. These channels can be open or closed in milliseconds by the external application of glycine. The on–off switch of ion transportation in combination with sodium chloride symporter allows modulating rapidly the electro-chemical potential across the membrane controlling transporters. This may be used to externally control the gene expression inside the protocell. Therefore, protocells with switchable pores, e.g. pH- or mechano-sensitive, can feature simple feedback loops and rudimentary perception of the environment. This would allow us to couple gene expression to mechanical cues in artificial bottom-up systems on the way towards the artificial cell and tissues.

2. Setup of the basic model

An adequate supply of nutrients is achieved by the creation and insertion of pore proteins in the protocells' membrane. The resulting change in concentration of the amino acids, $\dot{c}_{k,\text{in}}(t) = \dot{N}_k(t)/V$, with the number of amino acids N_k of type k (in units of mole/l), of a protocell is expressed as

$$\dot{c}_{k,\text{in}}(t) = -\frac{1}{V}\left[b_k \dot{P}(t) + J_k(t) A N_\text{A} P(t)\right], \tag{1}$$

where N_A is the Avogadro constant and b_k is the number of amino acids of type k required to build the pore proteins P (in units of mol). The supply of amino acids is served by all inserted pore proteins, with the cross-sectional area A of the pore channel, which enables a flux J_k of new amino acids entering from the surrounding solution into the protocell. Assuming a linear concentration gradient leading to diffusive transport of amino acids inside the pore channel, the flux can be determined from

$$J_k(t) = -D_{k,\mathrm{eff}}\,\hat{n}\cdot\vec{\nabla}c_k(t) = -\frac{D_{k,\mathrm{eff}}}{L}\left[c_{k,\mathrm{out}} - c_{k,\mathrm{in}}(t)\right] \tag{2}$$

with the length L of the pore channel, the concentrations $c_{k,\mathrm{in}}$ and $c_{k,\mathrm{out}}$ of amino acids inside and outside the protocell, the trans-membrane effective diffusion coefficient $D_{k,\mathrm{eff}}$ of the amino acids and the outside normal vector of the membrane $\hat{n}$.

In the scenario mentioned above, pore proteins are only expressed as long as amino acids are abundant. The expression process slows down if the concentration of even one type of amino acid runs low and eventually stops once the concentration of the amino acid reaches zero. The kinetics of each specific amino acid in equation (1) cannot be considered, as the precise concentrations of the feeding medium are unknown from the experiments of Noireaux and Libchaber (amino acid concentrations approximately 10–100 μm [14]). However, it turned out that the sum of the concentration of amino acids is sufficient: $c_{\mathrm{in}}(t) = \sum_k c_{k,\mathrm{in}}(t)$. For an extension, the buffer composition can be refined based on equations (1) and (2).

In our protocell messenger RNAs (mRNAs) are permanently produced, degraded (ribonucleases) and recycled. The mRNA concentration has been shown to stabilize rapidly [21], so we can assume a constant mRNA concentration for our model. We suppose that there is a sufficiently high concentration of the ribonucleotide (building blocks of mRNA) mixture, and assume saturated enzymes with an mRNA synthesis rate of approximately 10 base pairs per second [22]. α-Haemolysin is a pore-forming protein, which consists of self-assembling monomers forming a heptamer [23]. The synthesis of α-haemolysin monomers happens with a turnover rate of one to two amino acids per second, which corresponds to an assembling time of 5–10 min per α-haemolysin heptamer. The enzymatic reaction links a reversible binding and an irreversible synthesis step. Hence, the reaction follows the Michaelis–Menten kinetics:

$$\dot{P}(t) = \frac{v_{\max}}{N_A}\frac{c_{\mathrm{in}}(t)}{K_M + c_{\mathrm{in}}(t)} = r\frac{c_{\mathrm{in}}(t)}{1 + c_{\mathrm{in}}(t)/K_M} \tag{3}$$

with the amount of pore proteins P, the maximum reaction rate $v_{\max}$, the Michaelis constant K_M and the reaction activity defined by $r = v_{\max}/(N_A K_M)$ of the protocell. Combining equations (1)–(3) in the low-concentration approximation, $c_{\mathrm{in}}(t)/K_M \ll 1$, therefore $\dot{P}(t) = r c_{\mathrm{in}}(t)$, one obtains for the time-dependent amount of pore proteins:

$$LV\ddot{P}(t) + Lbr\dot{P}(t) + \left(\dot{P}(t) - r c_{\mathrm{out}}\right) D_{\mathrm{eff}} A N_A P(t) = 0. \tag{4}$$

3. Discussion

By rescaling the parameters and variables in equation (4), it becomes clear that only one parameter is relevant (time dependence omitted for clarity):

$$\frac{\mathrm{d}^2}{\mathrm{d}t^2}\tilde{P} + \frac{\mathrm{d}}{\mathrm{d}t}\left(\tilde{P} + \frac{1}{2}\tilde{P}^2\right) - f^2\tilde{P} = 0 \tag{5}$$

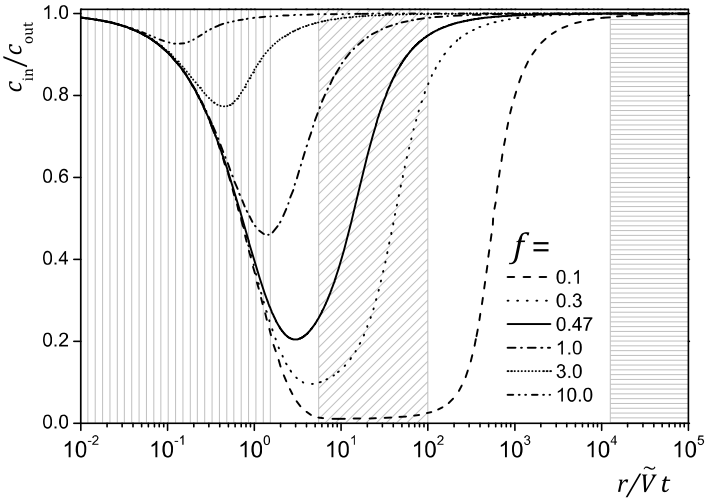

Figure 2. The amino acid concentration inside the protocell is shown, which is directly coupled to the membrane pore proteins via $\dot{P}(t) = rc_{\text{in}}(t)$. Small values of f (dashed) yield an increasingly pronounced depletion of basic components, resulting in a strongly reduced building rate of new pores. For $f = 0.1$ the short-, intermediate- and long-term domains are shown as highlighted areas.

with the coefficient $f = \sqrt{\tilde{V}\tilde{D}c_{\text{out}}}$ depending on the reduced volume $\tilde{V} = V/b$ and the reduced transport coefficient $\tilde{D} = D_{\text{eff}}AN_{\text{A}}/(Lbr)$ and we solve the equation for the $1/\tilde{D}$-rescaled amount of pore proteins $\tilde{P}$ with the rescaled time $t \to rt/\tilde{V}$.

Equation (5) has similarity to the harmonic oscillator, although without extensions it cannot provide oscillatory solutions because of the sign of the restoring force term, which results in a constant $\dot{\tilde{P}}$ for large times. The second term describes friction and is responsible for a permanent energy loss and damping of the dynamics.

For $f \lesssim 0.1$, which is equivalent to choosing a small protocell volume V, a low outer concentration c_{out} and a high reaction activity r (see the definition of f above), the numerical solution[4] displays, in general, characteristic behaviour on short, intermediate and long time scales. For short time scales and small initial concentrations, the continuous depletion of amino acids dominates the dynamics of the system. Assuming that the external concentration remains constant, the model only depends on the constant parameter f determining the shape of the pore concentration graph over time. Therefore, for short time scales, or with negligible trans-membrane transport, equation (4) is approximated by an exponential solution, $P(t) = (c_{\text{out}}V/b)\{1 - \exp[-br/(Vt)]\}$ (figure 2, the first highlighted area).

The intermediate time scale is dominated by the transient depletion of basic components in the protocell. In the beginning, the protocell consumes the stock of basic nutrients for the assembly of pores. Once a few pores have been formed through the membrane, new basic components are slowly provided to the protocell. Eventually, the system reaches the point of dynamic equilibrium where the loss and gain of basic components are balanced. In the case of $\dot{c}_{k,\text{in}}(t) = 0$

[4] The simulation was done with Mathematica 8, Wolfram Research, Inc., USA.

during the intermediate time scale, the pore protein amount increases exponentially:

$$P(t) = \frac{c_{\text{out}} V}{b} \exp\left(\frac{t}{\tau}\right), \quad \text{with } \tau = -\frac{b}{J_{\max} A N_{\text{A}}}. \tag{6}$$

Here the parameters determining the time scale τ can be extracted well since the equation is independent of the reaction activity r. $J_{\max} = D_{\text{eff}} c_{\text{out}}/L$ corresponds to the maximum possible flux, cf equation (2), through a membrane pore. The time scale τ gives the effective diffusion coefficient D_{eff}, which is the only unknown parameter. In addition, we also obtain from experimental data $c_{\text{out}} V/b$, corresponding to the number of α-haemolysin pores that can be produced by the initial stock of basic components within a permanently closed protocell volume.

With the growing number of membrane-bound pore proteins, the influx of basic components increases and eventually surmounts the loss due to pore protein synthesis and $c_{\text{in}}(t)$ increases again. The inner concentration approaches homoeostasis with the outer concentration on large time scales. Using $c_{\text{in}}(t) \approx c_{\text{out}}$ in equation (3) the low-concentration approximation, the increase of pore proteins for large time scales becomes simply $P(t) = r c_{\text{out}} t + \text{const}$.

In figure 2, the kinetics of the inner concentration, $c_{\text{in}(t)}/c_{\text{out}} = \dot{P}(t)/(r c_{\text{out}})$, is plotted for different values of f. It shows the influence of the specific reaction activity r/V. For smaller f, the basic components are steadily depleted for an increasing time span, which may lead to protocell death if activity is stopped for a time period.

This separation of time scales is well suited to the determination of the diffusion constant of amino acids through the pores, since the sensitivity of the model to the parameter values is dependent on f and increases for smaller values. With this goal in mind, it is advantageous to design the experiment for a small f in order to optimize the separation of the time scales and maximize the duration of the short and intermediate time scales.

In figure 3, we fitted the model curve to the experimental data by the mean-square method using the following parameters from [14]: $L \approx 10\,\text{nm}$, $A \approx 1.8\,\text{nm}^2$, $V \approx 4.2\,\text{pl}$ and $r \approx 7.1 \times 10^{-10}\,\text{pl}\,\text{s}^{-1}$. We note that $b = 3794$ represents the number of amino acids to build one pore-heptamer including seven attached enhanced GFPs. By fitting the curves for the evolution of membrane pore proteins, our model allowed us to determine the initial inner amino acid concentration of the vesicle and the hitherto unknown effective diffusion coefficient of amino acids through a pore: $c_{\text{out}} \approx 2.3\,\text{mM}$, $D_{\text{eff}} \approx 2.2 \times 10^{-15}\,\text{m}^2\,\text{s}^{-1}$. Furthermore, the predicted concentration of our model is slightly higher than the indicated amino acid concentration in [14].

4. Protein degradation

The effect of protein degradation, e.g. by proteases, or more general protein activity loss of the dynamics of our system has not been thoroughly investigated experimentally so far. Therefore, assumptions have to be made here. Long-term behaviour including protein activity loss may be integrated into the model by adding hypothetical terms for zeroth-order or first-order degradation.

Zeroth-order degradation is described by a constant degradation rate of pore proteins, $\dot{P}_{\text{deg}}(t) = -\lambda_0$, where first-order degradation is proportional to the number of undegraded pore proteins, $\dot{P}_{\text{deg}}(t) = -\lambda_1 P(t)$.

However, experimental studies of protein degradation, e.g. driven by AAA+ proteases ClpXP and ClpAP, is likely to follow Michaelis–Menten kinetics with small Michaelis constants

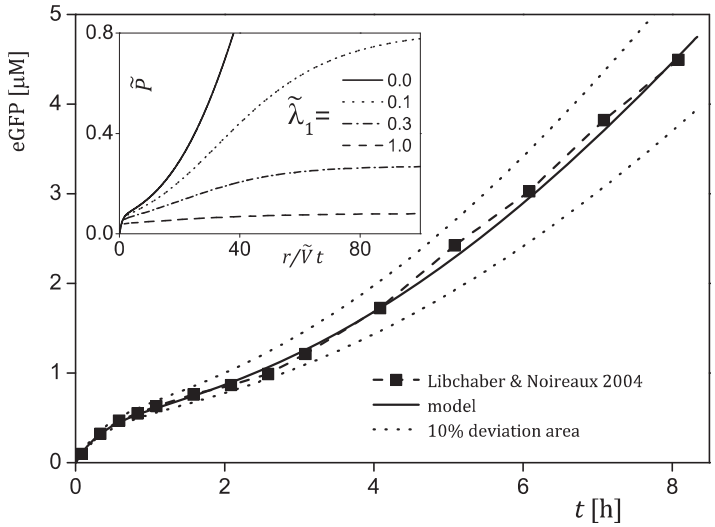

Figure 3. Comparison of the experimental data from Noireaux and Libchaber [15] to the presented model is shown here ($\tilde{\lambda}_1 = 0$, $\tilde{\lambda}_0 = 0$, $f = 0.47$) (see footnote 4). The dotted lines represent the maximum error of the model when varying c_{out}, D_{eff}, r and V by 10%. The inset shows the evolution of pore proteins inside the protocell including protein degradation for varying $\tilde{\lambda}_1$, $f = 0.3$ and $\tilde{d} = 0$. The data were obtained from [14].

$K_{\text{M,deg}}$ (approximately 1–100 nM), resulting in a pronounced zeroth-order degradation over a wide range of protein concentrations [21, 24, 25]. With increasing protein concentration, small Michaelis constants $K_{\text{M,deg}}$ lead to faster saturation of the degradation rate. Zeroth- and first-order degradation are the limit cases for high protein concentrations, $P(t) \gg K_{\text{M,deg}}$, and low protein concentrations, $P(t) \ll K_{\text{M,deg}}$, respectively.

In order to implement zeroth-order degradation, a constant decay rate λ_0, in units of mol s^{-1}, has to be subtracted from the right-hand side of equation (3). Further, $\lambda_0 d_k$ has to be added to the brackets in equation (1), where d_k is the amount of irreversible degraded amino acids of type k per degraded pore protein. The irreversible degradation probability $\tilde{d} = d/b$ refers to the purely reversible, $\tilde{d} = 0$, and purely irreversible, $\tilde{d} = 1$, degradation, respectively. Amino acids from reversible degradation may be reused to build new amino acids in contrast to the irreversible degradation case, e.g. where chemical modifications degrade functional ability and amino acids get irrecoverably lost. The corresponding rescaled degradation term to be added to the left-hand side of equation (5) is $\tilde{\lambda}_0 f^2(\tilde{P} + \tilde{d})$ with the reduced decay rate $\tilde{\lambda}_0 = \lambda_0/(rc_{\text{out}})$.

The first-order degradation terms are $-\lambda_1 P(t)$ to be added to equation (3), with λ_1 in units of s^{-1}, $\lambda_1 d_k P(t)$ to equation (1) and $\tilde{\lambda}_1(\dot{\tilde{P}} + \tilde{d}\tilde{P} + \tilde{P}^2)$ to equation (5), with $\tilde{\lambda}_1 = \lambda_1 \tilde{V}/r$.

The value for $\tilde{d}$ is arbitrarily chosen and serves as an exemplar of irreversible degradation ($\tilde{d} > 0$). We further discuss $\tilde{d} = 0.3$ to show the difference of reversible, figure 3 inset, and partially irreversible degradation, figure 4.

Figure 4 shows the qualitative difference of irreversible zeroth- and first-order degradation. In the case of zeroth order, no saturation in the number of pore proteins is found. A small enough degradation rate (short-dashed line, $\tilde{\lambda}_0 = 0.1$, left graph) decelerates the dynamics of the system.

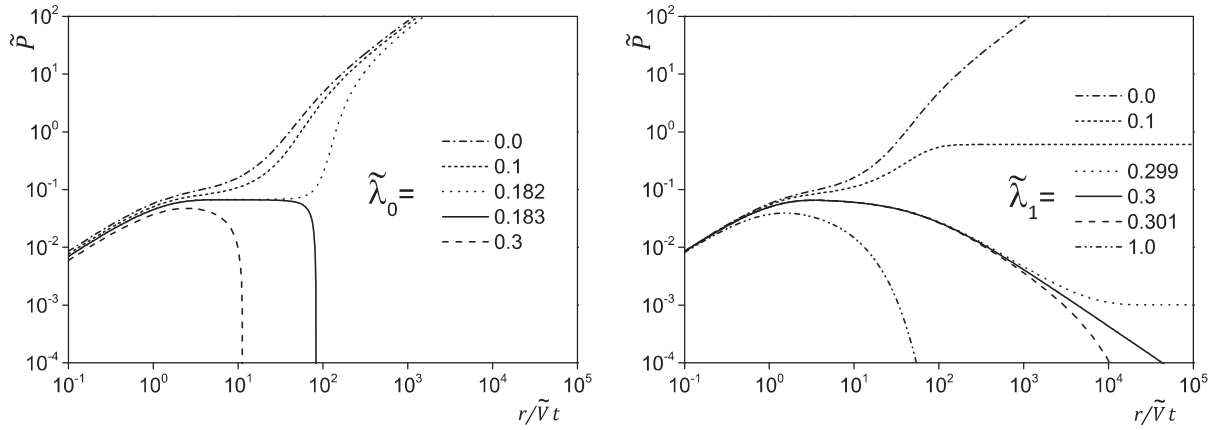

Figure 4. Evolution of pore proteins for zeroth-order (left) and first-order (right) protein degradation ($f = 0.3$). We have chosen $\tilde{d} = 0.3$ for convenience as an exemplar of irreversible degradation. The dynamics of the pore production slows down with increasing degradation rate. First-order degradation reveals saturation in the number of pore proteins for long-term scales. In both cases, a critical degradation rate can be seen ($\tilde{\lambda}_{0,\mathrm{crit}} \approx 0.182$ and $\tilde{\lambda}_{1,\mathrm{crit}} = 0.3$). Above these rates, the irreversible degradation of pore proteins, and therefore amino acids, becomes larger than the incoming flux of new amino acids. Eventually, this results in complete degradation of pore proteins and complete depletion of amino acids inside the protocell (dashed and dash-dot-dotted lines).

In contrast, above a critical degradation rate, the production grows on long-term scales. Below the threshold, we observed infinite growth in zeroth-order and stationary in first-order dynamics. The irreversible degradation rate exceeds the production of pore proteins. This diminishes the incoming flux of new amino acids and eventually results in complete depletion of the protocell and degradation of all pore proteins (dashed line, left graph). The protocell dies. For $f \lesssim 0.1$, the degradation rates for closing protocells has an upper bound $\tilde{\lambda}_{0,\mathrm{c}} > f^2/(\tilde{d} + f^2)$.

First-order degradation dynamics offers saturation of the number of pore proteins (short-dashed line, $\tilde{\lambda}_1 = 0.1$, right graph) up to a critical degradation rate (solid line, right graph). The system approaches steady state on the long-term scale. The inner concentration and the number of pore proteins for steady state can be calculated as $c_{\mathrm{s.s.}}/c_{\mathrm{out}} = 1 - \tilde{d}\tilde{\lambda}_1/f^2$ and $\tilde{P}_{\mathrm{s.s.}} = f^2 - \tilde{d}\tilde{\lambda}_1$. Above a critical rate, $\tilde{\lambda}_{1,\mathrm{c}} = f^2/\tilde{d}$, the degradation of pore proteins becomes larger than the production, decreasing the inflow of new amino acids. The number of pore proteins and the concentration of amino acids approach zero asymptotically. In this case, first-order degradation shares the same fate as zeroth-order on the long-term scale.

In conclusion, we found complex dynamics due to the two discussed degradation scenarios. If degradation surpasses a sharp threshold, all pores degrade, which amplifies this dynamics even more. In the case of zeroth order, this dynamics is strongly pronounced. In first-order case, below this threshold the system ends up in a stationary situation, which is not the case for zeroth-order degradation. The protocell is therefore required to sustain a production rate over this threshold to survive.

5. Summary

The discussed theoretical model describes the experimentally measured turnover dynamics of a simple protocell consisting of a liposome enclosing gene expression machinery. The protocell produces α-haemolysin pore proteins encoded in the included minimal genome. The impermeability of the membrane leads to basic component depletion, which shuts down the system turnover. Once the pores are inserted spontaneously into the membrane, the basic nutrients enter and the turnover increases again. Our one-parameter model describes quantitatively the transient dynamics. The model fits very well the corresponding experimental curve in [14], which allows us to predict numerical values for the amino acid diffusion through a single pore as well as the initial amino acid concentration of liposomes. We also considered the possible consequences of long-term degradation, although measurements are not yet available. The extended model describes zeroth- and first-order irreversible degradation of proteins and the qualitative differences on a long-term scale. Contrary to zeroth order, the number of pore proteins for first-order degradation will saturate on the long-term scale. Increasing the degradation rate up to the critical, well-defined threshold value slows down the pore production dynamics. For higher degradation rates, the protocells end up in equilibrium death.

Acknowledgments

We are grateful to Albert Libchaber (Rockefeller University, New York) and Vincent Noireaux (University of Minnesota) for providing data and support and Josef Käs for valuable and fruitful discussions and support. We also thank all the students who participated in the 2010 IPSP biophysics class at Leipzig University, for their lively discussion that was at the origin of the presented model. The work presented in this paper was made possible by funding from the German Ministry of Education and Research (BMBF, PtJ-Bio, 0315883).

References

[1] Miller S L and Urey H C 1959 *Science* **130** 1622–4
[2] Briones C, Stich M and Manrubia S C 2009 *RNA* **15** 743–9
[3] Miller S L and Urey H C 1959 *Science* **130** 245–51
[4] Fraser C L and Folsome C E 1975 *Orig. Life* **6** 429–33
[5] Lincoln T A and Joyce G F 2009 *Science* **323** 1229–32
[6] Monnard P A, Luptak A and Deamer D W 2007 *Phil. Trans. R. Soc.* B **362** 1741–50
[7] Deamer D W and Oro J 1980 *Biosystems* **12** 167–75
[8] Lazcano A and Miller S L 1994 *J. Mol. Evol.* **39** 546–54
[9] Stano P, Kuruma Y, Souza T P and Luisi P L 2010 *Methods Mol. Biol.* **606** 127–45
[10] Oberholzer T, Wick R, Luisi P L and Biebricher C K 1995 *Biochem. Biophys. Res. Commun.* **207** 250–7
[11] Oberholzer T, Nierhaus K H and Luisi P L 1999 *Biochem. Biophys. Res. Commun.* **261** 238–41
[12] Murtas G, Yutetsu K, Paolo B, Alberto D and Luisi P L 2007 *Biochem. Biophys. Res. Commun.* **363** 12–7
[13] Hanczyc M M and Szostak J W 2004 *Curr. Opin. Chem. Biol.* **8** 660–4
[14] Noireaux V and Libchaber A 2004 *Proc. Natl Acad. Sci. USA* **101** 17669–74
[15] Noireaux V, Bar-Ziv R H, Godefroy J, Salman H and Libchaber A 2005 *Phys. Biol.* **2** P1–P8
[16] Elowitz M B and Leibler S 2000 *Nature* **403** 335–8
[17] Garcia-Ojalvo J, Elowitz M B and Strogatz S H 2004 *Proc. Natl Acad. Sci. USA* **101** 10955–60
[18] Renner S, Bessonov A and Simmel F C 2011 *Appl. Phys. Lett.* **98** 083701

[19] Salbreux G, Joanny J F, Prost J and Pullarkat P 2007 *Phys. Biol.* **4** 268–84
[20] Mackenzie B and Erickson J D 2004 *Eur. J. Physiol.* **447** 784–95
[21] Karzbrun E, Shin J, Bar-Ziv R H and Noireaux V 2011 *Phys. Rev. Lett.* **106** 048104
[22] Abbondanzieri E A, Greenleaf W J, Shaevitz J W, Landick R and Block S M 2005 *Nature* **438** 460–5
[23] Song L, Hobaugh M R, Shustak C, Cheley S, Bayley H and Gouaux J E 1996 *Science* **274** 1859–66
[24] Hersch G L, Baker T A and Sauer R T 2004 *Proc. Natl Acad. Sci. USA* **101** 12136–41
[25] Wong W W, Tsai T Y and Liao J C 2007 *Mol. Syst. Biol.* **3** 130

Shen et al. Cancer Convergence (2020) 4:1
https://doi.org/10.1186/s41236-020-0010-1

Cancer Convergence

RESEARCH Open Access

Detecting heterogeneity in and between breast cancer cell lines

Yang Shen[1], B. U. Sebastian Schmidt[1], Hans Kubitschke[2], Erik W. Morawetz[2], Benjamin Wolf[3], Josef A. Käs[2] and Wolfgang Losert[1*]

* Correspondence: wlosert@umd.edu
[1]Institute for Physical Science and Technology, University of Maryland, College Park, MD 20742, USA
Full list of author information is available at the end of the article

Abstract

Background: Cellular heterogeneity in tumor cells is a well-established phenomenon. Genetic and phenotypic cell-to-cell variability have been observed in numerous studies both within the same type of cancer cells and across different types of cancers. Another known fact for metastatic tumor cells is that they tend to be softer than their normal or non-metastatic counterparts. However, the heterogeneity of mechanical properties in tumor cells are not widely studied.

Results: Here we analyzed single-cell optical stretcher data with machine learning algorithms on three different breast tumor cell lines and show that similar heterogeneity can also be seen in mechanical properties of cells both within and between breast tumor cell lines. We identified two clusters within MDA-MB-231 cells, with cells in one cluster being softer than in the other. In addition, we show that MDA-MB-231 cells and MDA-MB-436 cells which are both epithelial breast cancer cell lines with a mesenchymal-like phenotype derived from metastatic cancers are mechanically more different from each other than from non-malignant epithelial MCF-10A cells.

Conclusion: Since stiffness of tumor cells can be an indicator of metastatic potential, this result suggests that metastatic abilities could vary within the same monoclonal tumor cell line.

Keywords: Cancer, Heterogeneity, Single-cell, MDA-MB-231, MCF-10A, MDA-MB-436

Background

Recognized as early as 1958 (Huxley 1958), genetic heterogeneity is a well-established phenomenon in tumor cells, especially during metastatic stages (Torres et al. 2007; Park et al. 2010; Patel et al. 2014; Alizadeh et al. 2015). Studies have shown that cells from a single cancer typically contain multiple genetically distinct subgroups (Cleary et al. 2014; Meacham and Morrison 2013; Gay et al. 2016; Marusyk and Polyak 2010). Such high level of heterogeneity contributes to the reason why cancer is hard to cure (McGranahan and Swanton 2017; Mann et al. 2016; Koren and Bentires-Alj 2015). However, to-date the reason and extent of tumor cell heterogeneity is still not well-understood (Alizadeh et al. 2015). Two main theories have been proposed to explain the origin of tumor cell heterogeneity: the existence of cancer stem cells (Magee et al. 2012) and clonal evolution (McGranahan and Swanton 2017). These two theories try to explain the heterogeneity in ecological and evolutional aspects, respectively, and

evidence exists for each theory (Shackleton et al. 2009). Furthermore, new insight in gene regulatory networks provides a framework for explaining the broad heterogeneity without the need of excessive mutational activity (Huang 2012a; Huang 2013; Huang 2012b). Variations in gene expression lead to molecular variations which in turn affect cellular shape and function.

Another well-established phenomenon associated with tumors are changes in cellular stiffness. Cells actively structure and regulate the different elements of the cytoskeleton, the main contributor of cellular stiffness and compliance (Huber et al. 2013). In fact, different components of the cytoskeleton contribute to different structural and mechanical tasks, e.g. actin contributes to cell elasticity in response to small strains while microtubules affect responses to large strains (Lautenschlager et al. 2009; Kubitschke et al. 2017). The mechanics of cells has been studied with multiple experimental tools (Kubitschke et al. 2018; Pawlizak et al. 2015), including atomic force microscopy (AFM) (Hayashi and Iwata 2015), quantitative deformability cytometry (q-DC) (Nyberg et al. 2017), real-time deformability cytometry (Mietke et al. 2015; Otto et al. 2015), microfluidic optical cell stretchers (Farzbod and Moon 2018), and hydrodynamic flow stretchers (Dudani et al. 2013; Gossett et al. 2012). Since metastasis is responsible for more than 90% of cancer fatality (Wirtz et al. 2011; Mehlen and Puisieux 2006; Taketo 2011), great effort has been made to study the mechanical properties of metastatic tumor cells and to understand how mechanical properties of tumor cells affect their metastatic ability. A number of studies have found that metastatic tumor cells are softer than their non-metastatic counterparts as well as normal cells (Lekka et al. 2012; Plodinec et al. 2012; Swaminathan et al. 2011). In addition, studies have suggested the potential of using mechanical properties as a biomarker of metastasis (Xu et al. 2012) and for cancer diagnosis (Remmerbach et al. 2009).

In this paper we take first steps to link these two phenotypes of metastatic tumor cells – changes in cell heterogeneity and cell stiffness. Though most cell mechanics studies are carried out at the single-cell level, analysis and interpretation of data is generally confined to averages, thus omitting heterogeneity as an important aspect of the metastatic phenotype. Prior work (Plodinec et al. 2012; Kiessling et al. 2013) has yielded important hints that mechanical properties are in fact heterogeneous – the measured distributions for the viscoelastic properties of cells, even in a single cell line, are not Gaussian indicating that various mechanical phenotypes are present, for instance, represented by outliers of the usual long-tailed distributions.

In this paper, we use a microfluidic optical cell stretcher to measure and contrast mechanical properties of single cells from three epithelial cell lines: MCF-10A, MDA-MB-231 and MDA-MB-436, and we use the heterogeneity of the cell mechanical properties of each cell line to contrast the different phenotypes. These three cell lines represent a well-established breast cancer cell panel. MCF-10A is a non-tumorigenic epithelial cell line while MDA-MB-436 and MDA-MB-231 are breast carcinoma cell lines with a mesenchymal-like metastatic phenotype. With single cell data analysis, we show that heterogeneity of cellular stiffness exists both within and between cell lines. In particular, we observe two groups of MDA-MB-231 cells. Cells in one of the groups are significantly softer than cells in the other. In addition, we find that although MDA-MB-231 and MDA-MB-436 are both triple-negative breast cancer cell lines (i.e. they do not express estrogen receptors, progesterone receptors nor human epidermal growth factor receptor [HER]2) with metastatic tendency, they are rather distinct from each other compared to the nonmalignant cell line MCF-10A.

Results

We used a Microfluidic Optical Cell Stretcher to mechanically stretch individual cells from our breast cancer panel of cell lines and measure their stiffness (Kiessling et al. 2013; Lincoln et al. 2007a). Cells in suspension are not stimulated by their environment, and thus their cortical tension represents the cells' mechanical "ground state". Suspended single cells were trapped for 1 s and subsequently stretched for 2 s and then relaxed in trapping condition for another 2 s (Fig. 1). Images of cells were taken at the rate of 30 frames per second, and the length of the long axis was measured in each frame for each individual cell. In this paper, we use only two mechanical features calculated from these measurements: 1. Relative long axis deformation at the end of stretch (Deformation EOS), and 2. Relative long axis deformation after 2 s of relaxation (Relaxation EOE) (Fig. 1). The value of EOS is inversely proportional to the Young's modulus, where higher EOS value indicates lower Young's modulus (easier to stretch). On the other hand, EOE is a measure of the ability of a cell to restore its shape, where higher absolute value of EOE suggests greater ability to restore the original cell shape. The end-of-experiment deformation (EOE) can also be interpreted as the degree of cell plasticity of the cell under a given applied load or strain. This plasticity is in principle a coarse-grained property which contains contributions of the actin, microtubule and intermediate filament network (Kubitschke et al. 2017). Since both EOE and EOS are linear measurements, a two-fold change in the observed deformation corresponds to a two-fold change in elastic modulus.

In prior work where the mechanical measurements were parameterized by over 50 metrics, we identified deformation and relaxation as important independent

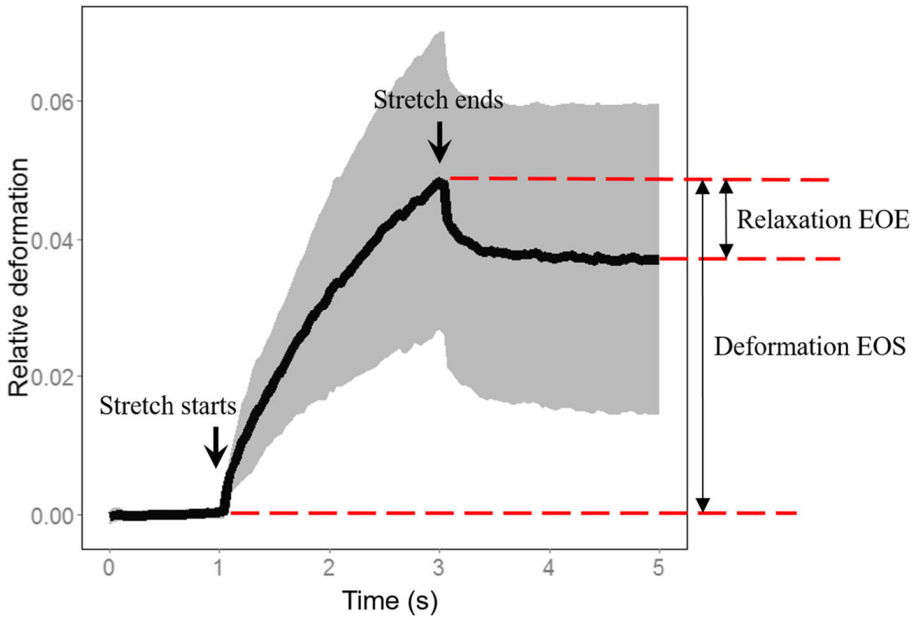

Fig. 1 An illustration of the whole deformability data set of the optical stretcher. The two arrows show the starting and ending time point of stretch respectively. The thick black line shows average deformation of the length of long axis of cell over 130 cells. The gray area captures one standard deviation above and below the average. The two mechanical properties used in this paper (relaxation EOE and Deformation EOS) are illustrated. For both measurements, the deformation at the beginning of the experiment is subtracted. Hence the values of EOS are mostly positive and values of EOE mostly negative

determinants of cell mechanics (Kiessling et al. 2013). Together, these two features give a good estimation of the elastic property of a single cell.

Using this technique, we measured cells from our breast cancer cell panel used to study the EMT. MCF-10A is a non-tumorigenic breast epithelial cell line which is used as a control cell line. MDA-MB-231 and MDA-MB-436 are both triple negative breast cancer cell lines that are epithelial in nature. Both have metastatic potential, with MDA-MB-231 considered more aggressive than MDA-MB-436 (Bianchini et al. 2016).

Two subgroups observed in MDA-MB-231 cells

We first identified two subgroups within MDA-MB-231 cells. One subgroup (cluster 2, Fig. 2) exhibited higher deformations at the end of stretch (EOS) and higher absolute values of relaxation at the end of experiment (EOE) than the other subgroup (cluster 1) (Fig. 2). Higher absolute values of both EOS and EOE indicate that cells in cluster 2 are softer and more elastic (easier to stretch and easier to restore original shape) compared to cluster 1, which overlaps with MDA-MB-436 and MCF-10A cells (Fig. 3a).

The more elastic group does not exist in MDA-MB-231 cells labeled for E-cadherin

Cadherins are responsible for cell-cell binding. E-cadherins are expressed in normal epithelial cells, while in mesenchymal carcinoma cells it is mainly N-cadherins. In our experiments, we also measured mechanical properties of MDA-MB-231 cells that were labeled with E-cadherin antibodies in order to activate extracellular binding sites. Since this is a mesenchymal-like cell line we found a low level of E-cadherin expression, as has also been quantified elsewhere (Pawlizak et al. 2015). In spite of the low expression levels, we observed a different stretching and relaxation behavior in the E-cadherin labeled and non-labeled MDA-MB-231 cells. E-cadherin labeled MDA-MB-231 cells only formed one cluster instead of the two clusters observed in unlabeled MDA-MB-231 cells. The labeled 231 cells overlap with the less elastic and less relaxing subgroup of

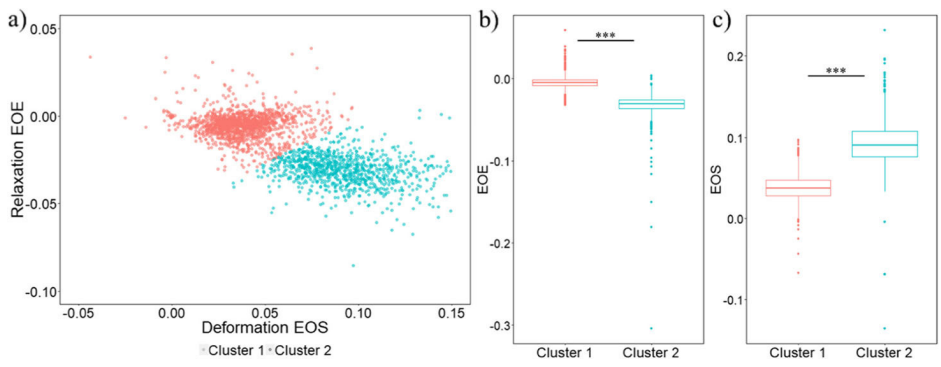

Fig. 2 Two clusters of MDA-MB-231 cells are observed. **a** Scatterplot of Relaxation EOE vs Deformation EOS for MDA-MB-231 cells. The two subgroups are identified with the k-means clustering algorithm and labeled by different colors (red: cluster 1, blue: cluster 2). Negative EOS values in the plot can have two causes: first, strongly rotating cells that influence the shape detection; second, active contractions under force activation (data not shown). Similarly, a positive EOE values can indicate a strongly rotating cells or continued deformation during the relaxation phase. **b** Boxplot comparing relaxation at the end of experiment between cluster 1 and cluster 2 of MDA-MB-231 cells (p value < 0.001). **c** Boxplot comparing deformation at the end of stretch between the two subgroups of MDA-MB-231 cells (p value < 0.001)

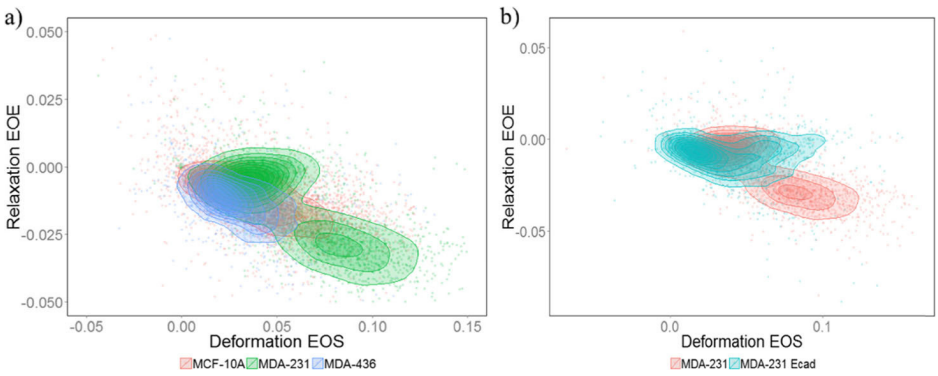

Fig. 3 MCF-10A, MDA-MB-436 and E-cadherin labeled MDA-MB-231 cells all overlap with cluster 1 (the less elastic group) in unlabeled MDA-MB-231 cells. **a** Scatterplot of Relaxation EOE vs Deformation EOE for MCF-10A (red), MDA-MB-231 (green) and MDA-MB-436 (blue) cells. **b** Scatterplot of Relaxation EOE vs Deformation EOE for E-cadherin labeled (blue) and unlabeled (red) MDA-MB-231 cells

MDA-MB-231 cells (cluster 1, Fig. 3b). Activation of the E-cadherin receptor by binding of the antibody leads to cadherin clustering and E-cadherin binding to the actin cortex, which upregulates the actin polymerization and cross-linking of the cytoskeleton (Perez-Moreno and Fuchs 2006). The decrease in deformation found in cluster 1 cells compared to cluster 2 cells is consistent with this change in mechanics due to E-cadherin activation since the elastic storage modulus strongly depends on crosslinking density and dynamics (Gardel et al. 2004; Lieleg et al. 2010; Strehle et al. 2011; Schnauß et al. 2016). In addition, the decreased cell relaxation of the cluster 1 subpopulation could also be explained with upregulated actin nucleation and aggregation while a destabilization of the microtubular cytoskeletal backbone may further result in a lack of relaxation and increased plasticity (Kubitschke et al. 2017).

MDA-MB-231 and MDA-MB-436 cells are more different from each other than from MCF-10A cells

While we showed above that cluster 1 of MDA-MB-231 cells greatly overlaps with MCF-10A and MDA-MB-436 cells, these three cell lines may still be separable at the single cell level. Since both MDA-MB-436 and MDA-MB-231 cell lines have a malignant mesenchymal-like phenotype, it is reasonable to expect they would be more similar to each other comparing to the epithelial-like MCF-10A cell line. To separate the cell phenotypes, we applied a k nearest neighbors (k-NN) algorithm for a pairwise classification of the three phenotypes. We first divided the cells into two groups: train and test. Phenotype labels were provided for cells in the training group but not for the test group. Then, given the position of a single cell in the test group, k-NN identifies its nearest k neighbors within the training group. The k neighbors then take a “vote” with their phenotype, and the cell from test group is assigned to the phenotype that has the highest number of votes. After classification, we calculate the sensitivity (true positive rate), specificity (true negative rate), and F1 score (a measure of classification result, the higher the score the better the classification; the maximum F1 score is 1) for each pair of classification. We found that classification between MCF-10A and MDA-MB-436 cells has the lowest sensitivity, specificity and F1 score regardless of the value of k

(green line in Fig. 4). On the other hand, classification between cluster 1 of MDA-MB-231 and MDA-MB-436 cells had the highest level of F1 scores (blue line in Fig. 4c) – which was even higher than the classification between MCF-10A and MDA-MB-231 cells (red line in Fig. 4c) for most values of k. Similar results were obtained with a different classification algorithm (SVM), where the classification between MDA-MB-231 and MDA-MB-436 cells also had the highest F1 value (Table 1). SVM takes a different approach in classification and aims to find the linear plane that best separates two groups to classify. In addition, when all four phenotypes were classified simultaneously, MDA-MB-436 cells were less likely to be miss-classified as MDA-MB-231 cells than as MCF-10A cells and vice versa (Fig. 5). Together, these results suggest that cells in cluster 1 of MDA-MB-231 are more different from MDA-MB-436 cells than from MCF-10A cells despite that MDA cells are phenotypically considered to be mesenchymal-like and MCF cells to be epithelial.

Discussion

Mechanical properties of tumors cells may be important markers for the metastatic potential of tumors. Studies have shown that metastatic tumor cells are on average softer than non-metastatic ones (Xu et al. 2012; Guck et al. 2005; Fritsch et al. 2010; Alibert et al. 2017; Mierke 2015). In this paper, we illustrate the heterogeneity of tumor cell stiffness both within and between cell lines. Based only on mechanical properties, we show that there are two distinct clusters within MDA-MB-231 cells. Cluster 1 greatly overlaps with MCF-10A and MDA-MB-436 cells, while cells in cluster 2 are softer and more elastic (easier to deform and restore to original shape). In addition, we found that the two malignant epithelial cell lines, MDA-231 and MDA-436, are more distinct from each other in their mechanical phenotype than from the non-tumorigenic MCF-10A cell line.

Our findings of mechanical heterogeneity within the MDA-MB-231 cell line complement prior findings indicating that the molecular single cell characteristics of MDA-MB-231 cells are also heterogeneous. For example, it has been shown that there are two distinct subgroups of MDA-MB-231 cells which differ significantly in the cell surface density of various cytokine receptors (CCR5, CXCR3, CXCR1) (Norton et al.

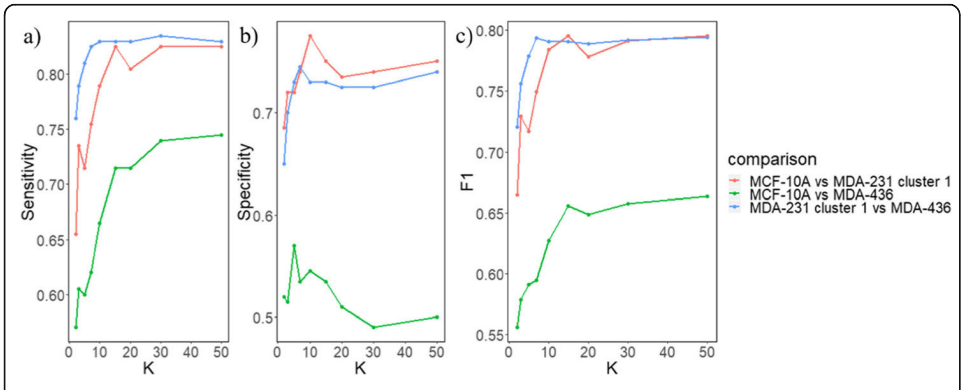

Fig. 4 Pairwise k-NN classification results show that MDA-MB-231 and MDA-MB-436 cells are more different from each other than from MCF-10A cells. **a** Sensitivity (true positive rate) for the three comparisons versus different values of k. **b** Specificity (true negative rate) for the three comparisons versus different values of k. **c** F1 score for the three comparisons versus different values of k

Table 1 Pairwise classification results by support vector machine (SVM)

	Sensitivity	Specificity	F1
MCF-10A (positive) vs MDA-MB-231 cluster 1 (negative)	0.71	0.72	0.71
MCF-10A (positive) vs MDA-MB-436 (negative)	0.58	0.66	0.60
MDA-MB-231 cluster 1 (positive) vs MDA-MB-436 (negative)	0.74	0.79	0.76

2015). In particular, CXCR3 was found to be overexpressed in metastatic tumor cells, and drugs targeting CXCR3 decreased tumor cell migration (Zhu et al. 2015). To link our observations of mechanical heterogeneity with molecular heterogeneity directly, future studies can combine the optical stretching with fluorescence imaging.

We also identified heterogeneity among different triple negative breast cancer (TNBC) cell lines, i.e. we found that MDA-MB-231 and MDA-MB-436 cells are quite distinct from each other, even more so than from the non-tumorigenic MCF-10A cell line. This finding is consistent with the perspective of the classical clonal evolution model, assuming the epigenetic and (more importantly) the phenotypic characteristics of normal breast tissue are similar among all women. Thus, both patients from which the MDA-MB-231 and MDA-MB-436 cell lines are derived, had initially breast tissue which is very similar to the MCF-10A tissue. From this healthy starting population of cells, different paths can be taken to reach a metastatic phenotype. In fact, an extensive gene similarity analysis based on The Cancer Genome Atlas (TCGN) revealed that on average approx. 40% of tumors of a given site, e.g. breast cancers, are likely genetically closer to tumors from other sites than to tumors of the same origin (Heim et al. 2014; Andor et al. 2016). It seems actually unlikely that two completely different patients accumulate the exact same cancer cell phenotype with the same optical stretching characteristics.

In addition, our findings may have important clinical implications. Patients with triple negative breast cancer are currently considered to have a very poor prognosis (Bianchini

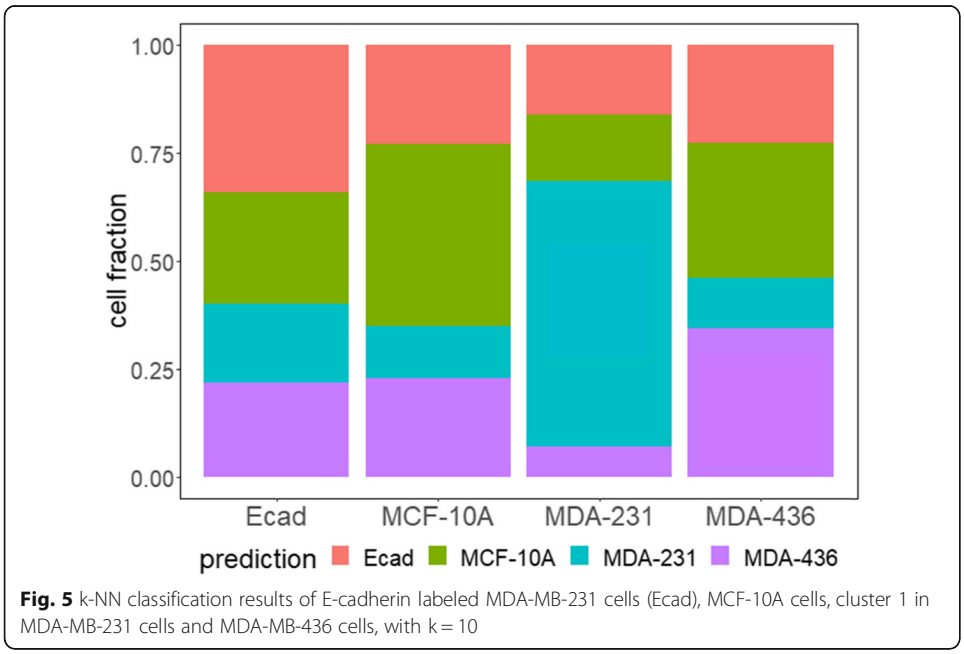

Fig. 5 k-NN classification results of E-cadherin labeled MDA-MB-231 cells (Ecad), MCF-10A cells, cluster 1 in MDA-MB-231 cells and MDA-MB-436 cells, with k = 10

et al. 2016; Lehmann and Pietenpol 2014; Denkert et al. 2017). However, there has been an emerging trend to regard TNBC as a heterogeneous group of patients with varying prognosis (Bianchini et al. 2016; Lehmann and Pietenpol 2014; Denkert et al. 2017). Furthermore, TNBCs can have very different molecular characteristics, potentially rendering some tumors more suitable to targeted therapies (Bianchini et al. 2016; Lehmann and Pietenpol 2014; Denkert et al. 2017). It is of paramount clinical importance to identify those patients. The present data is exciting in that it shows that two TNBC cell lines (which would be put into one prognostic basket clinically) are indeed very different. It is intriguing to speculate whether optical stretching analysis could be used to differentiate those TNBC cases with a better prognosis (i.e. a lower rate of relapse and distant metastasis) from those with a worse prognosis.

Moreover, our findings on the inter-cell-line heterogeneity is an indication that average based analysis methods could oversimplify tumor cell data. For example, MCF-10A, MDA-MB-436 and cluster 1 of MDA-MB-231 cells are mechanically similar to each other with probably minor difference in the average values (Fig. 3a). However, when classified with a more sophisticated algorithm like k-NN, reasonably good classification accuracy can be achieved. That is to say, even though cells from the three cell lines overlap on average, locally cells from a certain cell line are closer to cells from the same cell line than from other cell lines.

Lastly, our studies of E-cadherin labeled MDA-MB-231 cells reveal that antibody labeling can alter the mechanical phenotype significantly. We reason that this is because binding of the antibody to the E-cadherin receptor simulates cell-cell binding, which causes cadherin clustering and stimulates the actin cortex bound to cadherin. This is a good example of how antibody labeling may change the properties of cells, and how antibodies could provide insights into the changes in cancer cell behavior in response to their tumor microenvironment. Further experiments are needed to validate and provide molecular evidence for the role of E-cadherin antibody treatment in altering the mechanical phenotype of MDA-MB-231 cells.

Conclusion

In conclusion, we illustrated heterogeneity in cellular mechanical properties within and between cell lines. Future studies should examine how changes in chemokine receptor expression correlate with tumor cell stiffness. Additional investigations are needed to determine how mechanical properties of cancer cells could help identify distinct prognostic subgroups of triple negative breast cancer patients.

Methods and materials

Experimental procedures

The general setup of the optical stretcher (OS) is described in (Lincoln et al. 2007b) with additional improvements to the microfluidics, the computer-controlled stretching processes, and the thermally controlled stage described in detail in (Lincoln et al. 2007b; Guck et al. 2001; Schmidt et al. 2015). The mechanical properties of cells were determined by guiding the cell suspension into the automated microfluidic OS where single cells are consecutively trapped and stretched. The cells are trapped at 100 mW for 1 s and the cell radius along the laser axis is determined. The cell is afterwards

stretched at 875 mW for 2 s. The cells are allowed to relax for 2 s after stress cessation. A microscope-mounted camera takes images at 30 frames per second during the whole stretching process. Afterwards, an edge detection algorithm is used to extract cell shape and cell parameters and to sort out pathological cell (e.g. dead cells).

Cell culture and medium

MCF-10A cells (Cat.No. CRL-10317, ATCC) were cultured in DMEM/Ham's F12 medium containing l-glutamine (Cat.No. FG 4815, Biochrom) supplemented with 5% horse serum (Cat.No. 12449C, SAFC), 20 ng/ml human epidermal growth factor (Cat.No. E9644, Sigma-Aldrich), 10 μg/ml insulin (Cat. No.I9278, Sigma-Aldrich), 100 ng/ml cholera toxin (Cat.No. C8052, Sigma-Aldrich), 500 ng/ml hydrocortisone (Cat.No. H0888, Sigma-Aldrich) and 100 U/ml penicillin/streptomycin (Cat.No. A 2213, Biochrom).

MDA-MB-231 and MDA-MB-436 cells were cultured in DMEM containing 4.5 g/l glucose, l-glutamine (Cat.No. FG 0435, Biochrom) supplemented with 10% fetal bovine serum (Cat.No. S 0615, Biochrom) and 100 U/ml penicillin/streptomycin.

All cell lines were incubated at 37 °C in a 95% air and 5% CO2 atmosphere. The culture medium was changed every 2 to 3 days and cells were passaged every 4 to 5 days. To detach the cells, a PBS solution containing 0.025%(w/v) trypsin and 0.011%(w/v) EDTA (Cat.No. L 2113, Biochrom) was applied for several minutes.

Data analysis

The two clusters of MDA-MB-231 cells were identified using the *kmeans*() function in *R* (version 3.0.3) with 2 centers, 1000 iterations and 50 random initial conditions. For kNN classification, 1200 cells were first randomly selected from each cell line. From the 1200 cells, 200 were randomly selected as testing set and the remaining 1000 were used as training set for each cell line. The classification was done separately for each pair of cell line using the *knn*() function in R with 8 different values of k (2, 3, 5, 7, 10, 15, 20, 50). Similarly, simultaneous classification of the three cell lines were done. After classification, a false positive rate was calculated as FPR = (false positives) / (false positives + true positives), and a false negative rate was calculated as (FNR) = (false negatives) / (false negatives + true negatives). Finally, pairwise support vector machine (SVM) classifications were done based on all 1200 randomly selected cells using the *ksvm*() function with linear kernel and $C = 10$ in the *R* package *kernlab*. All plots were made with the ggplot2 package in *R*. The dataset is normalized to zero mean and unit variance before the aforementioned analysis.

Abbreviations

EOE: End of experiment deformation; EOS: End of stretch deformation; FNR: False negative rate; FPR: False positive rate; kNN: k nearest neighbors; OS: Optical stretcher; SVM: Support vector machine; TCGN: The Cancer Genome Atlas; TNBC: Triple negative breast cancer

Acknowledgements

Not applicable

Authors' contributions

YS analyzed data and wrote the manuscript, BUSS and BW helped interpret the data and edit the manuscript, HK and EWM carried out the experiment and edited the manuscript, WL and JAK supervised the project and edited the manuscript. All authors read and approved the final manuscript.

Funding
This project has received funding from the European Research Council (ERC-741350/HoldCancerBack) and we acknowledge funding from the European Commission H2020-PHC-2015-two-stage in the frame of the 'FORCE' project. W.L. was partially supported by AFOSR grant FA9550-16-1-0052. Y.S. was supported by the National Institutes of Health, National Eye Institute intramural research program. E.M. was supported by the European Union and the Europäischer Sozialfonds in Saxony (ESF – 100234741).

Availability of data and materials
Data is available upon request.

Ethics approval and consent to participate
Not applicable.

Consent for publication
Not applicable.

Competing interests
The authors declare that they have no competing interests.

Author details
[1]Institute for Physical Science and Technology, University of Maryland, College Park, MD 20742, USA. [2]Peter Debye Institute for Soft Matter Physics, Leipzig University, Linnéstr. 5, 04103 Leipzig, Germany. [3]Leipzig University Medical Center, Department of Obstetrics and Gynecology, Liebigstr. 20a, 04103 Leipzig, Germany.

Received: 7 June 2019 Accepted: 15 January 2020
Published online: 03 February 2020

References

Alibert C, Goud B, Manneville JB. Are cancer cells really softer than normal cells? Biol Cell. 2017;109(5):167–89.
Alizadeh AA, Aranda V, Bardelli A, Blanpain C, Bock C, Borowski C, et al. Toward understanding and exploiting tumor heterogeneity. Nat Med. 2015;21(8):846–53 Epub 2015/08/08.
Andor N, Graham TA, Jansen M, Xia LC, Aktipis CA, Petritsch C, et al. Pan-cancer analysis of the extent and consequences of intratumor heterogeneity. Nat Med. 2016;22(1):105–13 Epub 2015/12/01.
Bianchini G, Balko JM, Mayer IA, Sanders ME, Gianni L. Triple-negative breast cancer: challenges and opportunities of a heterogeneous disease. Nat Rev Clin Oncol. 2016;13(11):674–90 Epub 2016/10/19.
Cleary AS, Leonard TL, Gestl SA, Gunther EJ. Tumour cell heterogeneity maintained by cooperating subclones in Wnt-driven mammary cancers. Nature. 2014;508(7494):113–7 Epub 2014/04/04.
Denkert C, Liedtke C, Tutt A, von Minckwitz G. Molecular alterations in triple-negative breast cancer-the road to new treatment strategies. Lancet. 2017;389(10087):2430–42 Epub 2016/12/13.
Dudani JS, Gossett DR, Tse HT, Di Carlo D. Pinched-flow hydrodynamic stretching of single-cells. Lab Chip. 2013;13(18):3728–34 Epub 2013/07/26.
Farzbod A, Moon H. Integration of reconfigurable potentiometric electrochemical sensors into a digital microfluidic platform. Biosens Bioelectron. 2018;106:37–42 Epub 2018/02/08.
Fritsch A, Höckel M, Kiessling T, Nnetu KD, Wetzel F, Zink M, et al. Are biomechanical changes necessary for tumour progression? Nat Phys. 2010;6(10):730.
Gardel M, Shin J, MacKintosh F, Mahadevan L, Matsudaira P, Weitz D. Elastic behavior of cross-linked and bundled actin networks. Science. 2004;304(5675):1301–5.
Gay L, Baker AM, Graham TA. Tumour Cell Heterogeneity. F1000Res. 2016;5 Epub 2016/03/15.
Gossett DR, Tse HT, Lee SA, Ying Y, Lindgren AG, Yang OO, et al. Hydrodynamic stretching of single cells for large population mechanical phenotyping. Proc Natl Acad Sci U S A. 2012;109(20):7630–5 Epub 2012/05/02.
Guck J, Ananthakrishnan R, Mahmood H, Moon TJ, Cunningham CC, Käs J. The optical stretcher: a novel laser tool to micromanipulate cells. Biophys J. 2001;81(2):767–84.
Guck J, Schinkinger S, Lincoln B, Wottawah F, Ebert S, Romeyke M, et al. Optical deformability as an inherent cell marker for testing malignant transformation and metastatic competence. Biophys J. 2005;88(5):3689–98.
Hayashi K, Iwata M. Stiffness of cancer cells measured with an AFM indentation method. J Mech Behav Biomed Mater. 2015;49:105–11 Epub 2015/05/26.
Heim D, Budczies J, Stenzinger A, Treue D, Hufnagl P, Denkert C, et al. Cancer beyond organ and tissue specificity: next-generation-sequencing gene mutation data reveal complex genetic similarities across major cancers. Int J Cancer. 2014;135(10):2362–9 Epub 2014/04/08.
Huang S. Tumor progression: chance and necessity in Darwinian and Lamarckian somatic (mutationless) evolution. Prog Biophys Mol Biol. 2012a;110(1):69–86 Epub 2012/05/15.
Huang S. The molecular and mathematical basis of Waddington's epigenetic landscape: a framework for post-Darwinian biology? BioEssays. 2012b;34(2):149–57 Epub 2011/11/22.
Huang S. Genetic and non-genetic instability in tumor progression: link between the fitness landscape and the epigenetic landscape of cancer cells. Cancer Metastasis Rev. 2013;32(3–4):423–48 Epub 2013/05/04.
Huber F, Schnauss J, Ronicke S, Rauch P, Muller K, Futterer C, et al. Emergent complexity of the cytoskeleton: from single filaments to tissue. Adv Phys. 2013;62(1):1–112 Epub 2013/01/01.
Huxley J. Biological aspects of cancer: Harcourt, Brace; 1958.
Kiessling TR, Herrera M, Nnetu KD, Balzer EM, Girvan M, Fritsch AW, et al. Analysis of multiple physical parameters for mechanical phenotyping of living cells. Eur Biophys J. 2013;42(5):383–94 Epub 2013/03/19.

Koren S, Bentires-Alj M. Breast tumor heterogeneity: source of fitness, Hurdle for Therapy. Mol cell. 2015;60(4):537–46 Epub 2015/11/23.
Kubitschke H, Morawetz EW, Käs JA, Schnauß J. Physical Properties of Single Cells and Collective Behavior. In: Quantification of Biophysical Parameters in Medical Imaging. Cham: Springer; 2018. p. 89–121.
Kubitschke H, Schnauss J, Nnetu K, Warmt E, Stange R, Kaes J. Actin and microtubule networks contribute differently to cell response for small and large strains. New J Phys. 2017;19(9):093003.
Lautenschlager F, Paschke S, Schinkinger S, Bruel A, Beil M, Guck J. The regulatory role of cell mechanics for migration of differentiating myeloid cells. Proc Natl Acad Sci U S A. 2009;106(37):15696–701 Epub 2009/09/01.
Lehmann BD, Pietenpol JA. Identification and use of biomarkers in treatment strategies for triple-negative breast cancer subtypes. J Pathol. 2014;232(2):142–50.
Lekka M, Pogoda K, Gostek J, Klymenko O, Prauzner-Bechcicki S, Wiltowska-Zuber J, et al. Cancer cell recognition–mechanical phenotype. Micron. 2012;43(12):1259–66 Epub 2012/03/23.
Lieleg O, Claessens MM, Bausch AR. Structure and dynamics of cross-linked actin networks. Soft Matter. 2010;6(2):218–25.
Lincoln B, Schinkinger S, Travis K, Wottawah F, Ebert S, Sauer F, et al. Reconfigurable microfluidic integration of a dual-beam laser trap with biomedical applications. Biomed Microdevices. 2007a;9(5):703–10 Epub 2007/05/17.
Lincoln B, Wottawah F, Schinkinger S, Ebert S, Guck J. High-throughput rheological measurements with an optical stretcher. Methods Cell Biol. 2007b;83:397–423.
Magee JA, Piskounova E, Morrison SJ. Cancer stem cells: impact, heterogeneity, and uncertainty. Cancer Cell. 2012;21(3):283–96 Epub 2012/03/24.
Mann KM, Newberg JY, Black MA, Jones DJ, Amaya-Manzanares F, Guzman-Rojas L, et al. Analyzing tumor heterogeneity and driver genes in single myeloid leukemia cells with SBCapSeq. Nat Biotechnol. 2016;34(9):962–72 Epub 2016/08/02.
Marusyk A, Polyak K. Tumor heterogeneity: causes and consequences. Biochim Biophys Acta. 2010;1805(1):105–17 Epub 2009/11/26.
McGranahan N, Swanton C. Clonal heterogeneity and tumor evolution: past, present, and the future. Cell. 2017;168(4):613–28 Epub 2017/02/12.
Meacham CE, Morrison SJ. Tumour heterogeneity and cancer cell plasticity. Nature. 2013;501(7467):328–37 Epub 2013/09/21.
Mehlen P, Puisieux A. Metastasis: a question of life or death. Nat Rev Cancer. 2006;6(6):449–58 Epub 2006/05/26.
Mierke CT. Cellular stiffness and deformability. Bristol: Physics of Cancer: IOP Publishing; 2015. p. 3–31.
Mietke A, Otto O, Girardo S, Rosendahl P, Taubenberger A, Golfier S, et al. Extracting cell stiffness from real-time deformability Cytometry: theory and experiment. Biophys J. 2015;109(10):2023–36 Epub 2015/11/21.
Norton KA, Popel AS, Pandey NB. Heterogeneity of chemokine cell-surface receptor expression in triple-negative breast cancer. Am J Cancer Res. 2015;5(4):1295–307 Epub 2015/06/24.
Nyberg KD, Hu KH, Kleinman SH, Khismatullin DB, Butte MJ, Rowat AC. Quantitative deformability Cytometry: rapid, calibrated measurements of cell mechanical properties. Biophys J. 2017;113(7):1574–84 Epub 2017/10/06.
Otto O, Rosendahl P, Mietke A, Golfier S, Herold C, Klaue D, et al. Real-time deformability cytometry: on-the-fly cell mechanical phenotyping. Nat Methods. 2015;12(3):199–202 4 p following Epub 2015/02/03.
Park SY, Gonen M, Kim HJ, Michor F, Polyak K. Cellular and genetic diversity in the progression of in situ human breast carcinomas to an invasive phenotype. J Clin Invest. 2010;120(2):636–44 Epub 2010/01/27.
Patel AP, Tirosh I, Trombetta JJ, Shalek AK, Gillespie SM, Wakimoto H, et al. Single-cell RNA-seq highlights intratumoral heterogeneity in primary glioblastoma. Science. 2014;344(6190):1396–401 Epub 2014/06/14.
Pawlizak S, Fritsch AW, Grosser S, Ahrens D, Thalheim T, Riedel S, et al. Testing the differential adhesion hypothesis across the epithelial– mesenchymal transition. New J Phys. 2015;17(8):083049.
Perez-Moreno M, Fuchs E. Catenins: keeping cells from getting their signals crossed. Dev Cell. 2006;11(5):601–12.
Plodinec M, Loparic M, Monnier CA, Obermann EC, Zanetti-Dallenbach R, Oertle P, et al. The nanomechanical signature of breast cancer. Nat Nanotechnol. 2012;7(11):757–65 Epub 2012/10/23.
Remmerbach TW, Wottawah F, Dietrich J, Lincoln B, Wittekind C, Guck J. Oral cancer diagnosis by mechanical phenotyping. Cancer Res. 2009;69(5):1728–32 Epub 2009/02/19.
Schmidt B, Kießling T, Warmt E, Fritsch A, Stange R, Käs JA. Complex thermorheology of living cells. New J Phys. 2015;17(7):073010.
Schnauß J, Händler T, Käs JA. Semiflexible biopolymers in bundled arrangements. Polymers. 2016;8(8):274.
Shackleton M, Quintana E, Fearon ER, Morrison SJ. Heterogeneity in cancer: cancer stem cells versus clonal evolution. Cell. 2009;138(5):822–9 Epub 2009/09/10.
Strehle D, Schnauss J, Heussinger C, Alvarado J, Bathe M, Kas J, et al. Transiently crosslinked F-actin bundles. Eur Biophys J. 2011;40(1):93–101 Epub 2010/08/25.
Swaminathan V, Mythreye K, O'Brien ET, Berchuck A, Blobe GC, Superfine R. Mechanical stiffness grades metastatic potential in patient tumor cells and in cancer cell lines. Cancer Res. 2011;71(15):5075–80 Epub 2011/06/07.
Taketo MM. Reflections on the spread of metastasis to cancer prevention. Cancer Prev Res (Phila). 2011;4(3):324–8 Epub 2011/03/05.
Torres L, Ribeiro FR, Pandis N, Andersen JA, Heim S, Teixeira MR. Intratumor genomic heterogeneity in breast cancer with clonal divergence between primary carcinomas and lymph node metastases. Breast Cancer Res Treat. 2007;102(2):143–55 Epub 2006/08/15.
Wirtz D, Konstantopoulos K, Searson PC. The physics of cancer: the role of physical interactions and mechanical forces in metastasis. Nat Rev Cancer. 2011;11(7):512–22 Epub 2011/06/28.
Xu W, Mezencev R, Kim B, Wang L, McDonald J, Sulchek T. Cell stiffness is a biomarker of the metastatic potential of ovarian cancer cells. PLoS One. 2012;7(10):e46609.
Zhu G, Yan HH, Pang Y, Jian J, Achyut BR, Liang X, et al. CXCR3 as a molecular target in breast cancer metastasis: inhibition of tumor cell migration and promotion of host anti-tumor immunity. Oncotarget. 2015;6(41):43408.

Publisher's Note